DEEP STRUCTURE AND GEOPHYSICAL PROCESSES

BENEATH ISLAND ARCS

by

NORMAN HARVEY SLEEP

B.S., Michigan State University (1967)

M.S., Massachusetts Institute of Technology (1969)

SUBMITTED IN

PARTIAL FULFILLMENT

OF THE REQUIREMENTS FOR THE

DEGREE OF DOCTOR OF PHILOSOPHY

at the

MASSACHUSETTS INSTITUTE OF TECHNOLOGY

November, 1972 (i.e. Feb. 973)

Signature of Author...
Department of Earth and Planetary Sciences,
November 20, 1972

Certified by...
....
Thesis Supervisor

Accepted by..
Chairman, Departmental Committee on Graduate Students

ABSTRACT

Deep Structure and Geophysical Processes

Beneath Island Arcs

by

Norman Harvey Sleep

Submitted to the Department of Earth and
Planetary Sciences on January 17, 1973
in partial fulfillment of the
requirements for the degree of
Doctor of Philosophy

The deep structure and geophysical processes

associated with island arcs were examined as a problem in

heat and mass transfer. Particular attention was given to

the thermal behavior of lithosphere as it descends into

mantle, seismic transmission through descending slabs, the

origin of the magmas which erupt on island arcs, and the

cause of crustal spreading in intra-arc basins.

The factors affecting the thermal behavior of a

lithosphere slab descending into the mantle are so

complicated and numerous that only numerical methods can

accurately account for them. A series of finite-difference

calculations of the temperature field were made to test the

effect of phase changes, the dip of the slab, the thermal

conductivity, and the initial geotherm. Reasonable variations

in those parameters and geologically permissible variations in radioactive heating and adiabatic compression did not greatly effect the gross thermal structure calculated for the slab. Irregularities in slab movement on a time scale of less than 2 million years do not significantly effect the thermal field. Possible factors limiting the maximum depth of seismic zones include thermal assimilation of the slab due to latent heat from phase changes and thermal conduction, mechanical disruption of the slab, and the lack of stress at great depths due to lower density contrast between the slab and the mantle.

Theoretical ray paths through the numerically calculated thermal models of slabs were computed. The results were in good agreement with observed travel times. First motion amplitudes of P-waves at teleseismic distances were measured from long and short period WWSSN records of intermediate focus earthquakes in the Tonga, Kermadec, and Kurile regions and of nuclear explosions and shallow earthquakes in the Aleutian region. These amplitudes were corrected for source mechanism. The Aleutian data were sufficient to show that intermediate focus earthquakes in that region occur in the colder regions of the slab. At short periods shadowing effects which could be associated with the slab were not very marked, less than a factor of 2 reduction for epicentral distances greater than 50 degrees and possibly

more reduction for epicentral distances between 30 and 50 degrees. No systematic effects due to plates were found in the long period data. Some stations in the predicted shadow zone of a Tonga earthquake recorded low amplitude precursors which probably were greatly defocused waves which ran the full length of the slab. Simple diffraction is incapable of explaining the short period results.

Numerical and analytic models were constructed to examine four hypotheses for the origin of island arc volcanics: (1) melting at temperature lowered by inclusion of subducted material; (2) frictional heating related to the descent of the slab; (3) upwelling of material from the asthenosphere into the lithosphere of the island arc; (4) concentration of pre-existing melt in the asthenosphere. Presently available geochemical data is insufficient to resolve whether a significant portion of subducted material erupts on island arcs. This does not create a difficulty in evaluating the other hypotheses, as the observed eruption temperature of island arc volcanics is similar to that of basalt. The viscosity of the melt and the geometry of the asthenosphere are not conducive to segregation of melt. At low concentrations of melt, the regions with the highest concentration of melt contribute disproportionately to the magma which segregates. About 4 kb of shear stress is needed to cause melting above the slab. Frictional heating is not

likely to cause the widespread high crustal temperature observed beneath island arcs. Hypothesis 3 involves no obvious thermal or mechanical difficulties although the uncertain rheological properties of the region near the base of the lithosphere preclude the computation of a realistic, detailed model. However, it is both mechanically and thermally reasonable that the slab could entrain intermediate viscosity material near the base of the lithosphere. An influx of material from the asthenosphere to replace the entrained material could produce high crustal temperatures and provide a source region for island arc volcanics.

The hypotheses and models studied in relation to island arc volcanism are also relevant to spreading in intra-arc basins. Frictional heating above the slab is probably insufficient to cause this spreading. A numerical study was made to see if the extension could be related to viscous flow of material entrained with the slab. This calculated flow had the correct geometry to cause tension behind the island arc. Intra-arc spreading would be most likely to occur if the flow was induced in the intermediate viscosity region between the lithosphere and the asthenosphere.

ACKNOWLEDGEMENTS

This work might have proved intractable without the help of others. Especial thanks goes to my adviser, M. Nafi Toksöz, who endured my midwestern conservatism and suggested the topic of study and whose ideas and comments both clarified my thinking and improved this manuscript. I would also like to thank: Drs. John Minear and Bruce Julian for supplying computer programs which were subsequently modified; Drs. Jorge Mendiguren, Don Weidner and Professor Sean Solomon for helpful hints on reading seismograms; Dr. D. Joe Andrews for much advice on numerical and mathematical matters; Al Smith, Professors Richard Naylor, Seiya Uyeda and Sean Solomon for critical comments on various parts of the draft of this manuscript; and the above named people, Kei Aki, Patrick Hurley, Dai Davies, and William Bryan for useful discussions. Al Taylor provided assistance with using the seismic library. Ms. Sara Brydges typed the manuscript, translating it into standard English.

TABLE OF CONTENTS

CHAPTER 1. INTRODUCTION

The downwarping and descent of lithospheric plates into the mantle, as implied by the plate tectonic hypothesis has been widely accepted. Increasing amounts of geological, geochemical, and geophysical data are being explained in terms of descending slabs. In this thesis, the results of a series of analytical and numerical calculations on the evolution and properties of downgoing lithosphere and adjacent regions are described and compared with relevant observations. Rather than attempting to solve the convection problem for the entire earth, attention was given to problems which could be considered using observed plate motions as data. In particular, four areas were covered in detail:

1. Thermal evolution of a slab as it descends into the lithosphere (Chapter 2)

2. Teleseismic P-wave transmission through slabs (Chapter 3)

3. Origin of magmas which erupt on island arcs (Chapter 4)

4. Origin of intra-arc basins (Chapter 5).

The results of the thermal calculations were relevant to the subsequently considered problems. The seismic studies were concerned mainly with testing the implication of the thermal models to the gross structure of the slab

and with determining the spatial relationship between slabs and intermediate focus earthquakes. Physical models of several hypotheses on the origin of island arc volcanism and intra-arc basins involve the consideration of processes secondary to subduction.

The method of approach was well suited to the problems studied as the heat flow equation could be solved once the kinematics of subduction were known and since the mass transfer equation is most easily solved in regions directly influenced by the descent of the slab. As the kinematics of plate motion are used as input in the mathematics in this study, little information will be gained on the ultimate cause of this motion or on the flow and temperature at great depths far from slabs.

All protracted calculations were relegated to Appendix A. The physical models were kept simple using only the amount of detail warranted by knowledge of the physical parameters are by quality of the data to which the model was relevant. A better insight into the effect of various parameters was therefore obtained. Thermal and seismic calculations were generally more detailed; calculations involving viscosity were less detailed.

CHAPTER 2.   TEMPERATURE IN A DOWNGOING SLAB

Deep earthquake zones beneath island arcs are believed
to be related to slabs of subducted oceanic lithosphere
(e.g., Isacks et al., 1968).   The relatively simple pattern
of motion in these areas makes calculation of the tempera-
ture field practical without solving the full convection
problem for the earth.   Several solutions for the tempera-
ture in a slab have been obtained.   McKenzie (1969) used
a two-dimensional analytic solution which assumed the top
and the bottom of the slab were isotherms.   Griggs (1972)
included the effect of phase changes in a numerical
solution with similar boundary conditions.   Turcotte and
Oxburgh (1969) obtained a solution using boundary layer
theory.   Langseth et al. (1966), Minear and Toksöz (1970a,b),
Hasebe et al. (1970), and Toksöz et al. (1971) used two
dimensional numerical models in which the mantle surrounding
the slab was explicitly included so energy was conserved.

The purpose of this chapter is to use improved numer-
ical calculations similar to those used by Toksöz et al.
(1971) to test the effect of various physical parameters
on the evolution of the slab.   Questions unanswered by
previous studies include: the effect of slab geometry on
slab evolution; the factors which limit the length of the
slab; the sensitivity of the slab to thermal conductivity,
phase changes, and the initial geotherm, and the effect of

constant slab motion. The numerical methods used in this chapter are described in Appendix A.

2.1 Physical parameters

Certain physical constants such as mantle radioactivity, adiabatic gradient, density, and specific heat, can be shown to be well enough constrained from a knowledge of observational geophysics, solid state physics, and geochemistry that they can be considered known for purposes of constructing a model. The uncertainty in the value of other parameters, such as thermal conductivity and phase change relations, are large enough that these effects should be modeled. In addition, systematic parameters which themselves depend on the local physical constants, such as the unperturbed mantle geotherm, must be determined. The effect of frictional heating and its relation to volcanism are considered in Chapter 4.

The average density profile of oceanic crust (Press, 1970) and a specific heat of 1.3×10^7 erg/g-°C are sufficiently accurate for purposes of modeling the thermal structure of the slab (Minear and Toksöz, 1970a,b).

2.1.1 Radioactivity

The average radioactivity of the oceanic lithosphere is probably about equal to the radioactivity of the upper mantle, because differentiation at mid-oceanic ridges occurs

mainly above 30 km depth (Kay et al., 1970). Some radio-

activity is added to a plate by sediments and mid-plate

volcanism. It is not known to what extent this material

is subducted.

Radioactive heating in the upper mantle of the earth

is too low to effect the evolution of the slab. Estimates

of the quantity include 2.3×10^{-7} erg/gm-sec (MacDonald,

1959, 1963), 5.4×10^{-8} erg/gm-sec (Armstrong, 1968),

and 1.5×10^{-8} erg/gm-sec (Hurley, 1968a,b). The larger

radiactivity of MacDonald would increase the temperature

only 6°C in the 10 my descent of the slab. A more

important effect of radioactive heating is on the unperturbed

geotherm of the upper mantle.

The amount of radioactive heating in the upper mantle

is constrained by the abundance of Ar^{40} in the atmosphere

and the abundances of radiogenic and radioactive elements

in sampled rocks to the low values of Hurley (1968a,b)

and Armstrong (1968). The MacDonald radioactivity is based

on chondritic element abundances and calculated by distrib-

uting the radioactivity to obtain conductive equilibrium.

2.1.2 Adiabatic heating

The amount of heating due to adiabatic compression in

a downgoing slab can be calculated by $\rho g \alpha T v_z$ (Hanks and

Whitcomb, 1971). Other than α, all the parameters are known

at the start of any time step. As in Toksöz et al. (1971),

α (in units of 10^{-6} $°C^{-1}$) was calculated by exp(3.58-0.0072z), where z is depth in kilometers. The increase in slab temperature due to adiabatic heating is about 0.3 °C/km. Considering that the uncertainty in the unperturbed mantle geotherm is greater than this amount, adiabatic heat generation is known well enough for purposes of this chapter.

2.1.3 Thermal conductivity

Two possible schemes for calculating thermal conductivity in the interior of the earth were used in constructing models. The MacDonald (1959) formulation was used for most of the models calculated. Some models were calculated using an empirical formulation (Schatz, 1971). These formulae are given in Appendix A. The MacDonald conductivity is generally larger than the Schatz conductivity.

The conductivity change associated with the phase change at 400 km is probably not very large since ferrous iron, which increases opacity and reduces radiative conductivity, enters the common phases on both sides of the transition zone (Ringwood, 1970). If iron-free oxides such as MgO, Al_2O_3 or SiO_2 exist as minerals below the 600 km discontinuity, the radiative conductivity would be extremely high. Without direct experimental evidence at the phase relations of mantle materials at these pressures, no further speculation is warranted.

2.1.4 Phase changes

Several phase changes may occur in the upper mantle. Some such as slight partial melting in the low velocity zone do not effect bulk properties because only a minor portion of the material is involved. Other phase changes involving most of the material in the slab must be considered explicitly in a thermal model. If the vertical velocity through a phase change is fast enough, a few tenths of a centimeter per year for mantle material, the phase boundary will be moved from its normal position (Schubert and Turcotte, 1971). Except in a very rapidly convecting fluid the thermal gradient is locally sub-adiabatic near a major phase change (Verhoogen, 1965; Schubert and Turcotte, 1971; Ringwood, 1972). This inhibits small scale flow in this region, although large scale flow is enhanced by the density difference associated with the phase change.

An improved method was used to calculate the effects of phase changes in this paper. All points in the model, rather than just those points in the slab, were examined for phase changes at the end of each translation step and the change in the amount of each phase from the previous step recorded. Latent heat was calculated from this change and included as a heat source in the model. The translation routine for translating temperature was also used to translate the amount of each phase with the slab.

This calculation scheme works for phase changes going both ways whether or not the slab is assumed to move (Appendix A).

Three phase changes were considered in the models. Many of the models include a basalt-eclogite or equivalently a plagioclase peridotite-garnet peridotite reaction. The heating from this reaction was insignificant. Heat generation from the phase changes at 400 and 600 km is probably quite large. The 400 km transition has been studied experimentally (Ringwood, 1970). The slope of both phase changes is likely to be 20 to 30 bar/°C (Ringwood, 1972). For the models in which these changes were considered the phase diagram used by Toksöz et al. (1971) was used. One model was run with a seismically constrained phase diagram for the 400 km phase change; the effect was not greatly different.

2.1.5 Unperturbed mantle geotherm

In earlier papers the unperturbed geotherm of the mantle was either assumed to be adiabatic (McKenzie, 1969), the conductivity geotherm (Minear and Toksöz, 1970a,b; Toksöz et al., 1971), or to be controlled by the solidus temperature of peridotite (Griggs, 1972). In this study a crude approximation to the average geotherm in a convecting earth was obtained so that the importance of the unperturbed geotherm on the final results could be tested. For purposes of

calculation it is assumed that the downwelling parts of the
flow do not interact thermally with a significant volume of
the mantle, and that the upwelling flow can be approximated
with a uniform, steady-state upward flow necessary to
conserve mass. The latter assumption is reasonable since
the migration of ridges with respect to trenches precludes
a steady-state cell with a trapped flow in its core. At
some depth heat must be added to the convection pattern to
heat material which has sunk from the surface. In this
region, which could conceivably include the lower part of
the upper mantle, a conductive geotherm would exist.

Once these assumptions have been made, a "convective"
geotherm can be calculated in a straightforward manner
(Appendix A), if the surface heat flux, the average age of
oceanic crust, and the dependence of conductivity on
temperature and pressure are known. The results of the cal-
culations are shown in Figure 2.1. Below 160 km the average
thermal gradient is adiabatic. The gradient is increased
in the region of the phase change due to the increased amount
of heat generation there. Within the phase change region
the gradient is locally subadiabatic since the latent heat
of the phase change is conducted to the surrounding regions.
The choice of conductivity does not greatly effect the
geotherm. The conductive geotherm did not grossly differ
from the convective geotherm as the effects of ignoring
convection and placing all the heat sources in the upper

mantle have opposite signs.

2.2 Computational results

Due to the increased efficiency of the improved
numerical scheme, it was possible to calculate several
models with small time and space increments (Table 2.1).
Adiabatic heat generation, density, pressure, and specific
heat were not varied between models. To facilitate com-
parison with earlier calculations, most of the models used
the MacDonald (1959) radioactivity and temperature distri-
bution and the phase boundaries by Minear and Toksöz (1970a,
b). Models were calculated to test the importance of the
depth of the slab, the unperturbed geotherm, and the
conductivity. Frictional heating and its relevance to
intra-arc basins and island arc volcanism is considered in
Chapters 4 and 5.

A model similar to those calculated by Toksöz et al.
(1971) is used as a base model with which to appraise the
effects of changes in the parameters (Figures 2.2 and 2.3).
The temperature field in this model is in good agreement with
the most similar earlier model (Toksöz et al., 1971, Figure
8). Upward migration of the phase boundaries into the
coldest part of the slab should be noted. The second phase
change produced a kink in the isotherms, but did not cause
the slab to assimilate. Latent heat from the lower phase
change heated the slab to the ambient mantle temperature.

Below the depth of the lower phase change this slab would

no longer be detectable by geophysical means.

The temperature field of a slab dipping 29 degrees

was computed using the physical parameters of the base

model (Figures 2.4 and 2.5). Although 16 my, as opposed to

11 my for the base model, was required for this slab to

penetrate to 650 km, the maximum depth of penetration of

both slabs is controlled by the lower phase change. The

maximum penetration of isotherms into the mantle is about

30 to 100 km less in the shallower dipping model.

The modeled slab remains cooler to a greater depth if

the Schatz conductivity formulation is used (Figures 2.6

and 2.7). The thermal gradients are steep along the bound-

aries of this slab, since the minimum conductivity is at

intermediate temperatures. This slab persists to some

extent below the lower phase change.

Use of the "convective" geotherm does not greatly alter

the temperature field (Figure 2.8). The lower phase change

was not included in constructing the geotherm of the model.

Unlike the models using the strongly superadiabatic MacDonald

(1959) geotherm, the temperature field is not greatly

influenced by the kinematics assumed for the slab, since

motions in the nearly adiabatic regions of the mantle effect

temperatures only slightly. It should also be noted that

the effect of 400 km phase change is evident, although this

reaction was explicitly included when constructing the geotherm.

It is conceivable that for a period of time a slab may become hung up at a trench such that no subduction occurs. Contraction of the lithosphere would presumably occur elsewhere. The numerical method used in this chapter corresponds to such a periodic stop-start case. In some of the less detailed models the translation distance was about 80 km and the translation time-step about 1 my. The effect on the temperature contours is barely noticeable (Figure 2.9). The geological record might contain evidence relating to irregularities in subduction rate. The observed irregularities in the seismic zone are thus more likely due to disruption of the slab than non-uniform descent rate.

Once subduction ceases it is most likely that the slab will detach and sink as it did in South America or the New Hebrides. Tension near the top of the slab would permit fracture and separation. Detachment would occur if new material was being subducted more slowly than the separation rate. The maximum amount of time a slab may remain beneath a locked subduction zone may be calculated by assuming that no motion of the slab occurs. Several such numerical models were calculated. It was found that after 3.6 my the slab was not greatly effected (Figures 2.8 and 2.10). After 16 my, the slab was still evident but the temperature anomaly was spread over a larger region. After 50 my only a very broad temperature anomaly remained (Figure 2.11). It is not likely that a seismic zone will remain active for much

more than 10 my after subduction ceases. Once the slab is
partially heated, detachment would be easier. The velocities
of plate motions are great enough that the former site of
a subduction zone could be rapidly separated from the
material produced by the assimilation of the slab.

2.3 Geophysical implications

The models computed by varying thermal conductivity,
ambient geothermal gradient, and dip differed only in fine
structure which would not be resolved by most geophysical
methods. This gives some confidence in the earlier con-
clusions drawn from earlier calculations (Toksöz et al.,
1971).

1. Significant contributions to heating the interior
   of the slab are in order of importance: (a) Conduc-
   tive and radiative transfer of heat from the
   surrounding mantle; (b) Adiabatic compression of
   the slab material, including the latent heat of
   phase changes; (c) Frictional heating. Heating from
   radioactive decay is insignificant on a 10 my time
   scale.

2. The slab penetrates to at least the level of the
   600 km transition zone in the mantle. The 400 km
   transition causes only fine structure.

3. Conductive heat transfer cannot explain high heat
   flow behind island arcs.

4. The slab models may be used as a basis from which

   to compute the gravity, seismic velocity, and stress

   fields.

Conversely, the insensitivity of the models to reasonable

variations in physical parameters makes the use of data on

slabs an inefficient way to determine these parameters.

Further discussion of the relevance of the models to

the maximum depth of earthquakes, the gravity anomalies

associated with island arcs, and of subducted continental

material is in order. Seismic transmission through slabs is

discussed in Chapter 3 and the island arc volcanism in Chapter

4.

2.3.1 Maximum depth of earthquakes

No earthquakes have ever been observed below a depth

of 650 to 700 km, although several seismic zones terminate

at shallower depth (Isacks et al., 1968). The absence of

well defined travel time anomalies for deep focus earthquakes

indicates that a well defined slab does not exist for a sig-

nificant distance below the earthquakes (Toksöz et al., 1971;

Mitronovas and Isacks, 1971; Sen Gupta and Julian, in prep-

aration). A broad region of somewhat reduced temperature

or a weak continuation of the slab below the depth of maximum

earthquakes cannot be excluded by the data.

This limited depth of earthquakes may be explained by

either the absence of stresses necessary to produce earthquakes

or by the absence of material which would undergo brittle failure. Hypotheses postulating the absence of brittle material below 650 km include:

1. Subduction has been active for only 10 my and the slabs have not had time to penetrate deeper (Isacks et al., 1968).

2. Thermal conductivity is high enough that the slab assimilates with the adjacent mantle (McKenzie, 1969).

3. A local subadiabatic gradient related to the latent heat of the phase change precludes convection below 650 km or adds heat to the slab. (Verhoogen, 1965; Toksöz et al., 1971).

4. Metastable minerals are necessary for deep earthquakes to occur and do not exist below 650 km (Ringwood, 1972).

5. High viscosity or iron content precludes convection below 650 km (McKenzie, 1966).

Possible causes of the absence of stress below 650 km include:

6. The 650 km phase change occurs at shallower depths in the slab and produces the stress for deep focus earthquakes; below 650 km there is less density contrast and, therefore, less stress (Smith and Toksöz, 1972).

7. The slab below 650 km is sufficiently fragmented to not act as a stress guide.

These hypotheses are not mutually exclusive, as
several factors may contribute to the absence of deep
earthquakes below 650 km. The models calculated above,
except for 1, 4, and 5, have some relevance to these
hypotheses. Hypothesis 4 is difficult to test; hypothesis
5 can be excluded since glacial rebound studies indicate
that a major barrier to convection such as a subadiabatic
gradient or an increase in iron content with depth does not
exist around 650 km (Cathles, 1971). Hypothesis 1 is
unlikely since there is little evidence for a major start-up
of sea-floor spreading 10 my ago. Magnetic lineation
correlation (e.g., Heirtzler et al., 1968), deep sea drilling
(e.g., Menard, 1972) and the relationship between topo-
graphic elevation and the age of the sea floor (Sclater
et al., 1971) tend to preclude this hypothesis.

To accurately model the assimilation of the slab as
in hypotheses 2 and 3 it is necessary to have a geotherm
consistent with the physical parameters and motion assumed
for the mantle. For example, a conductive geotherm must
exist below the depth where convection ceases since much of
the heat which flows at the surface must originate in the
deep interior of the earth (Hurley, 1968a,b). A lower
geothermal gradient may exist since convection could con-
tinue into the lower mantle after the thermal deficiency
in the slab has spread out over a broad region.

Equilibration through thermal conduction is not likely

to be the sole cause of a maximum depth for earthquakes
as earthquakes in some seismic zone, such as Tonga, do not
become progressively rarer with depth (Isacks et al., 1968).
The age differs by a factor of 2, from the nearly vertical
Mariana slab to the 30 degree dipping Japanese slab.
Thermal conductivity would have to increase with temperature
as in the models for the slab to heat up in 10 my since the
thermal time constant for oceanic lithosphere is about 35
to 50 my (Sleep, 1969; Sclater and Francheteau, 1970).

Several modeled slabs were heated to above the normal
mantle temperature after penetrating the 600 km phase change
(Figures 2.3, 2.5, and 2.9). These higher than normal
temperatures are a result of the artificial nature of the
assumed motion. In the physical situation the material
would move away laterally as soon as it became buoyant with
respect to the mantle. However, the excess temperature at
the base of the slab is not large and not found in all the
models including the 600 km phase change (Figure 2.7). Whether
a broad cool region can exist where the slab penetrates into
the lower mantle depends sensitively on the geothermal
gradient and on the latent heat of the 600 km phase change.
The geothermal gradient, however, depends whether mantle-
wide convection occurs. Models which assume the kinematics
of the motion and the geotherm are, therefore, unlikely
to resolve this problem.

The density contrast due to the 600 km phase change,

about 10%, is much larger than the 2% or 3% density con-
trast due to ordinary thermal contraction. If the phase
transition occurred at shallower depths in the slab,
considerable stress would be generated in the lower part
of the slab. This probably explains the high seismicity
of small detached segments of slab in Tonga and the New
Hebrides (Smith and Toksöz, 1972). Below the depth of the
phase transition in the mantle, where this density could not
exist, the stress might be insufficient to cause earthquakes.

A small detached fragment of a slab is not likely to
have enough stress for earthquakes although it may be
sufficiently cool for faulting. Sufficiently low subduction
rates cannot supply material to the slab as fast as a
detached block would sink on its own. Successive blocks
would not interact and no seismic zone would form. If the
empirical relation between dip and subduction rate
(Luyendyk, 1970) gives the minimum sinking rate, no slabs
should form from subduction below 2 or 3 cm/yr. This is
consistent with the observed absence of seismic zones near
poles of plate rotation.

A mechanical condition, such as a moderate increase
in viscosity around 650 km, might disrupt the slab without
interfering with mantle-wide convection or the response to
glacial rebound. The process of disruption is probably
active in the deeper part of the Tonga slab. Locally
vertical and horizontal dips are present in the highly

contorted region (Isacks et al., 1969). The stress patterns
of deep earthquakes are compressional along the dip of the
slab, indicating that the descent is being resisted from
below (Isacks and Molnar, 1971; Smith and Toksöz, 1972).
The horizontal dip of detached slabs in the New Hebrides
and South America and the horizontal portion of the Tonga
slab also indicate that the slab has mechanical difficulty
penetrating below 650 km. Once the slab is disrupted the
smaller fragments are easily thermally assimilated and
unlikely to accumulate enough stress to cause earthquakes.

2.3.2 Gravity anomalies

The gravity anomaly due to the slab can be calculated
in a straightforward manner if the coefficient of thermal
expansion is approximately known (Appendix A). The gravity
anomaly is relatively independent of the detailed structure
of the slab. Thermal conductivity can redistribute heat
over short distances, but the total amount of heat and
therefore the density anomaly is conserved. Thermal models
which consider the slab alone (McKenzie, 1969; Griggs, 1972)
cannot be used to calculate gravity, because heat is not
conserved at the artificial boundary with the surrounding
mantle.

Gravity anomalies which were calculated for six slabs
(Figures 2.12 and 2.13) are much larger than observed,
although conservative values of physical parameters were used.

The effects of the slab on the free surface of the earth
and perhaps the region near 650 km may compensate the
gravity anomaly. Hydrodynamic pressure will move a stably
stratified boundary in a slowly moving viscous fluid relative
to the pressure creating a density anomaly. Oceanic trenches
are a feature of this type (Elsasser, 1967; Morgan, 1965).
Stress equilibrium requires that the excess weight of the
slab be balanced by either hydrodynamic forces or rigid
support. The viscosity of the lower mantle determined from
glacial rebound is too low for that region to rigidly
support the slab (Cathles, 1971). The lithosphere is too
thin to have any great effect over regions larger than
its thickness.

Consideration of the dynamics as well as the kinematics
of convection is necessary to understand the small observed
amplitude of gravity anomalies near island arcs. Any
complete convection model must satisfy this data. Without
additional, more difficult calculations, all that can be
concluded is that the weight of the slab is supported by
hydrodynamic forces rather than the static strength of the
mantle.

2.3.3 Continent-continent collisions

Continents connected to oceanic plates may drift into
a trench causing a continent-continent collision. An
orogeny caused by that event is likely to be brief and abrupt,

since less dense continental crust cannot penetrate the mantle. Numerical slabs of an intra-continental subduction zone were constructed to obtain predictions on their behavior.

The large scale structure in the region of a continent-continent collision is in part inherited from the pre-existing active continental margin and in part due to the subducted continental crust. The qualitative effect of most subduction parameters can be easily determined. At normal subduction rates, the material in the slab cools the surrounding region. High geothermal gradients above the slab could result from frictional heating on the fault plane (e.g., McKenzie and Sclater, 1968) or from mass transfer with material from below. At subduction rates of a few centimeters per year frictional heating in the seismic zone cannot cause high geothermal gradients near the surface without convective heat transfer (Hasebe et al., 1970). For continental crust to have much effect on temperature during its subduction, the subduction rate would have to be low since the average radioactive heat production of continental crust, 4.1×10^{-6} erg/gm-sec (Hurley, 1968a,b; Armstrong, 1968), can cause a maximum temperature increase of 10°C/my.

A numerical model using extreme value of parameters was constructed showing that frictional heating along the fault plane, alone, could not produce extremely high geo-thermal gradients above a subducted continent (Figure 2.14).

After about 50 my the temperature returns to steady state
(Figure 2.15). We may conclude that orogeny is most likely
to occur during the collision or after about 50 my when the
subducted continental material has become heated. In the
former case the heat of the orogeny would be related to
volcanic activity along the active margin prior to the
collision. In the latter it would be radioactive decay in
the subducted material.

Mass transport of heat, probably necessary if high
geothermal gradients occur in the crust above the slab, can
be caused by igneous intrusions from the mantle, folding of
deep strata upward during the collision, and partial melting
and intrusion of continental crust. To determine the
extent to which these processes operated during a continent-
continent collision, the duration of igneous activity and
folding associated with the orogeny and the relative temporal
order of folding, metamorphism, and igneous activity must
be deduced from observed geology.

2.4 Conclusions

Numerical models of the temperature regime in a
downgoing slab were constructed using a more flexible version
of the numerical scheme used by Toksöz et al. (1971). The
results were not greatly dependent upon the reasonable changes
in the thermal conductivity, the unperturbed geotherm, and
the dip of the slab. This gives more confidence in the

results of the calculation.

The observed maximum depth of earthquakes is probably related to lack of cool brittle material due to increased thermal conductivity at high temperatures and the latent heat of the 600 km phase change; and to the lack of stress due to mechanical disruption of the slab and a smaller density contrast below the phase transition. A kinematic model which assumes the ambient mantle temperature cannot be expected to give a reliable answer on the maximum depth of convection in the mantle. Gravity anomalies are effected by hydrodynamic forces in the mantle and can be calculated only from a model which considers the response of the mantle to the slab. The ambient state of the mantle, which depends on the extent of convection, is needed to determine this response.

Models were also constructed which showed that: short term irregularities in slab motion would not significantly perturb the thermal state of the slab; once a slab has halted, it is not likely to remain seismically active for much greater than 10 my; and, about 50 my is needed for subducted continental crust to heat up due to its radio-activity.

TABLE 2.1: A summary of parameters used for temperature field calculations for different models. Phase changes are listed in Appendix A. "M" refers to MacDonald (1959) conductivity; "S" to Schatz (1970) conductivity; and "ML" to Mac-Donald conductivity below 30 km and lattice conductivity above 30 km. "A35" refers to value of parameter above 35 km; "B35" refers to value below 35 km. Geotherms 1 and 3 are shown in Figure 2.1. Geotherm 4 is in conductive equilibrium with a flux of 45 erg/cm^2-sec at 200 km.

Table 2.1

Figure	Subduction velocity cm/yr	Phase changes	Conductivity	Δx km	Δz km	Shear heating 10^{-5} erg/cm² sec	Geotherm	Dip	Radioactive heat 10^{-8} erg/gm sec	Points translated per step	Temperature iterations per step
2.2	8	1,2a,3	M	10	10	16	1	45	23 A465 1.7 B465	2	2
2.3	8	1,2a,3	M	10	10	16	1	45	23 A465 1.7 B465	2	2
2.4	8	1,2a,3	M	18	10	16	1	29	23 A465 1.7 B465	6	2
2.5	8	1,2a,3	M	18	10	16	1	29	23 A465 1.7 B465	6	2
2.6	8	1,2a,3	S	10	10	16	1	45	23 A465 1.7 B465	6	2
2.7	8	1,2a,3	S	10	10	16	1	45	23 A465 1.7 B465	6	2
2.8	8	2b	M	10	10	16	3	45	1.5	2	2
2.9	8	1,2a,3	M	10	10	16	1	45	23 A465 1.7 B465	6	2
2.10	0	1,2a,3	M	10	10	0	1	45	23 A465 1.7 B465	-	-
2.11	0	1,2a,3	M	10	10	0	1	45	23 A465 1.7 B465	-	-
2.14	1	-	M	12	5	1 A35 16 B35	1	23	410 A30 1.5 B30	3	15
2.15	1	-	ML	16	5	16	4	17	410 A30 1.5 B30	2	10

FIGURE CAPTIONS

Figure 2.1   Possible geotherms for the earth were calcu-
lated using different assumptions. Geotherm 1
is in conductive equilibrium assuming the
MacDonald (1959) conductivity formulation and
MacDonald's distribution of radioactivity.
Geotherms 2 and 3 were calculated using a radio-
active heat production of 1.5×10^{-8} erg/cm^3-
sec by assuming convective equilibrium. Geo-
therm 2 uses the Schatz (1970) conductivity
formulation and Geotherm 3 the MacDonald
(1959) formulation. The convective geotherms
are nearly adiabatic below 200 km except for
the effects of the phase change near 400 km.
The surface heat flux for all the geotherms
was 70 erg/cm^2-sec.

Figure 2.2   The base slab model after 3.6 my and 7.1 my
was calculated using the parameters given in
Table 2.1. Note that the second phase change
produces a sharp kink in the geotherms.

Figure 2.3   The base slab after 10.7 my was calculated
using the parameters given in Table 2.1. This
slab was assimilated by the latent heat of the
600 km phase transition.

Figure 2.4   This slab was calculated using the same

parameters as in Figure 2.3 except for a dip
of 29 degrees.

Figure 2.5   The slab in Figure 2.4 after 16 my was assimi-
lated by the 600 km phase change. The pene-
tration of isotherms into the mantle is slightly
less than for the base slab in Figure 2.3.

Figure 2.6   Temperature field of slab was calculated using
the parameters of the slab in Figure 2.3 except
that the Schatz (1970) conductivity formulation
was used. Steeper thermal gradients occur at
the boundaries of this slab.

Figure 2.7   The slab in Figure 2.6 after 10.7 my. Due to
the lower Schatz conductivity, this slab pene-
trated the 600 km phase change.

Figure 2.8   Temperature field in a slab penetrating into
a mantle having Geotherm 3 (Figure 2.1). The
parameters used for this slab and given in
Table 2.1 are self-consistent with the geotherm.
Penetration of the slab was stopped at 10.7 my,
and the lower right slab was allowed to equili-
brate with the mantle for 3.6 my.

Figure 2.9   The temperature field of this slab after 10.7 my
was calculated with identical parameters to the
slab in Figure 2.3, except that each translation
was 6 grid points rather than 2. The difference

between the two slabs is barely noticeable.
This confirms that the numerical scheme used
to translate the slab is a small source of
error in the calculations and that irregularities
in slab motion on a time scale of a million
years would have little effect on the thermal
regime.

Figure 2.10   The thermal field of the lower slab in Figure
2.2 after the slab was left at rest for an
additional 3.6 my. Note that equilibration is
retarded in the vicinity of the phase boundary
on the bottom part of the slab.

Figure 2.11   The thermal field of the slab in Figure 2.5
was left at rest for an additional period of
48 my. The temperature anomaly becomes pro-
gressively broader with time. It is unlikely
that the upper slab would be seismically active.

Figure 2.12   Gravity field calculated for the base slab
model in Figure 2.3 (1), and the upper (3)
and lower (2) parts of Figure 2.2. This gravity
anomaly is much larger than observed. The
horizontal zero point in Figures 2.2 and 2.3
is at 770 km.

Figure 2.13   The gravity field calculated for the slab in
Figure 2.8, upper left (1), upper right (2),

and lower left (3). The horizontal zero point
in Figure 2.8 is at 770 km. These anomalies
are also much larger than observed.

Figure 2.14 The temperature in a subducted continent is
shown after 7.7 my (above). The base of the
crust is indicated by M. After remaining
stationary for an additional 47 my, a thermal
maximum has formed in the subducted crust (be-
low).

Figure 2.15 Temperature field in subducted continent after
10 my was effected by extreme frictional heating
along the fault plane. The highly radioactive
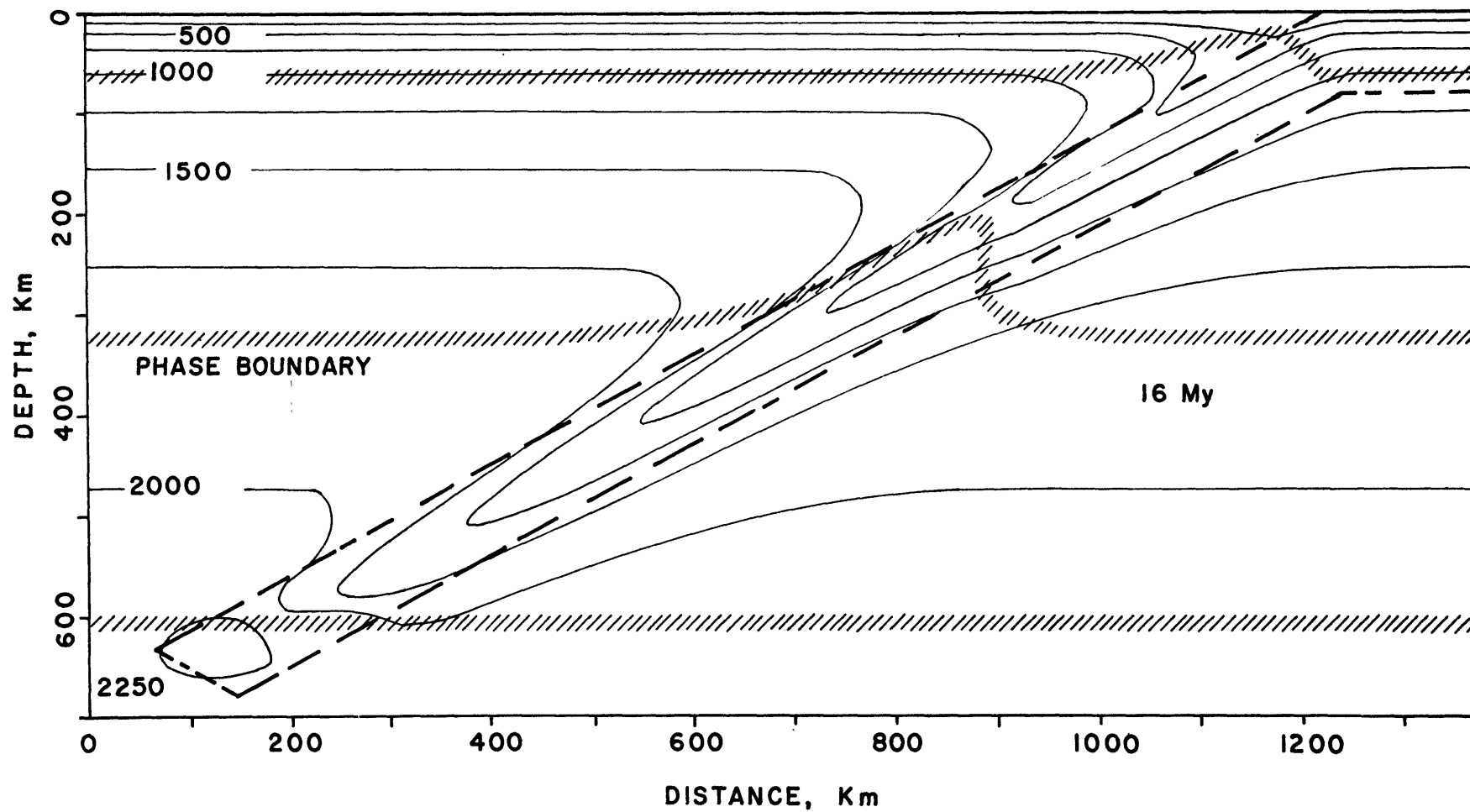continent crust is indicated by hatching.
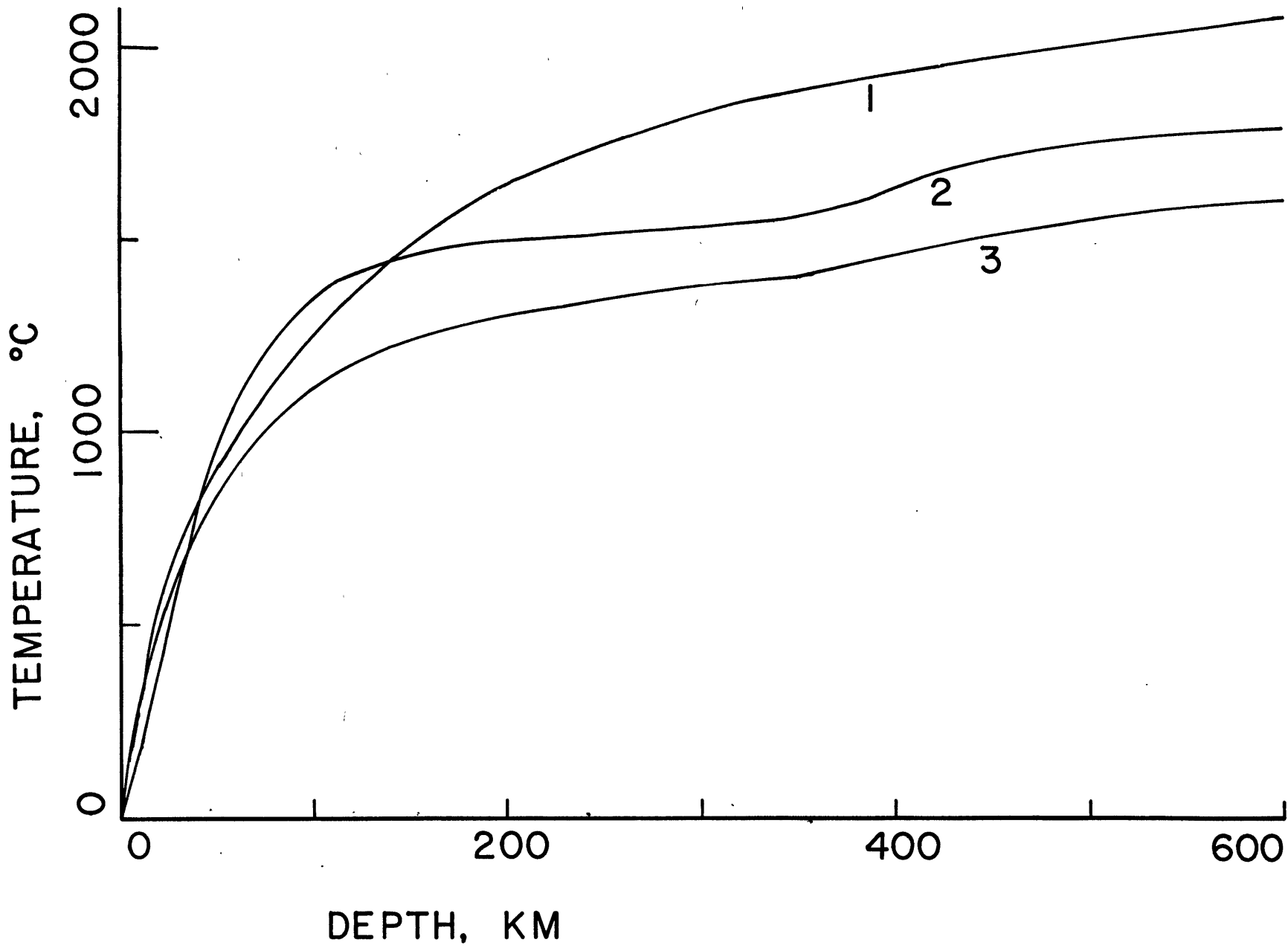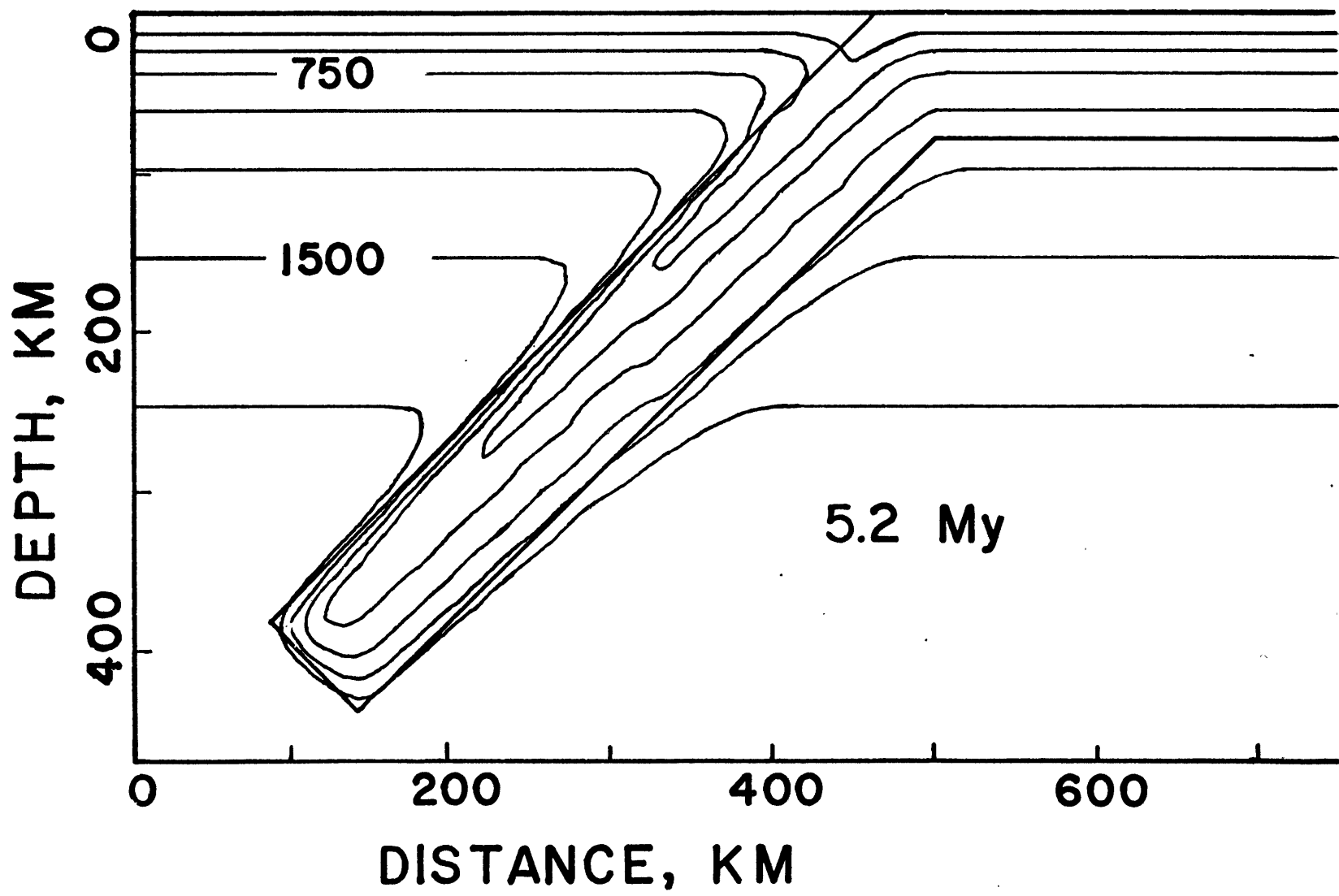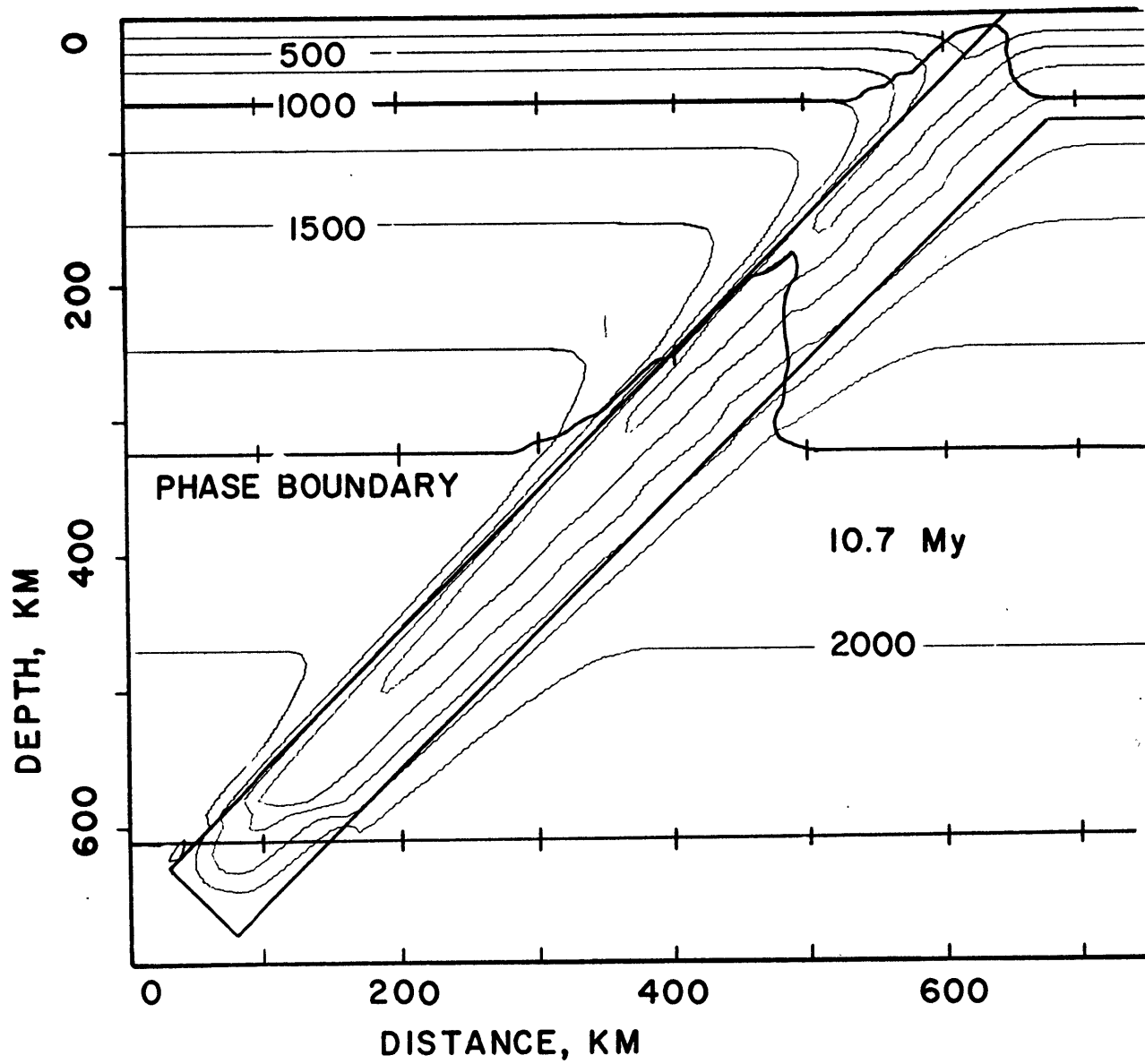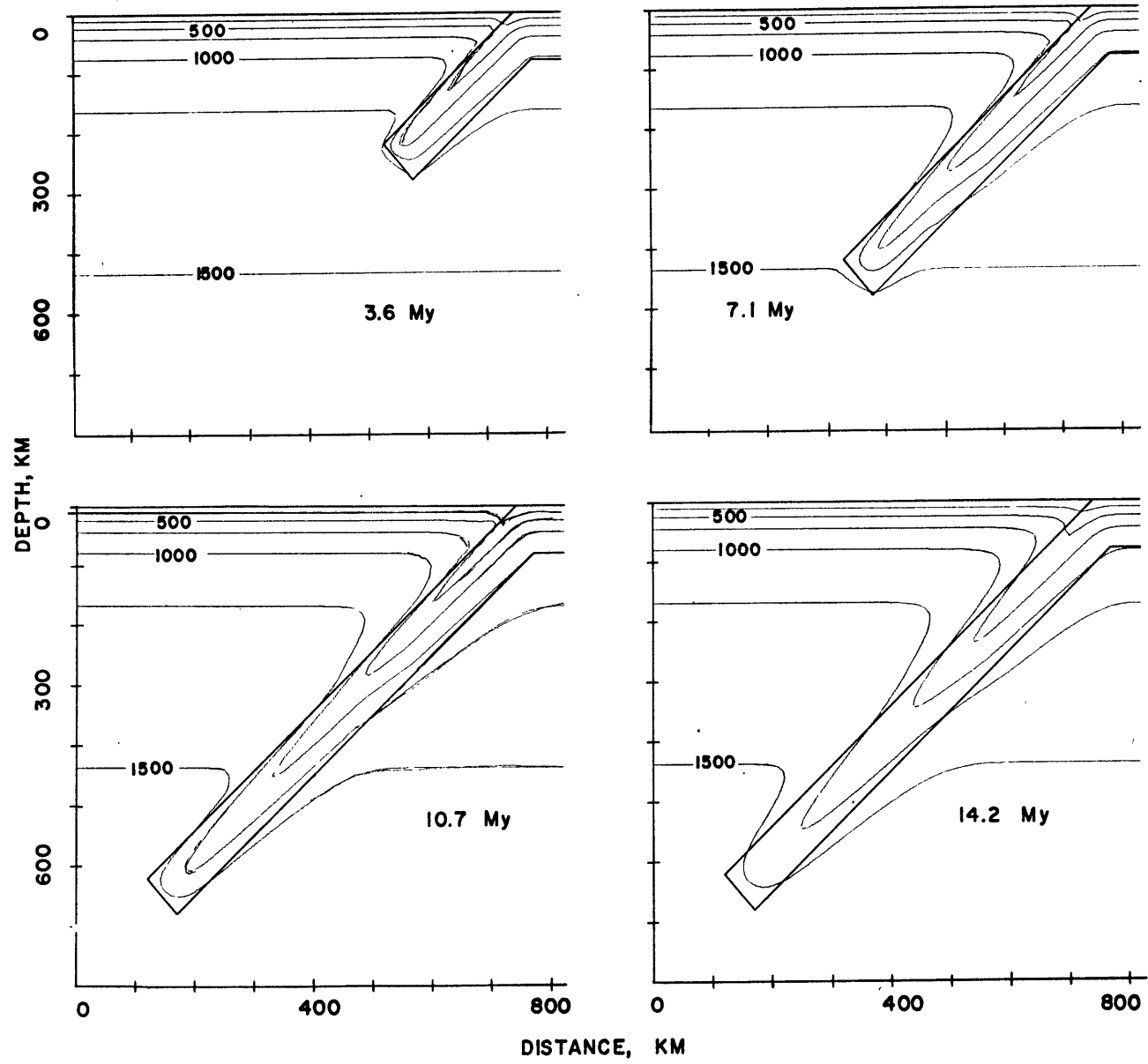
FIGURE 2.1
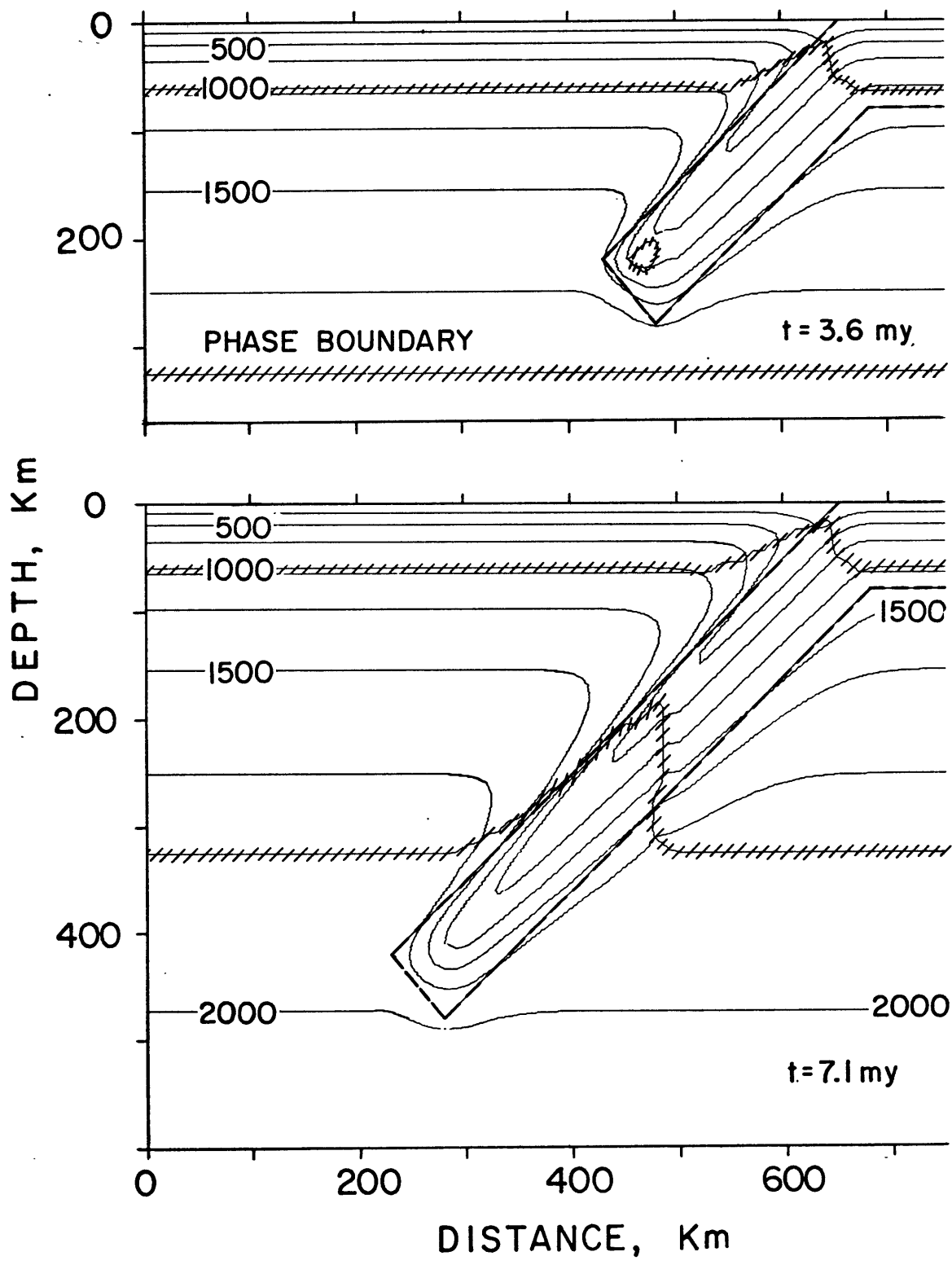
FIGURE 2.2
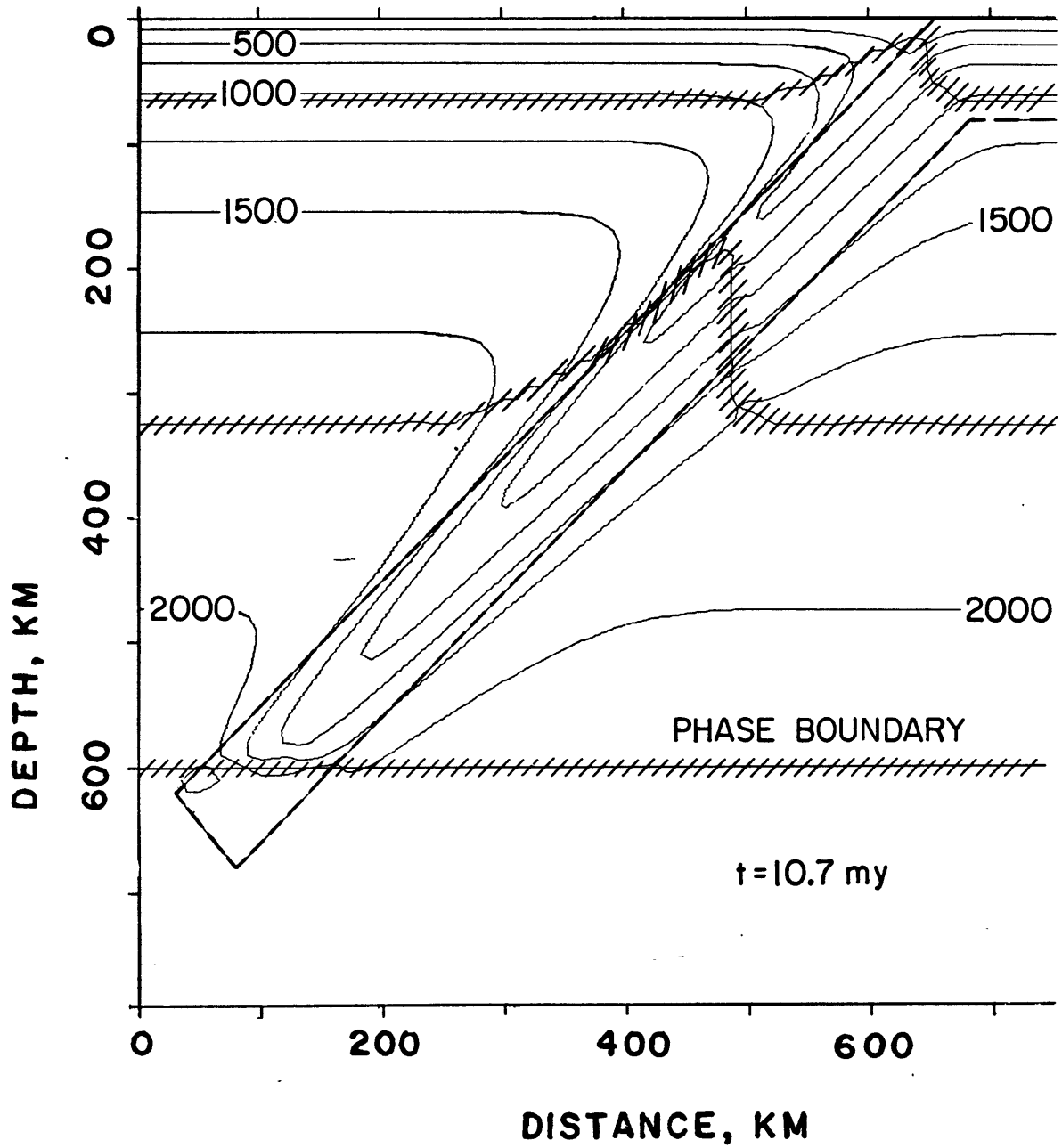
FIGURE 2.3
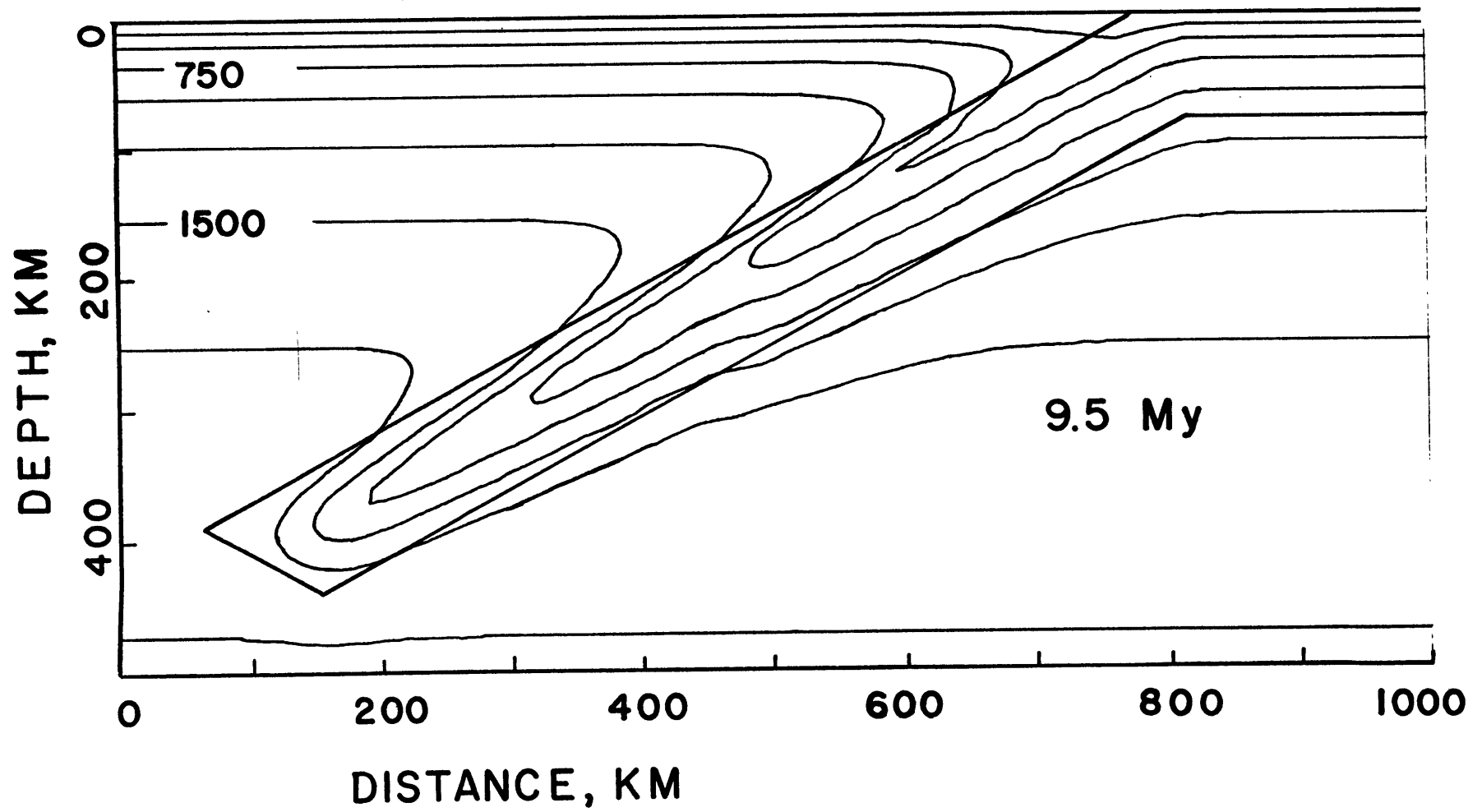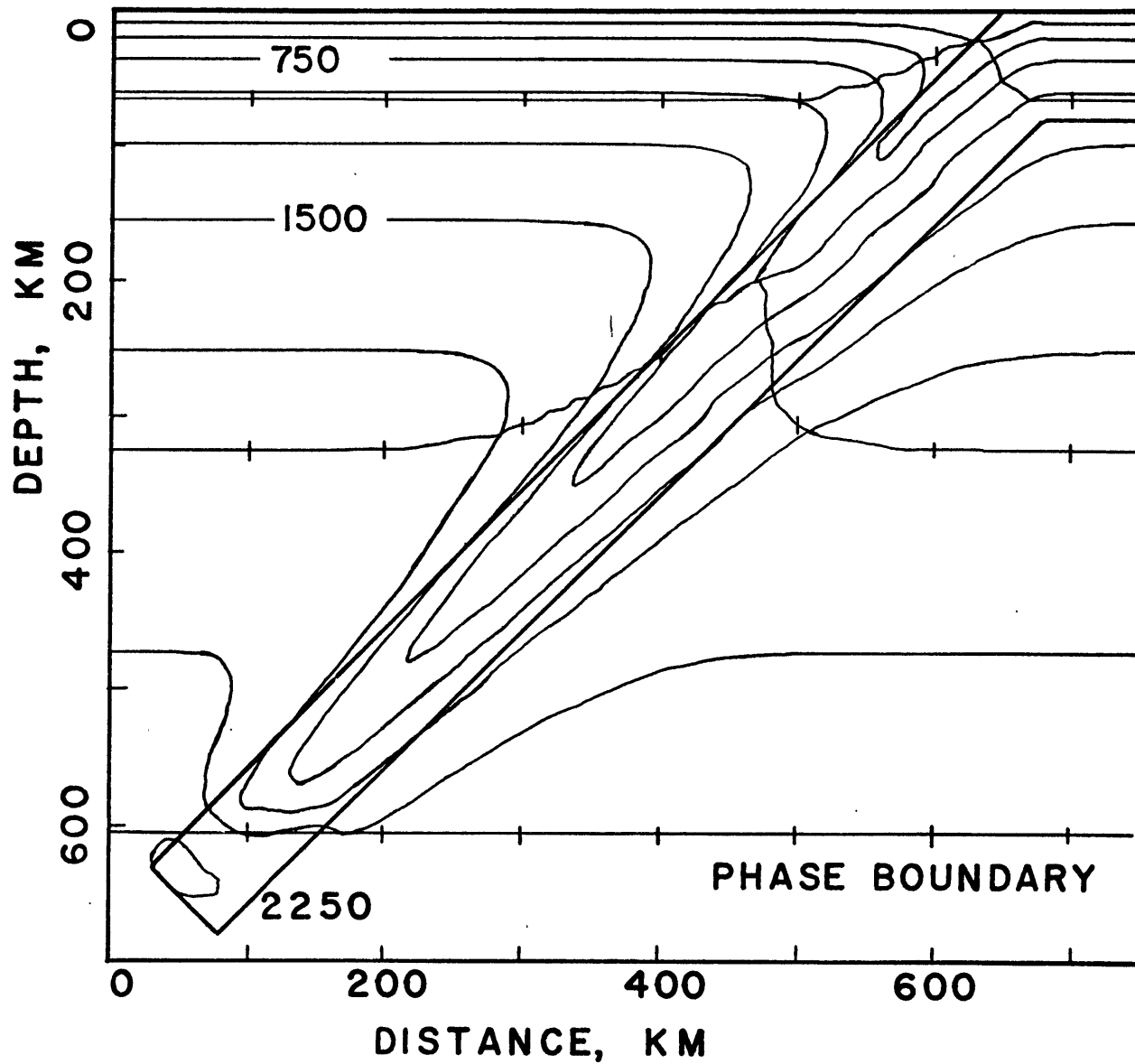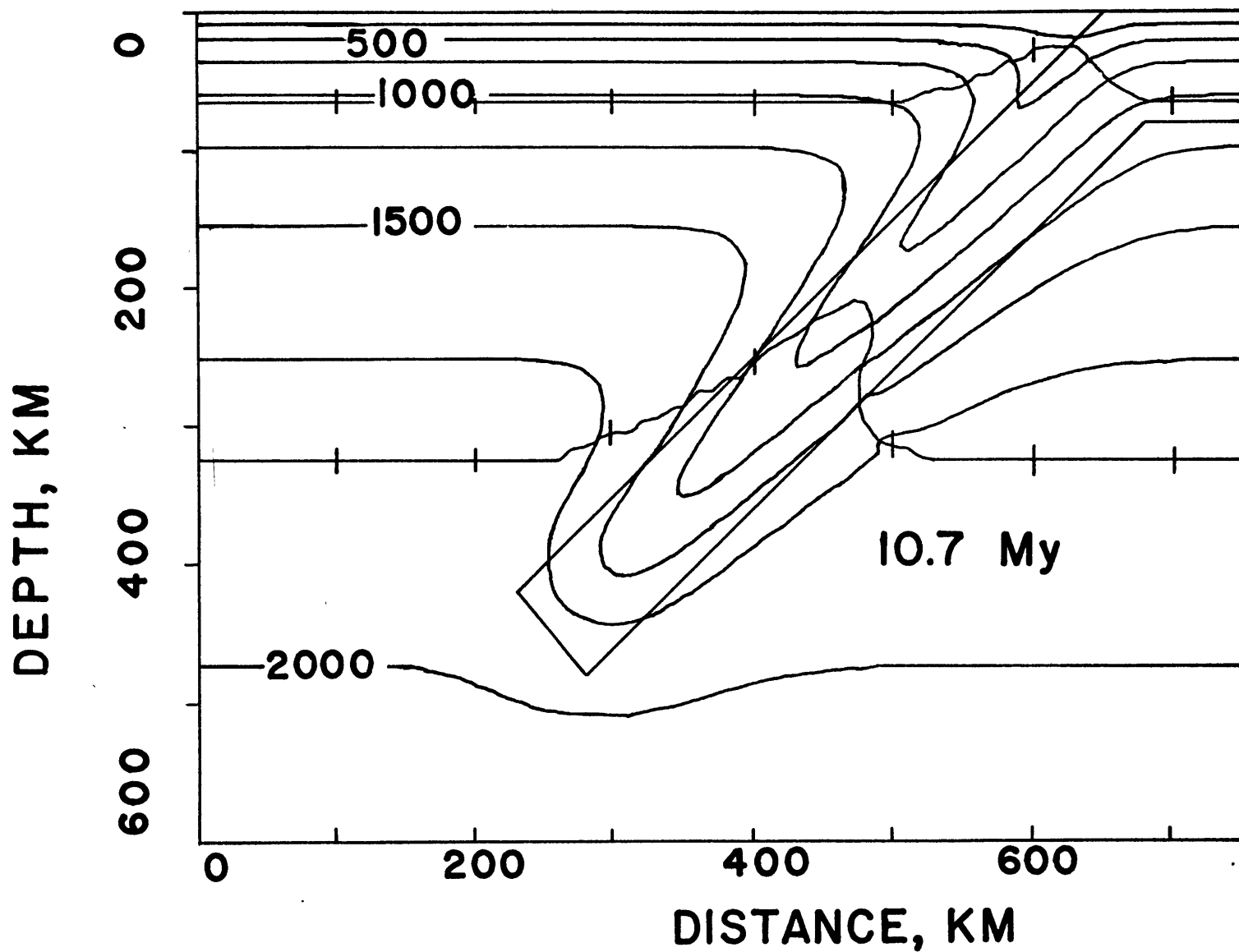
FIGURE 2.4

FIGURE 2.5
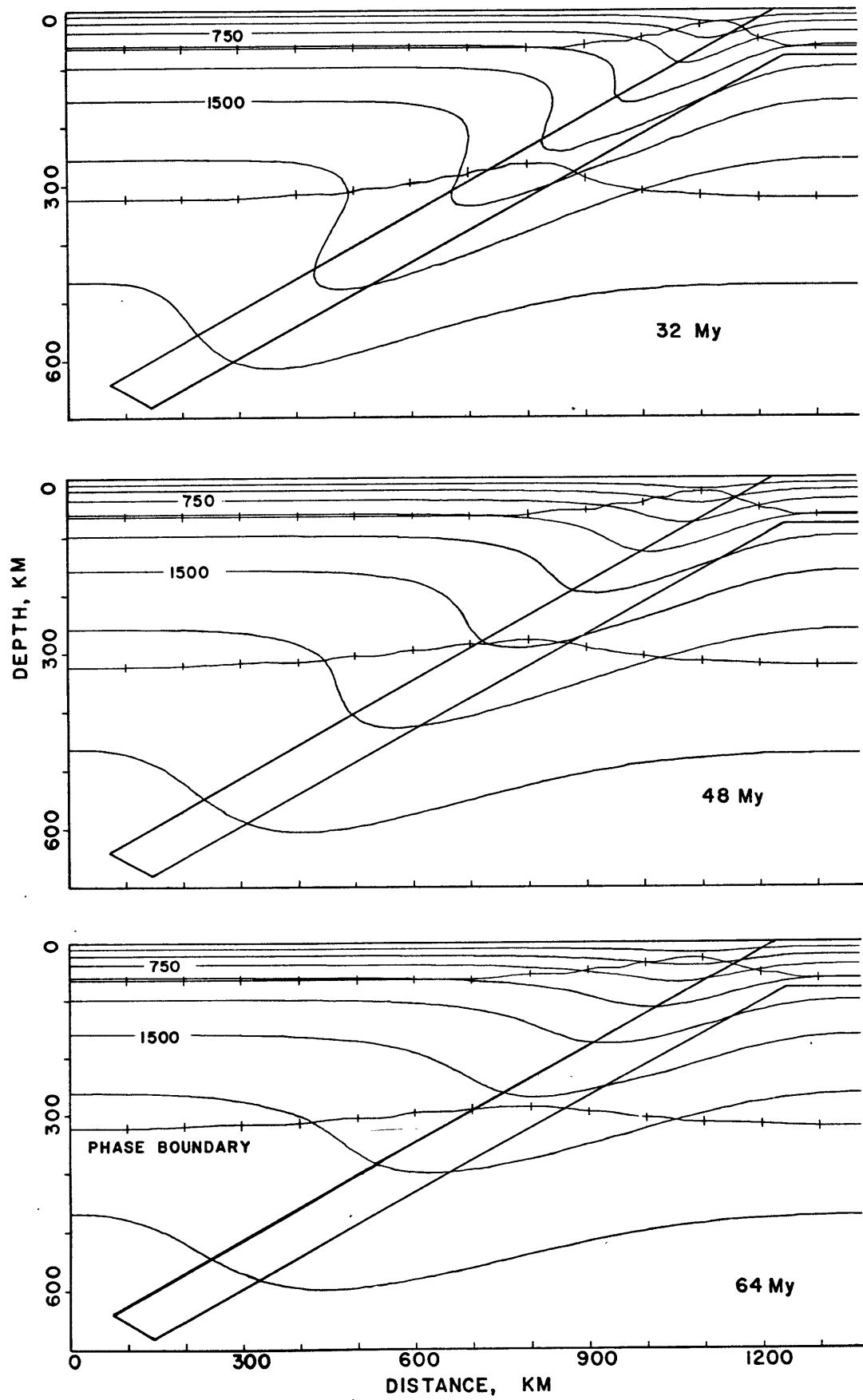
FIGURE 2.6

FIGURE 2.7

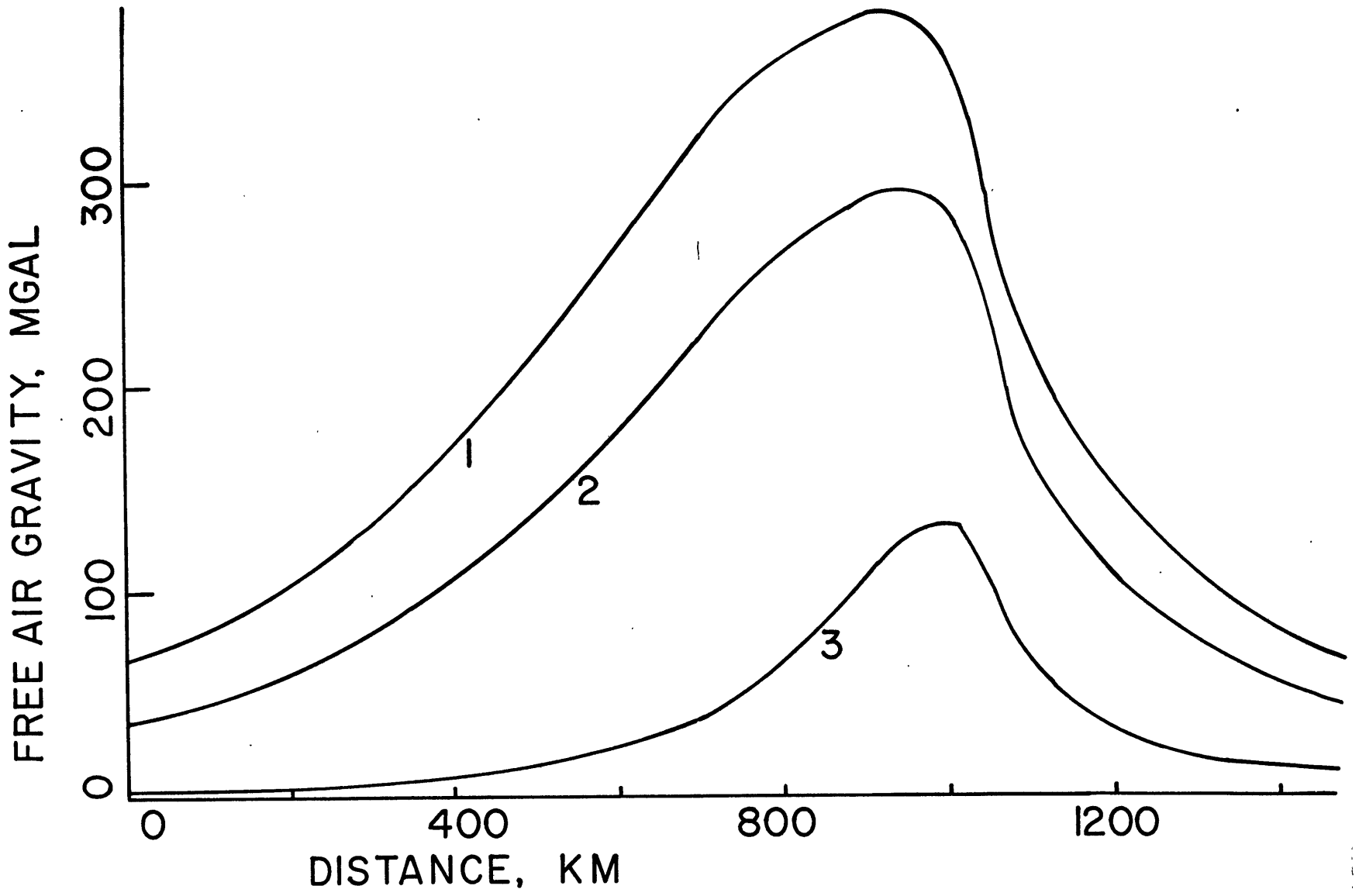FIGURE 2.8

FIGURE 2.9

FIGURE 2.10
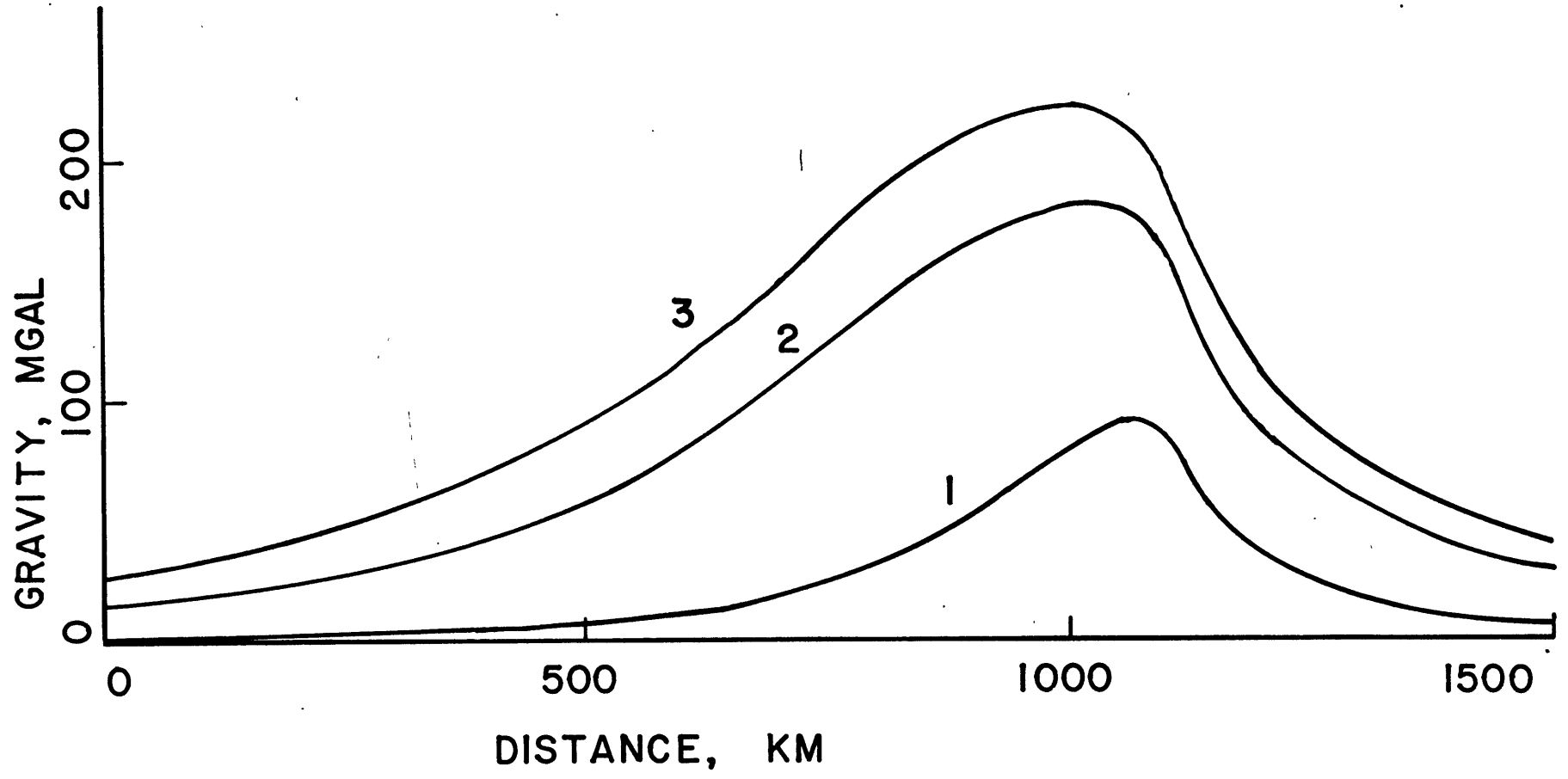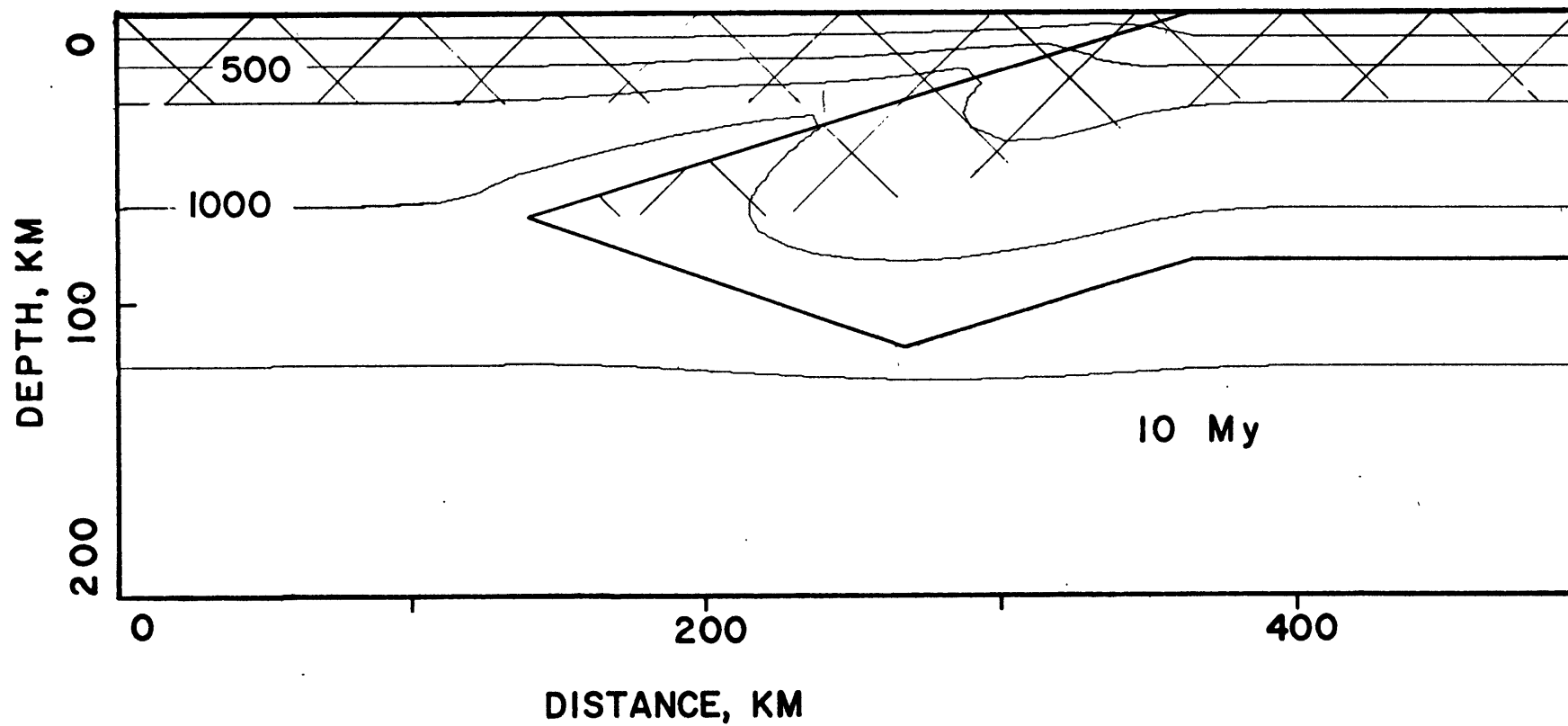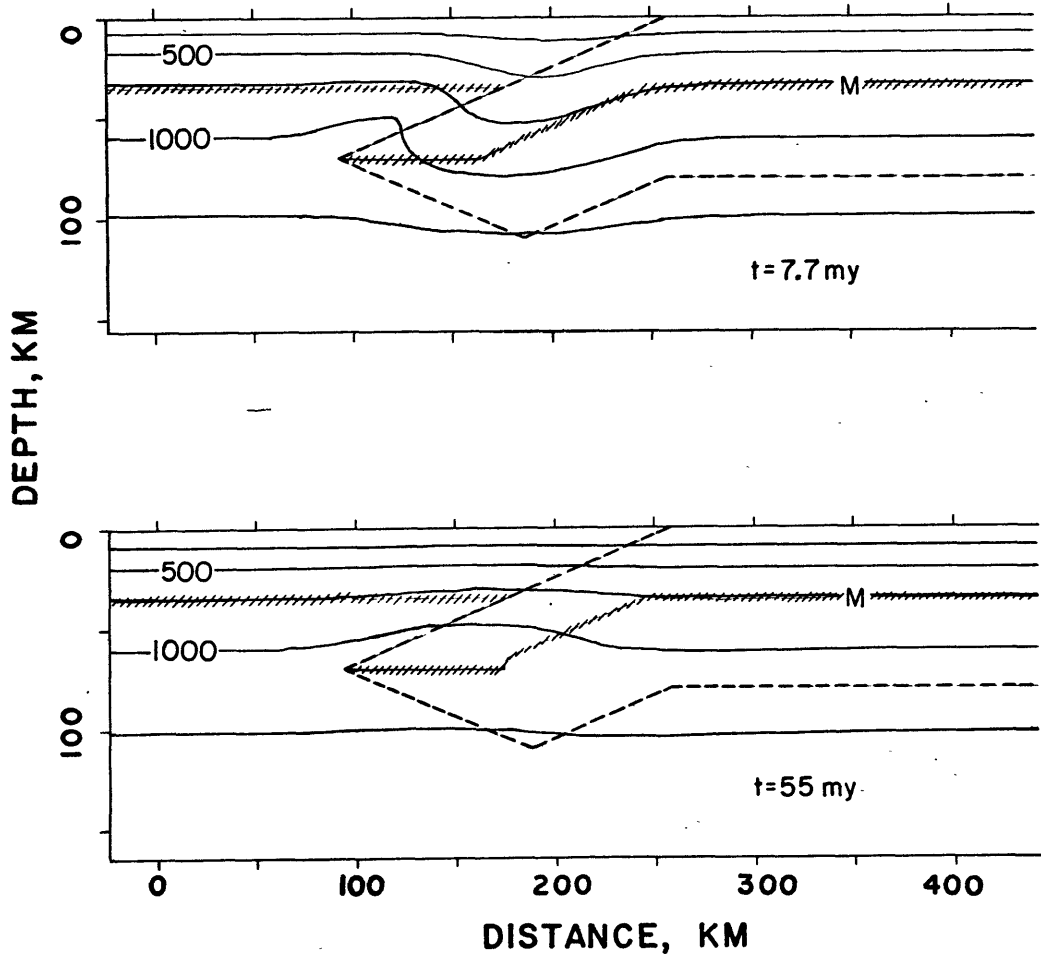
FIGURE 2.11

FIGURE 2.12

FIGURE 2.13

FIGURE 2.14

FIGURE 2.15

CHAPTER 3. SEISMIC WAVE TRANSMISSION THROUGH SLABS

Slabs of oceanic lithosphere subducted beneath island arcs at oceanic trenches are now believed to be the site of intermediate deep focus earthquakes and anomalous seismic transmission (e.g., Isacks et al., 1968; Utsu, 1971). Velocity and amplitude anomalies have been used to demonstrate the existence of the slab (Davies and McKenzie, 1969; Sorrells et al., 1971; Mitronovas and Isacks, 1971; Toksöz et al., 1971; Jacob, 1970, 1972; Abe, 1972a,b; Davies and Julian, 1972). Ray theory calculations have been made for only ad hoc, grossly simplified, or analytic models. Davies and Julian's model is probably the most realistic so far used. The purpose of this chapter is to use the thermal models of slabs calculated in the previous chapter to construct seismic models and to use ray theory to predict effects which can be compared with observations of P-waves at teleseismic distances. Local observations are too difficult to interpret since the upper mantle may vary regionally. Travel times and amplitudes of teleseismic phases other than P are too poorly known to confidently look for slab effects. Modeling of the attenuation of high frequency P and S-waves is beyond the scope of this chapter.

A numerical approach is necessary to model the transmission of P-waves through slabs, as analytic solutions cannot give sufficient resolution. A ray tracing method

(Julian, 1970) was used in preference to more complete solution. Even this simplified calculation proved so protracted that an exhaustive development of models would have been uneconomical. Although direct calculation of amplitude was not practical by the numerical method used, the amplitude could be quantitatively estimated from the spacing of emerged rays. Models were constructed mainly to test the sensitivity of travel time and amplitude to the location of a source with respect to the slab. The velocity distribution through which rays were traced was obtained from numerically calculated thermal models (Chapter 2).

3.1 Geology of source regions

The Tonga and Aleutian slabs were selected for study, since data from suitable seismic events are available and since the geometric parameters relevant for constructing a thermal model are reasonably known. An event from the Kurile area was also used for data. A short review of the geology and geometry used in constructing the thermal and velocity models is in order.

The activities of the nuclear testing range on Amchitka island (Figure 3.1) have included the passive location of earthquakes by a local network of seismometers (Engdahl, 1971). Reliable epicentral locations also exist for a region near Adak island (Murdock, 1969a,b). The seismic zone dips

about 60 degrees to the north and extends to about 200 km depth in those regions. Geological evidence indicates that the short length of the Aleutian slab is due to recently commenced subduction. The initiation of island arc volcanism in the Aleutians has been dated at 1.8 my from studies of the distribution of volcanic ash in deep-sea cores (Hays and Ninkovich, 1970). This upper Pliocene age is consistent with the geology on land (Burk, 1965). Several deep-sea sedimentary fans were beheaded from their source region when subduction began in the Pliocene (Mammerickx, 1970).

A thermal model was calculated using the subduction rate normal to the arc at Amchitka island, 4.5 cm/yr (Figure 3.2) (Morgan, 1968; LePichon, 1968). The arc in this region has a radius of curvature of 12 degrees and extends suffi- ciently far from Amchitka that no teleseismic rays would emerge from the ends of the slab.

Deep earthquakes occur down to about 650 km depth in the Tonga-Kermadec region (Sykes, 1966). As the date of initiation of subduction has not been determined from geology, the thermal model for the Tonga slab was calculated to obtain the observed length of the slab. A subduction rate of 8 cm/yr and a dip of 45 degrees were assumed in the model. The actual subduction rate decreases southward from 9 cm/yr to 5 cm/yr (Morgan, 1968; LePichon, 1968). The subduction rate of the Kurile slab is about 8 cm/yr (Morgan, 1968; LePichon, 1968). The dip and length of this slab are similar

to the Tonga slab. One thermal model (Figure 2.3) was used
to model both long slabs.

3.2 Computations of velocity models

These velocity models were constructed from numerical
thermal models calculated for parameters relevant to the
Aleutian, Tonga, and Kurile slabs using a linear relation,
including phase changes, as given by

$$v(x,z) = v_0(z)+\partial v/\partial T(T_0(z)-T(x,z))+\Sigma_m \partial v/\partial m(m_0(z)-m(x,z))$$

$$(3.1)$$

where

v = seismic velocity

T = calculated temperature

0 (subscript) = unperturbed quantity

x,z = horizontal and vertical coordinates

m = amount of phase present

Model CIT 204 (Julian and Anderson, 1968) was used as a
base from which to calculate anomalous velocities and
delays.

The low velocity zone below 80 km and the rapid velocity
gradients at 400 and 600 km are probably caused by phase
changes (e.g., Anderson and Sammis, 1970; Ringwood, 1970,
1972). The amount of seismic velocity increase and the
position of the phase change were adjusted such that the
phase diagram was consistent with the unperturbed temperature

and seismic velocity profiles (Figure 3.3). A linear slope of the 400 km phase transition curve of 9°C/km was used (Ringwood, 1970), and the width of the phase change adjusted to give self-consistency. Partial melting was assumed to cause a variation of 0.5 km/sec over a temperature range of 300°C. The solidus curve, adjusted to give self-consistency, was in reasonable agreement with high pressure experiments (Lambert and Wyllie, 1970). The 600 km phase change was not included in the calculations.

A trade off exists between the thermal coefficient of velocity ($\partial v/\partial T$) and the assumed unperturbed geotherm in the mantle. It is also not clear that the laboratory value of the parameter is relevant to the mantle. A coefficient of -0.5×10^{-3} km/sec°C has been measured in short term experiments on several possible materials (Anderson et al., 1968). However, several strongly multivariant phase transitions which cannot be calibrated directly from the dependence of seismic velocity on depth may occur in the mantle. Possible reactions include the formation of garnet, olivine, and jadeite at the expense of aluminous pyroxene, spinel, and plagioclase (Green and Ringwood, 1967b; O'Hara et al., 1971). There is insufficient experimental data to correct directly for these reactions and for partial melting in a velocity model. The gross geometry of the slab is well enough determined from the location of deep earthquakes that it is better to calibrate the coefficient of velocity with

observed travel time anomalies to a predetermined slab geometry than it is to adjust the slab shape to use a preconceived velocity coefficient.

Travel times from the LONGSHOT event and the Aleutian slab model were used to obtain the value of the thermal coefficient of seismic velocity used to calculate theoretical ray paths. The observed advance for rays down dip of the slab is slightly over 2 sec (Jacob, 1972; Abe, 1972a). This value, relatively independent of shot location, was given by a coefficient, which does not include the effect of partial melting, of -9×10^{-4} km/sec°C (Figure 3.4). In agreement with Jacob (1972) a velocity contrast of about 10% is required. The resulting velocity models are shown in Figure 3.5 and Figure 3.6.

3.3 Theoretical ray paths

Theoretical travel times and ray paths were calculated for 6 surface locations on the Aleutian velocity model, 4 surface locations on the long slab model, and 7 intermediate depth locations on the long slab model. The computed travel times and assumed take-off parameters are plotted as a function of the emergence point of the rays on Figures 3.7, 3.8, and 3.9. The models are symmetric with respect to the dip of the slab.

The Aleutian locations were spaced at 0.1 degree [11 km] intervals (Figure 3.2). The travel time anomalies were found

to be slowly varying functions of terrestrial coordinates
(Figure 3.7). The size of the travel time anomaly is
greatest for locations C and D and smaller on either side.

The shadow zones for locations A, B, and C are similar.
South of location C the size of the shadow zone decreases,
becoming insignificant at location F. Two branches of
teleseismic rays travel north from location A. At distances
less than 35° the arrival consists of a small precursor
which traversed the slab and a normal arrival which missed
the slab. For locations north of A the normal arrival
emerges at increasingly larger distances. No multiple
arrivals were found for more southerly shot locations. For
location C the amount of defocusing in the shadow reduces
amplitude by a factor of about 8. The defocusing reduces
the amplitude more at locations A and B. The effects of
defocusing are somewhat canceled by the effect of attenuation
since the defocused rays going through the slab miss the
high attenuation of the low velocity zone.

For the long slab model a pronounced shadow zone
existed for all sources (Figure 3.8). The results for
surface positions A and B are nearly identical as the shadow
zone results from rays being critically refracted off the
slab (Figure 3.6). The edge of the shadow is a complex
region of multiple arrivals. The predicted amplitudes in
the shadow were so low that rays entering some areas could
not be obtained although the take-off angle of the rays was

incremented by 0.001 degrees. The shadow zone is smaller

for surface positions C and D. The maximum travel time

anomaly for a ray running the full length of the slab from

position C is 7.8 sec early. Again it was numerically

difficult to obtain rays entering the shadow.

Amplitudes and delays for intermediate earthquake

locations A through E are not significantly different,

since the shadow zone is caused by critical refraction

(Figure 3.9). The maximum time anomalies are about 6 sec

early. The size of the shadow zone decreases for loca-

tions near the base of the slab. At position G the shadow

zone does not extend out to the core shadow and the delays

are somewhat smaller. The amplitudes in the shadow zone

are reduced to one one-hundredth of normal. The edge of

the shadow zone is again a region of complex multiple

arrivals.

3.4 Travel time anomalies

Although the arrival time of P-waves can often be

measured to 0.1 sec, care is required to resolve anomalous

effects due to slabs, since errors on the order of a second

may exist in published travel time tables and station

corrections. If earthquakes rather than controlled explo-

sions are used as sources, lack of knowledge of the origin

time and location of the event further complicates the

analysis. Discussion is confined to travel time anomalies

which vary as a function of station location. World-wide

constant advances and delays are difficult to interpret and

mostly unresolvable from systematic errors in the tables.

Three nuclear explosions, LONGSHOT, MILROW, and CANNIKIN

were used as sources for the Aleutian region (Figure 3.1).

LONGSHOT data is primarily considered, as the explosions

were in close proximity and as the LONGSHOT data was more

carefully analyzed (Lambert et al., 1970). A check of the

PDE reports showed no systematic differences among the

travel times from these events. It was necessary to station

correct the LONGSHOT data since the station effects were

of the same order as the source effects and correlated with

broad geographic regions (Jacob, 1972). After station

corrections were made, there was so much scatter that it was

necessary to average the data from geographical areas

(Jacob, 1972; Abe, 1972a). Averaging over 10 x 10 degree

quadrangles in a polar epicentral project left over a

second of scatter in the travel time residuals (Jacob, 1972).

The station corrected data averaged over all tele-

seismic distances and 15 degree intervals of azimuth (Abe,

1972a) were used as data with which to test the theoretical

model (Figure 3.10). A good fit resulted. The location of

LONGSHOT with respect to the slab cannot be accurately

constrained from the travel time data since the data were

insufficient to resolve the anomaly as a function of

epicentral distance and since theoretical travel time

anomalies were insensitive to shot point location.

Abe (1972a) noted that arrivals were later at stations between 10 and 30 degrees azimuth than at adjacent azimuth intervals and postulated a gap in the slab. Errors in either the travel time table or the station corrections are alternative explanations, however, since only 4 different stations were involved.

No controlled events are located suitably with respect to long slabs such as Tonga. Travel time residuals were calculated relative to locations obtained from a network of local stations for numerous earthquakes near Tonga (Mitronovas and Isacks, 1971). After spatially averaging these residuals for teleseismic stations, the effect of the slab is clearly evident (Figure 3.11). The theoretical travel time anomaly fits the observed data reasonably well. Although the data were insufficient to give a clear-cut relationship between epicentral distance and delay, the largest advances were observed around $\Delta = 60°$ in agreement with the theoretical model. Again, little resolution could be obtained on the spatial relationship between the slab and the earthquakes.

3.5 Amplitude anomalies

The amplitudes of 3 nuclear explosions and 15 shallow and intermediate focus earthquakes were measured to obtain improved information on the location and structure of the slab (Table 3.1). Amplitudes observed only on World Wide

Standard Seismographs (WWSS) were used in this study to avoid error due to faulty correction for instrument response. Thirty-five millimeter films were generally used; comparison with full scale reproductions, where available, showed that the films were adequate for the purpose of this chapter. High quality copies of the LONGSHOT event were used (Lambert et al., 1970).

The normal definition of magnitude is unsuitable, since different parts of the coda may be measured at different stations. It was most convenient to measure the amplitude of the first peak-to-peak motion. Following Cleary (1967) and Nuttli (1972) the frequency of the first arrival was assumed to be constant at all stations. This made it unnecessary to know the period of the arrival at each station, which would be nearly undeterminable on the short period record. No variation of frequency between stations was evident for any of the events studied.

In order to look for amplitude anomalies, it is necessary to have a wide distribution of stations. All stations were used where it was possible to find the first arrival. Rejection of weak arrivals would have biased the results against finding any shadow zones.

In order to interpret amplitude data, it is necessary to correct for variations in amplitude as the result of heterogeneities in the radiation pattern at the source and as a result of systematic variations with epicentral distance. Unlike travel time corrections, the uncertainty in amplitude

corrections is the same order as the amplitude itself.

The amplitudes of earthquakes were corrected for source mechanism (to the value at the axis of maximum compression) using double couple solutions (Stauder, 1968; Isacks et al., 1969; Isacks and Molnar, 1971).

$$F(x,y) = |Sin(2\theta) Cos(\phi)| \qquad (3.2a)$$

$$A_f(x,y) = A(x,y)/F(x,y) \qquad (3.2b)$$

where

F = focal plane correction

x = location of station

y = location of earthquake

ϕ = co-latitude of ray on focal sphere measured about null axis

θ = longitude of ray on focal sphere measured about null axis and from the nodal plane

A_f = source corrected amplitude

A = measured amplitude

Source corrections were restricted to a maximum value of a factor of 10 since it was felt that the nodal planes were not accurate to more than 3 degrees. Poor location of a nodal plane that does not emerge at teleseismic distances does not effect the results significantly, since the source correction is large only if a station is near a nodal plane and only a weak function of the location of the more distant nodal plane. Errors in the location of the earthquake only weakly effect the position of a station on the focal

sphere, since all earthquakes studied were in the upper

mantle where the angle of emergence is a slowly varying

function of depth and distance for teleseismic rays. If

the slab should strongly refract a ray emerging near a

nodal plane, the angle of emergence given in the table might

give a spurious value of source correction. No source

correction is necessary for nuclear explosions.

The source corrected amplitudes must also be corrected

for epicentral distance

$$A_\Delta(x,y) = A_f(x,y)/G(\Delta) \qquad (3.3)$$

where

A_Δ = distance and source corrected amplitude

Δ = epicentral distance

G = distance correction.

Although the amplitude-distance relationship is poorly

known for P-waves, the choice of this function is not

critical if a good distribution of stations can be obtained.

The amplitude-distance curves were used to divide the

observed data for each event into interval classes differing

by factors of two. A simple continuous curve consisting of

four line segments was used in this chapter to correct

short period amplitudes for epicentral distance (Figure 3.12).

Previously published amplitude curves are neither simple nor

in agreement with each other nor with the Gutenberg and

Richter (1956) curve. Curves derived from nuclear explosion

data (Carpenter et al., 1967; Kaila, 1970) are biased since

most of the arrivals at some distances are in the shadow

zone of LONGSHOT, and are discontinuous. The various curves

differ most strongly between 30 and 40 degrees. Errors

of a factor of two could easily be introduced by faulty

correction of amplitude for epicentral distance. A

systematic biasing is much less likely.

An amplitude distance curve measured at a period of

about 2.5 sec on the long period WWSS (Nuttli, 1972) was

used to correct the long period results for distance. This

curve is more accurate than the short period curve as the

scatter due to local station effects is much larger at

short periods.

A combined station and distance correction can be

obtained if an event whose rays, uneffected by the slab,

is located suitably close to the event being studied. The

station corrected amplitudes of the slab event (A_s) can

be obtained by

$$A_s(x,y_1) = A_\Delta(x,y_1)/A_\Delta(x,y_2) \tag{3.4}$$

where

y_1 = event studied

y_2 = reference event.

This formula is independent of $G(\Delta)$ to the first order

since the epicentral distance corrections of y_1 and y_2 are

similar and cancel out on the right hand side of equation

(3.4). These station corrections should not be interpreted

as being invariant properties of the local geology of the
stations, since they include the amplitude distance curve
and are determined for only one event.

3.5.1 Aleutian amplitude results

The amplitudes of 3 nuclear explosions and 6 earth-
quakes around Amchitka island were measured. The nuclear
explosions and two normal faulting earthquakes in the
Aleutian trench generated the best data.

Short period amplitudes measured for LONGSHOT and
MILROW are plotted in Figure 3.13. Arrivals from CANNIKIN
were generally off-scale on short period records, except
at stations in the shadow zone or those with unusually
small magnification. Long period amplitudes for MILROW
and CANNIKIN are plotted in Figures 3.14, 3.15, and 3.16.
Although there is considerable scatter in the data, it is
evident that the shadow zone extends from about 310° to
50° azimuth for distances between 70° and the core shadow.
The shadow zone observed for LONGSHOT with Canadian stations
extends to 70° azimuth at distances between 30° and 40°
(Davies and Julian, 1972). The shadow zones for MILROW
and CANNIKIN are similar at long periods and slightly larger
than the short period shadow for LONGSHOT. The difference
between LONGSHOT and MILROW may not be real since the best
data for each event were measured on instruments with
different frequency response (SPZ for LONGSHOT, LPZ for
MILROW).

The amplitudes of two normal faulting earthquakes in the trench near Amchitka were measured to obtain station corrections for LONGSHOT and MILROW. These earthquakes occurred seaward enough that teleseismic rays would not be effected by the slab. The path through the deep mantle and up to the station for rays emerging from LONGSHOT is nearly identical to this portion of the path from the earthquakes. The data for the June 2, 1966 earthquakes were of superior quality since the nodal planes emerge away from teleseismic stations. There were no interfering events. No shadow zone was observed at either long or short period for either event (Figures 3.17 and 3.18).

Long and short period amplitudes of four underthrusting earthquakes belonging to the Rat island sequence of Feb. 1965 were measured from WWSSN records. The long period record from three other earthquakes proved too difficult to untangle. Contamination of the measured amplitudes with pP could have occurred on the noisier long period records. It was difficult to consistently pick the first motion on the short period records since the amplitude did not usually peak by the third half cycle. The first arrival was frequently missed at stations near the nodal plane. These stations showed considerable scatter with the high-noise, low-magnification stations giving higher measured amplitudes. It is possible that some of the earthquakes were true multiple events. The number of reliable measurements of rays

which probably missed the slab is limited, since one of the nodal planes generally emerged near the western United States and Australia.

The data for these earthquakes, plotted in Appendix B, precludes the possibility of a large shadow zone with an average reduction factor greater than 10 at short periods, but the scatter is sufficiently large that a shadow zone comparable to the LONGSHOT shadow would not be detectable. No attempt was made to use station corrections. No long period shadow was evident for any of the events.

The observed short period amplitudes for LONGSHOT and MILROW were station corrected using the June 2, 1966 event (Figure 3.13). An insufficient number of station corrected amplitudes were obtained for MILROW. The amplitudes after station correction in the shadow zone between -50° and 50° azimuth are about a factor of 2.5 below the other amplitudes (geometric average). The scatter in the data is greatly reduced by the station correction and there is little overlap between shadow zone and non-shadow zone amplitudes. Note that the stations at northern azimuths and small epicentral distances have low station corrected amplitudes. The slab location preferred in this paper places this region in the shadow zone.

The amplitude data for LONGSHOT are sufficient to locate the shot between locations C and D (Figure 3.2). Considerable scatter in the edge of the shadow is expected

to result from crustal structure and minor irregularities
in the slab. This location of LONGSHOT with respect to
the slab is significantly south of the position suggested
by Davies and Julian (1972) and not grossly different from
the position proposed by Jacob (1972). The position
suggested herein can be shown to be more likely by considering
multiple arrivals which were observed at teleseismic distances.
A normal ray which misses the slab may be preceded by a low
amplitude precursor which travelled the length of the slab.
Rays which miss the top of the slab will appear at small
distances and northern azimuths. Rays which miss the
bottom of the slab will emerge south of the shadow zone out
to large azimuths. Unless the slab is extremely thin, both
types of multiple arrival cannot occur for one shot. For
LONGSHOT, multiple arrivals were observed south of the
shadow zone at large azimuths at western Canadian stations
(Davies and Julian, 1972). A multiple arrival north of
LONGSHOT at Point Barrow, Alaska, may be a refraction off
the 600 km discontinuity (Jacob, 1972).

The slab location deduced from LONGSHOT is such that
intermediate depth earthquake epicenters fall in the coldest
region of the slab model (Figure 3.19). This is expected
since intermediate earthquake mechanisms can be attributed
to tension (or compression in other regions) along the dip
of the slab (Isacks et al., 1969; Isacks and Molnar, 1971;
Smith and Toksöz, 1972) but not to shearing on the boundary

of the slab. For mechanical reasons brittle fracture should
occur in the coldest part of the slab (McKenzie, 1969).

3.5.2 Long slab amplitude results

Long and short period amplitudes were measured for
six intermediate focus earthquakes in the Tonga-Kermadec
region (Figures 3.20 and 3.21). The use of intermediate
depth earthquakes eliminates problems resulting from
contamination with pP and from attenuation of normal rays
in the low velocity zone. The measured amplitudes were
corrected for source mechanism using earthquake solutions
by Isacks et al. (1969) and Isacks and Molnar (1971). A
nodal plane often emerged moderately near the western
United States. The results of the measurements are plotted
in Figures 3.22 thorugh 3.27.

Low short period amplitudes were observed only within
45 degrees to the west of the epicenters. Although this
is the location of the predicted shadow zone, it is possible
that errors in the distance correction effected the results.
Short period amplitudes at stations beyond 50 degrees from
the source were independent of azimuth for all the earth-
quakes studied. Distance and source corrected long period
amplitudes were independent of azimuth for all the earth-
quakes in the Tongan region. Slight variations in the long
period amplitudes are probably due to measurement errors
and errors in the distance and source corrections and to
station differences.

Reasonable quality amplitude data were obtained from
one intermediate event near the center of the Kurile arc
(Figure 3.28). Although there is some scatter in the data,
an average of a factor of 2 reduction in short period ampli-
tude in the predicted shadow zone between 255 and 15 degrees
azimuth is observed (3.29). The data reduction was fairly
insensitive to errors in the amplitude distance curve since
the stations in and out of the predicted shadow zone are
distributed over a similar range of distances. The source
corrections for data in both regions are similar. There
were no suitable events to use for making station corrections
for the Tonga and Kurile earthquakes. An attempt to use a
nearby earthquake, which occurred 80 km deep beneath the
Kurile trench, for station corrections failed since few
reliable amplitudes could be obtained. The nodal planes
for this event passed near many stations. Away from the
nodal plane it was difficult to pick the first arrival.
The error in the location of this earthquake may be abnormally
large since many stations picked later parts of the coda
as the first arrival. The long period signal from this
event was often too small to measure reliably.

Low amplitude precursors occurring 1 to 3 sec before
the main arrival were observed in the predicted shadow zone
for the earthquake of 21 July 1964 near Tonga. The
amplitude of these precursors was small enough that they
would have been missed on noisy records. Tracings of

relevant seismograms are plotted in Figure 3.30. Possible precursors were observed for some of the other events but the shape of the wave form away from the shadow zone was such that these arrivals could not be confidently identified as precursors. Some of the scatter in the amplitudes measured inside of 45 degrees from the source may be due to inconsistent picking of the main arrival or the precursor.

The small precursors to the 21 July 1964 arrival were considered to be strongly defocused waves which ran the full length of the slab rather than evidence of a foreshock, since the time delay between the precursor and the main arrival was variable, since the amplitude ratio of the main signal was variable, and since no precursors were observed outside the predicted shadow zone. The multiple P-wave arrival corresponds to no known seismic phase (Jeffries and Bullen, 1958; Herrin, 1968). It is very unlikely that local station effects would cause precursors only at stations in the predicted shadow zone. Although it was not possible to compute the spectra, it is evident from the records that the frequency content of the precursor and main arrival is similar. There is some interference between the two arrivals at CTA and PMG.

The observed precursors can be easily explained as defocused waves which have run the full length of the slab. The more difficult problem is explaining why the amplitudes in the shadow zone for the Tonga and Kurile slabs are not

smaller than for the shadow zone for the much shorter

Aleutian slab. Although the data is better for the Aleutians,

the Tonga and Kurile data can support, at most, amplitude

reduction of a factor two for epicentral distances greater

than 45 degrees and a factor of eight between 30 and 40

degrees. These amplitudes observed in the shadow zone were

much larger than the amplitudes predicted from the ray

theory. This is unlikely to be the result of too high a

theoretical slab velocity, since the velocity model was

calibrated to give observed travel time anomalies. Possible

explanations for the larger observed than predicted amplitudes

include: diffraction, gaps in the slab, large fault length,

occurrence of the earthquake near the base of the slab, and

guided or converted phases. The implications of these

possibilities are discussed below.

The long period observations can be explained by

diffraction (Ward, 1971; Davies and Julian, 1972) since the

wavelengths were comparable to the width of the slab. The

source determinations used in this paper are unlikely to be

in error due to refraction, since long period data were used

in the determination. Simple diffraction, however, cannot

explain the short period results, since normal or slightly

reduced amplitudes were observed for rays which would emerge

over 10 degrees into the shadow zone. An analytical solution

for wave propagation in a one-dimensional slab indicates

that ray theory will work with respect to diffraction for the

1 to 3 second waves measured in this paper (Ward, 1971).

Irregularities, tortuosities, or gaps in the slab may cause the shadow zone to be absent. A local dip of 30 degrees in the slab is sufficient to let normal rays emerge at distances beyond 60 degrees. The Tonga slab when viewed in detail varies significantly from the average dip of 45 degrees, being overhanging in some places and nearly flat in others. Significant advances relative to normal mantle velocity could still be expected for rays which escape from the slab since rays emerging from an earthquake near the center of the slab remain in the slab for a considerable distance. For a slab dipping 45 degrees, large variations from the average dip would be necessary to let rays emerging at epicentral distances between 30 and 45 degrees escape, since these rays take off at close to the dip of the slab. These rays could escape at locally vertical sections on the top of the slab as well as locally flat sections on the bottom.

Large true gaps in the slab are unlikely since high frequency waves efficiently propagate to the surface from deep earthquakes (Barazangi et al., 1972). Small gaps in the slab such as suggested by Abe (1972a) for the Aleutian slab might be sufficient to let normal amplitude rays escape without effecting high frequency transmission.

The fault length of intermediate focus earthquakes in the magnitude range used in this study is probably

insufficient to account for the arrivals in the shadow zone.
Although the fault for the largest earthquakes extends
through the slab (Kanamori, 1971b; Fukao, 1972), the fault
length of moderate size intermediate earthquakes has been
determined to be 10 to 20 km by seismic moment studies
(Wyss and Molnar, 1972; Brune, 1970). Unless the rupture
started in the lower part of the slab, the shadow zone
for P-waves would still exist.

Intermediate focus earthquakes are not likely to occur
in the high temperature region at the base of the slab,
where no shadow zone would be present, since the stress
drop for intermediate focus earthquakes is high (Wyss and
Molnar, 1972) and since fracture would begin in the coldest
and strongest area. The seismic plane in Tonga is as narrow
as can be resolved by epicenter location, about 25 km
(Sykes, 1966). If intermediate depth earthquakes occurred
in the high temperature region beneath the slab, a greater
spatial scatter would be expected since mechanical con-
ditions in that region vary slowly with position.

The normal amplitude arrivals in the predicted shadow
zone could be a phase not predicted by the simple ray theory
calculation. The converted or guided phase must satisfy
several restrictions. This phase must arrive within 1 to
3 seconds of a low amplitude precursor, the wave must have
the correct polarity, and the arrival must have normal
amplitude. Conversion of S to P-waves on the bottom of the

slab is unlikely since this wave would arrive too late unless the earthquake was near the bottom of the slab anyway. Reflections off the top of the slab are refracted with the same shadow zone as a source in that region. However, rays might be trapped in the slab by reflection off its boundaries at a low angle. A more sophisticated calculation would be required to evaluate the amplitude of any reflected or guided wave having the correct arrival time. The quality of the data presently available precludes any appraisal which requires detailed knowledge of the spectral characteristics of the signal.

3.6 Conclusions

Velocity models for downgoing slabs were constructed from theoretical temperature profiles and calibrated by considering travel time anomalies for nuclear tests on Amchitka island and intermediate focus earthquakes in Tonga. The LONGSHOT event was located with respect to the slab by using variations in P-wave amplitude observed at teleseismic distances. The locations of intermediate focus earthquakes correspond with the coldest region of the theoretical slab model. Normal faulting earthquakes in the Aleutian trench were used to obtain station corrections. It was determined that the shadow zone extends northward into Greenland and Northern Canada. The observed shadow for

LONGSHOT is definitely not a network bias.

Although some low amplitude precursors were observed for Tonga earthquakes, the amount of amplitude reduction in the part of the predicted shadow zone beyond 45 degrees epicentral distance, was less than a factor of 2 for short period measurements of intermediate Tonga and Kurile events. The short period amplitude may be more reduced at epicentral distances between 30 and 45 degrees. Any long period shadow zone could be at most a reduction of a factor of 2. The precursors can be explained as defocused waves which have run the full length of the slab, and the lack of reduction at long periods can be attributed to diffraction. The explanation, however, for the observed lack of reduction in amplitude in the predicted shadow zone is not clear-cut; possible hypotheses include irregularities in the slab, earthquakes at the base of the slab, and guided or converted seismic phases.

The data used in this chapter were the highest quality data available which had good spatial distribution. An improvement in the quality of travel time data would increase its utility as the resolution was lost by the need to spatially average. This improvement is unlikely in the near future since a major difficulty is systematic errors rather than poor measurements. The amplitude interpretations would be greatly improved by digital records with good spatial distribution, by the wide-spread installation of

arrays which could detect low amplitude precursors, and by improved knowledge of distance and station corrections. Until these improvements are made, additional knowledge of seismic transmission through slabs is most likely to come from the study of phases other than teleseismic P-waves.

TABLE 3.1: The source parameters of earthquakes for which

the amplitudes were measured. The number refers

to the source of the focal plane correction

(S, Stauder, 1968; ISO, Isacks et al., 1969;

IM, Isacks and Molnar, 1971). Quality refers

to the difficulty of recognizing the first

arrival (1, no difficulty at most stations;

2, serious difficulty at many stations; 3,

records too difficult to untangle).

Table 3.1

No.	Month	Day	Year	Hour	Min	Sec	Lat	Long	Depth	Mag	Qual
						Aleutian Earthquakes					
S1	02	04	1965	05	01	28	51.3N	178.6E	40	6.0	3
S2	02	04	1965	12	06	04	52.6N	172.1E	25	5.8	3
S3	02	04	1965	14	18	28	53.0N	171.0E	30	5.7	3
S4	02	05	1965	09	32	09	52.3N	174.3E	41	5.9	2
S5	02	05	1965	20	47	13	51.9N	174.6E	35	5.7	2
S6	02	06	1965	04	02	53	52.1N	175.7E	35	5.9	2
S7	02	07	1965	02	17	09	51.4N	173.4E	40	6.0	1
S8	02	07	1965	09	25	51	51.4N	179.1E	30	5.3	2
S14	06	02	1966	03	27	53	51.1N	176.0E	41	6.0	1
						Tonga-Kermadec Earthquakes					
ISO 18	03	18	1965	06	22	10	19.9S	175.9W	219	5.5	1
ISO 19	08	10	1966	05	01	10	20.2S	175.3W	95	5.6	1
ISO 20	08	20	1965	21	21	50	22.9S	176.1W	79	6.1	1
ISO 21	07	21	1964	03	48	57	26.0S	177.9W	200	5.8	1
ISO 23	08	05	1964	11	06	01	32.2S	179.8E	216	5.8	1
IM 56	08	12	1967	09	39	43	24.7S	177.5W	134	5.8	1
						Kurile Earthquakes					
IM 118	08	04	1964	17	24	28	46.6N	151.4E	86	5.9	1
IM 122	04	05	1965	13	52	12	44.5N	150.9E	76	5.7	3

FIGURE CAPTIONS

Figure 3.1   Index map of southern Amchitka island showing

the locations of LONGSHOT (L), MILROW (M), and

CANNIKIN (C). The relation of Amchitka to

neighboring islands is shown in the inset. The

islands immediately north of Amchitka are

volcanic, while Amchitka is part of the frontal

arc.

Figure 3.2   Theoretical temperature contours at 250°C

interval were calculated for a slab dipping at

57 degrees. The subduction rate is 4.5 cm/yr.

Ray theory travel times and amplitudes were

calculated for surface explosions at locations

A through F. Point C is 12 degrees from the

center of curvature of the arc.

Figure 3.3   The CIT-204 velocity profile was used for

unperturbed regions of the mantle. The straight

lines were used to determine the change of

seismic velocity with respect to phase changes

in a way consistent with the unperturbed velo-

city model.

Figure 3.4   Calculated delays for rays going parallel to

the dip of the slab were calculated for various

velocity coefficients and shot locations. The

number indicates for velocity coefficient in

10^{-4} km/sec-°C; the letter indicates the shot
site in Figure 3.2. A coefficient of 9×10^{-4}
km/sec-°C was needed to fit observed delays.

Figure 3.5   Theoretical velocities determined from the
temperature profile in Figure 3.2 are contoured
at 0.25 km/sec intervals. The velocities out-
side of a cone about 38 degrees wide from the
shot site are of no significance to this paper
since only teleseismic data was used in this
paper. No attempt was made to include a
detailed crustal model of Amchitka island.

Figure 3.6   Calculated ray paths for a model of the Tonga
slab are plotted above the theoretical velocity
used to model that region. Letters indicate
source locations. Rays were stopped near their
source and darkened for clarity. The rays are
refracted away from the slab creating a shadow
zone. The contour interval for velocity is 0.25
km/sec.

Figure 3.7   Calculated travel time residuals (advances
positive) are plotted on the left of an equi-
distant azimuthal projection about the shot
point. Calculated initial ray parameters for
rays emerging on the projection are plotted on
the right. Initial take off angles in degrees

are contoured at 3 degree intervals, with 1
degree intervals indicated by thin lines and
0.5 degree intervals by dashed lines. Initial
take off azimuths are contoured at 40 degree
intervals by dashed lines. The stippling
indicates the area of significantly reduced
amplitudes. The letters refer to shot locations
in Figure 3.2. The northward limit of normal
rays which miss the top of the slab at location
A is indicated by the dashed line L.

Figure 3.8   The results for ray tracing from surface
sources above the Tonga slab are plotted as in
Figure 3.7. Rays running the full length of the
slab were difficult to obtain for numerical
reasons. Later multiple arrivals at the edge of
the shadow zone are not plotted. Letters refer
to surface locations in Figure 3.6.

Figure 3.9   The results of ray tracing from 200 km deep
sources, indicated by letters in Figure 3.6, are
plotted as in Figure 3.7.

Figure 3.10 Calculated delays at site C (Figure 3.2) are
compared with observed station corrected delays
averaged over interval of azimuth and over
delta (Abe, 1972a). The fit is obtained by
assuming the strike of the arc is N82W.

Figure 3.11   The theoretical delays for intermediate
earthquake location C (Figure 3.6) at a
distance of 60 degrees are compared with
averaged observed delays computed with respect
to locations computed from local stations
(Mitronovas and Isacks, 1971).

Figure 3.12   Amplitude distance relations of various
authors show little similarity. Curve 1
(Gutenburg and Richter, 1956), curve 2
(Kaila, 1970), and curve 3 (Carpenter, et al.,
1967) were not used in this paper. Curve 4
is this smoothed curve assumed in this paper
for short period waves. Curve 5 (Nuttli, 1972)
was used for long period data.

Figure 3.13   Observed short period amplitudes for the
LONGSHOT (above) and MILROW (below) events are
plotted on equi-distance azimuthal projections
about the shot points. The amplitudes given
on a $\log_2$ scale are given in Appendix B. The
raw amplitudes for both events (right) are
generally low between about 310 and 50 degrees
azimuth. The station corrected amplitudes on
the left show that the shadow zone is real.

Figure 3.14   Long period amplitudes for the MILROW event
(Nuttli, 1972) are plotted on an equi-distant

azimuthal projection about the shot point.
Circles indicate normal amplitudes and triangles
reduced amplitudes. A shadow zone to the
north is indicated although it is somewhat
undefined.

Figure 3.15   The observed long period amplitudes of CANNIKIN
are plotted as a function of epicentral distance,
delta. Amplitudes at stations between 310 and
50 degrees azimuth, indicated by triangles, have
somewhat lower amplitudes than other stations,
indicated by circles. Nuttli's (1972) curve
is used to divide the data into two groups.
Stations used in order of increasing delta
include: MAT, COR, SHK, GUA, DUG, GOL, TUC,
KEV, KTG, DAL, FLO, HNR, NUR, SCP, PMG, BLA,
SHA, CHG, COP, ESK, SNG, QUE, BEC, STU, TRI,
LEM, PTO, PDA, RIV, SJG, JER, and WEL.

Figure 3.16   Long period amplitudes for CANNIKIN plotted
as in Figure 3.10. Note the shadow zone.

Figure 3.17   The observed short (above) and long period
amplitudes of the earthquake of 2h on 7 FEB
1965 are plotted on equi-distant azimuthal
projection about the source. The amplitudes
are expressed on an arbitrary $\log_2$ scale.
The amplitudes on the right have been corrected

for the effect of a double couple source.
The observed amplitudes are plotted as a
function of delta in Appendix B. No shadow
zone is evident on either instrument. This is
earthquake number 7 (Stauder, 1968a).

Figure 3.18 Observed amplitudes for the 2 JUN 1966 event
are plotted as in Figure 3.17. These ampli-
tudes were used to source correct the LONGSHOT
and MILROW amplitudes. This is earthquake
number 14 (Stauder, 1968a).

Figure 3.19 The theoretical temperature anomaly associated
with the best fitting seismic model of the
Aleutians is plotted with respect to observed
earthquake epicenters (Engdahl, 1971). Note
that the epicenters of intermediate depth
earthquakes fall in the calculated low temper-
ature region of the slab.

Figure 3.20 Index map shows the location of intermediate
earthquakes used in this paper to the Tonga
seismic zone (modified after Isacks and Molnar,
1971). Numbers indicate: 1, 18 MAR 1965; 2,
10 AUG 1966; 3, 20 AUG 1965; 4, 12 AUG 1967;
5, 21 JUL 1964. The numbers assigned to
these earthquakes in Isacks and Molnar's
catalogue are 52, 51, 55, 56, and 57 respectively.

Figure 3.21   Index map shows the relation of the earthquake

of 5 AUG 1964 to the Kermadec seismic zone

(modified after Isacks and Molnar, 1971,

catalogue number 61).

Figure 3.22   Amplitudes for the earthquake of 21 JUL 1964

are plotted as in Figure 3.17. The 'p'

indicates the stations where low amplitude

precursors were observed.

Figure 3.23   The amplitudes of the earthquake of 5 AUG 1964

are plotted as in Figure 3.17.

Figure 3.24   The amplitudes of the earthquake of 18 MAR 1965

are plotted as in Figure 3.17.

Figure 3.25   The amplitudes of the earthquake of 20 AUG 1965

are plotted as in Figure 3.17.

Figure 3.26   The amplitudes of the earthquake of 10 AUG 1966

are plotted as in Figure 3.17.

Figure 3.27   The amplitudes of the earthquake of 12 AUG 1967

are plotted as in Figure 3.17.

Figure 3.28   The location of the earthquake of 4 AUG 1964 is

compared with the seismic zone of the Kurile

arc (modified after Isacks and Molnar, 1971,

catalogue number 118).

Figure 3.29   The amplitudes of the earthquake of 4 AUG 1964

are plotted as in Figure 3.17.

Figure 3.30 Tracing of the short period P-wave arrivals

from the earthquake of 21 JUL 1964 show

precursors at PMG, CTA, BAG, and ANP. Normal

appearing arrivals at TUC and SBA are shown

for reference.
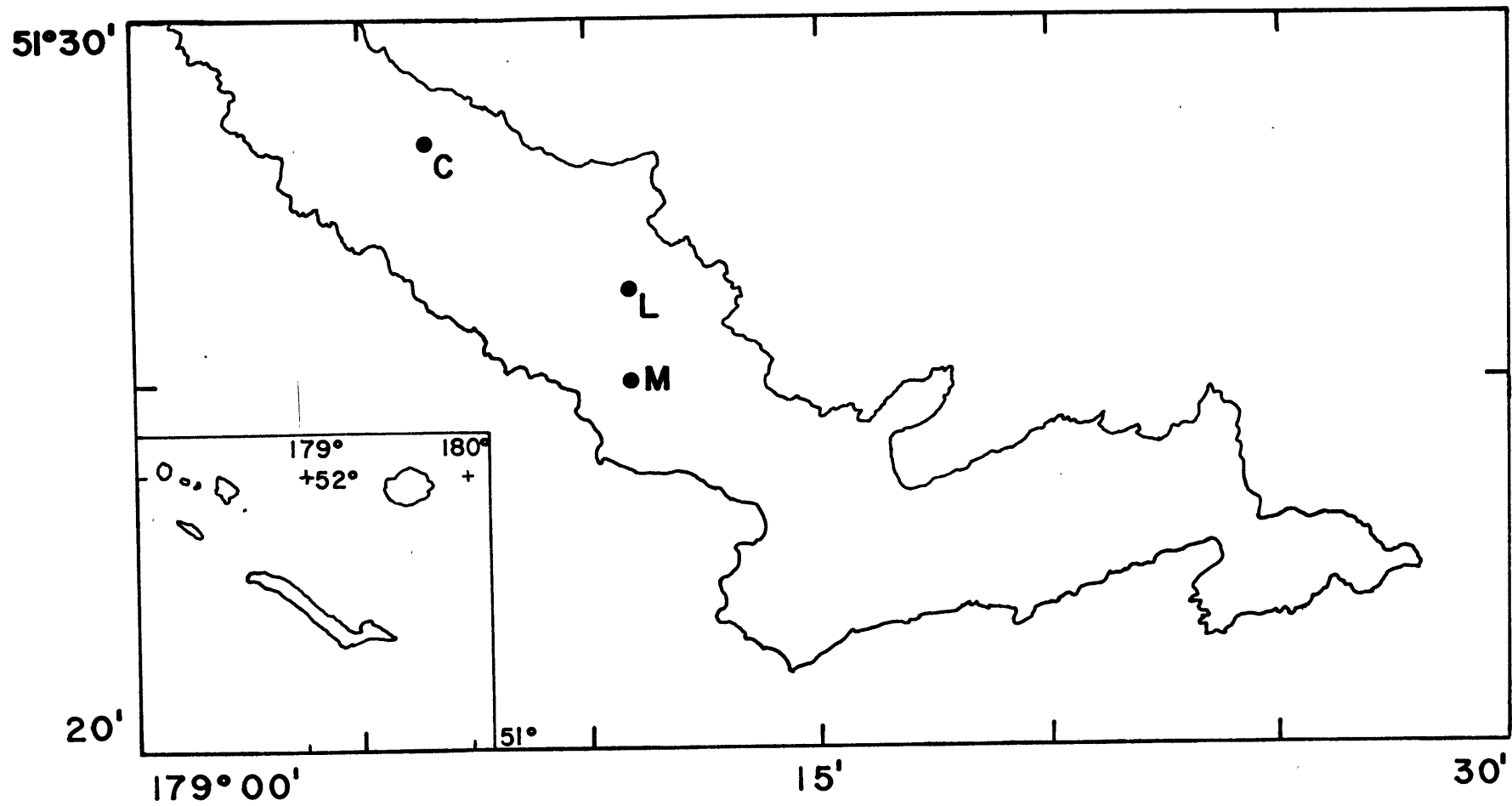
FIGURE 3.1
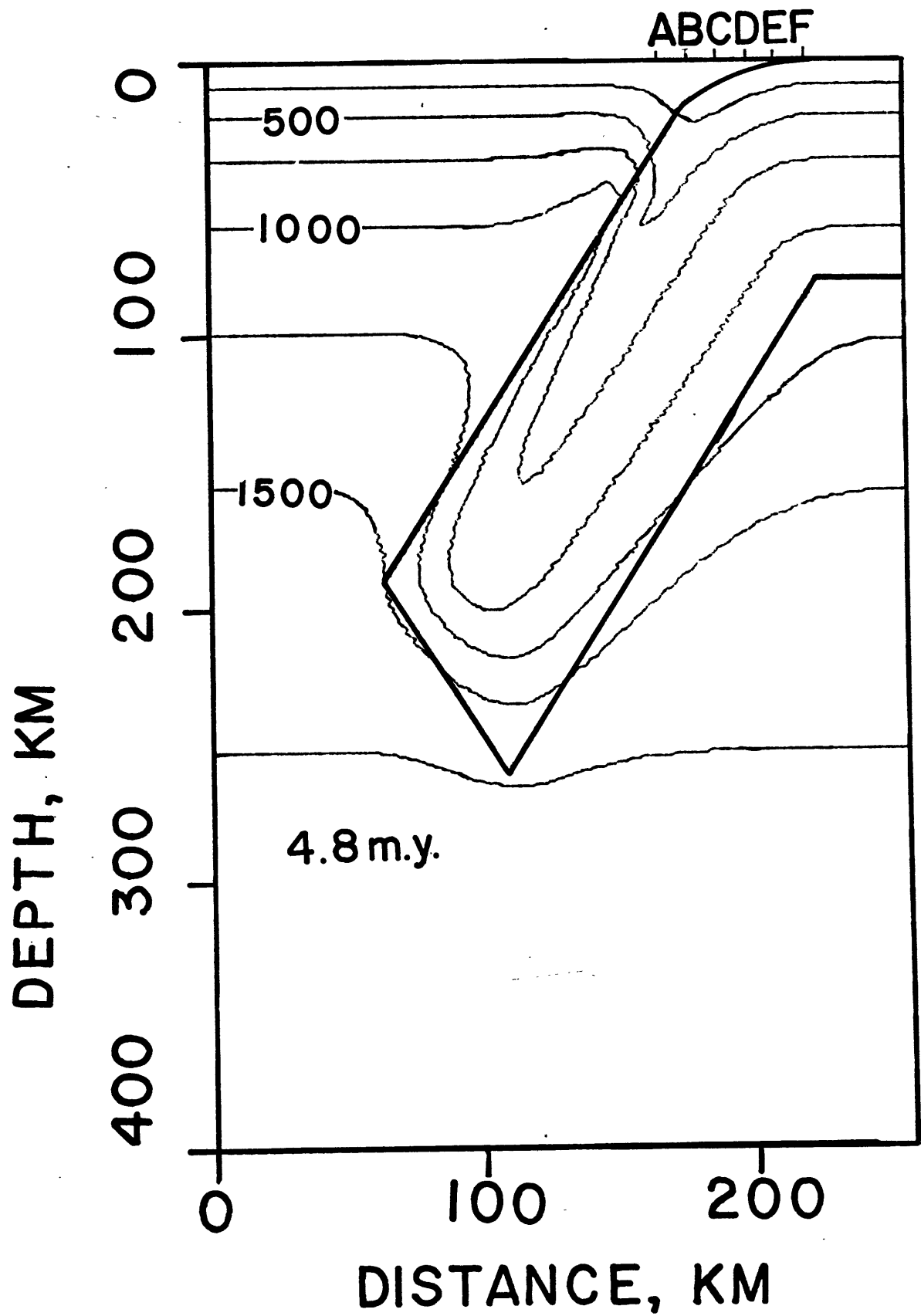
FIGURE 3.2
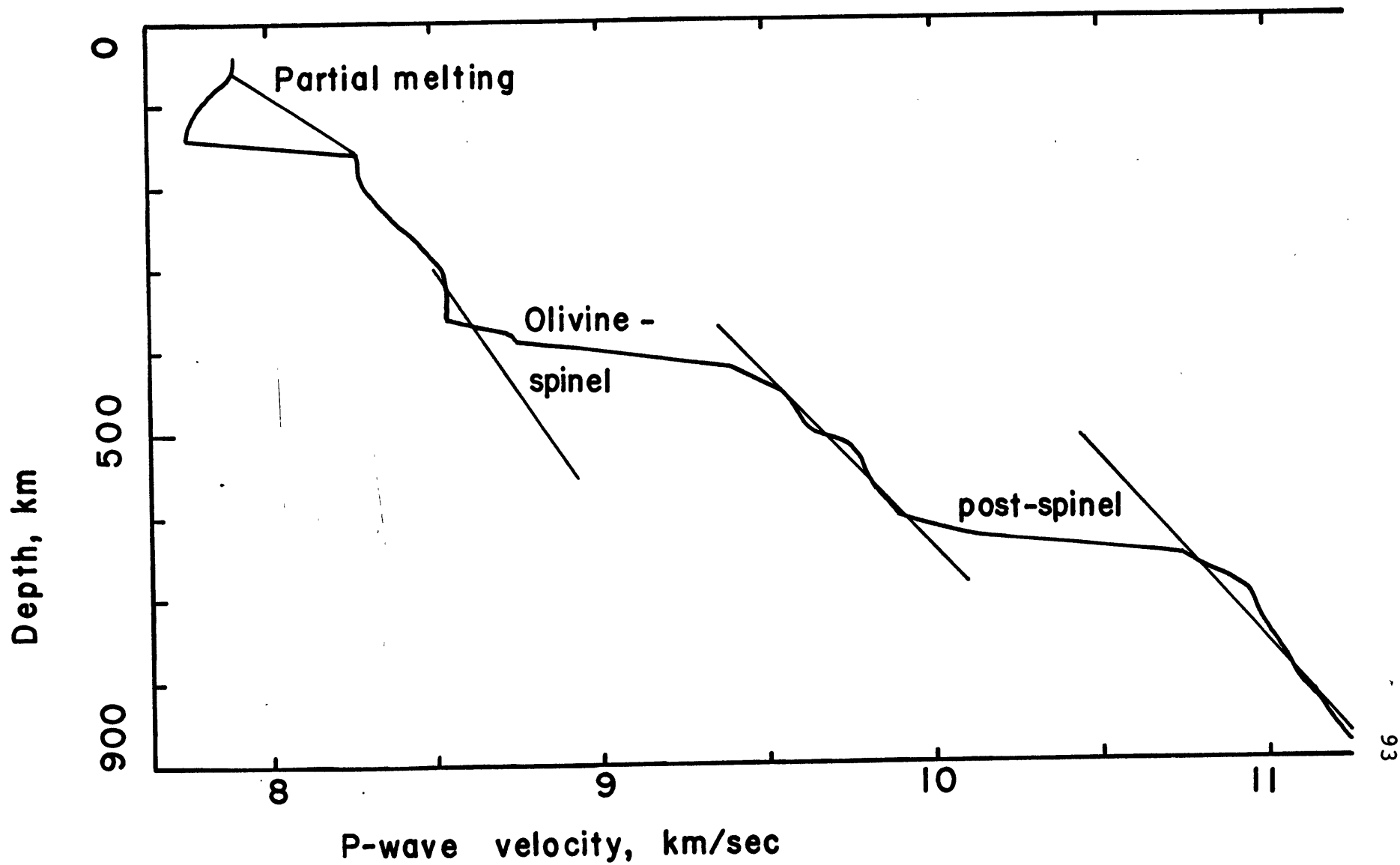
FIGURE 3.3

FIGURE 3.4

FIGURE 3.5

SHADOW ZONE

P-WAVE VELOCITY
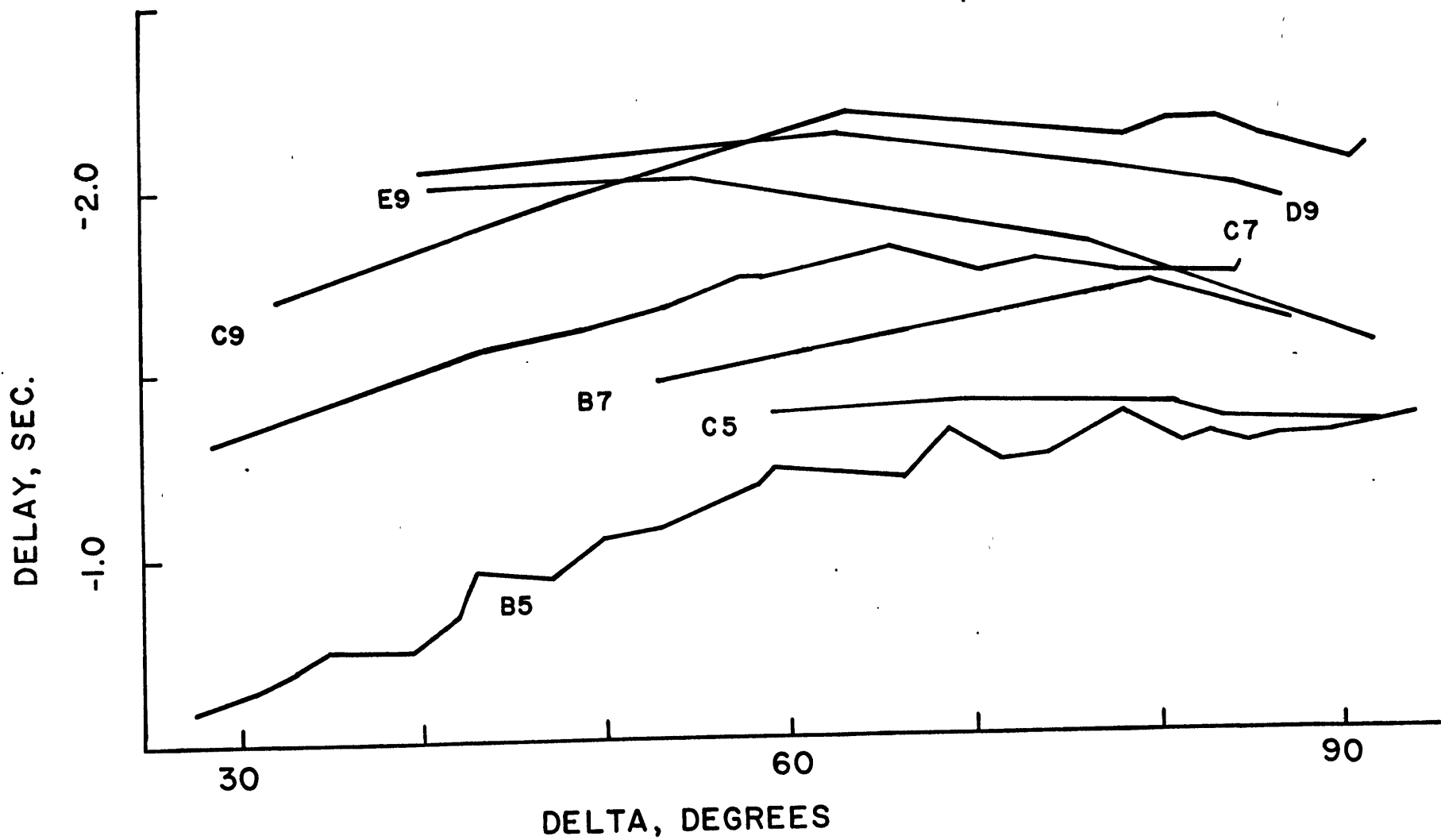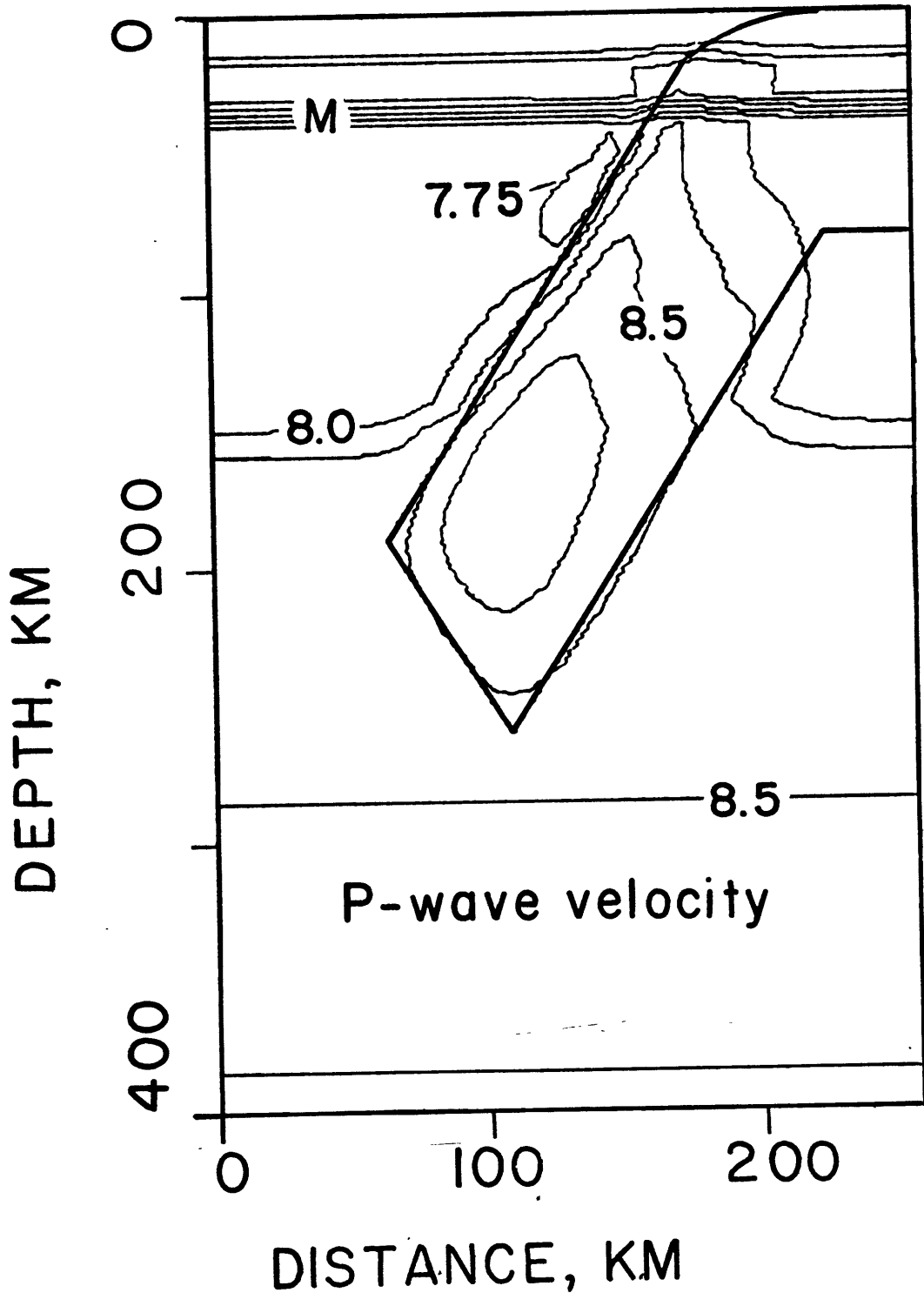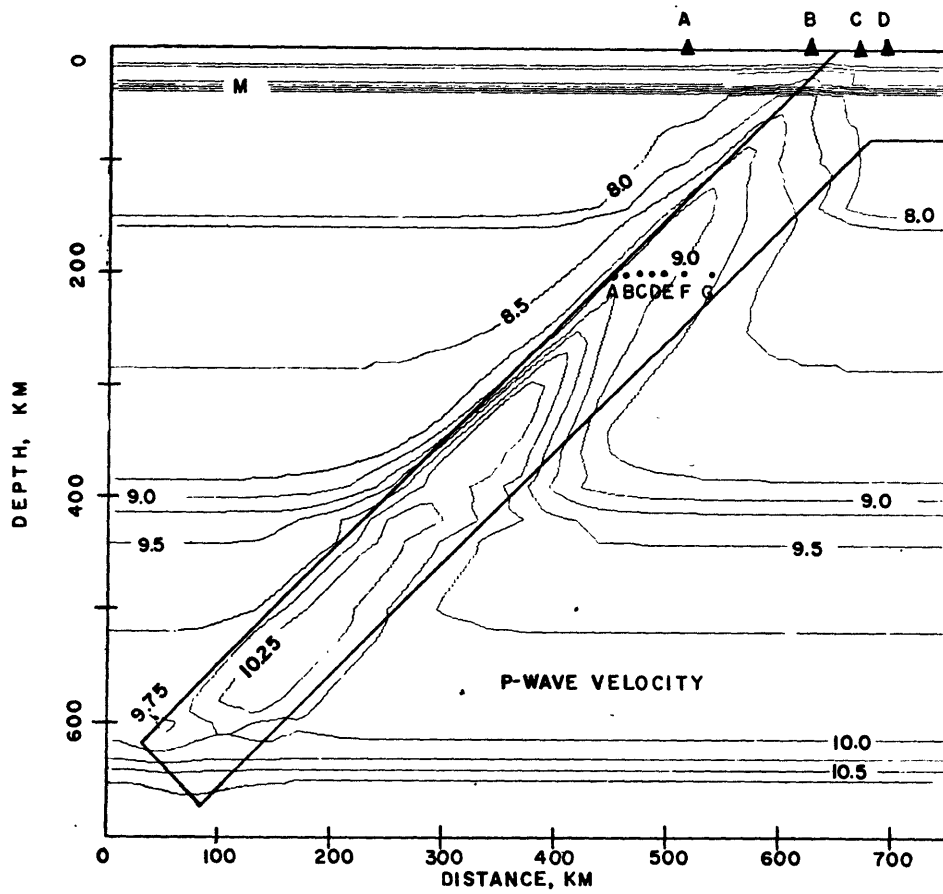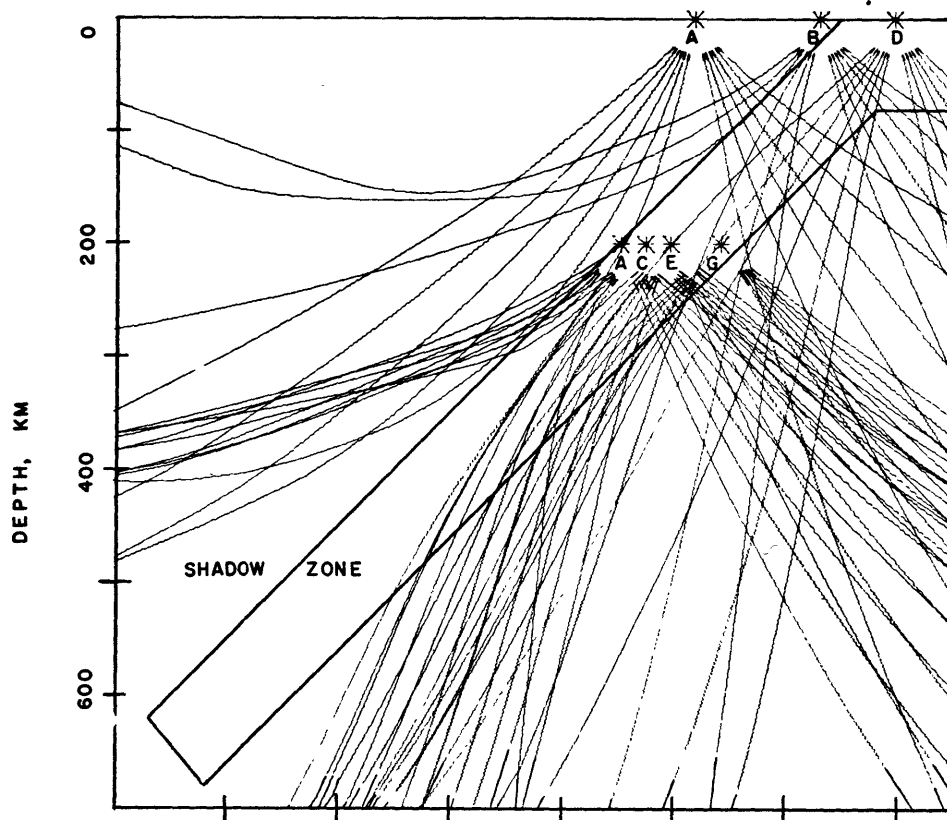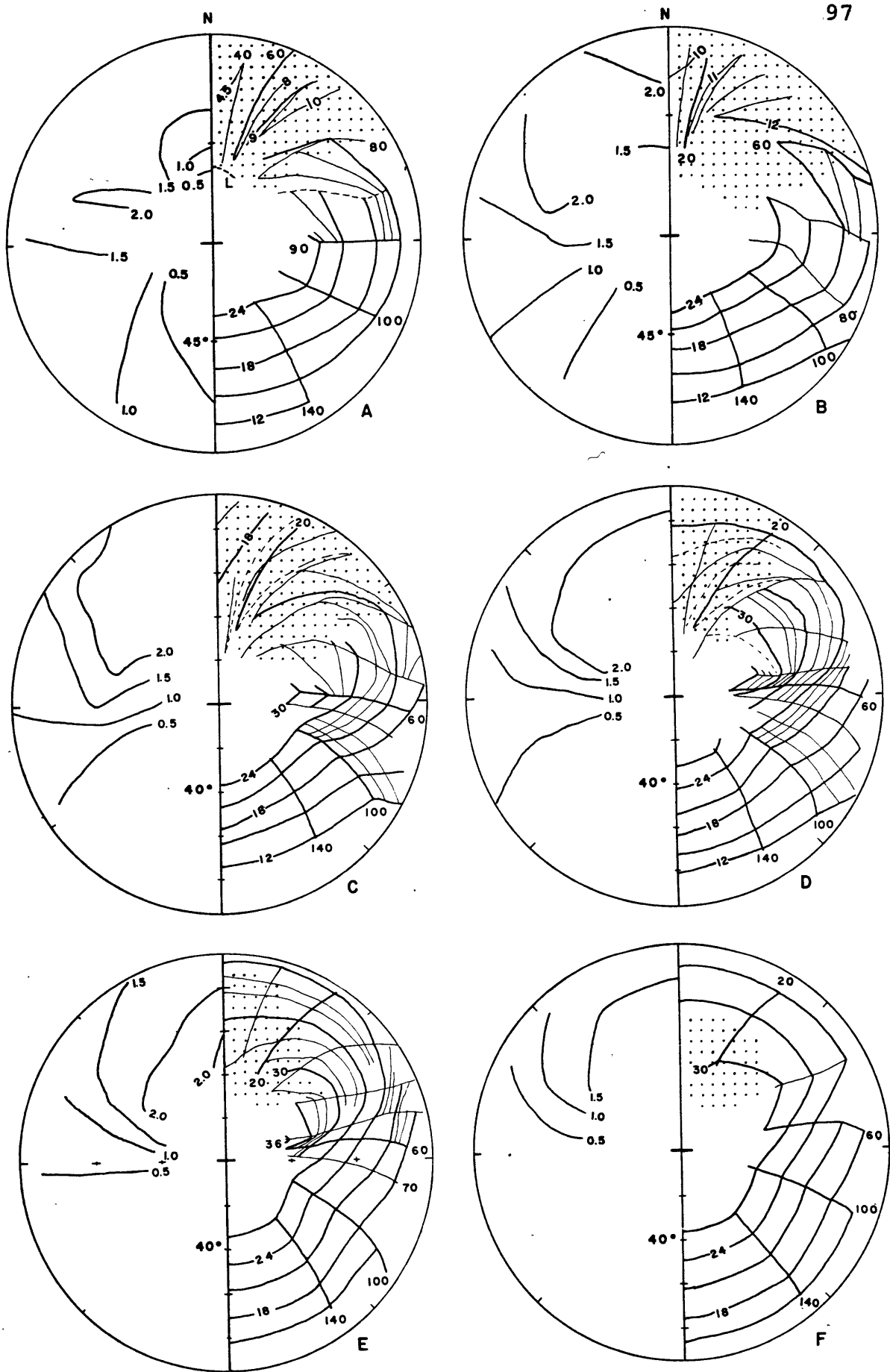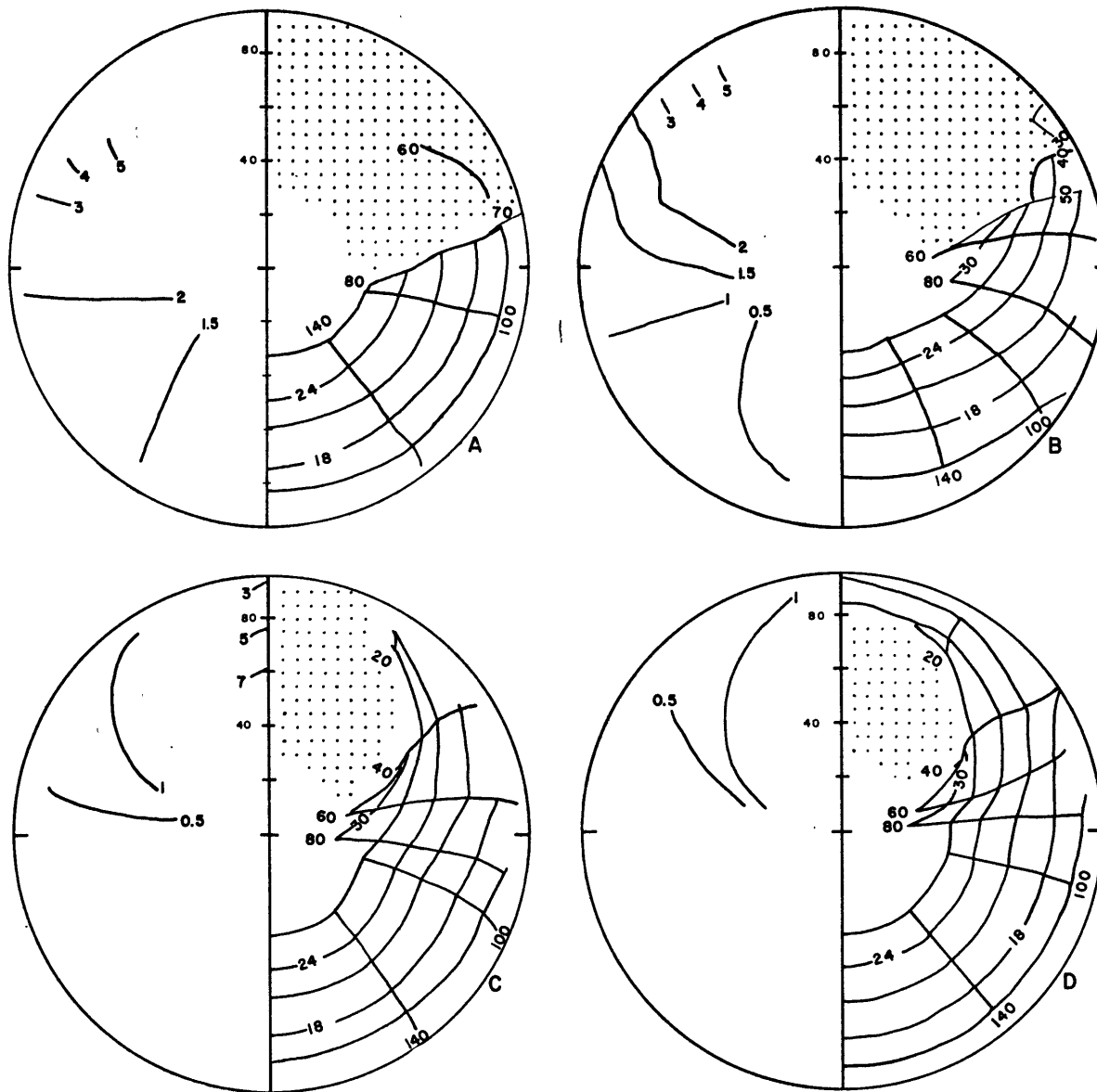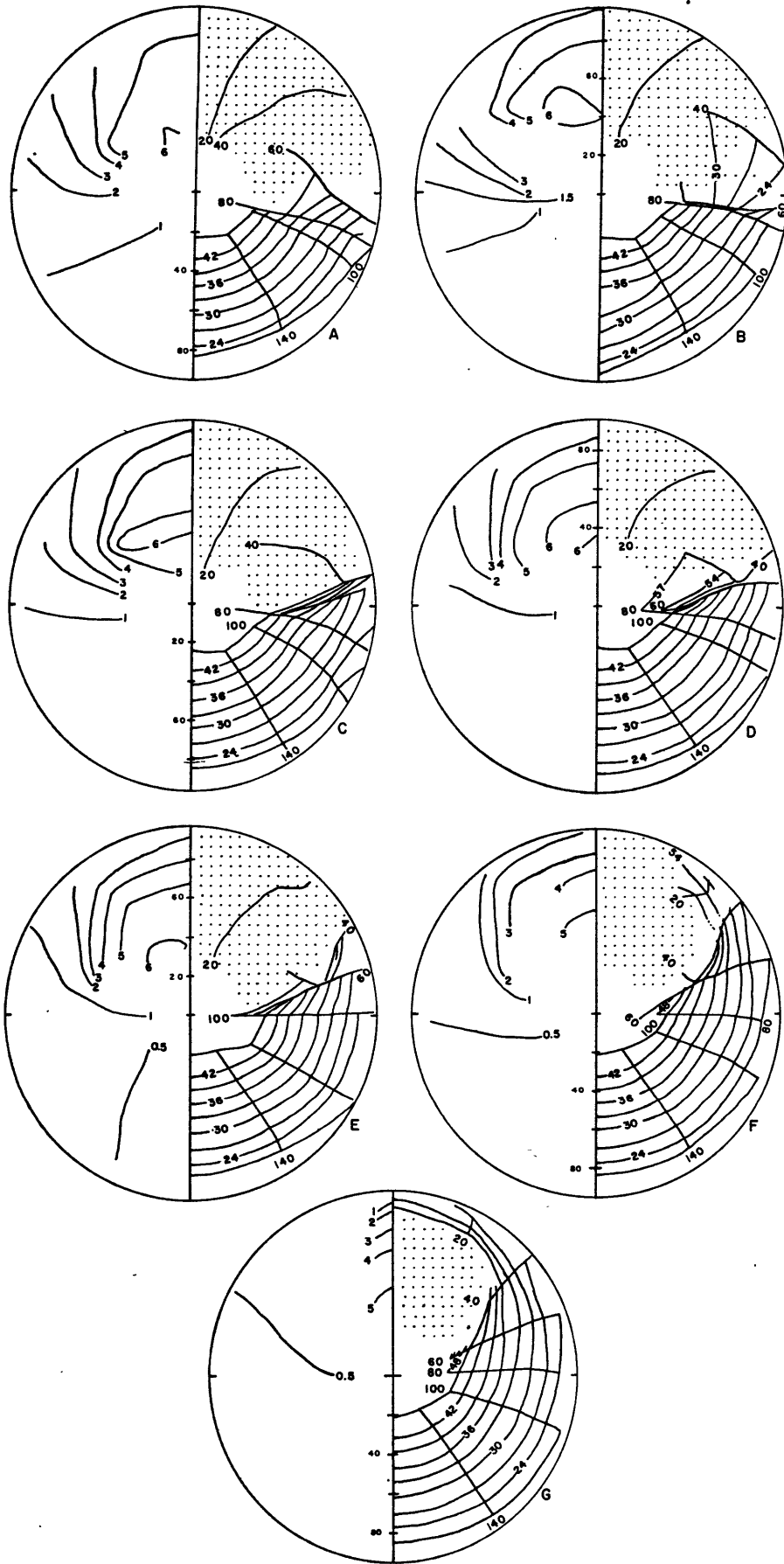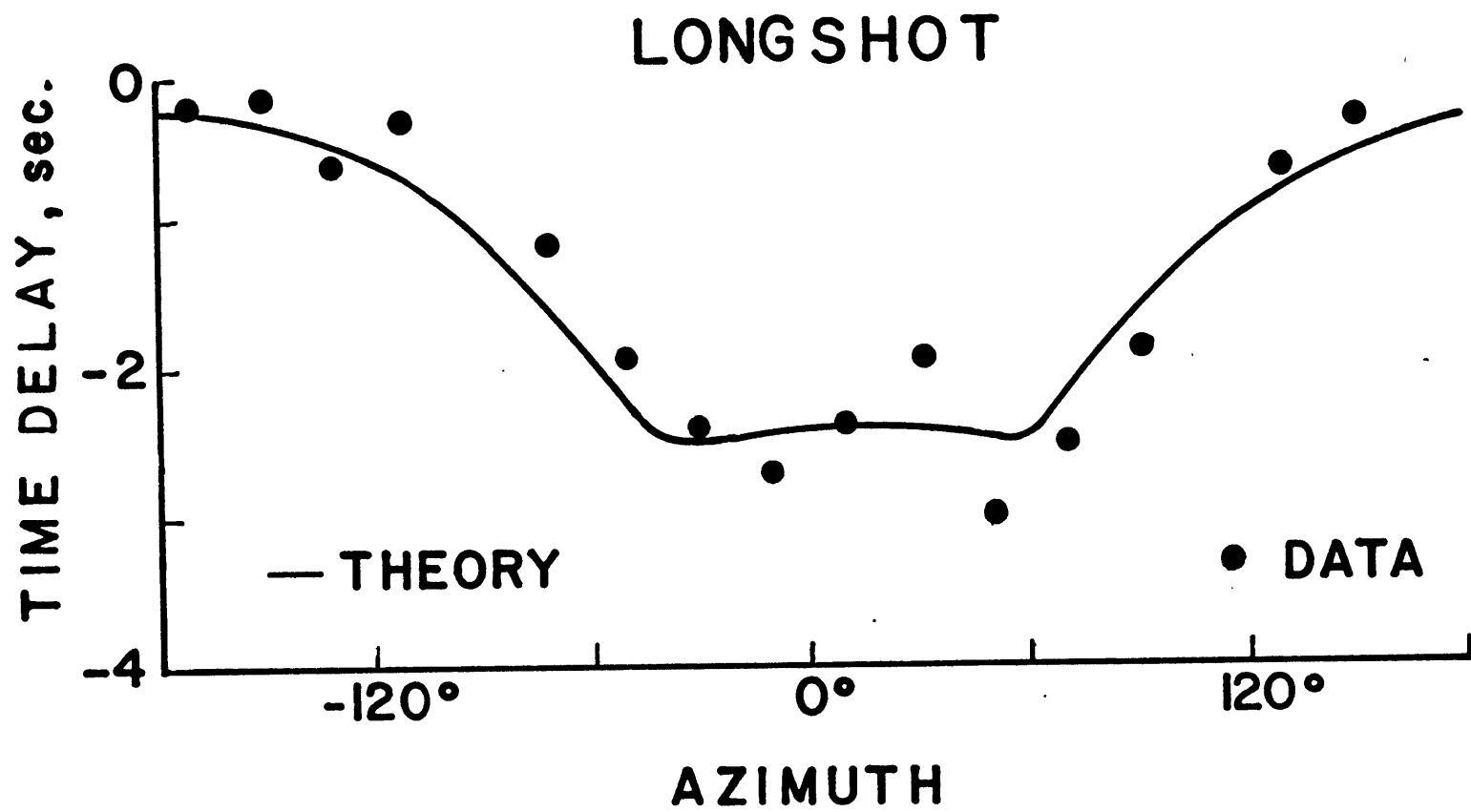
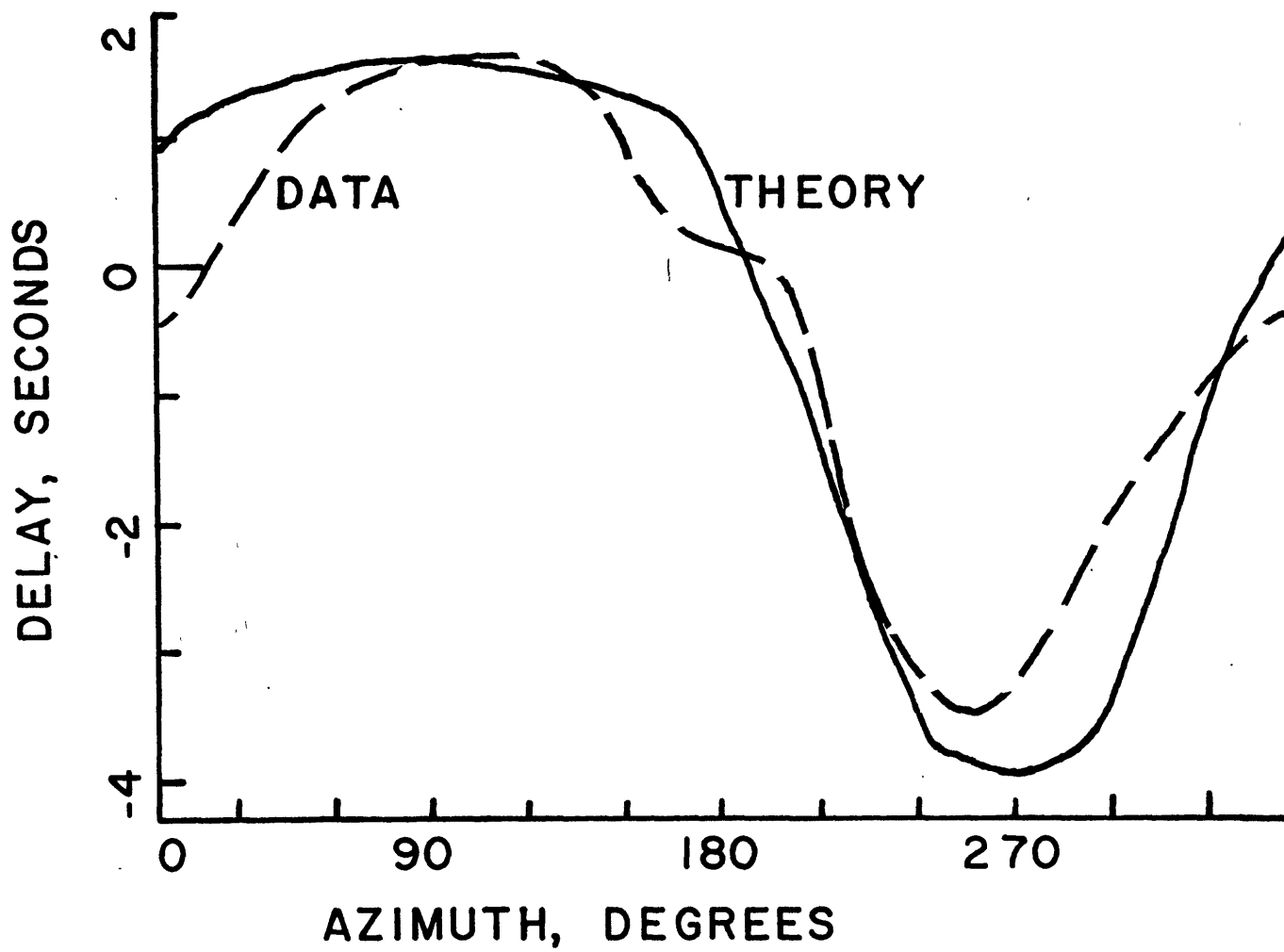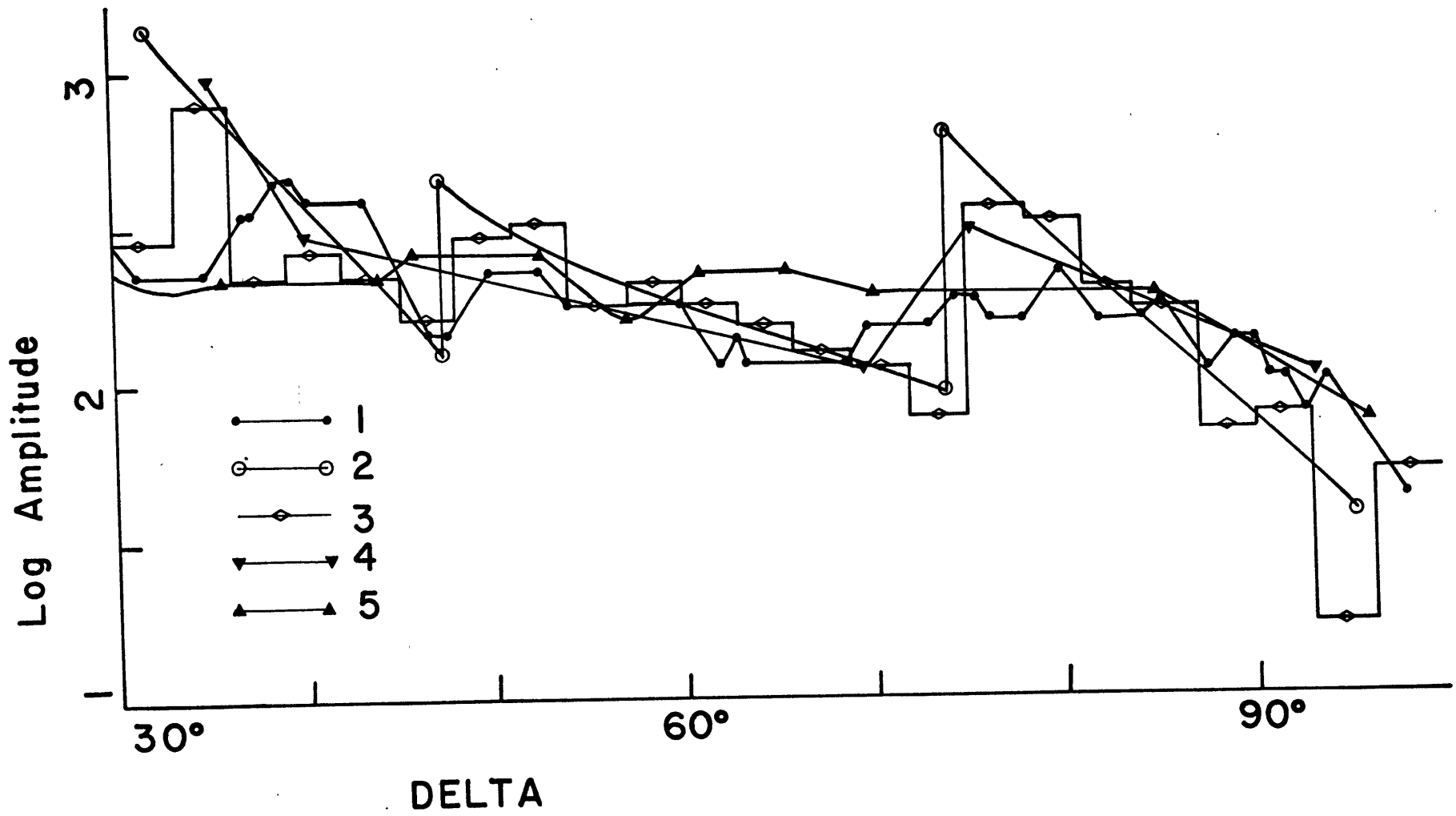FIGURE 3.6
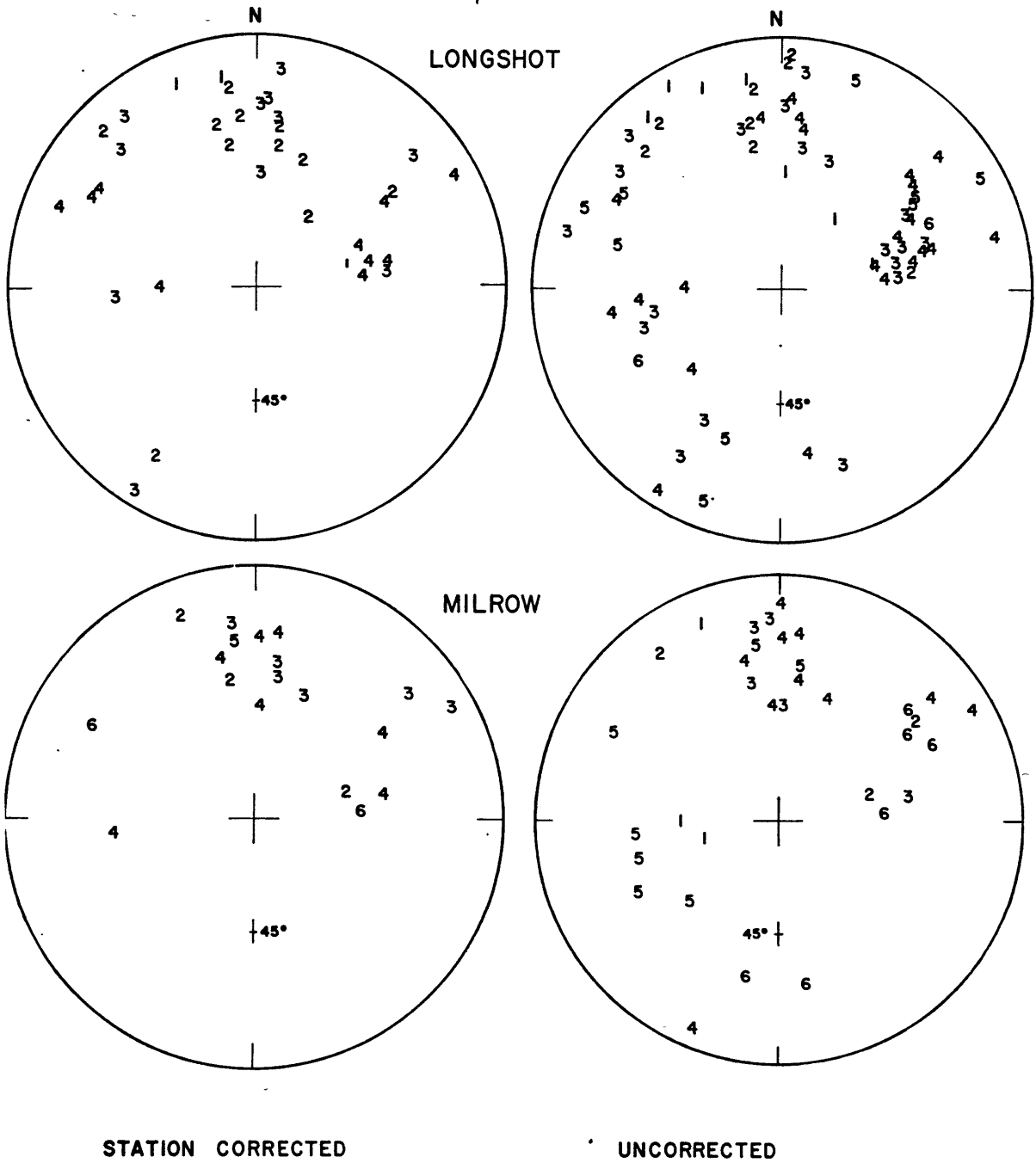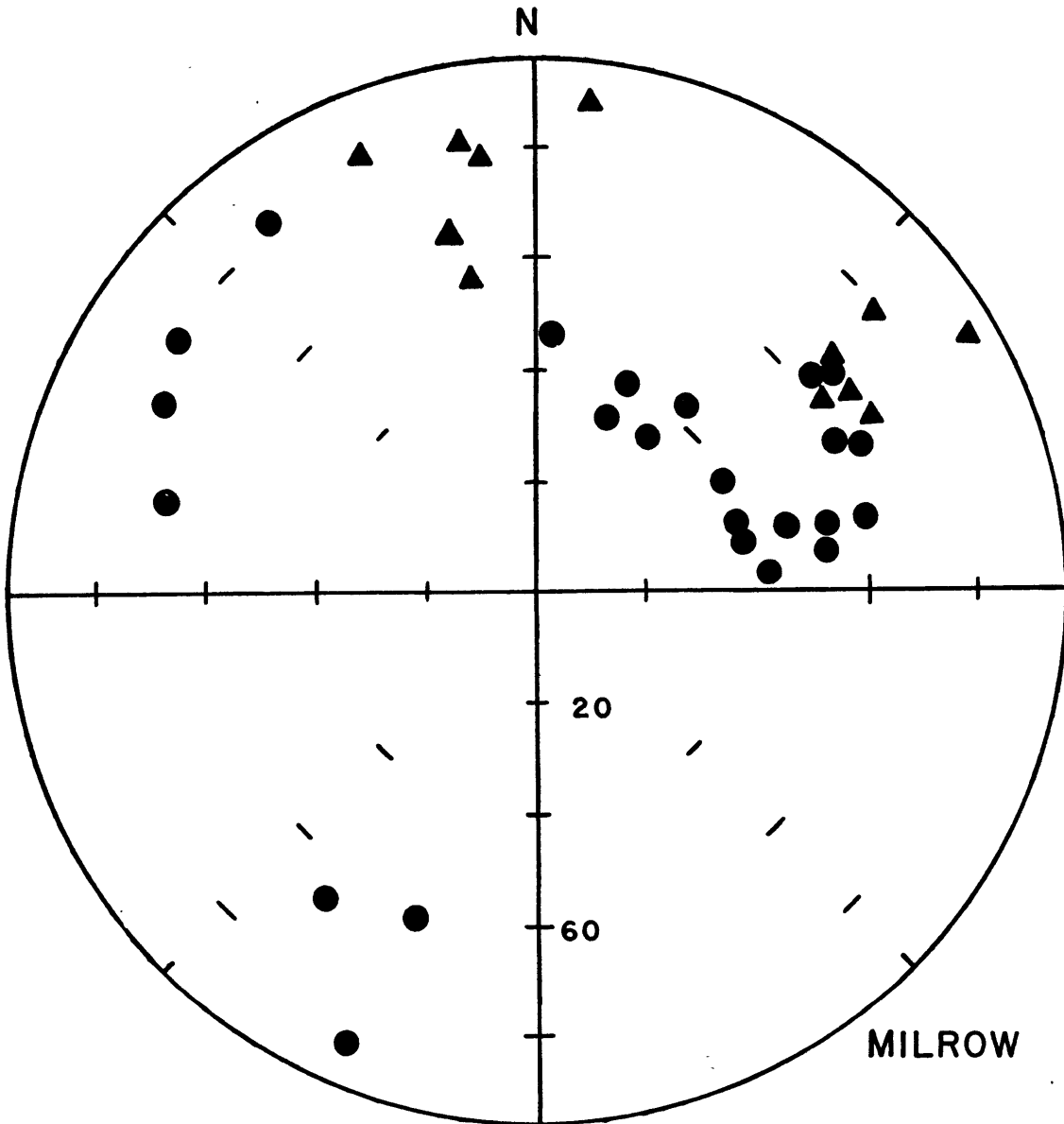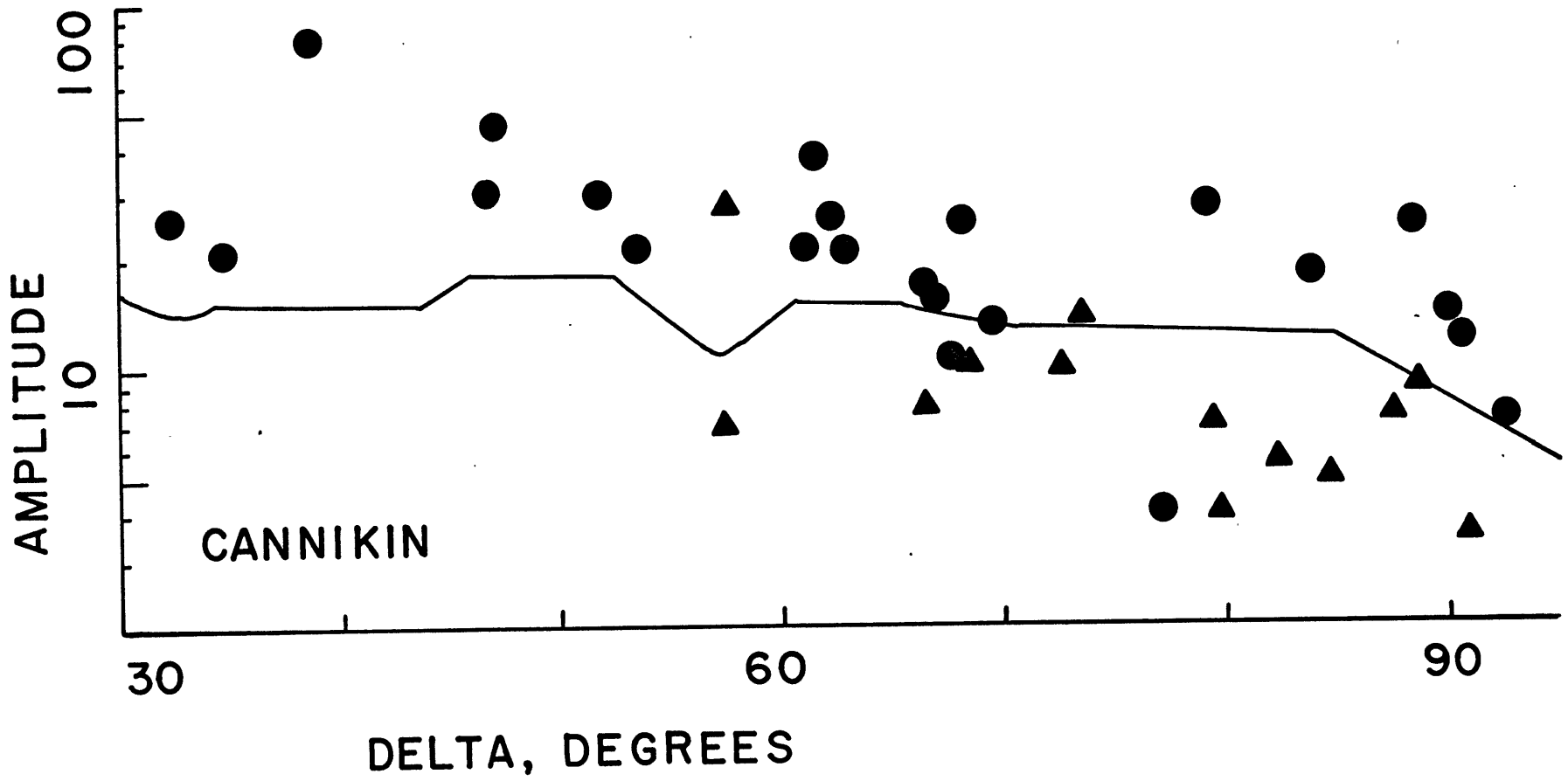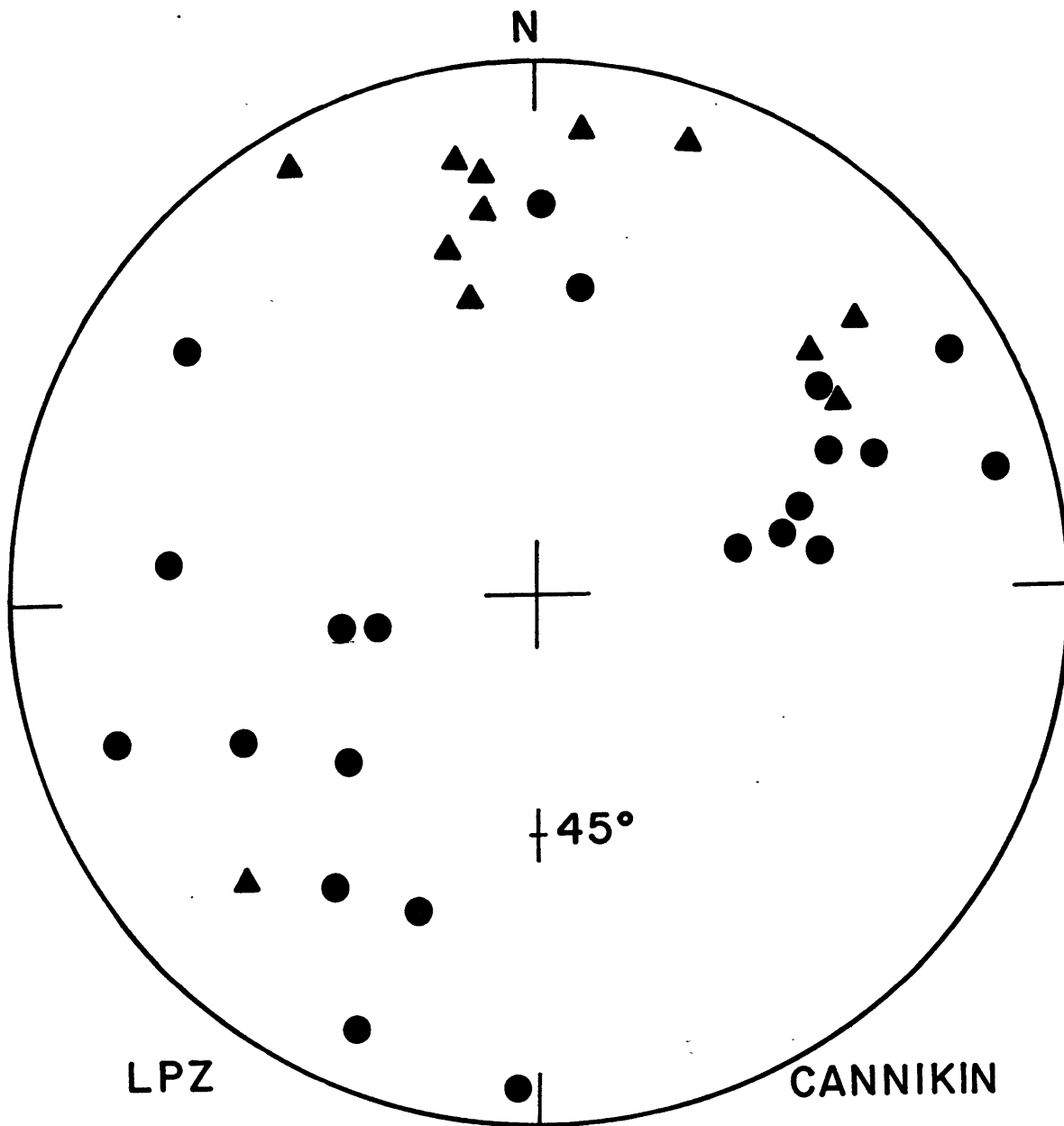
FIGURE 3.7

FIGURE 3.8

FIGURE 3.9

LONGSHOT

FIGURE 3.10

FIGURE 3.11

FIGURE 3.12

FIGURE 3.13

FIGURE 3.14

FIGURE 3.15

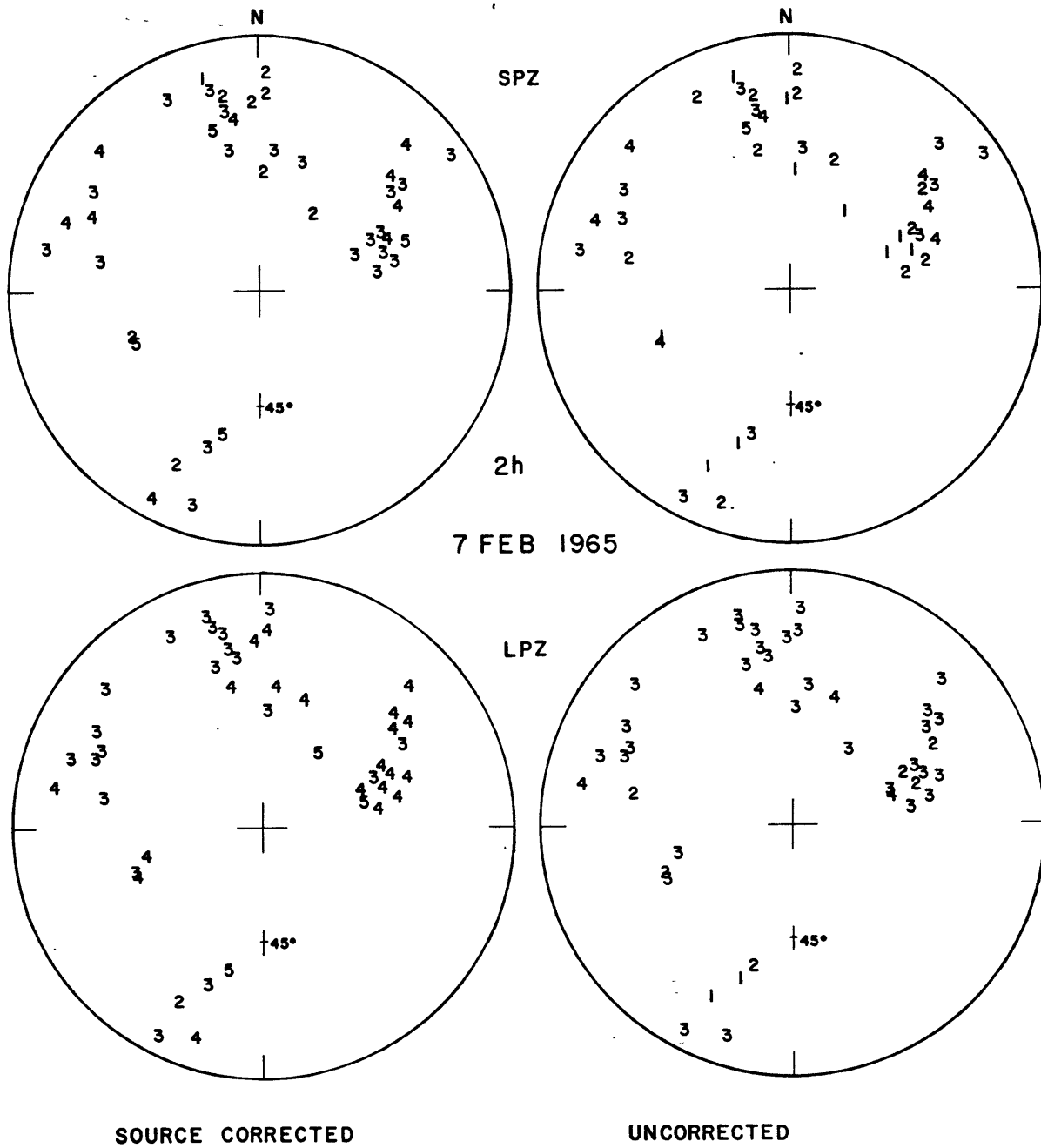FIGURE 3.16
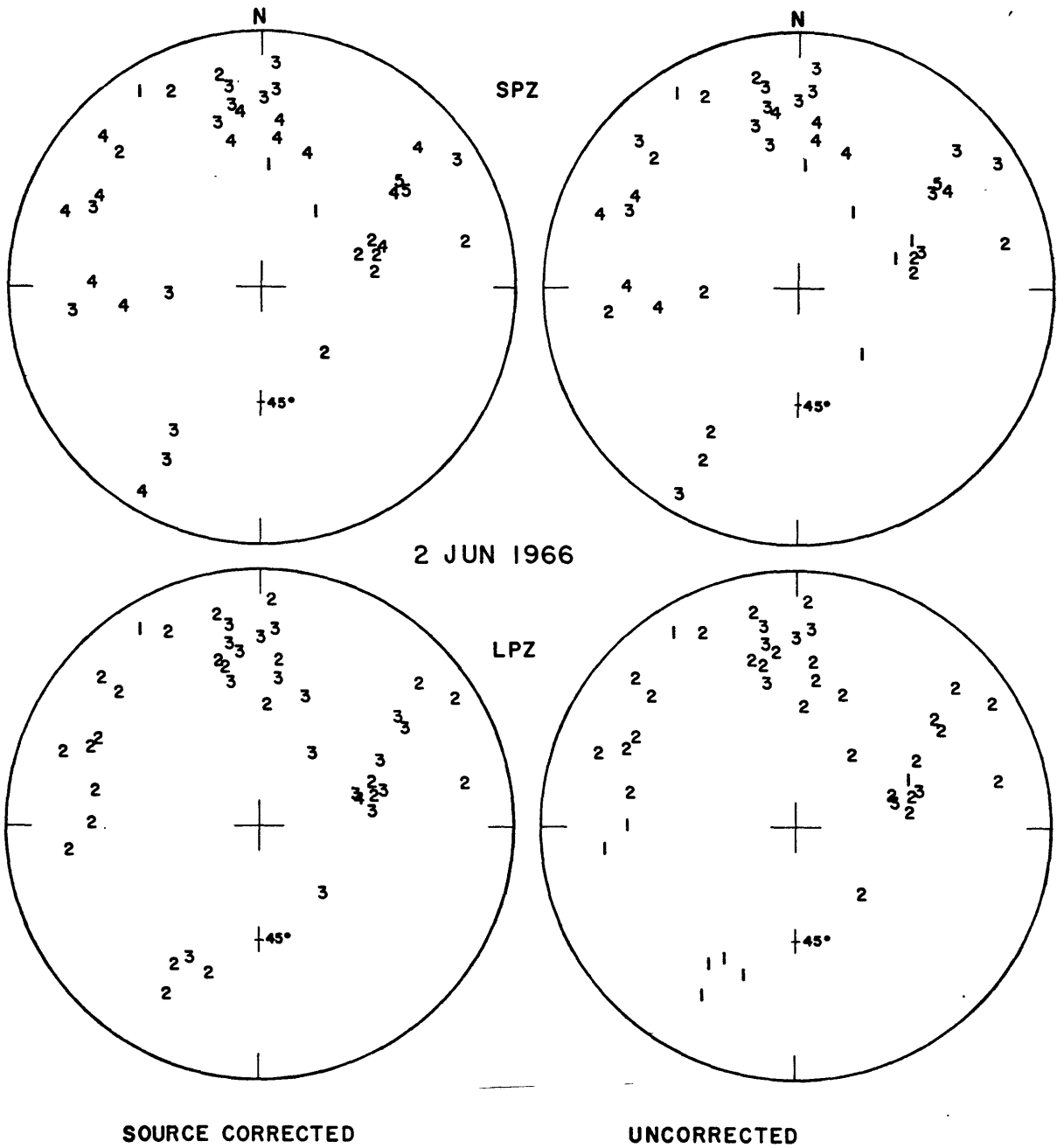
SPZ

2h

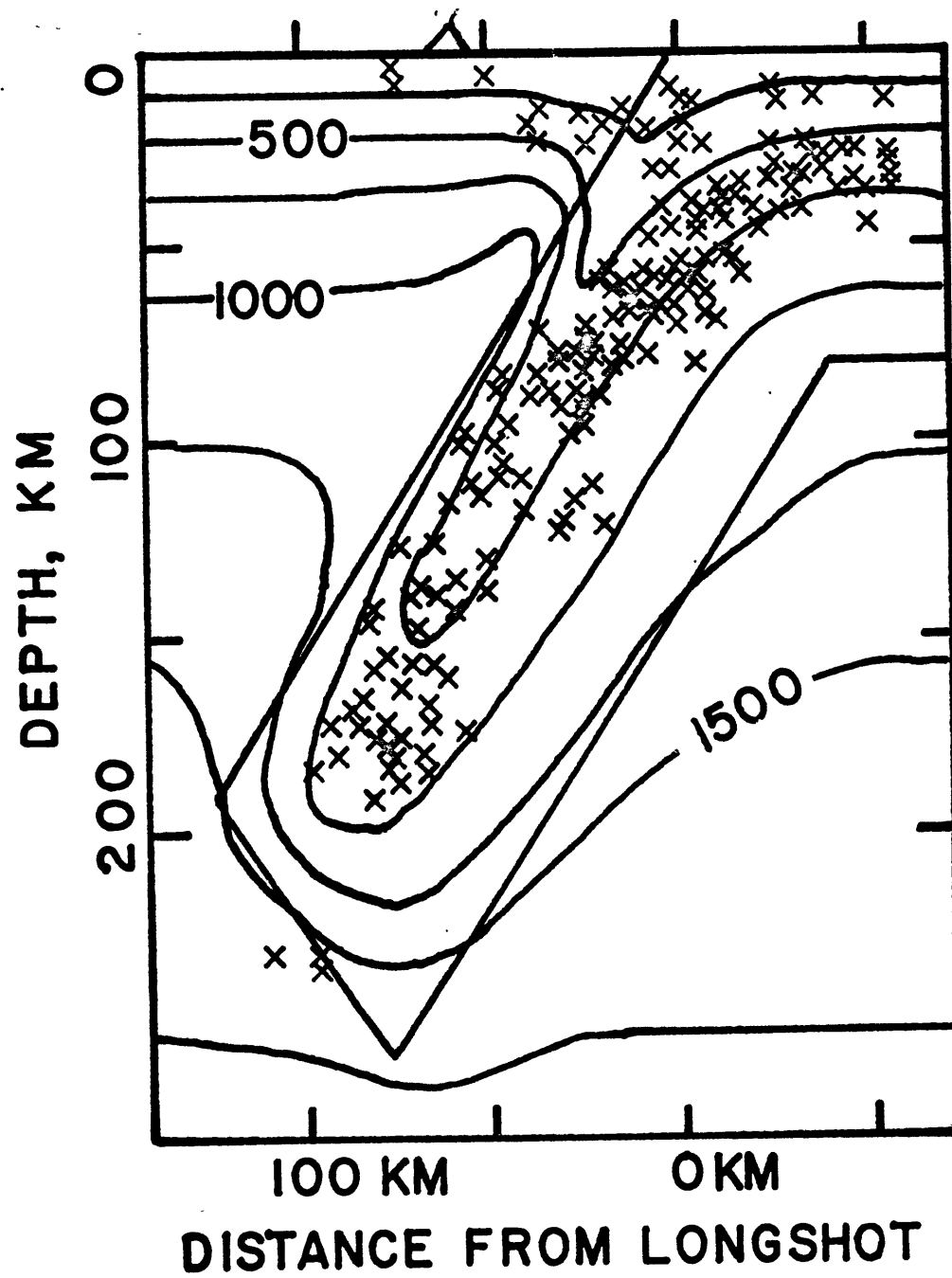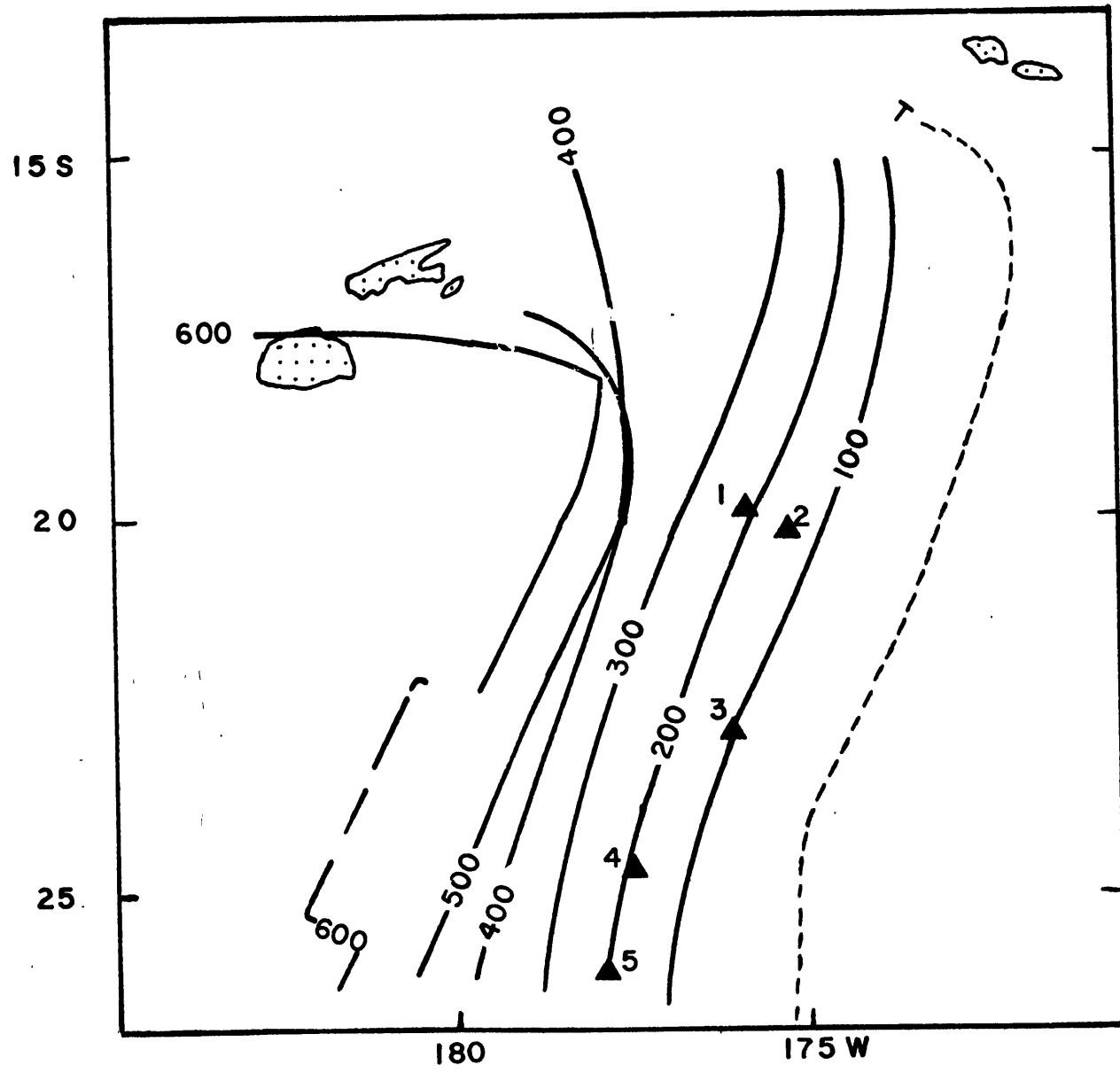7 FEB 1965
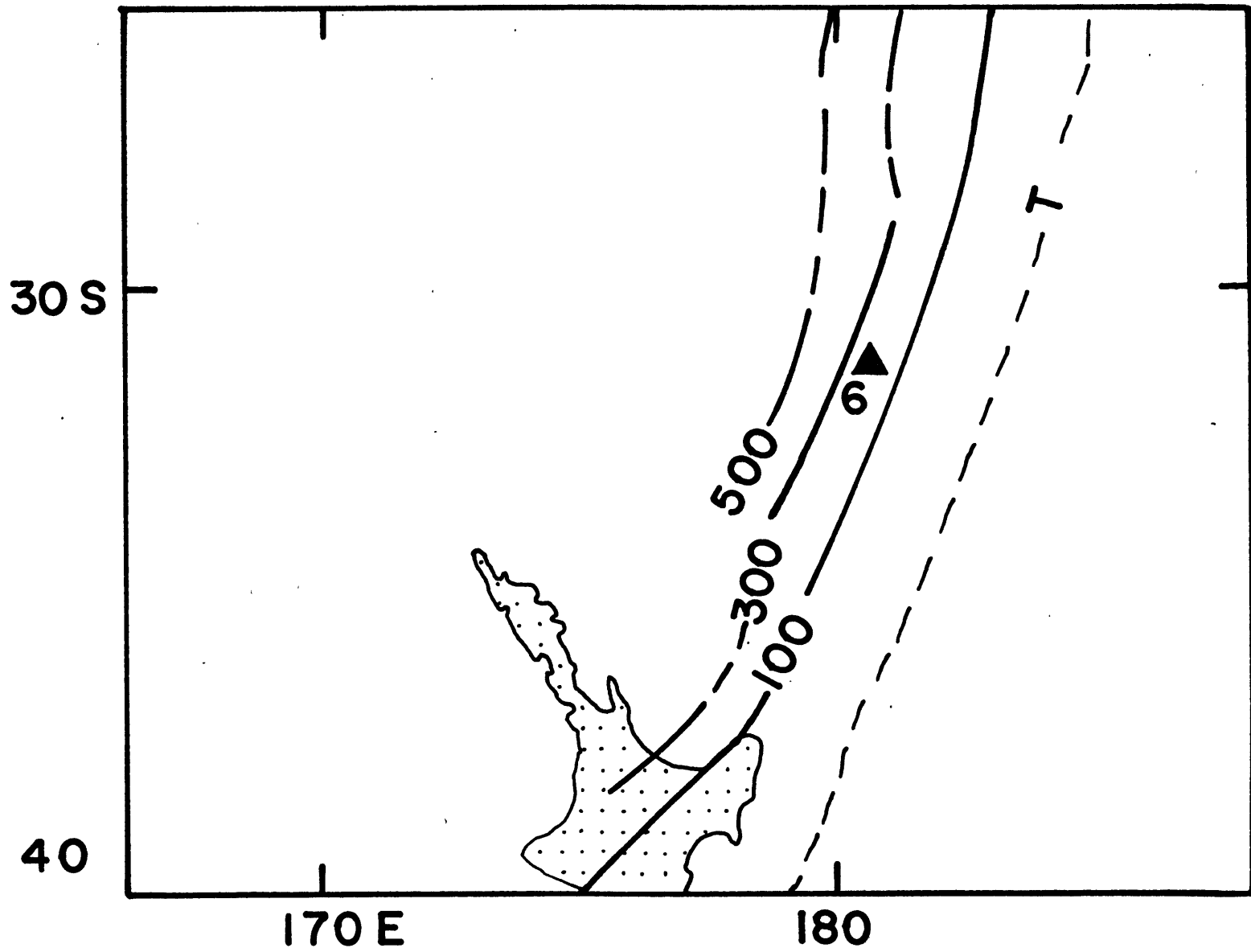
LPZ

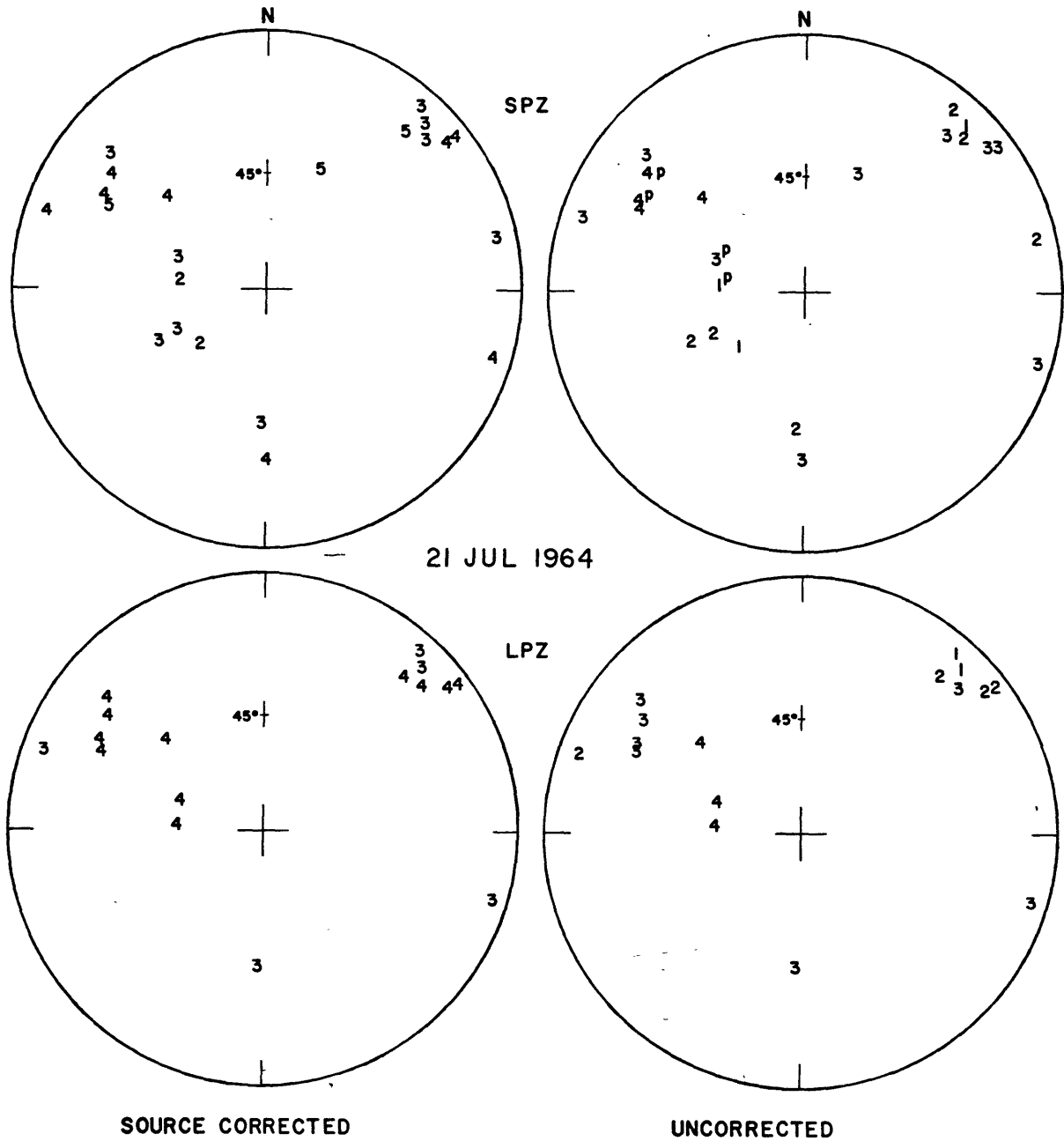SOURCE CORRECTED

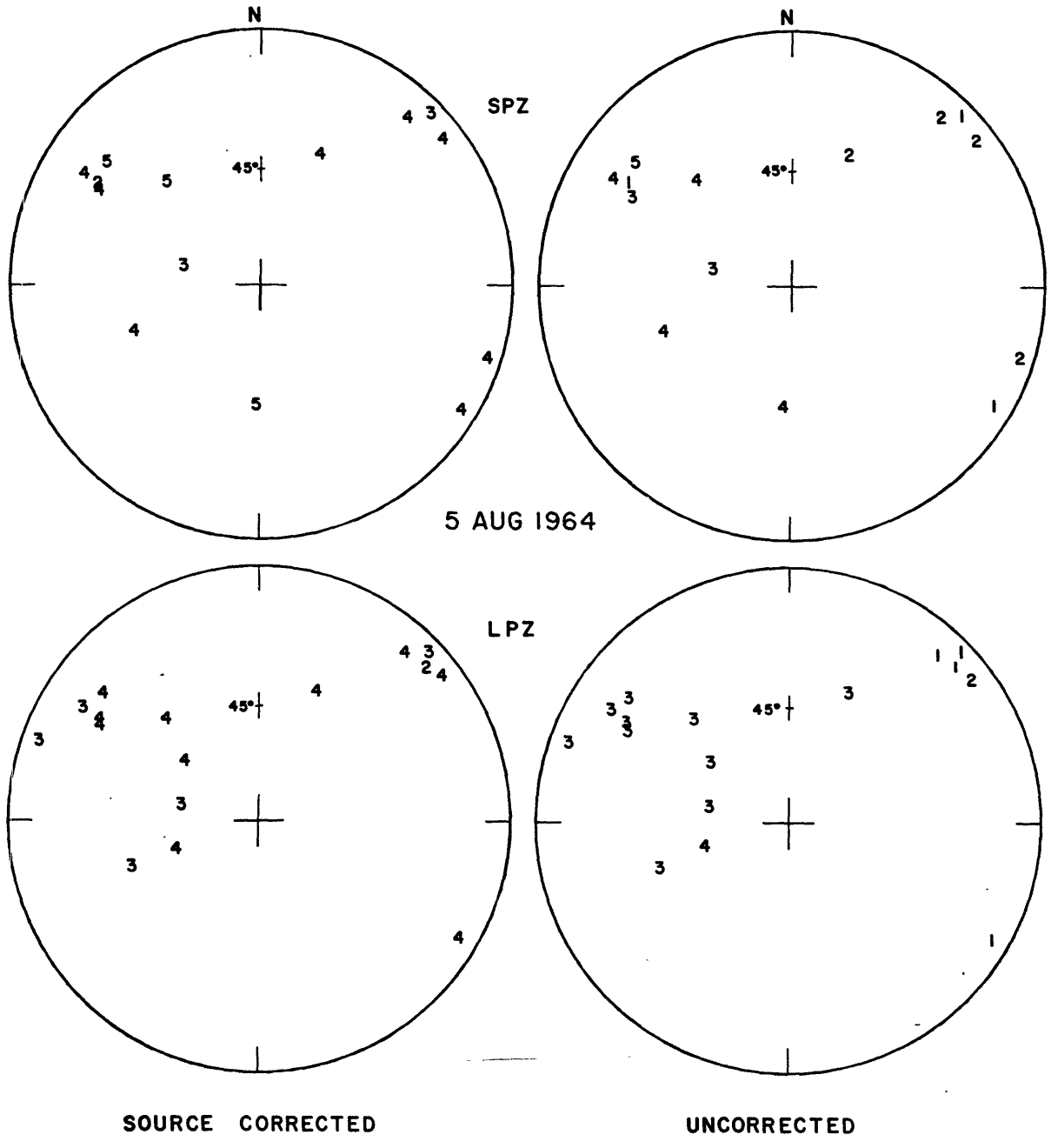UNCORRECTED

FIGURE 3.17

FIGURE 3.18

FIGURE 3.19

FIGURE 3.20

FIGURE 3.21

FIGURE 3.22

FIGURE 3.23

FIGURE 3.24

FIGURE 3.25

FIGURE 3.26

12 AUG 1967

SOURCE CORRECTED   UNCORRECTED
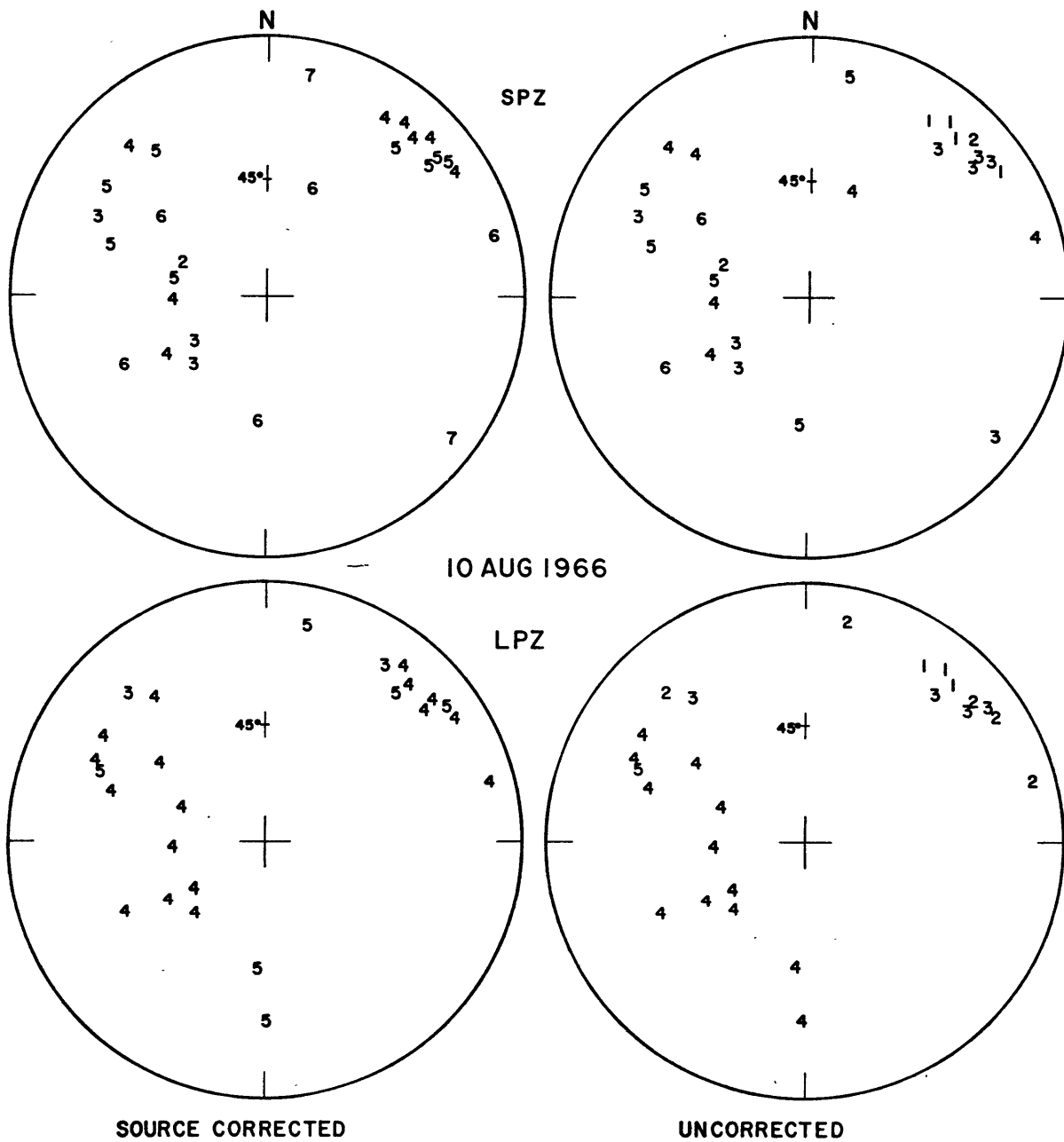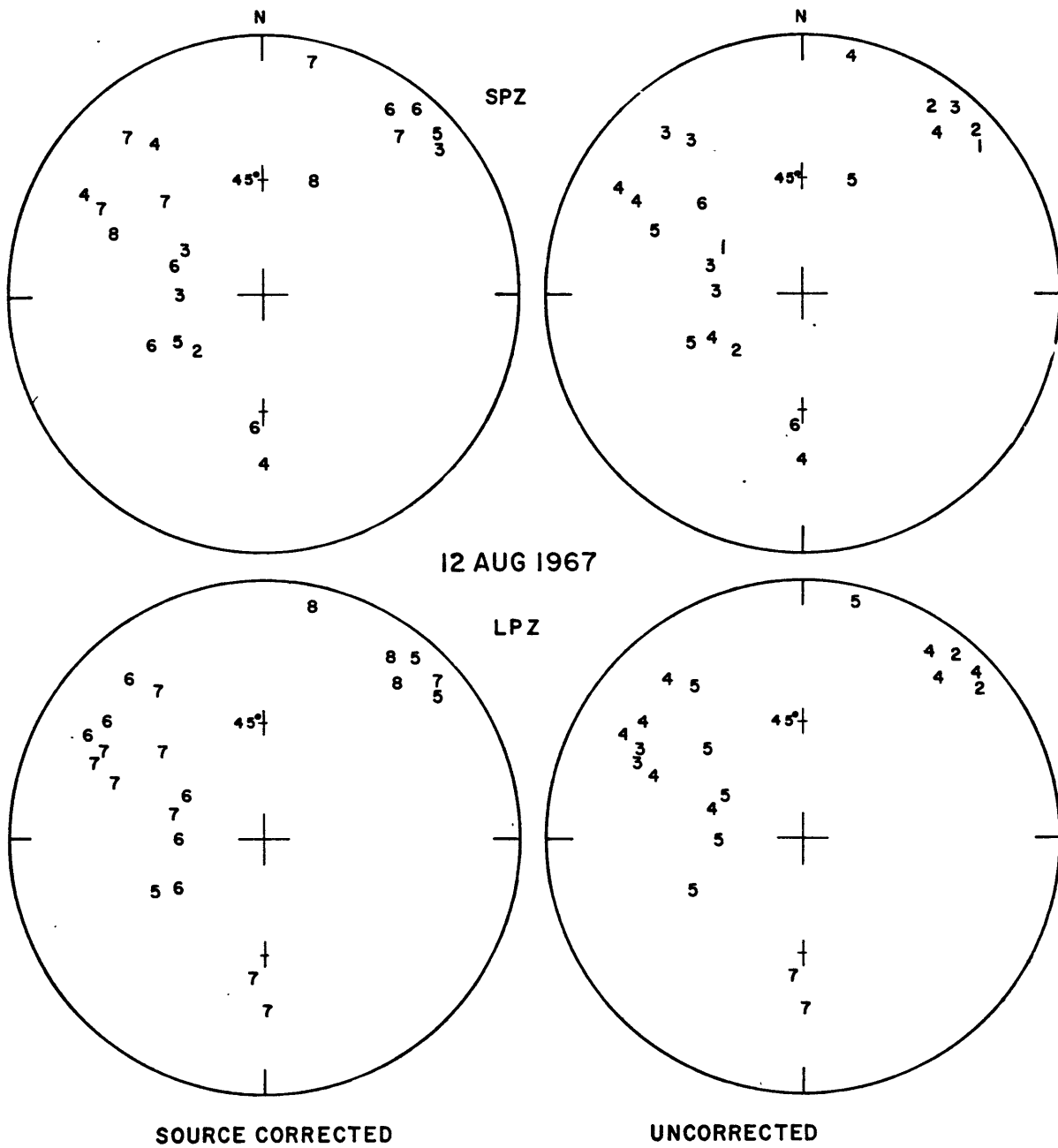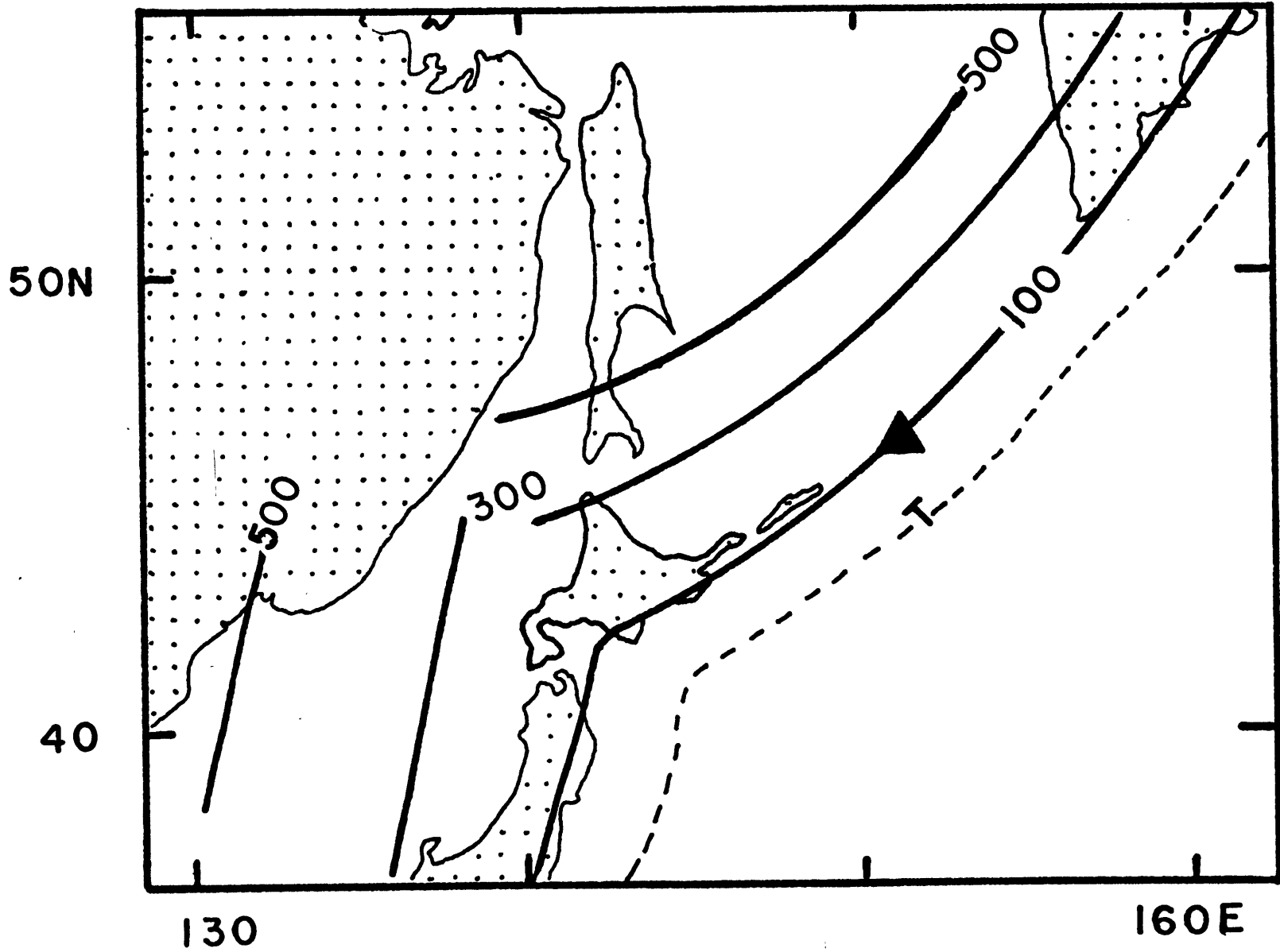
FIGURE 3.27
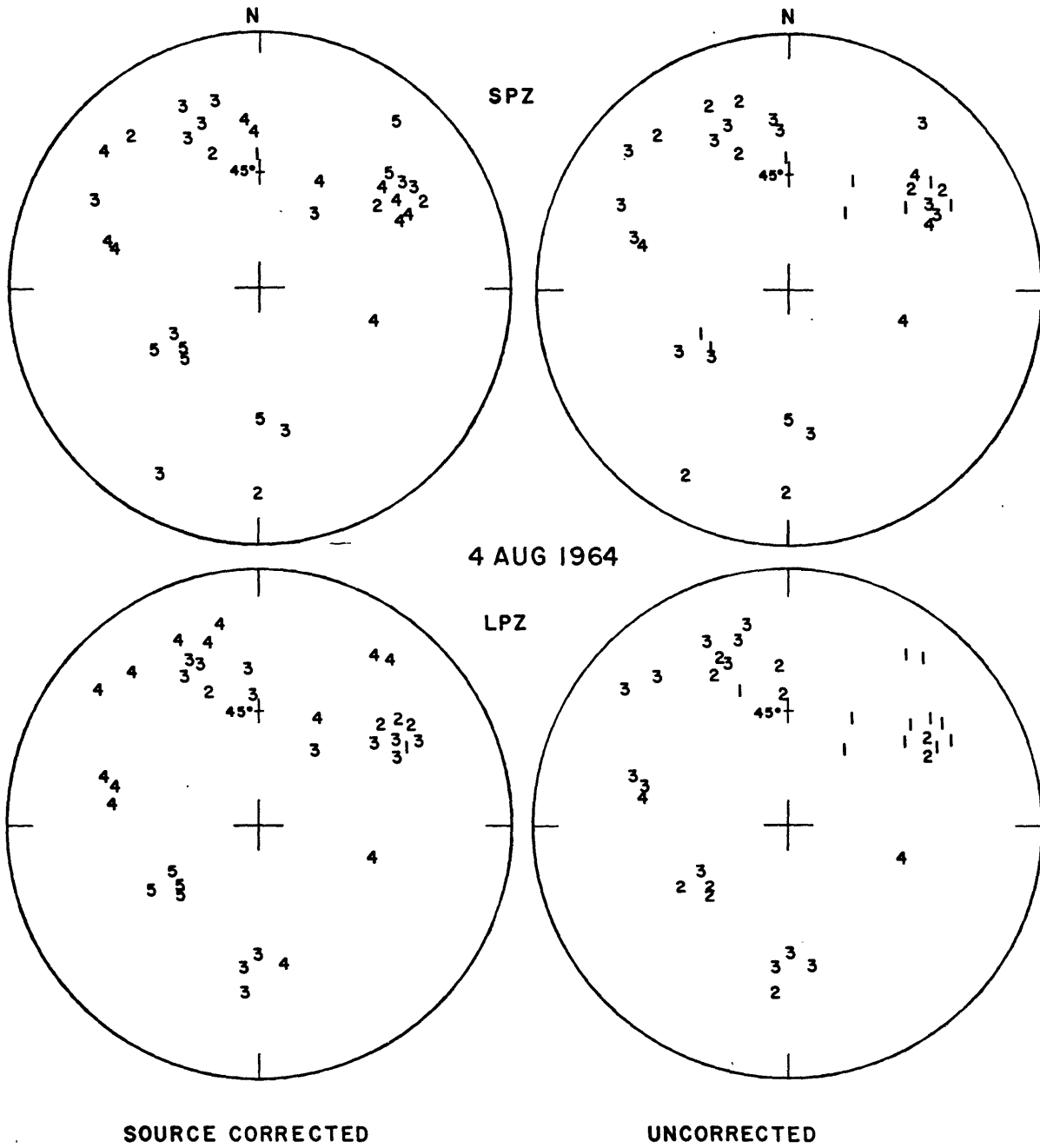
FIGURE 3.28

FIGURE 3.29
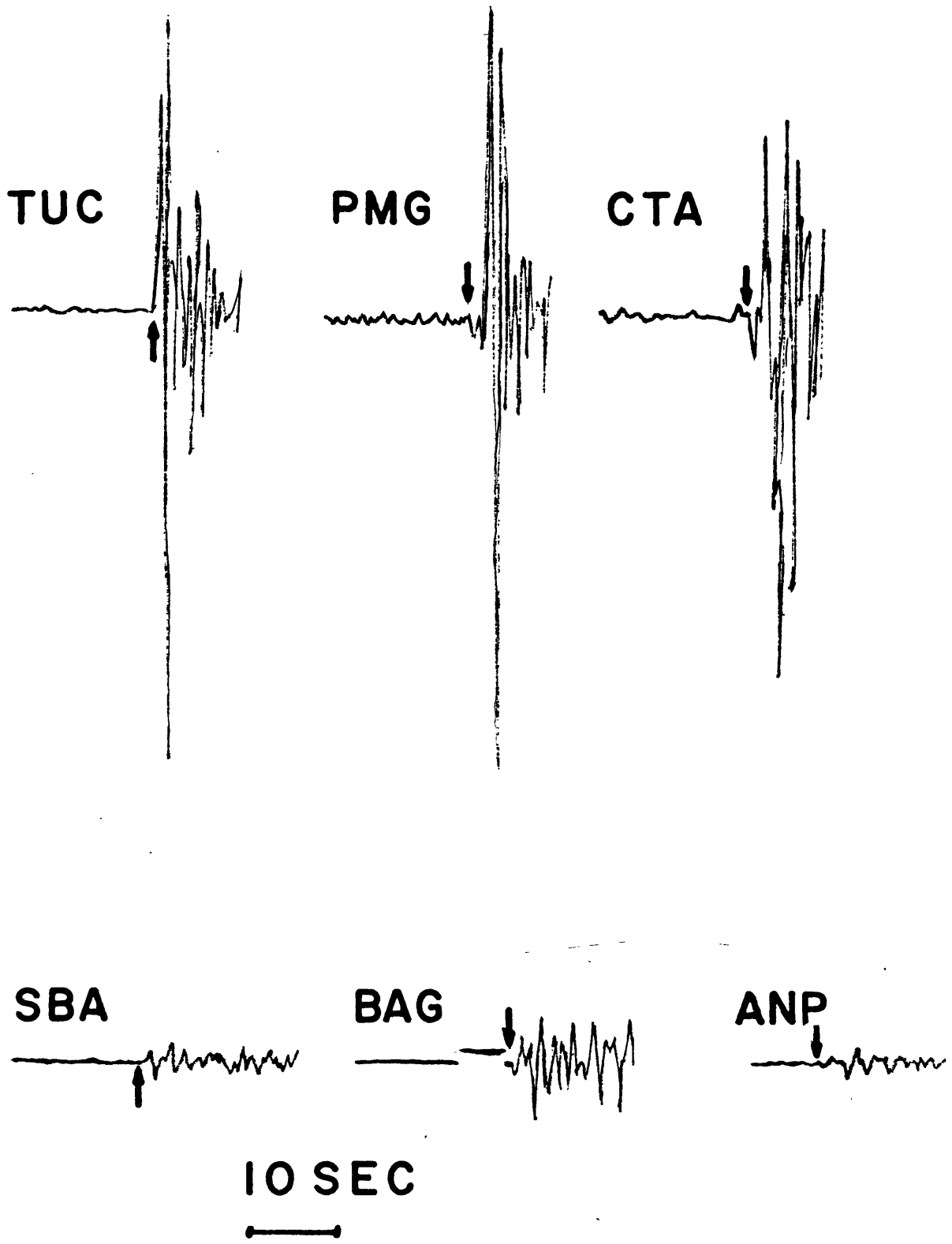
FIGURE 3.30

CHAPTER 4. ISLAND ARC VOLCANISM

Volcanoes, an obvious feature of island arcs, have been extensively studied by geologists and geochemists. Geophysical contributions to the understanding of the processes of generation of magma have been of a more general nature consisting of the gross understanding of the kinematics of plate tectonics (e.g., Isacks et al., 1968) and the delineation of the seismic zone (Benioff, 1955; Sykes, 1966). Numerical convection models (Turcotte and Oxburgh, 1968, 1969; Minear and Toksöz, 1970; Toksöz et al., 1971; Hasebe et al., 1970) do not have the resolution to give a definitive answer. The purpose of this chapter is to apply the laws of heat and mass transfer to the problem of the origin of the primary magmas for island arc volcanics. Numerical and analytical models will be constructed to test the feasibility of various hypotheses by comparison with observed data. Geochemical sampling of eruptives, the extent and duration of volcanism, and geophysical data relating to the stress and thermal structure beneath island arcs are relevant to the origin of island arc volcanics. The usefulness of geochemical data is enhanced by low and high pressure geochemical experiments. Geophysical experiments, however, are so generally intractable that numerical and mathematical modeling of the processes provides more lucid results.

There is little agreement on the ultimate origin of
the magma which erupts on island arcs other than that a
mantle process, rather than partial melting of the crust
under the island arc, is involved. Possible origins
suggested in current literature include (See Figure 4.1):

1. Partial melting of subducted material

    a. Partial melting of the basaltic, oceanic
       crust at the top of the subducted plate (T.
       Green and Ringwood, 1968a, 1969; Taylor, 1969;
       Fitton, 1971).

    b. Partial melting of the subducted oceanic crust
       with the addition of subducted ocean sediments
       (Coats, 1962; Hess, 1965; Rayleigh and Lee,
       1969).

    c. Upward migration of water from the downgoing
       slab thereby lowering the melting point of
       the mantle (McBirney, 1969).

2. Melting due to frictional heating related to earth-
   quakes on the fault plane which separates the down-
   going slab from adjacent mantle (McKenzie and
   Sclater, 1968; Turcotte and Oxburgh, 1969; Oxburgh
   and Turcotte, 1971; Minear and Toksöz, 1970;
   Hasebe et al., 1970).

3. Upwelling of material from the asthenosphere
   related to tectonic stresses (Gorshkov, 1969a,b,
   1970; Isacks et al., 1968).

4. Concentration of pre-existing magma in the astheno-

      sphere by inhomogeneities or hydrodynamic forces

      (Scheinmann, 1968, 1971).

These hypotheses are by no means naturally exclusive.
Direct geochemical evidence of subducted oceanic crust or
sediments alone could be sufficient to appraise hypothesis
1. Hypotheses 2 and 3 imply melting at similar depths in
the mantle. If the melting point of the volcanics is not
greatly reduced as in hypothesis 1, geochemical evidence
would be little help in choosing between hypotheses 2 and
3. Numerical modeling of the physics of frictional heating
along the fault plane and of the nature of tectonic forces
associated with the slab is more relevant. The physics
governing the separation of a partial melt from an ultra-
basic mush are relevant to all the hypotheses.

4.1 Data and constraints

Island arcs and their volcanics have been extensively
studied for various purposes. Data which are useful for
establishing constraints on the physical and chemical nature
of the source region of the volcanics are most relevant to
the purpose of this paper. Little attention will be given
to work relating to near surface processes. Abundant
geological and petrological data forms the framework within
which the more sophisticated results of geochemistry and
geophysics must be considered.

4.1.1 Geology and petrology of island arc volcanics

Unlike mid-oceanic and seamount lavas, which erupt with limited duration at one location of the crust within zones of tension, most island arc volcanics erupt on the same part of the crust for tens of millions of years in zones of compression (Matsuda and Uyeda, 1971). Extensive study and classification of magmas has indicated that several varieties erupt on island arcs, the more voluminous of which are not found elsewhere (e.g., Kuno, 1966).

A group of eruptives from a single volcano or a group of closely spaced volcanoes over a limited period of time is known as a petrographic series, whose variations are assumed to be caused by near surface differentiation. Although intermediate members of the series are most abundant, the parental magma is generally believed to be the most basic member of the series which is not a cumulate (Kuno, 1966, 1969). Four petrographic series are associated with island arcs.

The calcic, pigeonitic, or island arc tholeiitic series is low in potassium and shows iron enrichment during the middle states of differentiation (Peacock, 1931; Kuno, 1950, 1966; Jakes and Gill, 1970; Joplin, 1964). The differentiation sequence ranges from "tholeiitic" basalt through granophyre. When present, the pigeonitic rock province is the most seaward and has a sharply defined volcanic front (Kuno, 1966; Sugimura, 1967, 1968; Matsuda and Uyeda, 1971).

Approximately 85% of island arc volcanics are pigeonitic (Sugimura, 1968; Jakes and White, 1971). Pigeonitic provinces include the South Sandwich islands (Baker, 1968a), Tonga islands (Bryan et al., 1972), the central Kurile islands (Gorshkov, 1970), and the seaward belt in Japan (Kuno, 1950).

The calc-alkaline, or hyperthenic, or andesitic rock series has moderate amounts of potassium and shows little iron enrichment during the main part of differentiation (Peacock, 1931; Kuno, 1950, 1966; Joplin, 1964). This sequence includes high alumina basalts, sensu-stricta andesites, dacite, and rhyolites. About 12% of all island arc volcanics belong to this series (Sugimura, 1968; Jakes and White, 1971). Recent calc-alkaline rocks are found, for example, in the Aleutian islands (Coats, 1962; Forbes et al., 1969), the Cascade mountains (McBirney, 1968; Kuno, 1969), and Japan, where pigeonitic rocks occur in close proximity (Kuno, 1950, 1966). A continuous gradation may exist between the two series (Kuno, 1966). Pigeonitic rocks are commonly believed to be the first eruptive on young island arcs (Baker, 1968a; Jakes and Gill, 1970; Bryan et al., 1972). On the Aleutian islands, however, volcanic activity began 1.8 my ago (Hayes and Ninkovich, 1970), yet the volcanics are calc-alkaline, not pigeonitic.

Rocks of the nepheline normative alkaline series erupt far inland from the arc (Sugimura, 1968; Kuno, 1966).

The shosonitic series of Joplin (1964) is a subclass of this series. The alkaline series also occurs in non-orogenic areas with a similar mode of emplacement (Forbes and Kuno, 1965).

The other series sometimes found on island arcs is the Andean series (Joplin, 1964; Jakes and White, 1971) which includes voluminous rhyolitic ignimbrites. Strontium isotope studies indicate that these rocks originate from the melting of continental crust (McBirney and Weill, 1966).

Both pigeonitic and calc-alkaline volcanics are sufficiently voluminous to build island arcs in oceanic areas. A significant portion of the continental crust may form these rocks (e.g., Dickinson and Luth, 1971; Taylor and White, 1966; Jakes and White, 1971). The mantle between the crust of the arc and the slab could only be a transient source of island arc volcanic, since only a small fraction (ca. 2%) yield of these volcanics is possible from average mantle composition (Armstrong, 1971). Either the more enriched elements in island arc volcanics are added from subducted material or the depleted residuum is somehow removed after differentiation.

The eruptives further inland appear to have fractionated at greater depths and constitute smaller fractions of the source material (e.g., Kuno, 1966; Jakes and White, 1970). "Incompatible" elements such as potassium are more abundant farther inland. These trends have been ascribed to partial

melting at progressively deeper levels along the seismic
zone (e.g., Kuno, 1968; Jakes and White, 1970; Dickinson
and Hatherton, 1967; Dickinson, 1968; Hatherton and
Dickinson, 1969; Fitton, 1971; Green, 1972). Alternatively
the material heated along the seismic zone may ascend for
some distance as a diapir before melting occurs (Green and
Ringwood, 1967a). It is expected that any direct evidence
for melting on the fault plane would be subtle, since the
eruption temperature of island arc volcanics including
calc-alkaline andesites is not greatly reduced in comparison
with basalts (Osborn, 1969b). Geochemical and isotopic
evidence relevant to this problem is reviewed below. A
brief review of relevant high pressure experiments and
geophysical data also follows.

4.1.2 Geochemistry

Calc-alkaline magmas are most likely to show chemical
evidence of subducted material since they are richer in
"incompatible" elements. However, the effects of near-
surface fractionation on these magmas are not thoroughly
understood.

The differentiation of calc-alkaline magmas is in-
fluenced by high water content, and possibly by high alkali
and silica content of the parent magma. The initial com-
position of the parent magma has been difficult to determine
since the phenocrysts in an eruptive may have formed at

different water and oxygen fugasities than the bulk of the
cumulate. Proposed parental magmas vary from high-alumina
basalt to andesite itself. Direct evidence of the source
region is lacking as peridotite xenoliths are not found
in calc-alkaline rocks and high pressure, 10 to 20 kb,
garnets are only found rarely (Green and Ringwood, 1969b).
It is sometimes contended that a silica rich andesitic
magma could not ascend through the mantle since it would
react with olivine in the wall rock (Osborn, 1969b). How-
ever, once a reaction rim was established in the conduit
the reaction rate would be very low.

Low pressure petrological experiments have been dif-
ficult to perform since it is necessary to control the
oxygen fugacity as well as the partial pressure of water.
Vapor transport, which may be important in nature (Anderson
and Gottfried, 1971), is difficult to measure in the
laboratory. Much confusion has resulted since it has not
been considered that the observed eruption temperature and
liquidus of andesite are close to those of basalt, about
1200°C (Osborn, 1969b).

Minerals commonly observed in ejected cumulate blocks
and calc-alkaline gabbros include magnetite, titanous
aluminous hornblende, calcic plagioclase, olivine, calcic
clinopyroxene, apatite, biotite and sphene. If care is
taken, it is possible to fit major element compositions of
andesites to a differentiation model of the observed

phenocryst from high-alumina basalts (Baker, 1968b; Osborn, 1969b,c; Anderson and Gottfried, 1971). Petrological experiments have confirmed that plagioclase precipitating from a hydrous melt is calcic (Yoder, 1965, 1969; Osborn, 1969b). The association of plagioclase and olivine in cumulates limits the depth of fractionation to 20 km (Yoder, 1969).

Osborn (1969a) favors the country rock as the source of the water in calc-alkaline melts. This seems unlikely since recent calc-alkaline rocks are found only on island arcs, but intrude a variety of rock types which would have different porosities and permeabilities with respect to water and are found inland of and in close association with pigeonitic rocks intruding the same rock types.

Trace element compositions in calc-alkaline rocks are difficult to reconcile with the fractional crystallization of andesite from high-alumina basalt magma. Vanadium and scandium which would be depleted by magnetite precipitation, are not strongly depleted in andesites with respect to the associated high-alumina basalts. Other "normally" concentrated elements (K, Rb, Cs, Ba, rare earth elements, Th, U, Zr, Hf, and Li) are not greatly enriched in andesite with respect to the associated high-alumina basalts. Nickel contents of high-alumina basalts and andesites are low but similar (Taylor and White, 1966; Taylor, 1969; Taylor et al., 1969a,b; cf. Osborn, 1969c). On this evidence, Taylor

(1969) proposes a source region depleted in refractory elements with a composition of one part basalt to two parts peridotite.

4.1.2.1 Daughter isotopes

Relatively unambiguous evidence on the source region of volcanics can be obtained from isotopic ratios of heavy elements, which are not effected by chemical reactions. Most importantly remobilized continental crust (or subducted sediments) can be identified by measuring the ratios of stable daughter elements formed from the decay of long lived parents. Strontium (87) (from rubidium decay) and lead (206, 207, 208) (from thorium and uranium decay) are most useful. The daughter elements in the continental crust have more radiogenic isotopic ratios than in the mantle, since parent elements have been preferentially concentrated in the crust with respect to the mantle (Hurley, 1968a,b).

It is now evident that most island arc volcanics contain too few radiogenic isotopes to be formed only from remelted continental crust or by extensive mixing of continental material with basalt (Hedge, 1966; Ewart and Stipp, 1968; Lewis, 1968; Pushkar, 1968; Kurasawa, 1968; Yoder, 1969; Tatsumoto and Knight, 1969; Hedge and Knight, 1969; Tatsumoto, 1969; Gill, 1970; Hedge et al., 1970; Peterman et al., 1970b,c). The strontium Sr (87/86) ratios for island arc volcanics generally range between 0.7030 and 0.7045 (Hedge

et al., 1970; Peterman et al., 1970b,c; Gill, 1970; Yoder, 1969; Pushkar, 1968), although in some areas more radiogenic ratios of about 0.7060 have been observed (Pushkar, 1968; Ewart and Stipp, 1968). Abyssal tholeiites generally are less radiogenic than island arc volcanics having Sr (87/86) ratios of 0.7010 to 0.7030 (Hart, 1971; Ozima et al., 1971; Hedge and Peterman, 1970). Hawaiian basalts, seamount basalts, and certain continental basalts have the same range of strontium isotopic ratios as island arc volcanics (Laughlin et al., 1971; O'Neil et al., 1970; Peterman et al., 1970a, Powell and Delong, 1966; Ozima et al., 1971; Leggo and Hutchinson, 1968). Continental rocks generally have Sr (87/86) ratios greater than 0.7100.

Lead isotopes in island arc volcanics are generally more radiogenic than in abyssal tholeiites (Figure 4.2) (Tatsumoto, 1966a,b; Hedge and Knight, 1969; Tatsumoto and Knight, 1969; Armstrong, 1971). Tatsumoto (1969) stated that Japanese alkali basalts are less radiogenic than Japanese tholeiites; however, only three points were available for alkali basalts and the distributions of both rock types overlap.

Lead isotopic ratios have been used to show that island arc volcanics originate from a mixture of subducted oceanic sediments and abyssal basalts (Armstrong, 1971; Armstrong and Cooper, 1971; Tatsumoto, 1969). When Icelandic basalts and basalts from small oceanic islands are considered, the

case becomes much less convincing. In Figure 4.2 it is
evident that the Pb (206/204) vs. Pb (208/204) co-ordinates
of abyssal tholeiites and island arc volcanics overlap. The
distribution of lead isotopes in island arc volcanics and
Icelandic volcanics is similar. Some rocks from small
Atlantic islands are much more radiogenic than island arc
volcanics (Oversby and Gast, 1968, 1970).

The scatter in lead isotopic ratios is due to mantle
inhomogeneities, possibly related to convection and previous
episodes of differentiation (Oversby and Gast, 1970;
Oversby et al., 1971; Armstrong and Cooper, 1971). Two-stage
model ages for lead found on oceanic islands are about 2 by
(Oversby and Gast, 1970; Oversby et al., 1971).

Isotope studies thus confirm the conclusion of trace
element studies that the source region of island arc
volcanics is enriched in non-refractory elements. This is
compatible with but not necessitating the incorporation of
subducted material into the volcanics.

Mid-ocean ridge basalts alone cannot be the parent or
the source regions of island arc volcanics, since potassium,
heavier alkalis, vanadium, and radiogenic lead and strontium
are much more abundant in island arc volcanics than mid-
oceanic basalts (Taylor et al., 1969a; Armstrong, 1971).

4.1.2.2 High pressure geochemistry of calc-alkaline rocks

High pressure petrological experiments have been

hampered by the lack of knowledge of the primary melt which forms the calc-alkaline series.

Some type of multistage process may be necessary to form calc-alkaline melts, since silica saturated magmas cannot form under dry conditions at pressures exceeding 5 kb (O'Hara, 1963a,b; Boyd and England, 1963). Under wet conditions both high-alumina basalts and andesites can form from mantle rocks in the lithosphere, 10 to 30 kb (O'Hara, 1965; Yoder, 1969). Andesitic melts can also form from the partial melting of a quartz eclogite at 80 to 150 km depth or from the fractional crystallization of a hydrous basalt between 15 and 80 km depth (Green and Ringwood, 1967, 1968a, 1969). The melting temperature of the hydrous andesites produced by Green and Ringwood (1968a, 1969) is probably too low when compared to the observed eruption temperature of calc-alkaline rocks.

The range in depth, 30 - 150 km, of differentiation for island arc volcanics implied by these experiments is so broad that no useful constraints on the genesis of these volcanics can be obtained.

4.1.3 Geophysical data

The distribution and focal mechanisms of earthquakes in the seismic zone beneath island arcs are too well known to need a review. Other geophysical data relevant to the problem of the origin of island arc volcanics and also of

intra-arc spreading includes studies of the seismic velocity and attenuation beneath island arcs, heat flow measurements, and electrical conductivity measurements. The mechanism and distribution of earthquakes located away from the seismic zone is more relevant to the origin of intra-arc basins (Chapter 5).

Geophysical data indicates that the upper most mantle beneath western Japan is exceptionally hot and possibly partially molten. Heat flow values often exceed 80 erg/cm^2-sec (Uyeda and Horai, 1964; Matsuda and Uyeda, 1971). Low seismic velocity and high seismic attenuation exist in the upper most mantle of this region (see Utsu, 1971 for a review). The deep electrical conductivity is also high (Rikitake, 1969).

Metamorphic rocks from similar regions in the geologic record show the effects of metamorphism with a high geo-thermal gradient (Dewey and Bird, 1970; Oxburgh and Turcotte, 1970; Matsuda and Uyeda, 1971). Partial melting at the base of the lithosphere sometimes produces voluminous rhyolitic ignimbrite deposits (McBirney and Weill, 1966; Pushkar et al., 1972). It should be noted that the volcanics which actually erupt do not constitute a major part of the heat budgets of island arcs (Sugimura, 1968).

Compressive stress in the region of island arc volcanoes must impede the ascent of magma at least to some extent. (Alkaline volcanics ascend rapidly to the surface and

probably erupt in zones of tension as in non-orogenic

environments.) It would therefore be expected that the

magmas which eventually erupt are more differentiated than

they would otherwise be. There is little evidence, however,

relevant to the relationship between transient variations

in local stress associated with the occurrence of great

earthquakes and volcanism. Tokarev (1971) was unable to

detect any correlation between earthquakes and volcanoes in

the Kurile region other than a correlation for the entire

arc. He believed that the correlation was not a simple

cause and effect because the earthquakes and volcanoes

occurred at opposite ends of the arc. Kanamori (1972) found

a correlation between eruptions of a volcano near an arc-

arc-arc triple junction and great earthquakes on the arcs

not associated with the volcano. In this case the volcano

was located immediately in front of a trench and was there-

fore subjected to tension after great earthquakes.

4.1.4 Geological, geochemical, and geophysical constraints

Any physical model of island arc volcanics must be

compatible with the following data:

    A. Island arc volcanics erupt continually within

        zones of compression.

    B. The eruption temperature of island arc volcanics

        is similar to that of basalts.

    C. There is a sharp volcanic front on the seaward

side of island arcs. Inland the volcanics become
more fractionated and less voluminous.

D. The source region of the volcanics is rich in
incompatible or nonrefractory elements and radio-
genic isotopes compared with the source region
of mid-ocean basalts.

E. High heat flow and crustal temperatures sometimes
are associated with island arcs.

The data are sufficient neither to prove nor to reject a
fundamental role of subducted material in island arc vol-
canics. The association of these volcanics with the
subduction process is well established, but available data
appear to be insufficient to directly resolve the problem.

4.2 Theoretical modeling and testing of hypotheses

Physical models of the proposed mechanisms for the
origin of island arc volcanics were constructed for comparison
with observed data. Incorporation of subducted material in
the volcanics, if any, is not sufficient to be of concern
in a thermal model. The physics governing the segregation
of melt from an ultrabasic mush is treated first as it has
relevance to all of the mechanisms under consideration.

4.2.1 Segregation of melt from mush

For magma to erupt at the surface it is necessary for
the partial melt to segregate from the crystal which formed

it. Once a substantial volume of melt is present, it can ascend by elastic crack propagation (Weertman, 1971). This process, however, is too slow for melts trapped between grain boundaries. A small fraction of partial melt can segregate if a hydraulic pressure gradient is present and if the geometry of the grains and the conduit are suitable.

4.2.1.1 Mathematical model of segregation

A model with an analytic solution is available to demonstrate the dimensional dependence of this effect (Figure 4.3). The equations governing the flow in a dike-like region bounded by rigid boundaries and containing two fluids with different viscosities are (Faizullaev, 1969):

$$f_1 \eta_1 \frac{\partial^2 u_1}{\partial y^2} + \chi(u_1 - u_2) = f_1 \frac{\partial p}{\partial x} \tag{4.1a}$$

$$f_2 \eta_2 \frac{\partial^2 u_2}{\partial y^2} + \chi(u_2 - u_1) = f_2 \frac{\partial p}{\partial x} \tag{4.1b}$$

where

  u_1, u_2 - velocity

  f_1, f_2 - fraction

  η_1, η_2 - viscosity

  1, 2 (subscripts) - fluid 1, fluid 2

  y - direction normal to dike

  x - direction of flow

  χ - empirical coefficient

It is evident from the equations that two end member regimes are possible. Both fluids may move at the same rate and obey Poiseuille's law or the less viscous fluid may move rapidly with respect to the more viscous one and obey Darcy's law. The problem of flow induced segregation reduces to determining the transition between these two types of flow, since differential movement of the two fluids is a necessary condition for the less viscous fluid to become enriched downstream.

For an ultrabasic mush, $f_1 << f_2$ and $\eta_1 << \eta_2$. As Darcy's law must be obeyed at the limit of $\eta_2 \to \infty$, the empirical coefficient χ can be identified with the permeability k.

$$\chi = f_1^2 \eta_1 / k \tag{4.2}$$

The permeability, which depends only on the geometric arrangement of the two fluids can be calculated from a variety of assumptions and an expression of the form

$$k = C f_1^3 / s^2 \tag{4.3}$$

where

C - a constant

S - ratio of area to volume

The constant C must in practice be assumed ad hoc for each set of data. For materials having tortuous pores, C can be significantly smaller than the theoretical value of about 0.5. Fortunately, free energy requirements prohibit highly

tortuous grain boundaries in a chemically active system such as an ultrabasic mush. (See Scheidegger (1960) for a detailed review of how equation 4.3 is derived.) Assuming $C = 0.5$ and a-sided cubical grains, equation 4.3 becomes

$$k = f_1^3 a^2 / 72 \tag{4.4}$$

Equation 4.1 can be solved exactly (Faizullaev, 1969). The expression relating the difference in velocities at the center of the flow is sufficient for our purpose of determining in which flow regime an ultrabasic mush is:

$$U = \frac{u_{1max} - u_{2max}}{u_{1max}} = \eta - 1 / \left[\eta - \frac{\eta}{(f_1 + f_2 \eta)} \right.$$

$$\tag{4.5}$$

$$\left. + \frac{H}{2f_1 f_2} \left(\frac{\cosh\left\{ \left(\frac{\frac{f_1}{\eta} + f_2 H}{f_1 f_2} \right)^{1/2} \right\}}{\cosh\left\{ \left(\frac{\frac{f_1}{\eta} + f_2(H-1)}{f_1 f_2} \right)^{1/2} \right\}} \right) \right]$$

where $\eta \equiv \dfrac{\eta_2}{\eta_1}$ $H \equiv \chi h^2 / 4\eta_1 = f_1^2 h^2 / 4k$

For large f_2, η, and H (3) reduces to

$$U = \eta / (\eta + H/f_1) \tag{4.6}$$

A dimensionless constant $P = 2\eta f_1 / H$ thus determines whether there is Darcy flow (P>>1) or Poiseuille flow (P<<1). An

expression of the form of (4.6) also results from
Faizullaev's (1969) solution for flow in a cylindrical
conduit. Substituting the expression derived for permeability one obtains

$$P = a^2 f_1^2 \eta / 9h^2 \tag{4.7}$$

Note that segregation is most likely if the conduit is
narrow, the viscosity of the grains large, or the fraction
of melt large. Adjacent domains in the conduit with
different fractions of melt could segregate independently.

4.2.1.2 Discussion of model

The relatively simple geometry of seamounts and mid-ocean ridges permits a test for gross validity of the
mathematical model for segregation. It is believed on
petrological grounds that magma segregation under mid-ocean ridges begins at about 5% partial melt (Kay et al.,
1970; Ringwood, 1969; Green et al., 1967). In agreement
with this observation a fraction of 3% melt at the beginning
of differentiation can be obtained by using parameters
applicable to mid-oceanic ridges. (The value of η is
approximately the ratio of the viscosity below the asthenosphere (10^{22} to 10^{23} poise, e.g., Cathles, 1971) and
basaltic melts (10^3 to 10^4 poise, e.g., Bottinga and
Weill, 1972).)

$$\eta = 10^{19} \qquad h = 30 \text{ km} \qquad a = 0.1 \text{ cm}$$

The oceanic crust, if it is produced from segregated melt, should be somewhat thicker at low spreading rates where the conduit is narrower. However, this effect is not likely to be large since the increase due to adiabatic decompression of the fraction of melt from 5% to 30% in a small depth range above 30 km (Kay et al., 1970; Ringwood, 1969; Green et al., 1967) would dominate over the dependence of fractionation on conduit width. The observed relatively constant thickness and the composition of oceanic crust are thus compatible with the model.

Magma formed away from ridge axes at seamounts differentiates at greater depths and smaller fractions of melt than magma formed at ridge axes. From thermal considerations only a relatively narrow conduit can exist at depth for a minor source of magma. If only a small fraction of melt segregates, the regions with the highest concentrations of partial melt contribute disproportionally to the magma since the rate of segregation is a strong function of the fraction of melt present. At high concentrations, such as found at mid-ocean ridges, all regions contribute to the melt. The melt erupted on seamounts has more radiogenic isotopes than magma erupted on ridges. For geochemical reasons, radioactive isotopes and therefore their products are found with the lowest melting fraction. A reasonable cause for the postulated heterogeneities is segregation at ridge crests and island arcs during previous cycles of

mantle convection (Armstrong and Cooper, 1971). Viscous flow, such as that commonly observed in metamorphic rocks, deforms inhomogeneities but does not eliminate them. Considerable randomness in mantle composition on a local scale is probable since no fixed cores of convection cells can exist if ridges migrate with respect to trenches. Thus, virtually any mechanism for producing island arc volcanics is compatible with the apparent enrichment of the source region in radiogenic isotopes and nonrefractory elements, as long as segregation occurs at a small fraction of melt. There is no need to require that the radiogenic isotopes come directly from subducted sediments.

A very small conduit thickness is necessary for differentiation segregation of melt from the asthenosphere if the viscosity and fraction of this melt determined from seismic attenuation are not in gross error. For the 1% melt and 10^7 poise viscosity of the melt in this region (Solomon, 1972), a conduit less than a kilometer wide is needed for segregation to occur. (An analytic solution (McKenzie, 1969) indicated that flow this constricted occurs only within a few kilometers of the intersection of the fault zone and asthenosphere. Island arc volcanoes occur over a much larger region.) The permeability of such a material would be so low that little melt could diffuse through it. Assuming

grain size - a = 0.3 cm

specific weight of melt - $\mu = 3 \times 10^3$ dynes/cm^3

viscosity of melt - $\eta = 10^7$ poise

hydraulic gradient - $\Delta \ell' = 0.1$

and calculating the permeability using equation (4.4), a
flux of 1 cm/my of melt results. Unless there is a gross
error in these parameters, no significant amount of melt
could be directly concentrated in the asthenosphere. This
calculation, however, says nothing about the possibility
of non-differentiated material rising from the astheno-
sphere.

4.2.2 The fault zone and frictional heating

The details of the region near the trench where the
slab turns down are probably exceedingly complicated. It
is highly unlikely that the top of the slab remains the
simply stratified section of oceanic sediments, extrusive
basalts, intrusive crust, and mantle that is sometimes
shown in schematic diagrams. The active fault plane
between the island arc and the slab is likely to vary in
location, sometimes entraining parts of the lithosphere
of the arc in the slab, sometimes leaving behind ophilite
complexes. As with most large faults observed in the field
and with ophilites, extensive mixing of material can be
expected.

The existence of a fault plane on top of the slab
is relevant to the production of island arc volcanics and

intra-arc spreading since friction along the fault may
provide a heat source, and in addition, the flow pattern
in the mantle above the slab would be modified by the
existence of any shear zones. A detailed numerical model
is necessary to determine the amount of frictional heating
needed to cause increased temperatures. The conditions for
a shear zone to exist above the slab within the fluid
regions of the mantle can be determined from a simple
analytical model, as can the time necessary for a diapir
of material heated in such a shear zone to ascend.

4.2.2.1 Frictional heating in the rigid mantle

Great earthquakes occur where the slab is thrust
against the lithosphere of the island arc. The hypothesis
that frictional heating along the fault plane associated
with these earthquakes causes melting beneath island arcs
can be tested mathematically, for the relevant parameters
except for the amount of frictional heating are known
reasonably well. It does not matter whether the melting
occurs in subducted oceanic crust or in the mantle since
the temperature needed to produce the observed volcanics
is constrained by their observed high eruption temperatures.
Two variants of the hypothesis are considered: each earth-
quake may melt its own batch of magma; or the heat may
build up continually. The former case results in mechanical
and geochemical difficulties; in the latter case, the mode

which frictional heating is usually assumed to take requires thorough modeling.

The possibility that each great earthquake produces its own batch of magma is very unlikely since the observed mode of volcanism would be difficult to explain. Great earthquakes occur on the order of every 50 years (Kanamori, 1971a). For the hypothesis to work, almost all the melt produced would have to escape from the fault zone before the next earthquake and, also, without losing significant heat to the walls of the fault zone. Almost total melting would be required for the material to flow out in a short time span, thus conflicting with the highly differentiated character of island arc magmas with respect to the mantle and the lack of mantle derived ultra-basic xenoliths in these magmas.

The stress needed to rapidly raise even a thin sheet above its melting temperature is excessive. Assuming a latent heat of 8×10^9 ergs/cm^3, 10 kb of stress are required to melt 5 m layer of rock every 50 years. Unless the flow of material from the fault zone is extraordinarily rapid, most of the heat from a thinner zone would be lost to the sides of the fault zone.

Partial melting near the fault zone may also result from the buildup of heat over long periods of time (Hasebe et al., 1970; Oxburgh and Turcotte, 1970, 1971; Minear and Toksöz, 1970a,b). Stress heating is likely to adjust

itself in such a way that the temperature is at most
slightly above the solidus since appreciable melting re-
duces friction.

Extensive frictional heating on the uppermost 20 or
30 km of the fault plane is unlikely, since those melange
sequences which are believed to form in that environment
exhibit the effects of very low rather than high tempera-
ture metamorphism (e.g., Ernst et al., 1970). Frictional
heating on a shear zone in the more fluid parts of the
mantle is limited by a variation principle which requires
that the frictional energy dissipation on the fault plane
be less than the dissipation which would have resulted if
a great proportion of shear had occurred in the fluid.
There is also the requirement that energy dissipation not
exceed the amount of work available from the convection
process.

Two-dimension numerical models of descending slabs
were calculated with different amounts of frictional
heating near the fault plane (Figure 4.4). Approximately
6.4×10^{-4} ergs/cm^3-sec of heating in a 14 km wide shear
zone were needed to produce an 80 km deep region of
slightly elevated temperature. Less than a million years
are needed for the temperature to reach dynamic equilibrium.
A detailed numerical model with a grid spacing of 2.5 km,
a 3.5 km wide shear heating zone, and a translation dis-
tance of 5 km confirms that the amount of frictional

heat required for melting is relatively independent of the
shear zone and that the less detailed numerical models
were reasonably accurate (Figures 4.5 and 4.6). For normal
subduction rates, the stress required to produce melting
is independent of subduction rate; most of the heating goes
into heating the moving slab and frictional heating is
proportional to velocity at constant stress.

The frictional heating in both the more and the less
detailed models is equivalent to a stress of 4 kb at the
assumed subduction rate of 8 cm/yr, about the same as
deduced by Minear and Toksöz (1970). There is no obvious
violation of the conservation of energy or the variational
principle for viscous flow, since frictional heating is
necessary only next to the lithosphere of the island arc.

The calculated value of stress is high compared to
the apparent stress drops of about 100 bars which define
a lower limit of stress for thrusting earthquakes (Brune,
1968, 1970; Wyss, 1970). This value is, however, in
agreement with the stress required to produce the observed
uplift on the outer rise of the Japan trench (Hanks, 1971).

Great thrusting earthquakes are less frequent in
regions where a low velocity zone has developed between
the crust of the arc and the slab (Kanamori, 1971a). It is
difficult to see how a shear zone could continue to pro-
duce significant amounts of frictional heat after such a
large zone of heated mantle has developed above it. Once

a moderate viscosity region developed above the slab, forced convection would begin if the stress of the fault plane was high enough to cause melting. Widespread high temperatures in the uppermost mantle beneath island arcs indicated by geophysical measurements, by the eruption of voluminous products of crustal anatexis and by the implacement of granite batholiths are too hot to be explained by frictional heating above the slab.

This does not preclude frictional heating along the fault plane providing the heat source of volcanism on young island arcs where the crustal temperatures are not high. Minor amounts of frictional heating may also be important in material which is already hot for some other reason. A mechanism other than or in addition to frictional heating is needed to explain the association of high lithospheric temperatures with island arc volcanism.

4.2.2.2 Shear zones in fluid mantle

A brief examination of the physics controlling a shear zone is in order as hypotheses under examination propose the existence of a shear zone above the slab in the fluid parts of the mantle. Equations for the velocity and temperature distribution in a shear zone have been solved by Turcotte and Oxburgh (1968). For the purpose of this paper the conditions necessary for the existence of the shear zone, itself, are more relevant.

The variational principle for viscous flow limits the amount of viscous heating in the shear zone. An attempt to increase the amount of viscous heat generation in a shear zone by decreasing its thickness or increasing its viscosity would cause a large amount of the flow to concentrate outside the shear zone. The total amount of heat generation with a low viscosity shear zone cannot exceed the amount with the shear zone absent.

An analytical solution is easily obtained to approximate this effect. Let the region above the slab be modeled by two fluids bounded by parallel planes, a shear zone with viscosity η_1 and thickness d_1 and the normal mesosphere with viscosity η_2 and thickness d_2. Stress is conserved at the boundary between these fluids

$$\eta_1 v_1/d_1 = \eta_2 v_2/d_2 \tag{4.8}$$

where v_1 and v_2 are the velocity changes across each fluid. The total energy dissipation in each of the fluids is given by

$$\eta_1 v_1^2/d_1 \tag{4.9}$$

Substituting for v_1, the ratio of energy dissipation in the shear zone to the energy dissipation in the entire region is

$$E = \eta_2 d_1/(\eta_1 d_2 + \eta_2 d_1) \tag{4.10}$$

Setting $E = 0.95$ and $d_1/d_2 = 0.05$, the ratio of the viscosities is 380. As this ratio is well within the range of

viscosities normally considered in earth models it is not unreasonable to presume that a shear zone is present above the slab in the asthenosphere. However, assuming a normal mesosphere viscosity of 10^{23} poise (e.g., McConnell, 1968; Cathles, 1971) and a distance from the slab to the lithosphere of the arc of 150 km, the maximum stress that could result would be 2 kb for 8 cm/yr spreading. If the shear zone in the example developed, the stress would drop to 100 bars. Frictional heating would then be too small to maintain any excess temperature in the shear zone. The shear zone however might be maintained by a strain rate dependent viscosity.

It is thus unlikely that a thermal maximum could result from shear heating adjacent to the slab in the mesosphere. Since the viscosity of the asthenosphere is about 10^{20} to 10^{21} poise, significant frictional heating in the asthenosphere is even less likely.

Even if a thermal maximum did result from frictional heating adjacent to the fluid part of the mantle, the time required for a thermal diapir to rise from the shear zone is geologically significant. This can be seen by modeling the diapir with a fluid sphere. The rate of ascent is then

$$u = R^2 \Delta \rho g / 3 \eta_2 \tag{4.11}$$

R is the radius of the sphere. The density difference due to the maximum possible viscous heat generation is (setting

d_1 = 2R and assuming no heat is lost)

$$\Delta\rho = \rho t v^2 \alpha \eta_2 / (C_p 2Rd_2) \qquad (4.12)$$

where t is the time of heating. By assuming that heating

and ascent are concurrent, one can set $u = d_2/t$ to obtain

$$t^2 = 6C_p d_2^2 / Rv^2 \rho g \alpha \qquad (4.13)$$

Setting   specific heat $C_p = 10^7$ erg/°C-gm

thickness of mesosphere d_2 = 100 km

radius of diapir R = 50 km

velocity of subduction v = 10 cm/yr

acceleration of gravity $g = 10^3$ dynes/gm

coefficient of thermal expansion $\alpha = 4\times10^{-5}$°C^{-1}

density ρ = 3 gm/cm^3

one obtains that 10 my are required for a diapir to form

and rise. Note that the estimate is independent of

viscosity and that the model and the parameters were chosen

to minimize the ascent time and that any heat loss by

conduction was ignored. It thus is both unlikely that

significant frictional heating could occur adjacent to the

slab below the lithosphere and that a thermal diapir could

rise from that zone of heating in a reasonable time.

In partially molten regions below the island arc

where the viscosity of the melt and the geometry of the flow

are conducive to segregation, any additional heat due to

friction would increase the fraction of melt, thereby con-

tributing to the volcanism. As shown above, the asthenosphere

is not likely to be a region favorable for segregation.
A large increase in the percentage of melt would, therefore,
be required for any melt to ascend directly from the astheno-
sphere to the surface. Shear heating in the fluid part of
the mantle, therefore, is even less likely to cause island
arc volcanism, than heating in the shear zone between the
lithosphere of the island arc and the slab. Even if some
shear heating did occur, it is unlikely that the heated
region would rise as a diapir or that the additional melt
could segregate directly from it.

4.2.3 Intrusions from asthenosphere

Intrusions of the asthenosphere into the lithosphere
of island arcs may be the source region for island arc
volcanics (Gorshkov, 1969a,b, 1970). The feasibility of
this hypothesis is somewhat hard to appraise since the
lithosphere beneath the volcanic belt is the most difficult
region to represent, since the stress pattern there is not
constrained by abundant direct evidence and since con-
tinuous flow and brittle fracture are possible means of
deformation in its lower portion. (A problem of semantics
exists here since the lithosphere is commonly considered
rigid. Clearly, lithosphere and asthenosphere are artificial
divisions. Rather than create new terminology, high vis-
cosity upper asthenosphere is used herein to refer to the
region near the base of the lithosphere which is much more

viscous than the asthenosphere, yet subject to significant deformation.) Calculation of the shape and extent of the intrusion is difficult without some direct evidence since brittle fracture may cause intrusions to penetrate cooler parts of the lithosphere.

If flow is induced in the high viscosity upper asthenosphere, hotter, less viscous material rising from the asthenosphere would replace the material entrained with the slab. This process would be somewhat self-generating, since new intrusions would raise the temperature of the lithosphere beneath the arc, increasing the area subject to coupling with the slab. An adequate source of magma could result this way since depleted residuum would be later entrained with the slab and carried away. The entrained material probably continues down to a considerable depth since the forced convection cell would become depleted in magma and heat if it were too tightly closed.

The problem of determining whether the asthenosphere intrudes the lithosphere of island arcs thus reduces to determining whether the high viscosity upper asthenosphere can deform at a rate such that the intruding asthenosphere can supply the observed magma and excess surface heat flux. Analytical models giving the rate of flow induced by coupling of the high viscosity upper asthenosphere and the slab and the rate of flow needed to maintain high crustal temperatures were constructed. A numerical calculation was made to

obtain the general geometry of the flow.

4.2.3.1 Mechanical model for flow in high viscosity
upper asthenosphere

Models of flow in the high viscosity upper astheno-
sphere are difficult to construct since relevant mechanical
properties and boundary conditions are not evident. It
may be reasonably expected, however, that viscosity would
vary continuously with depth and that a region having a
viscosity 2 or 3 orders of magnitude higher than the
asthenosphere exists near the base of the lithosphere.
Theoretical viscosity calculations assuming solid state
creep indicate that this region would be 10 or 20 km thick
(Weertman, 1970). It is easy to show that the amount of
friction, calculated to cause melting on the fault between
the lithosphere of the island arc and the slab, would in-
duce significant flow in such a region. For example,
assuming that

stress on the fault = 3 kb

viscosity = 10^{23} poise

thickness of high viscosity upper asthenosphere = 10 km

a flow of 1 cm/yr results directly from the definition of
viscosity. Stresses of this magnitude might also cause
faulting in the lithosphere adjacent to the slab.

A numerical model was computed to simulate flow caused
by coupling of the slab to the high viscosity upper

asthenosphere (Figure 4.7). A no-slip boundary was assumed to exist between the asthenosphere and the slab and the lower lithosphere was assumed to be partially coupled to the slab. An approximately equidimensional eddy resulted in the upper more viscous region probably due to the different boundary conditions in the two layers. Calculations in Chapter 5 indicated that viscosity stratification alone was insufficient to cause a separate eddy in the higher viscosity region. Other models calculated using different boundary conditions along the slab in the upper layer gave geometrically similar flow patterns as long as some coupling along the boundary was assumed.

If the gross shape of the flow pattern calculated above is correct, that fraction of melt in the flow would increase seaward since melting curves being steeper than adiabats cause the fraction of melt to increase upward in an ascending material (Figure 4.8). The volume of magma erupted would thus increase seaward. The fraction of incompatible elements in the erupted magma, such as potassium, would increase landward since these elements are most enriched if a small fraction of melt is formed. A sharp volcanic front could form at the turning point of the flow as it would be difficult for differentiation to occur in the descending part of the flow where the material is cooler and the fraction of melt is decreasing.

The flow pattern actually present is probably more

complicated, since brittle fracture in the lithosphere of the island arc may permit irregular and intermittent flow into cooler regions. These intrusions would be favorable regions for magma segregation due to the smaller dimensions of their conduits. Heat lost by conduction during the cooling of an intrusion into a cooler part of the lithosphere would increase the regional temperature, the surface heat flux, and the region below the island arc capable of viscous flow.

4.2.3.2 Thermal considerations on flow in high viscosity upper asthenosphere

If material which intrudes from the asthenosphere to replace the material in the high viscosity upper asthenosphere that was entrained with the slab is the source region for island arc volcanism, the velocity of upwelling must be great enough for the material to remain hot. An analytic solution is easily obtained to show that flow at a small fraction of observed subduction rates can remain hot if it upwells beneath island arcs. Heat lost to the surface from this flow, an obvious source for the observed high flow on island arcs, is a limiting factor on the depth of the top of the upwelling.

$$q = K(\frac{T}{z} - \frac{T}{\ell}) \tag{4.14}$$

q = heat flux at surface

T = temperature of asthenosphere

K = thermal conductivity

z = depth of top of upwelling

ℓ = thickness of asthenosphere

This heat must be balanced by heat brought up by convection.

$$q = \rho c v T r \qquad\qquad (4.15)$$

ρc = volume specific heat

v = vertical velocity in upwelling

r = fraction of cooling of convection of material

Solving for V, one obtains

$$V = \kappa \left(\frac{\ell - z}{z \ell r}\right)$$

κ = thermal diffusivity

Letting

r = 1/10

$\kappa = 0.01 \ cm^2/sec$

ℓ = 100 km

z = 50 km

one obtains an average velocity of 0.3 cm/yr.

The heat lost from the flow would continually raise the temperature near the base of the lithosphere, increasing the region subject to viscous flow. This attrition of the lithosphere would reach equilibrium either when the heat lost to the surface by conduction balanced the heat brought up by mass transport or when melting of the lower crust caused efficient heat transfer to the surface. The growth of the asthenosphere at the expense of the lithosphere

might take several million years if the induced flow was
a moderate fraction of the subduction rate, say about
1 cm/yr. No obvious mechanical or thermal difficulties
therefore arise from the suggested flow of the astheno-
sphere into the lithosphere of the island arc. Unlike
the mechanism of frictional heating, intrusions from the
asthenosphere could provide a source of magma and the
observed high heat flow on island arcs.

4.3 Summary and conclusions

Four classes of hypotheses for the origin of island
arc volcanics: (1) melting temperature lowered by subducted
material; (2) frictional heating on fault zone; (3) up-
welling of material into the lithosphere of island arc;
and (4) concentration of pre-existing melt in asthenosphere
were appraised by constructing physical models for com-
parison with observed data. To be valid, an hypothesis
should be compatible with the following characteristics
of island arc volcanism.

(A) <u>Continual eruption with zone of compression</u>.
This volumetric constraint is satisfied easily by hypo-
theses (1) and (2) since a new source region is continu-
ously supplied by subducted material. For hypothesis (3)
reflux of material from the lithosphere back into the
asthenosphere must be postulated for the source of

volcanics to be adequate. Hypothesis (4) seems to imply

insufficient generation of magma.

(B) <u>High eruption temperature</u>.

This eliminates hypothesis (1) as far as thermal models

are concerned although some subducted material could be

incorporated in the magma, without greatly modifying the

melting point.

(C) <u>Sharp volcanic front and landward diminution</u>

<u>of volcanism</u>. Hypotheses (1) and (2) can be expected to

satisfy this since less melting would occur at greater

depths. Hypothesis (3) is compatible as the intrusion

would be shallower nearer to the arc. It is difficult

to explain the widespread nature of volcanism with

hypothesis (4).

(D) <u>Enriched incompatible elements in source region</u>.

Any of the hypotheses would satisfy this because regions

with greater fractions of melt contribute disproportionately

to the final melt if segregation occurs at small fractions

of melt.

(E) <u>High heat flow and crustal temperatures</u>.

Only a large scale flux of material from the asthenosphere

seems capable of causing this. A hot region between the

slab and the crust of an island arc would reduce friction

on the fault plane. The friction necessary to cause melting

would also probably induce flow in the lower lithosphere.

It is conceivable that frictional heating may be important

beneath island arcs which do not have high crustal temperatures. Friction might also increase the temperature of previously hot material which upwelled from the asthenosphere.

It may thus be concluded that serious objections exist to all the hypotheses except induced flow beneath the island arc. Unfortunately this hypothesis is most difficult to model physically, since protracted mathematics and unknown physical parameters would be involved. Flow voluminous enough to be the source of island arc volcanics could reasonably occur beneath island arcs, but little can be said on the detailed geometry of such flows without additional direct data.

FIGURE CAPTIONS

Figure 4.1   Schematic diagram shows proposed origins of
island arc volcanics. Upper left: subducted
oceanic crust or sediments melt at a reduced
temperature. Lower left: frictional heating
along the fault plane raises the temperature
until melting occurs. Upper right: pre-
existing magma in the low velocity zone is
concentrated by the geometry of the slab or by
hydrodynamic flows in the flow pattern. Lower
right: material from the low velocity zone
intrudes the lower lithosphere and partially
melts as it rises.

Figure 4.2   Initial Pb (208/204) is plotted against initial
Pb (206/204) for various recent volcanic rocks.
No correction has been made for inter-labora-
tory biases. Island arc volcanics: small
open circles (Armstrong, 1971); small filled
circles, Japan (Tatsumoto and Knight, 1969);
"V", Vesuvius (Oversby and Gast, 1968), and
filled squares, alkali basalts (Tatsumoto,
1969). Oceanic volcanics: large open circles,
Tristan island (Oversby and Gast, 1968); open
squares, Azores islands (Oversby, 1971);
vertical diamonds, Canary islands (Oversby
et al., 1971); open triangles, Easter island

(Tatsumoto, 1966); and horizontal diamonds, mid-oceanic tholeiites (Tatsumoto, 1966a,b); and "I" Iceland (Welke et al., 1968). Note that the isotope ratios of island arc and oceanic volcanics overlap.

Figure 4.3   Schematic diagram of the model used to obtain the conditions necessary for melt to segregate from a mostly crystalline mush. The grains and the melt (speckled) are assumed to act as two viscous fluids whose interaction is governed by the relative viscosity of the materials, the width of the conduit (h) and the grain size (a). Rigid boundary conditions are assumed at the edges of the conduit.

Figure 4.4   Slab models were calculated numerically with a 20 km distance translation on a 10 km grid spacing for various amounts of frictional heating applied between 40 and 90 km depth. The upper figures show the slab after 1.1 my of 8 cm/yr subduction. The lower figures are after 2.1 my of subduction. The amount of frictional heat corresponds to stresses of 4, 3, and 1 kb from left to right. Note that a region of excess temperature is present in the leftmost model.

Figure 4.5   Detailed thermal model of a slab sinking at

8 cm/yr shows the effects of large amounts of

frictional heating. Heat equivalent to a stress

of 4 kb is applied in a 3.5 km wide shear zone

at the top of the slab between 40 km and 90

km depth. A region of temperature sufficient

to cause partial melting has formed by 1.42 my.

The calculation technique is described in

Chapter 2.

Figure 4.6   Detailed thermal model in Figure 4.7 after

0.30 my more subduction. Above: the

frictional heating continues down to 120 km.

Below: the frictional heating is stopped at

90 km. Note that the heated region corresponds

to the high temperature region above the slab.

Figure 4.7   Substantial flow in the high viscosity upper

asthenosphere induced by a small amount of

coupling with the slab. The viscosity of

the upper fluid is 1000 times the lower fluid.

In this model the slab is assumed to be com-

pletely decoupled from the high viscosity

upper asthenosphere except within a short

distance of the asthenosphere-upper asthenosphere

boundary. The details of the flow pattern in

the upper region are sensitive to the choice

of boundary conditions although the geometry
of the pattern is not. Note that the flow in
the lower region is similar to the flow in
Figure 5.5. The width of the upper eddy is
the same order as the thickness of the upper
fluid. The numerical method used to compute
the model is described in Appendix A.

Figure 4.8   Schematic diagram shows the preferred hypo-
thesis for the origin of island arc volcanics.
Material near the base of the lithosphere be-
comes entrained with the slab and is carried
to depth. Material from the low velocity zones
ascends to take its place and melts due to
adiabatic decompression. The volcanoes which
tap the flow near the turning point are most
active since the fraction of partial melt
is highest there. Volcanoes farther landward
are less voluminous and tap a partial melt
richer in incompatible elements. The residuum,
a depleted mantle, is returned to depth
completing the cycle.

FIGURE 4.1

Lead isotopes
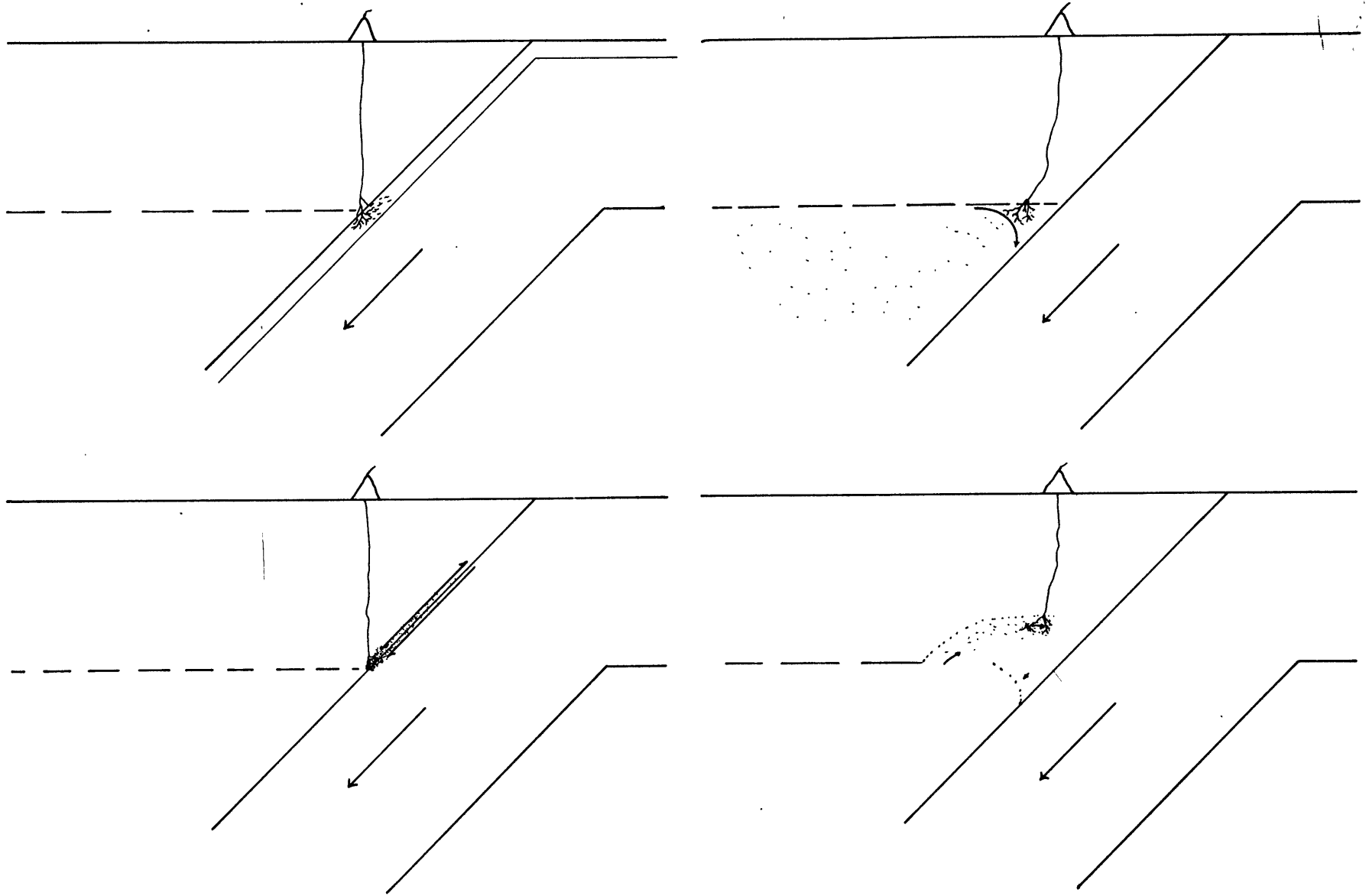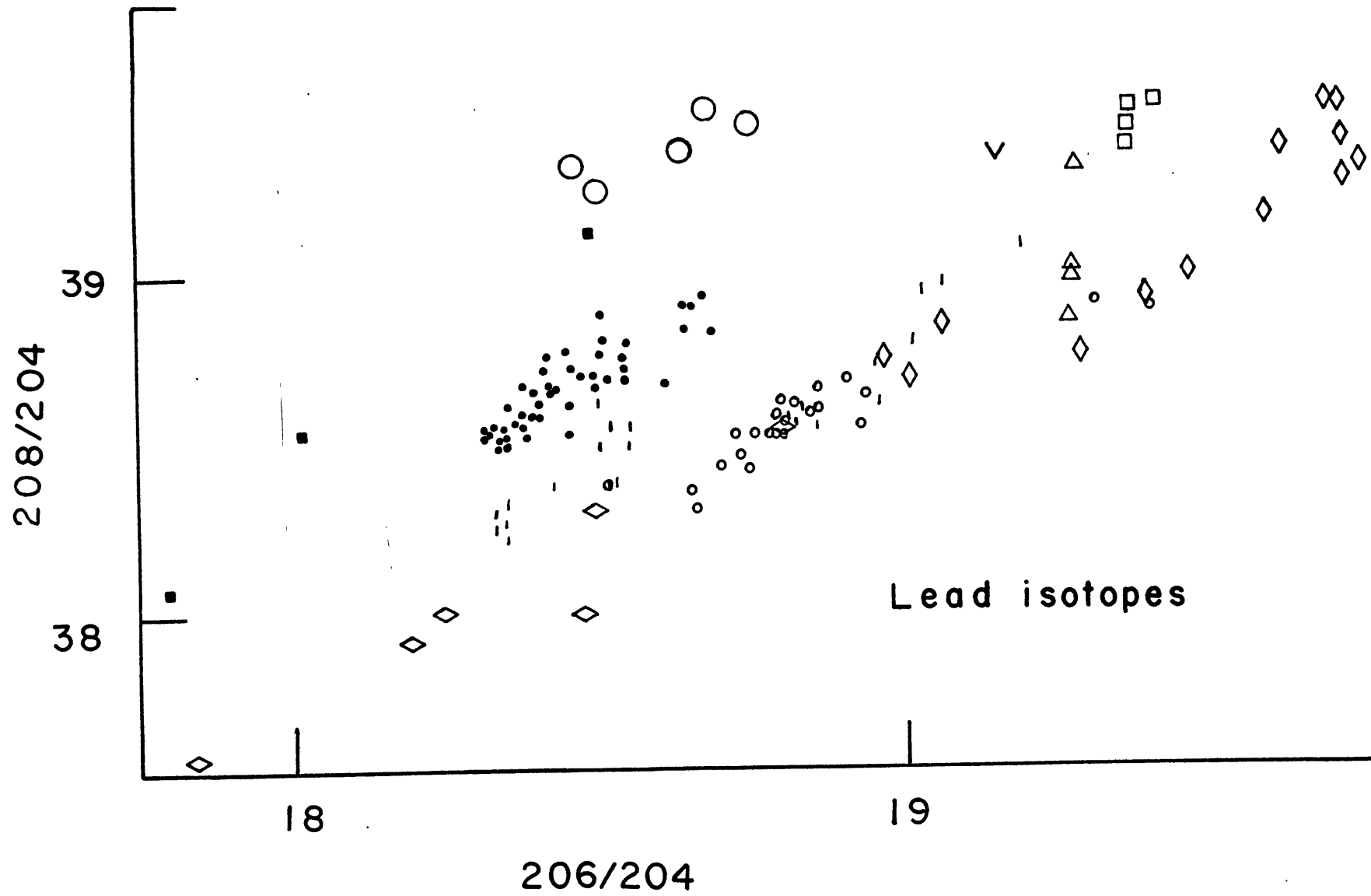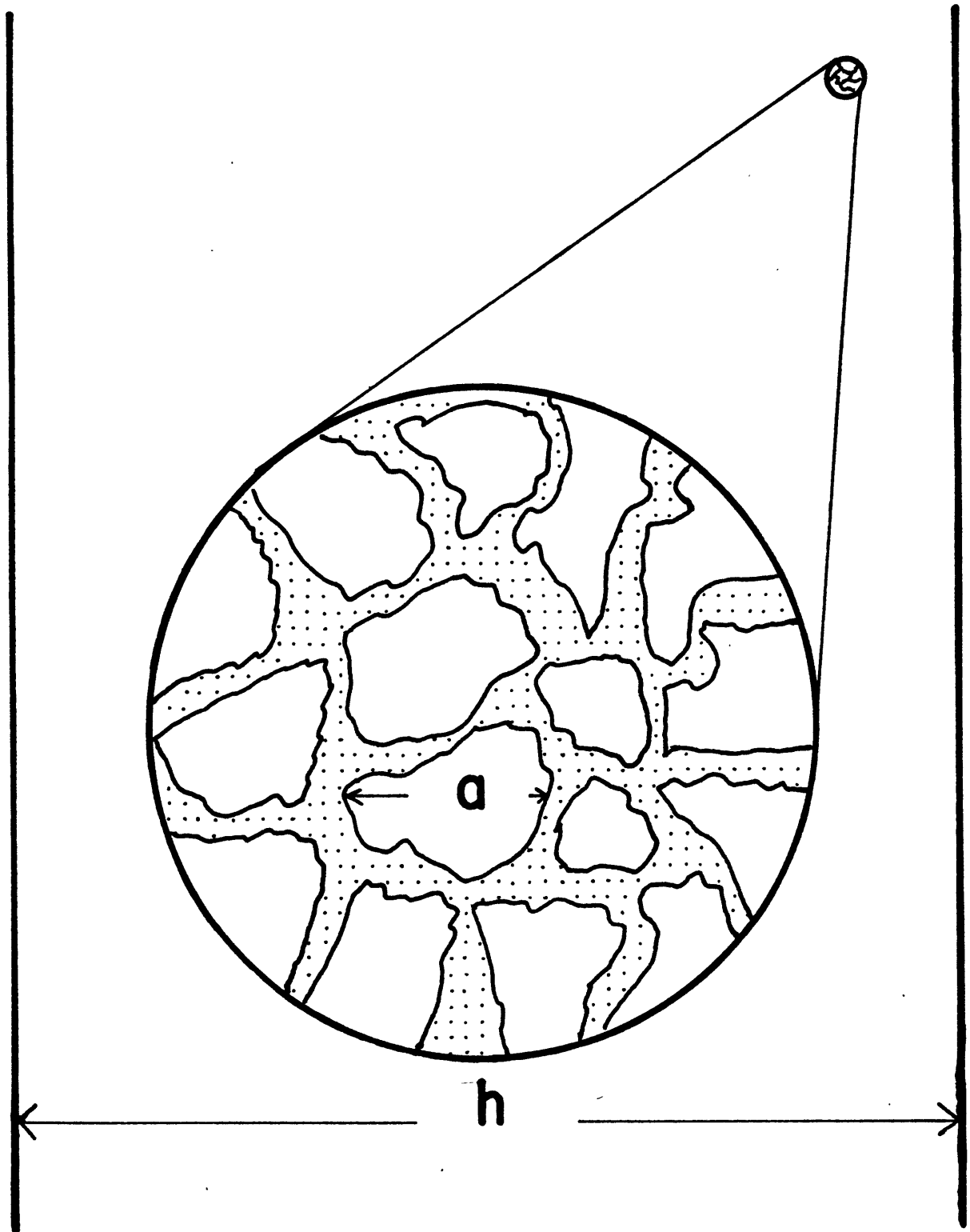
FIGURE 4.2

FIGURE 4.3
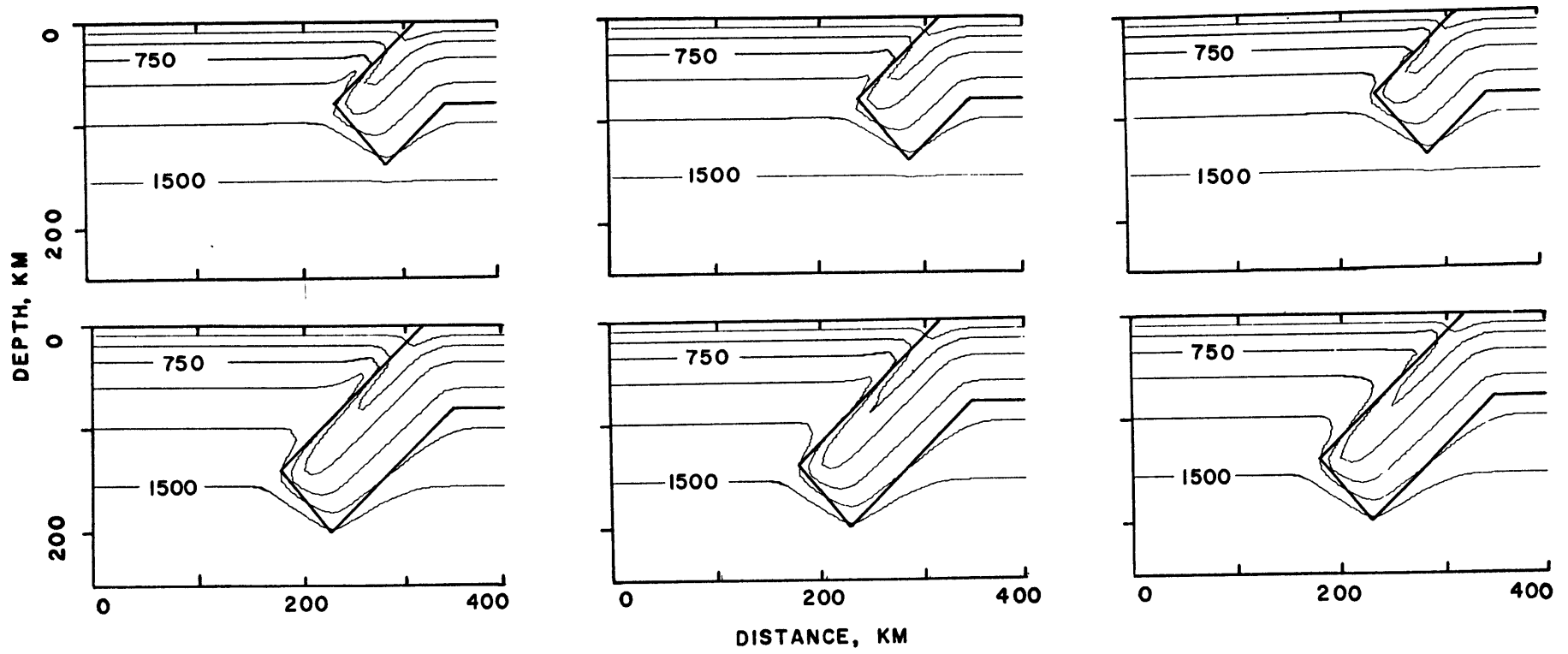
FIGURE 4.4
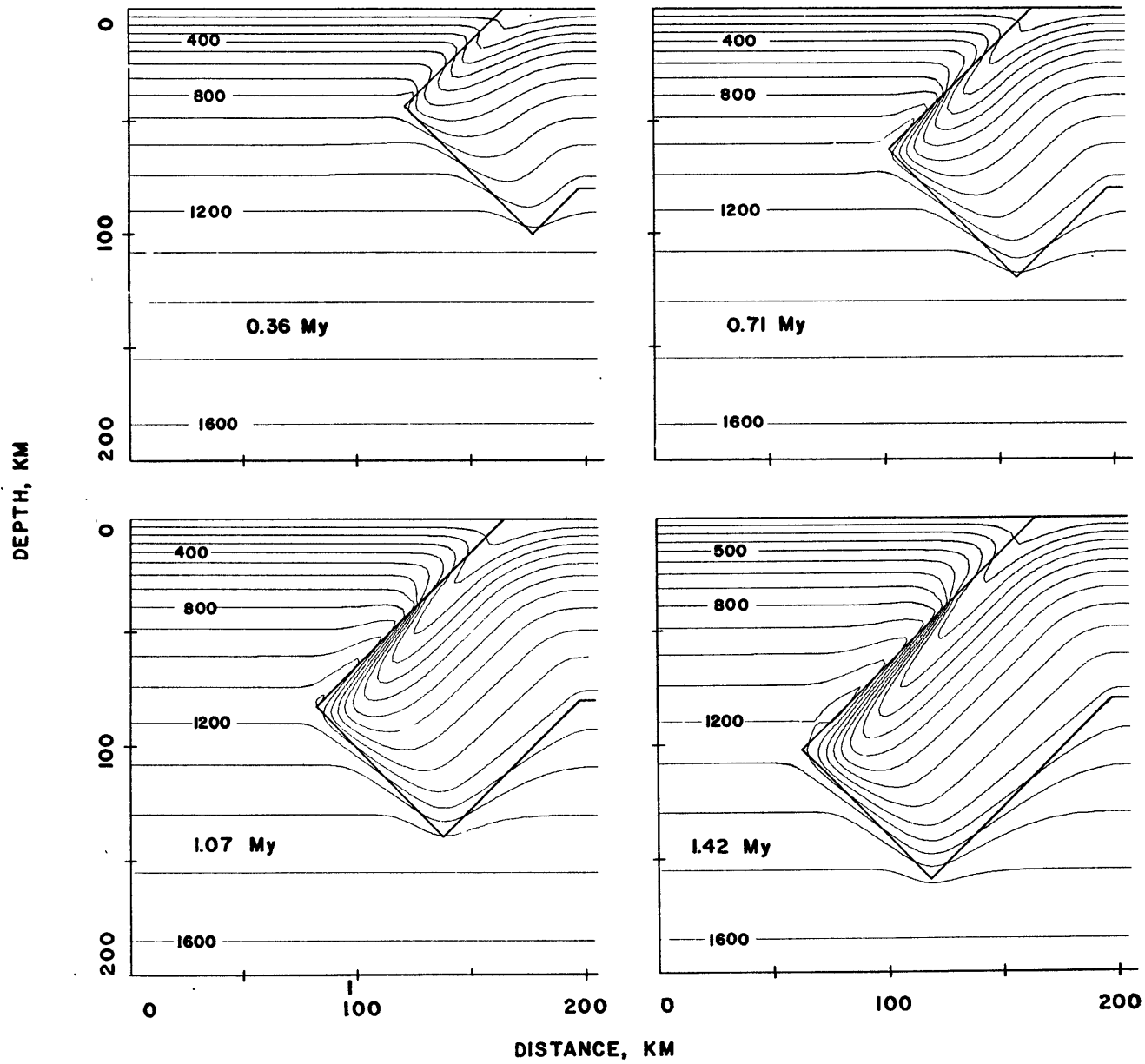
FIGURE 4.5
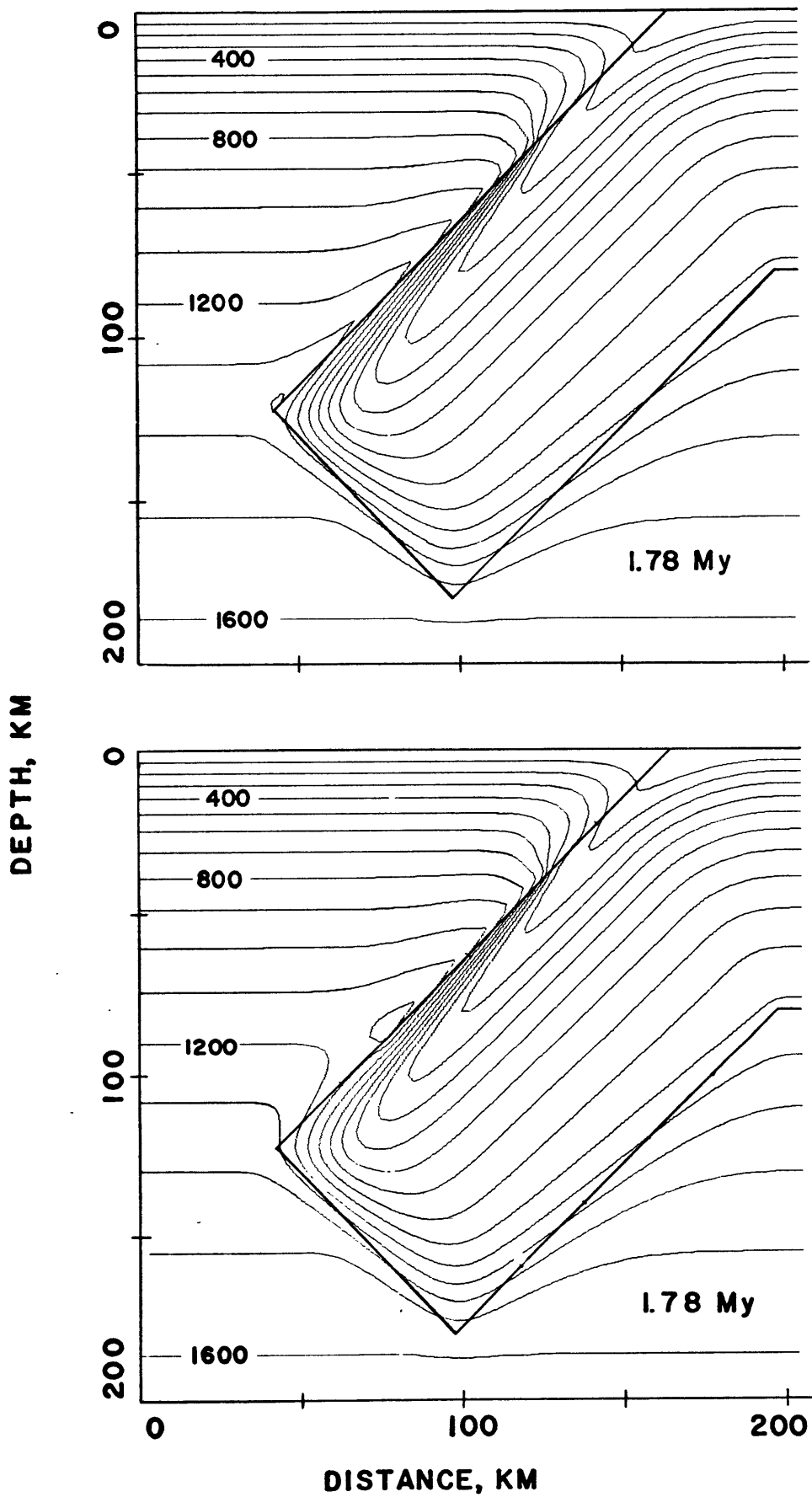
FIGURE 4.6
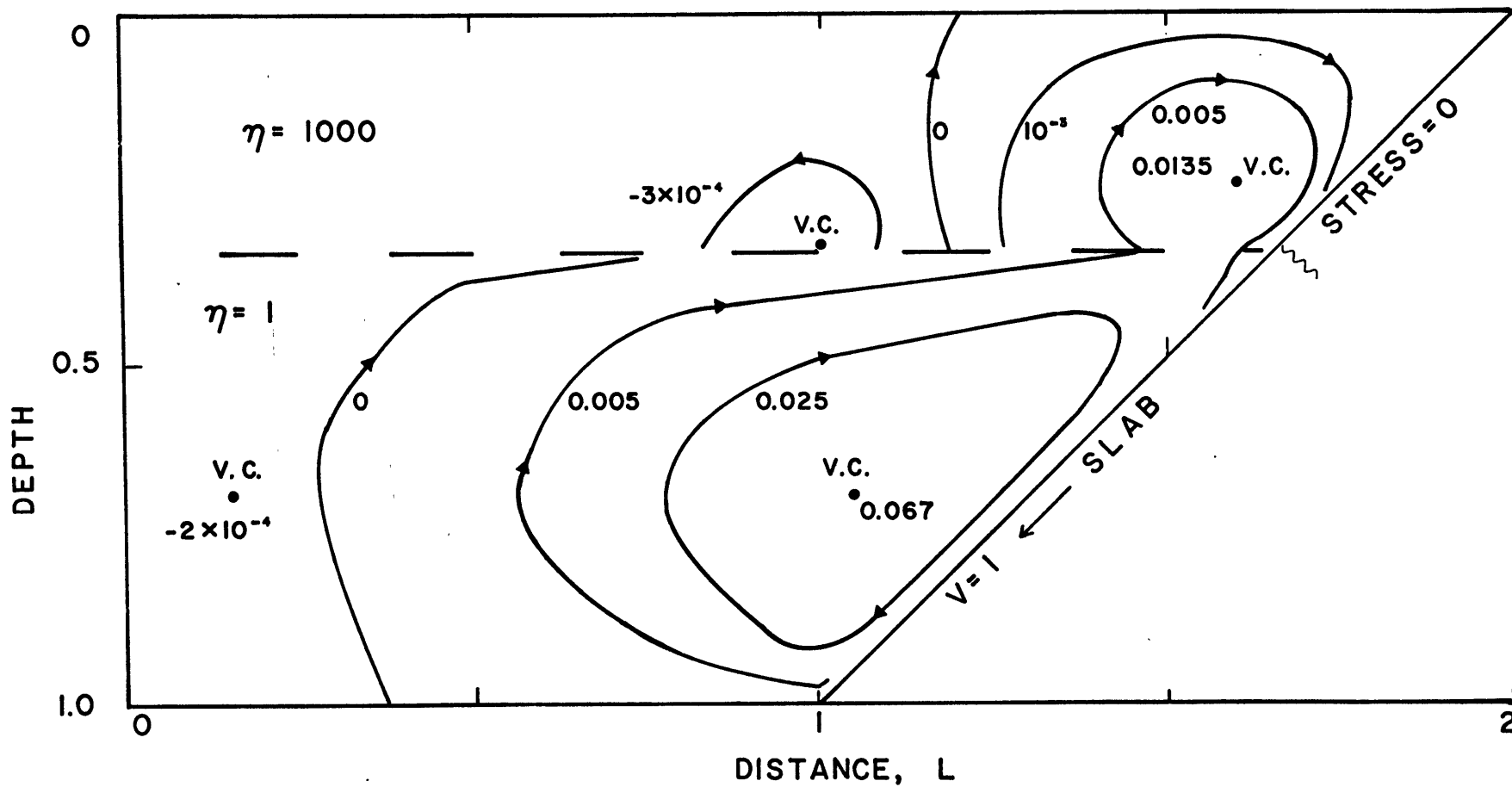
FIGURE 4.7
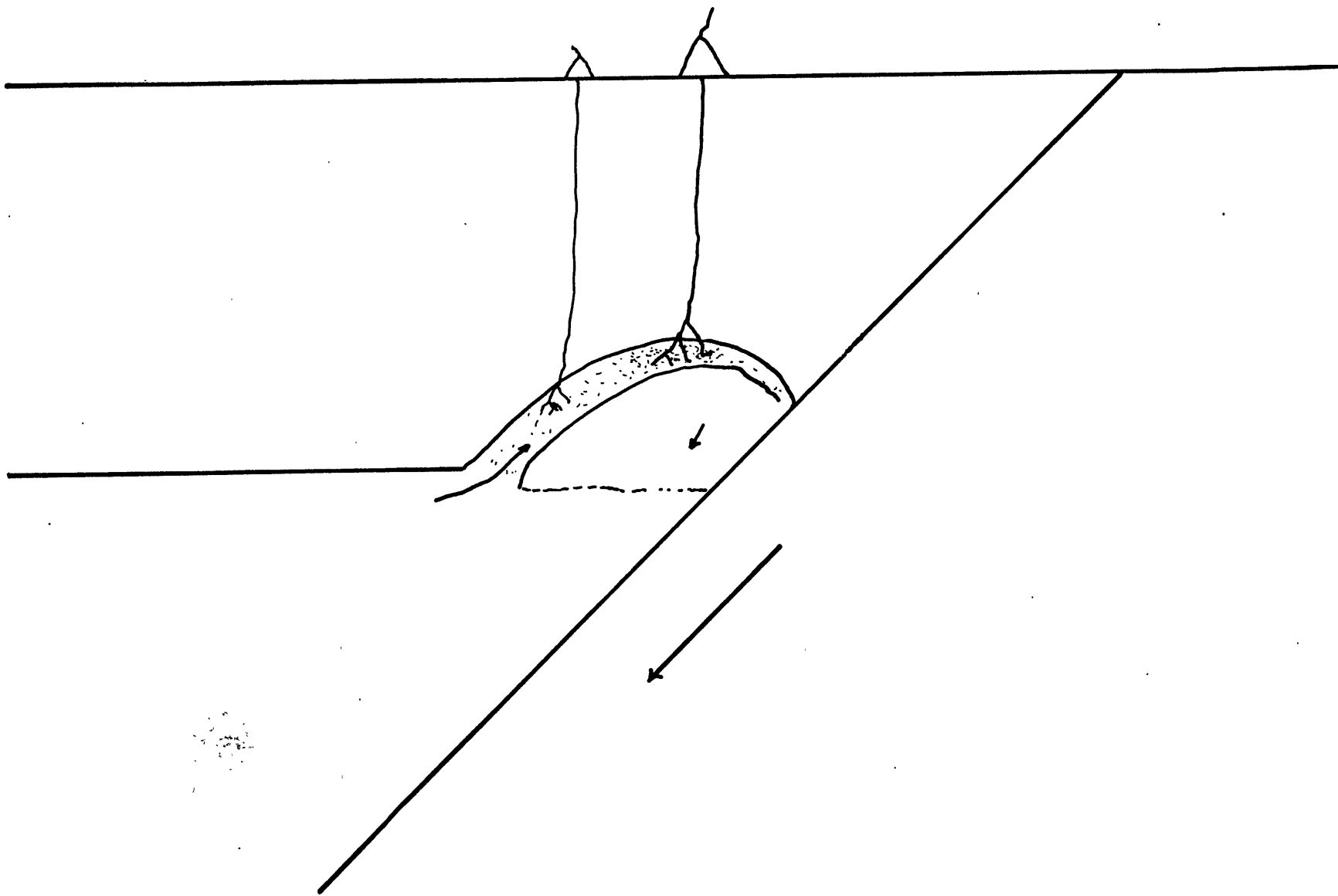
FIGURE 4.8

CHAPTER 5. INTRA-ARC BASINS

Small basins, floored by oceanic crust, often exist behind island arcs (Menard, 1967; Karig, 1970). Most of these basins are in the western Pacific, including the Sea of Okhotsk, the Sea of Japan, and the Lau-Havre basin. Other such basins include: the Andaman Sea behind the Indonesian arc, the Aves basin behind the Lesser Antilles arc, the Tyrennian Sea behind the Calabrian arc and the basin behind the south Sandwich arc. The basins are generally less than a few hundred kilometers wide. Some are much narrower, including the Taupo depression, a continuation of the Lau-Havre basin into New Zealand, the Okinawa trough, and the Bouldir depression, behind the Aleutian arc.

Vening Meinesz (1951) first considered these basins in relation to convection currents in the earth. Recent advances in global tectonics and a large accumulation of oceanographic data have resulted in interest in these basins (e.g., McKenzie and Sclater, 1968; Karig, 1970). A discussion of the origin of these basins is in order since proposed mechanisms for their origin are similar to those proposed for island arc volcanics. The physical models developed in Chapter 4 are directly relevant to this problem.

5.1 Spreading origin of intra-arc basins

Although it is possible that certain intra-arc basins may be underlain by older oceanic crust trapped behind a younger arc, geological evidence such as anomalously thin sediments, truncation of older geologic features, and freshly erupted basalts (Belousov and Rudich, 1961; Rodolfo, 1969; Karig, 1970, 1971a,b, 1972; Karig and Glassley, 1970; Sclater et al., 1972) indicates that some type of crustal spreading or oceanization formed the basins. Geophysical evidence including the attenuation of short period seismic waves (Molnar and Oliver, 1969; Barazangi and Isacks, 1971; Utsu, 1971), shallow seismicity (Sclater et al., 1972) and high heat flow (McKenzie and Sclater, 1968; Yasui et al., 1970) support the same hypothesis. Extensive material transport of heat to shallow depths is necessary to explain this high heat flow in intra-arc basins, since heat generated near the slab cannot be conducted to the surface in a reasonable amount of time (McKenzie and Sclater, 1968; Minear and Toksöz, 1970a,b; Toksöz et al., 1971; Hasebe et al., 1970).

The crust in wider intra-arc basins is not distinguishable from crust produced at normal mid-ocean ridges (Menard, 1967; Murachi et al., 1968; Sclater et al., 1972). Magnetic anomaly patterns have been found in the Sea of Japan (Yasui et al., 1967) and the Lau-Havre basin (Sclater et al., 1972) but are not suitable for determining a spreading

history. In some cases geological evidence indicates that the spreading rate is a sizable fraction of the subduction rate at the associated trench (Karig and Glassley, 1970; Karig, 1971a,b). The direction of spreading may not be perpendicular to the arc (Karig, 1972; Sclater et al., 1972). Intra-arc spreading apparently begins on a well-defined fracture about 50 or 100 km landward of the volcanic front as both sides of younger basins are usually bounded by well-developed escarpments which appear to have once been conjunct.

Only limited evidence on the temporal relationship between the initiation of island arc volcanism and intra-arc spreading is available. Geological evidence indicates that spreading in the Sea of Japan began in the Early Miocene soon after the arc became volcanically active (Minato et al., 1965). The Bouldir depression has formed in the Aleutian arc since the Pliocene, although subduction also began as recently as the Pliocene (Hays and Ninkovich, 1970; Burk, 1965).

Horizontal tension probably exists beneath intra-arc basins and compression beneath the volcanic belt as mechanisms of shallow earthquakes are probably compressional normal to the arc near the volcanic belt and tensional in the intra-arc basin behind the arc. In Japan some of the compressional earthquakes are exceptionally large and have many aftershocks (Ichikawa, 1966). In other regions,

earthquakes away from the slab which are large enough to determine focal mechanisms are fairly rare. Two earthquakes in the Andamen Sea, an intra-arc basin behind the Indonesian arc, were extensional. However, the axis of tension of only one of those earthquakes was normal to the strike of the arc (Fitch, 1970). Two new earthquake mechanisms were obtained in this study (Figure 5.1). One earthquake located near the volcanic Tonga arc was compressive (Figure 5.2). The other earthquake located in the Lau-Havre basin behind the arc was tensional (Figure 5.3). The data were not sufficient to resolve the strike of the nodal planes for either earthquake.

5.2 Mechanism of spreading

The mechanism for spreading in intra-arc basins is probably related directly to the descent of the slab. Spreading centers are abandoned after they have migrated away from the arc. Basins occur behind arcs on several plates including both east and west dipping subduction zones in the western Pacific. The mechanism causing the opening of the basin must be secondary to the primary formation of sea-floor, for only about 5% of the earth's oceans are intra-arc basins (Menard, 1967).

Two classes of mechanisms have been proposed. Friction along the fault plane may heat the mantle and cause a

thermal diapir to rise beneath the arc (Hasebe et al.,
1970; Oxburgh and Turcotte, 1971; Karig, 1971; Matsuda
and Uyeda, 1971); or hydrodynamic forces or other stress
related to the descent of the slab may create local tension
beneath the arc allowing hot material from the low velocity
zone to upwell passively (Holmes, 1965; Isacks et al., 1968;
Kraus, 1971; Wiggins, 1971; Sleep and Toksöz, 1971). Data
which establish the existence of spreading in intra-arc
basins are not likely to be relevant in discriminating be-
tween these hypotheses. The time scale on which the
mechanisms operate and the stress distribution which the
mechanisms imply are likely to be useful if compared with
observed data.

There are serious objections to the hypothesis that
frictional heating along the fault plane is the cause of
intra-arc basins. As was shown in Chapter 4, it is highly
unlikely that a shear zone along the slab in the astheno-
sphere or the mesosphere could generate enough heat to
cause a thermal maximum. Even if this heating occurs, it
would take a much greater time than observed for intra-arc
spreading to begin, since the rate with which a thermal
diapir can ascend is low. Induced flow in the mantle
would also tend to convect downward any material heated near
the slab.

Forces related to the descent of the slab are a more
probable cause of intra-arc spreading, although constructing

a physical model is somewhat difficult. Any mechanism of
this type would be compatible with earthquake source mech-
anisms which imply that the stress in the lithosphere near
the fault plane is compressive while the stress further
away is tensional.

A qualitative picture of the forces acting on the
lithosphere of an island arc can easily be obtained. The
lithosphere beneath the island arc is acted on horizontally:
by friction along the fault plane, by viscous coupling to
any forced flow in the asthenosphere, by the component of
pressure normal to the fault plane, and by forces associated
with intra-arc basins or island arc volcanism (Figure 5.4).
The force on the fault plane tends to push the island arc
landward, yet some thought is required to determine the
sign of the other forces. Note that no rigid hinge exists
at point H (Figure 5.4) where the arc turns down. If
extension or contraction of the lithosphere occurs at the
island arc, point H is free to move with respect to the
adjacent continent, point C. The depression associated
with the trench is probably an indication of underpressure
resulting from the viscous head loss associated with the
descent of the slab (Morgan, 1965; Elsasser, 1967). This
underpressure may act across the fault plane putting tension
on the lithosphere at the arc. As shown below, flow in the
asthenosphere at the base of the lithosphere is toward the
slab.

Flow in the asthenosphere appears to be the only one of the forces which could produce tension away from the island arc and compression near it. It is unlikely that underpressure on the fault plane dominates the stress balance, since tension, not the observed compression, would then occur immediately behind island arcs. Friction along the fault plane has the wrong sign.

Numerical and analytical models of the flow induced by the slab were constructed to obtain quantitative constraints on the distribution of flow induced by the descent of the slab and to determine whether this flow could cause intra-arc spreading. Several models of increasing complexity were computed for flow in this wedge shaped region above the slab. These models included: an infinite wedge shaped region of a single viscosity, a region of a single viscosity bounded by a rigid boundary below, a region consisting of two viscous fluids and bounded by a rigid boundary below. The numerical method is described in Appendix A.

The properties of the more fluid parts of the mantle relevant to the calculation of flow induced by the slab are directly constrained from isostatic rebound studies. The viscosity of the upper mantle below the low velocity zone is about 10^{23} poise (McConnell, 1968; Cathles, 1971). The low velocity zone may have a viscosity of about 10^{20} or 10^{21} poise (Crittenden, 1967). The bottom boundary of the low viscosity zone is not likely to convect with the flow

since this boundary is probably controlled by pressure
dependent substitution of $(OH)_4^{-4}$ for $(SiO_4)^{-4}$ (Sclar,
1970). The lower boundary of the lithosphere is determined
by the presence of partial melt. This boundary can convect
with the flow since melting is both temperature and pressure
dependent.

The flow at the lithosphere-slab corner can be approx-
imated by an analytical solution for flow in a wedge shaped
region, since slow viscous flow solutions depend most
strongly on the nearest boundaries (Moffatt, 1964; McKenzie,
1969). The flow in the asthenosphere at the base of the
lithosphere is seaward. Intense underpressure tending to
pull the lithosphere at the arc downward is also produced
by the flow. Unlike horizontal movements, the vertical
movements caused by this force cease when the surface mass
deficiency balances the force. If the lithosphere of the
island arc is modeled as a free surface rather than a rigid
boundary, a maximum velocity of intra-arc spreading of
about half the subduction rate can be obtained from a
similar analytic solution (Moffatt, 1964). No information
on a preferred point of intra-arc spreading can be obtained
from either analytic solution. Models containing some
stratification, therefore, need be considered.

A somewhat realistic numerical model presumes a rigid
boundary at the base of the flow (Sleep and Toksöz, 1971)
(Figure 5.5). The rigid boundary may be thought of as

representing the top of the mesosphere or the top of the lower mantle. In either case for the model to be realistic, insignificant flow must be excited in the lower region modeled as a rigid boundary. A series of eddies inside the region of flow, each about 1.4 zone widths wide, resulted in the calculation. All eddies other than the one nearest the slab are only of mathematical interest since the amplitude ratio of successive eddies is about 1/350 (Moffatt, 1964). A model (Figure 5.6) showed that stratification of viscosity in the mantle would not significantly effect the flow pattern induced by the slab. (For numerical reasons it is easier to calculate steady state flow with the boundary of the fluids fixed. Because the boundary does not move a significant distance in the time mechanical equilibrium is established, the streamlines calculated are valid instantaneous streamlines.) When a shear zone was assumed to exist along the slab in a high viscosity region above the asthenosphere, the flow in the asthenosphere was not greatly altered and an additional eddy developed in the high viscosity region (Figure 4.7).

Each of the three models has a point of maximum tension on the lithosphere of the island arc at the divergence point of the first eddy. Intra-arc spreading would be expected to begin there, unless the point of initial break-up was controlled by weaknesses in the lithosphere of the arc. In the constant viscosity model this region is about twice

the thickness of the asthenosphere from the lithosphere-slab corner. In the two layer, constant slab velocity model, it is about 1.5 thicknesses of the region away from the corner. In the shear zone model (Figure 4.7), the point of divergence is twice the thickness of the upper high viscosity layer from the corner. The former two models place the point of maximum tension too far landward from the observed points of initial intra-arc spreading, although the ultimate widths of intra-arc basins are in agreement with this spreading location. An initial spreading center a few tens of kilometers from the volcanic front, as observed, is predicted by the shear zone model. Theoretical viscosity calculations indicate that the intermediate viscosity region at the base of the lithosphere, which, as in the model might couple partially to the slab across a shear zone, is about 10 or 20 km thick (Weertman, 1970).

Induced flow in the intermediate viscosity region near the base of the lithosphere is a reasonable cause for intra-arc spreading since more traction on the base of the more rigid part of the lithosphere would result from flow of a more viscous fluid. Once started, flow in the high viscosity upper asthenosphere would alter the stress balance in the more rigid part of the lithosphere towards tension since the area of the fault plane between the lithosphere of the island arc and the slab is decreased and the area and

viscosity of the fluid acting on the bottom of the litho-
sphere are increased (Figure 5.7).

The observed self-limiting nature of intra-arc
spreading can be explained qualitatively if this mechanism
causes spreading. Since spreading is more or less symmet-
rical (Sclater et al., 1972), for geometrical reasons the
dip of the slab must decrease if intra-arc spreading occurs
at a significant fraction of the subduction rate. This
would increase the area of the fault plane and also the
percentage of friction contained in the horizontal com-
ponent. This would cause the stress balance to become
more compressive and retard spreading. Once migration has
gone far enough, the stress on the lithosphere near the
trench is too small to cause rapid intra-arc spreading.
Spreading may then either cease or restart at a new spreading
center closer to the arc.

A time dependent convection model thus would be
necessary to model this process in detail. Variations in
the dip and hinge point of the slab, which are relevant to
the problem, would be hard to consider in any tractable
numerical scheme. As often happens involving convection in
the earth, semi-quantitative constraints can be easily
obtained, but any added sophistication would involve a
morass of undetermined free parameters and interminable
mathematics.

Flow from the asthenosphere into the lower part of

the lithosphere, the preferred hypothesis in the previous chapter for the origin of island arc volcanics, appears capable of causing spreading in intra-arc basins. A complete model of this process was too intractable to construct. Frictional heating appeared to be insufficient to cause the secondary spreading. The observed initial axis and limited duration of intra-arc spreading centers are compatible with the preferred hypothesis.

FIGURE CAPTIONS

Figure 5.1   First arrivals determined from WWSS records

for two earthquakes west of Tonga are plotted

on the focal plane projection for shallow

focus crustal earthquakes. Compressions are

indicated by circles and rarefactions by

triangles. The "X" indicates a low amplitude

arrival believed to be near the nodal plane.

Possible fault planes are shown for reference

only. Although the focal mechanism cannot be

unambiguously determined, it is clear that the

earthquake of JUL 21, 1965, is reverse faulting

and the earthquake of OCT 3, 1966, is normal

faulting.

Figure 5.2   The locations of earthquakes for which focal

mechanisms were determined are plotted relative

to other shallow earthquake epicenters indicated

by "X". The Tonga trench is indicated by

stippling. Earthquake A is OCT 8, 1966.

Earthquake B is JUL 21, 1965. (Modified after

Sclater et al., 1972).

Figure 5.3   The location of the earthquake of JUL 21, 1965

(hexagon) is shown in relation to other nearby

earthquakes. Large dots are more accurately

located epicenters. The seismic stations NIU,

TGU, PAG, and EUA are situated on the non-
volcanically active part of the island arc,
while TFA is situated near an active volcano.
(Modified after Isacks et al., 1969.)

Figure 5.4   The lithosphere of an island arc is subjected
to several kinds of horizontal forces.
Friction along the fault plane, σ_{ij}, tends to
push the island arc toward the continent at
point C. Fluid drag, τ_{xz}, at the base of
this lithosphere and the underpressure, P_{ii},
on the fault plane tend to pull the arc away
from the continent. Since no rigid hinge
exists at point H, the trench, point T, can
move with respect to the continent when intra-
arc spreading occurs. Island arc volcanism
and intra-arc spreading cause additional forces.

Figure 5.5   Numerically calculated streamlines in an
asthenosphere bounded above and below by
rigid plates, and by a moving slab are plotted
in dimensionless units. The stress, τ_{xy}, and
underpressure, P, at the base of the litho-
sphere are strongly concentrated near the slab-
lithosphere corner. An intra-arc spreading
axis at the divergence point of the first eddy
is predicted by this model. (After Sleep and
Toksöz, 1971.)

Figure 5.6   Two fluid model for the upper mantle is similar

to the one fluid model in Figure 5.5.   The

viscosity ratio of the upper fluid to the

lower fluid is 1:1000.   If no shear zone

develops in high viscosity regions, viscosity

stratification in the upper mantle would have

little effect on the flow induced by the slab.

Concentration of the flow in the less viscous

fluid, however, is noticeable.

Figure 5.7   Flow in the high viscosity region near the

base of the lithosphere would change the stress

balance in the lithosphere from compressive

(above) to tensional (below) since the area

of the fault plane below the slab and the

lithosphere is decreased and the more viscous

fluid acting on the base of the lithosphere

produces more drag.   This tensional stress is

the suggested cause of intra-arc spreading.
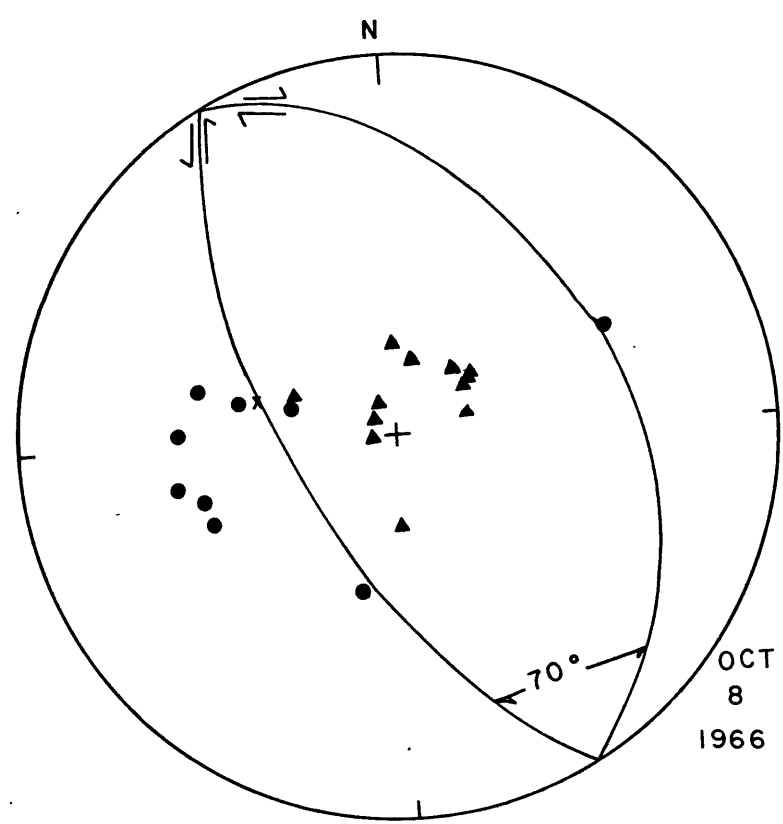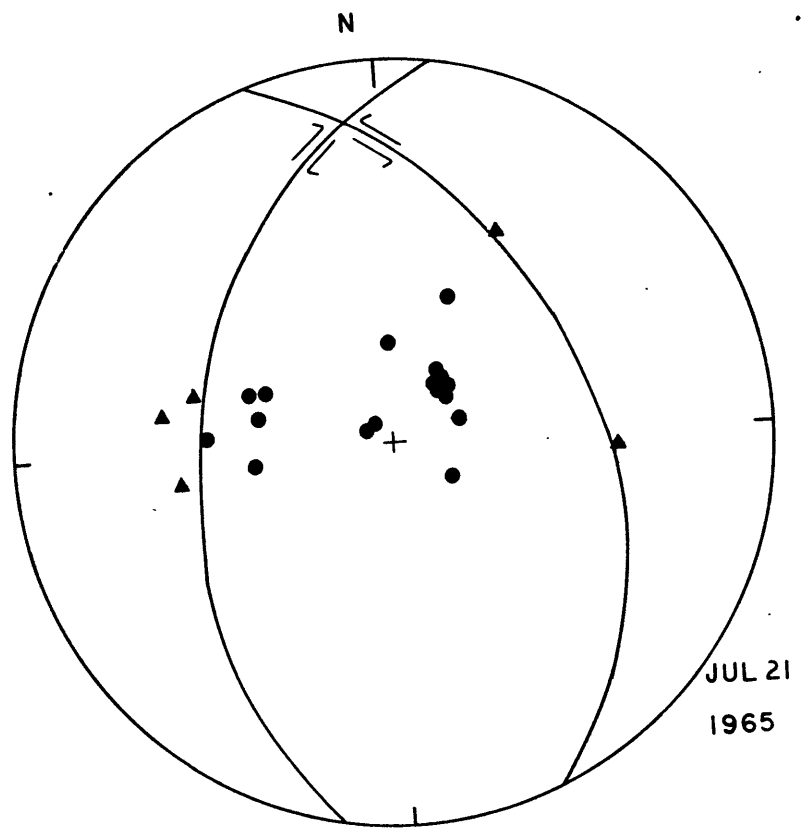
FIGURE 5.1

FIGURE 5.2

DISTANCE, KM
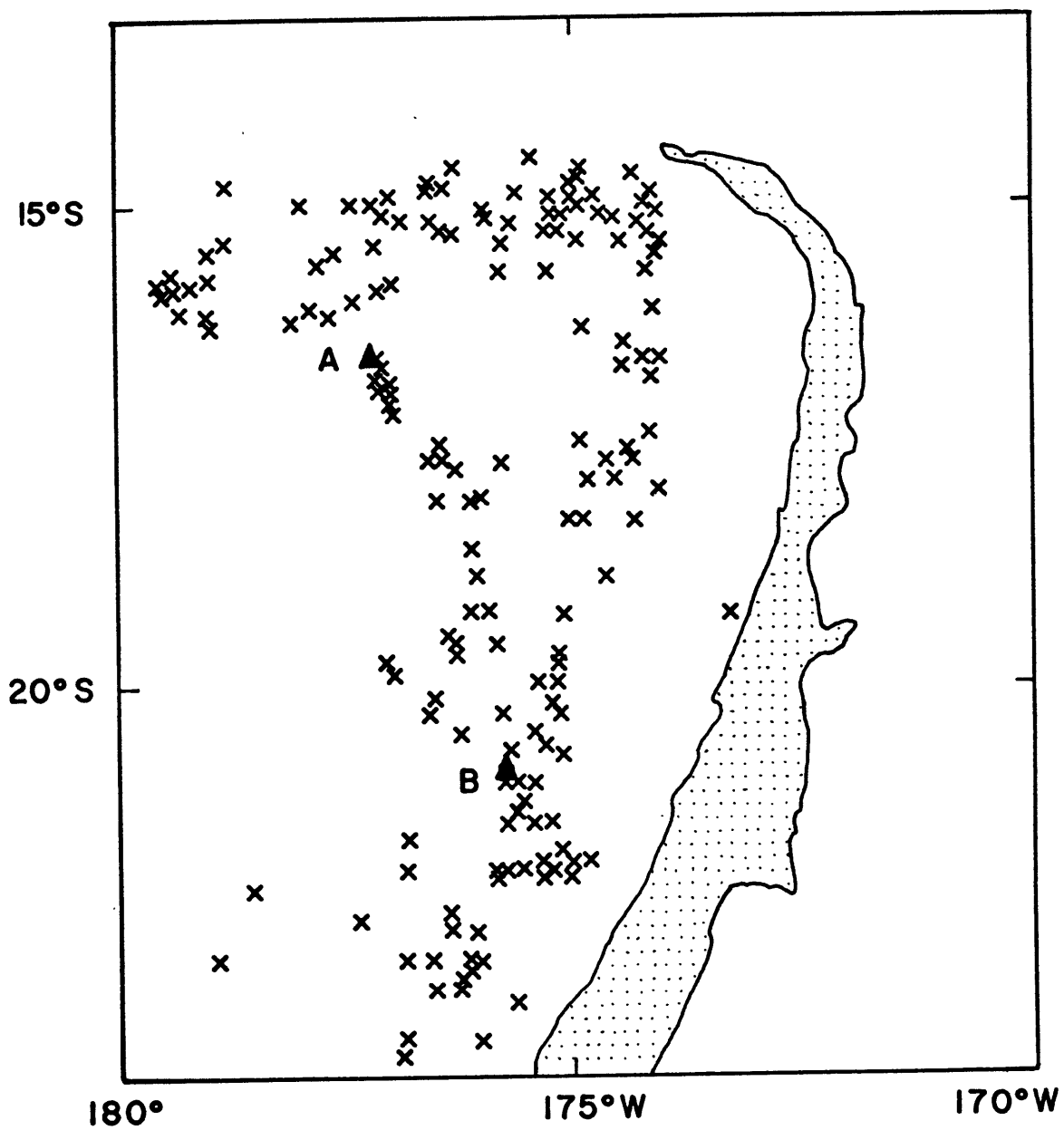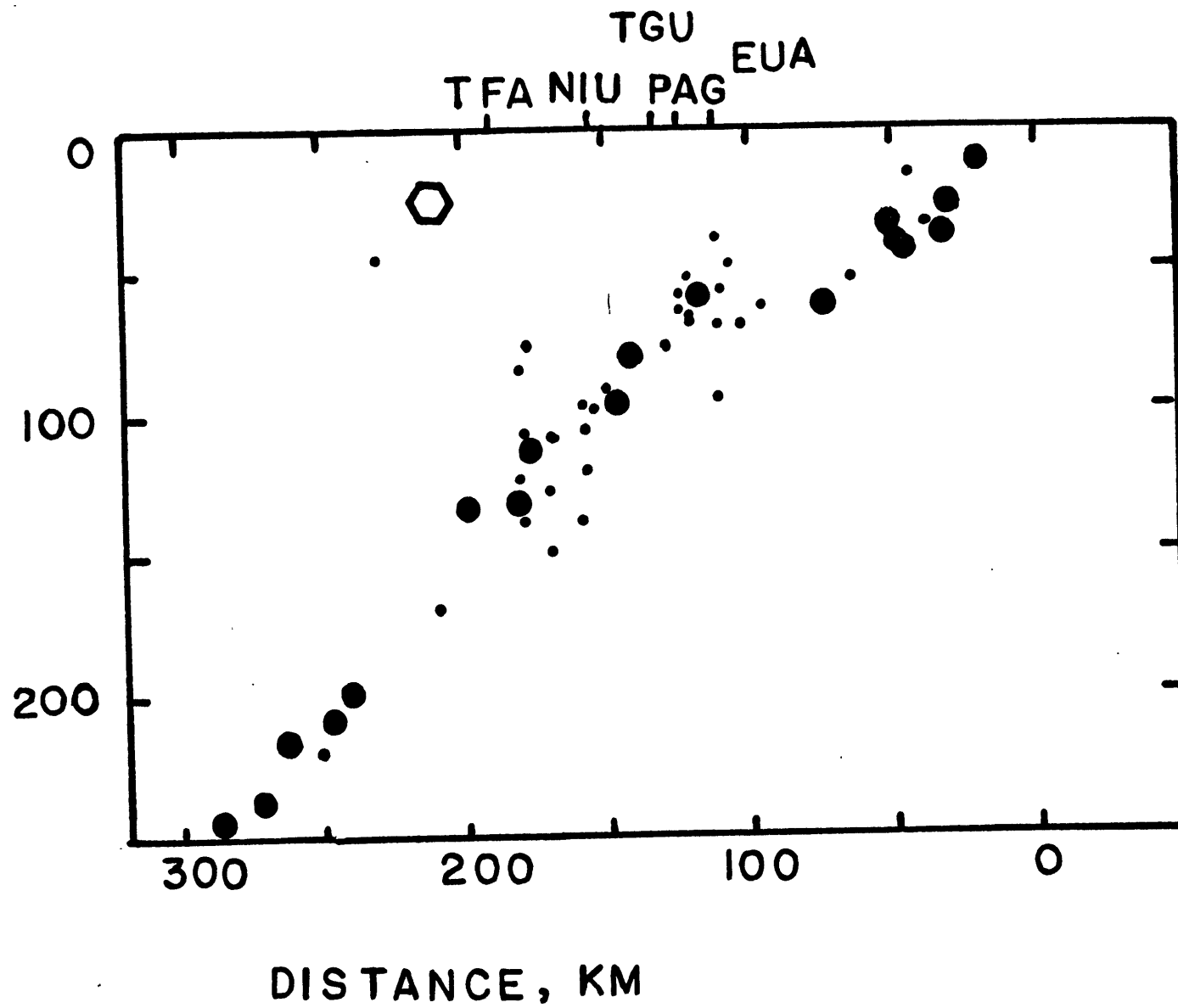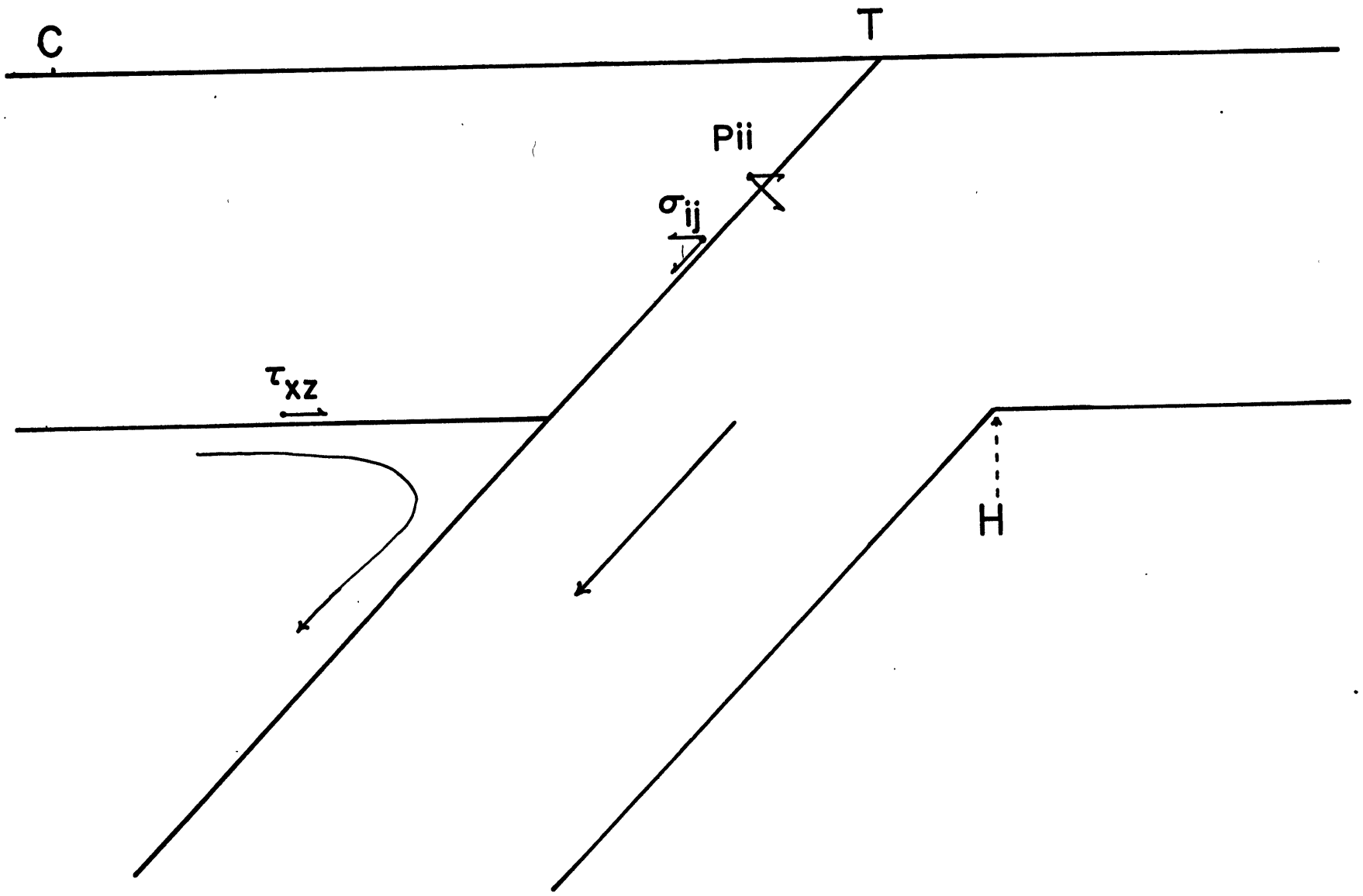
FIGURE 5.3

FIGURE 5.4
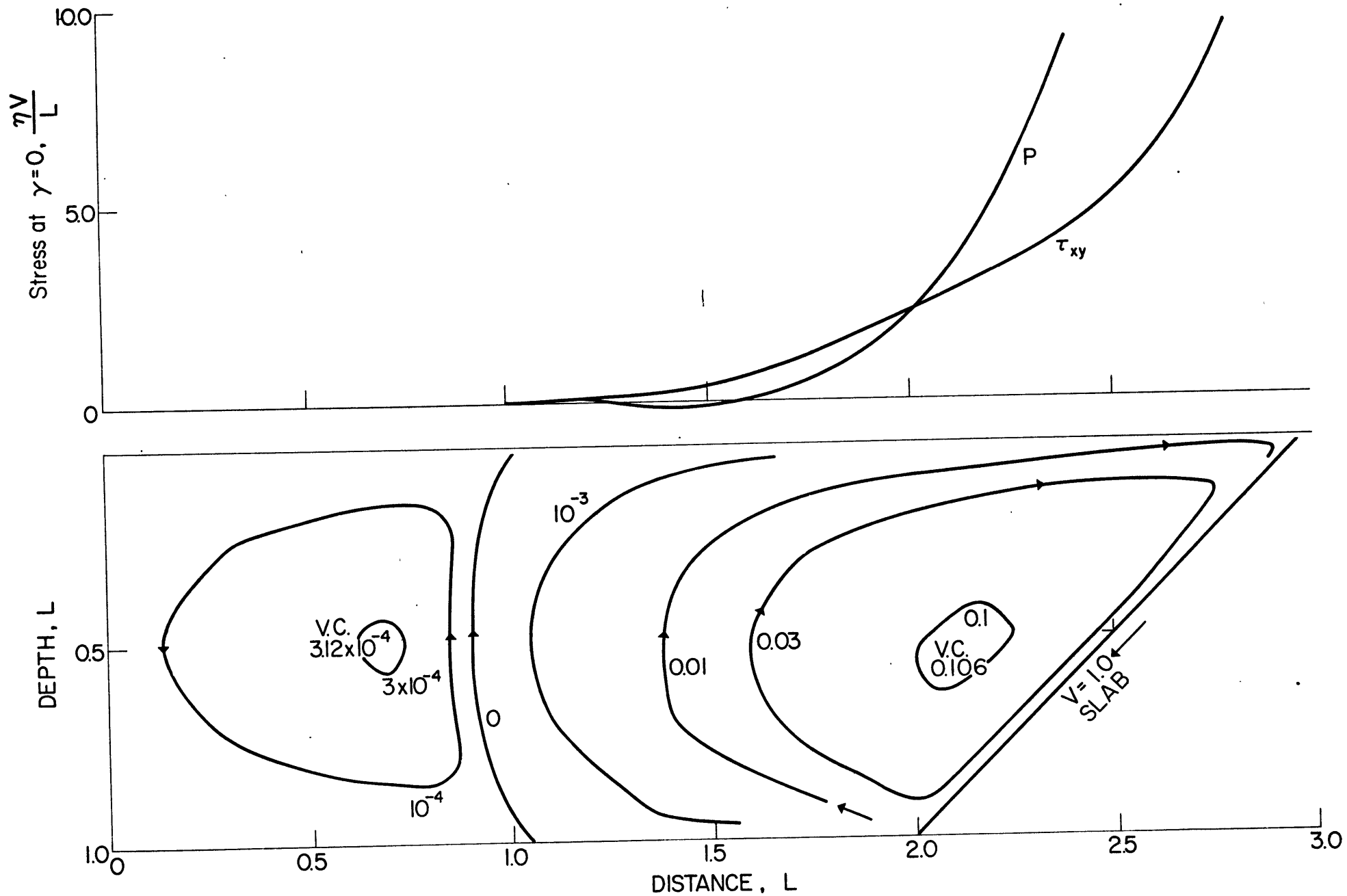
FIGURE 5.5
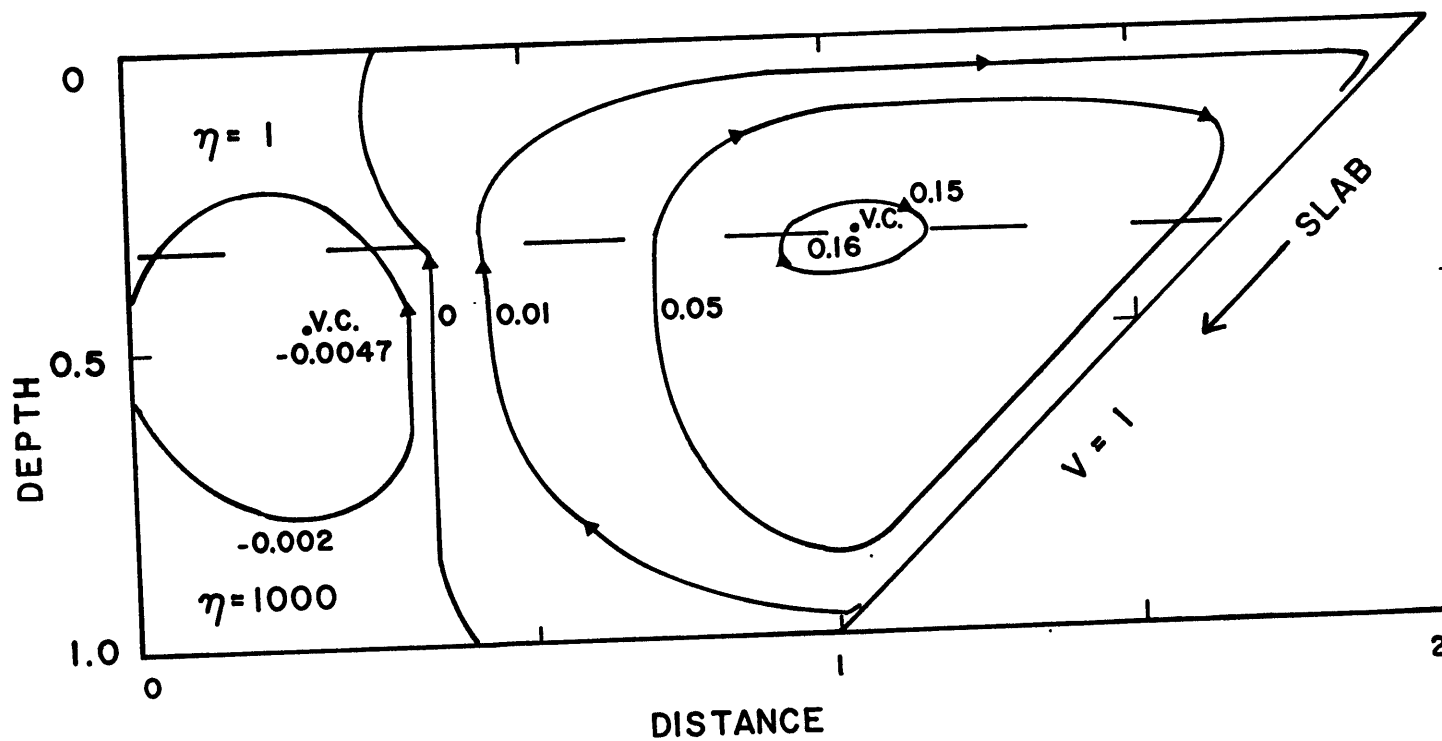
FIGURE 5.6
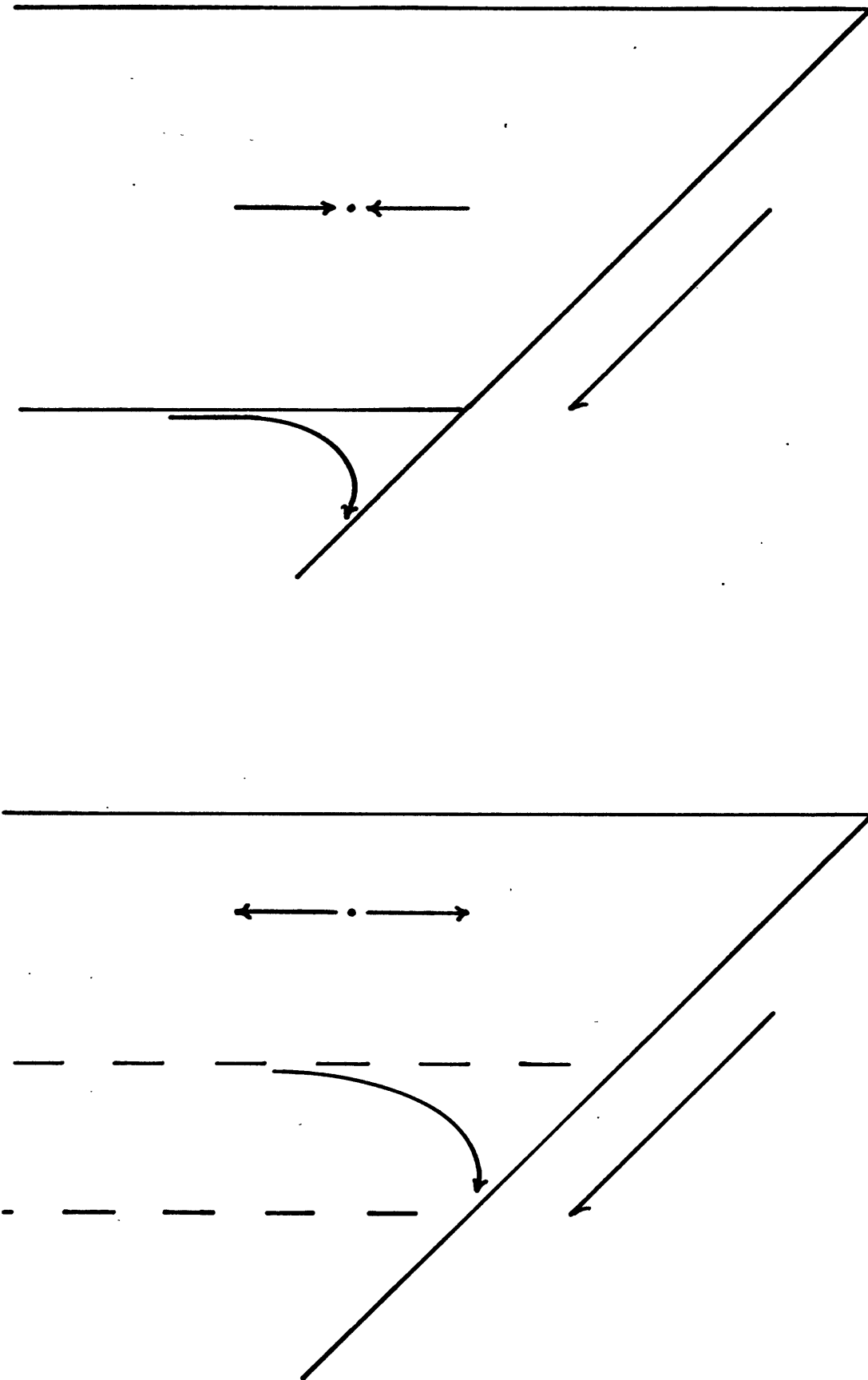
FIGURE 5.7

CHAPTER 6. CONCLUSIONS AND AFTERTHOUGHTS

This study was undertaken in order to understand the deep structure and geophysical processes beneath island arcs. Mathematical models of physical processes including the gross thermal structure of the slab due to subduction, ray theory P-wave transmission through the slab, detailed effects of frictional heating above the slab on temperature, segregation of melt from a partially molten mush, and secondary flow induced by the descent of the slab, were constructed and compared with observations. Results were limited not so much by the mathematical and numerical difficulties, but by the lack of knowledge of the physical parameters in the interior of the earth, and by the limitations of the approach to the problem which presumed the large scale kinematics.

The gross thermal structure of the slab was found to be insensitive to reasonable variations in the values of physical parameters. Gravity anomalies indicate that much of the weight of the slab is somehow compensated. The dynamics of the entire convection pattern would probably have to be considered to explain the observed maximum depth of earthquakes.

Anomalous seismic travel times and amplitudes confirmed that a slab of high velocity material is associated with deep seismic zones. The interpretation of the data was

limited by difficulties in resolution of the effects of the slab. Improved travel time tables and station corrections would increase the worth of the available data.

Frictional heating along the fault plane, concentration of pre-existing melt in the asthenosphere by hydrodynamic forces, and intrusions of asthenospheric material into the lithosphere of the island arc induced by tectonic forces were considered as causes for island arc volcanism. The latter mechanism was most feasible although lack of knowledge of mechanical properties near the base of the lithosphere precluded construction of a detailed physical model. Frictional heating might be significant in some cases. Improved geochemical constraints on the depth of origin of the magma are needed.

Intra-arc basins behind island arcs are the result of crustal spreading. Induced flow, related to the descent of the slab, is the most plausible mechanism for the formation of such basins. The seismicity of the basins can be explained by such a mechanism. Again, lack of knowledge of physical properties near the base of the lithosphere precluded detailed modeling.

The results of this study were in general compatible with the plate tectonic hypothesis. Useful results were obtained by the process of physical modeling. It is likely that additional results can be obtained by applying the calculations of this study to different problems.

Consideration of the dynamics in addition to the kine-
matics of gross plate motions will be necessary in some
cases.

REFERENCES

Abe, K., 1972a, Seismological evidence for a lithospheric tearing beneath the Aleutian arc, Earth Planet. Sci. Letters, 14, 428-432.

Abe, K., 1972b, Lithospheric normal faulting beneath the Aleutian trench, Phys. Earth Planet. Interiors, 5, 190-198.

Anderson, A., and Gottfried, D., 1971, Contrasting behavior of P, Ti, and Nb, in a differentiated high-alumina olivine tholeiite and a calc-alkaline andesite suite, Bull. Geol. Soc. Amer., 82, 1929-1942.

Anderson, D., and Sammis, C., 1970, Partial melting in the upper mantle, Phys. Earth Planet. Interiors, 3, 41-50.

Anderson, O., Schreiber, E., Liebermann, R., and Soga, N., 1968, Some elastic constant data on minerals relevant to geophysics, Rev. Geophys. Space Phys., 6, 491-524.

Armstrong, R., 1968, A model for the evolution of strontium and lead isotopes in a dynamic earth, Rev. Geophys., 6, 175-199.

Armstrong, R., 1971, Isotopic and chemical constraints on models of magma genesis in volcanic arcs, Earth Planet. Sci. Letters, 12, 137-142.

Armstrong, R., and Cooper, J., 1971, Lead isotopes in
    island arcs, Bull. Volcanol., 35, 27-37.

Baker, P., 1968a, Comparative volcanology and petrology of
    the Atlantic island arcs, Bull. Volcanol., 32, 186-206.

Baker, P., 1968b, Petrology of Mount Misery volcano, St. Kitts,
    West Indies, Lithos, 1., 124-150.

Barazangi, M., and Isacks, B., 1971, Lateral variations of
    seismic wave attenuation in the upper mantle above the
    inclined earthquake zone of the Tonga Island arc:
    Deep anomaly in the upper mantle, J. Geophys. Res.,
    76, 8493-8517.

Barazangi, M., Isacks, B., and Oliver, J., 1972, Propagation
    of seismic waves through and beneath the lithosphere
    that descends under the Tonga Island arc, J. Geophys.
    Res., 77, 952-958.

Beloussov, V., and Ruditch, E., 1961, Island arcs in the
    development of the earth's structure (especially in
    the region of Japan and the Sea of Okhotsk), J.
    Geology, 69, 647-658.

Benioff, H., 1955, Seismic evidence for crustal structure
    and tectonic activity, Geol. Soc. Amer. Spec. Paper,
    62, 61-75.

Benioff, H., 1955, Seismic evidence for crustal structure and tectonic activity, Geol. Soc. Amer. Spec. Paper, 62, 61-75.

Bottinga, Y., and Weill, D., 1972, The viscosity of magmatic silicate liquids: a model for calculation, Amer. Jour. Sci., 272, 438-475.

Boyd, F., and England, J., 1963, Effect of pressure on the melting of enstatite, Carnegie Inst. Wash. Yr. Bk., 62, 118-119.

Brune, J., 1968, Seismic moment, seismicity and rate of slip along major fault zones, J. Geophys. Res., 73, 777-784.

Brune, J., 1970, Tectonic stress and the spectra of seismic shear waves from earthquakes, J. Geophys. Res., 75, 4997-5009.

Bryan, W., Stice, G., and Ewart, A., 1972, Geology, petrography, and geochemistry of the volcanic islands of Tonga, J. Geophys. Res., 77, 1566-1585.

Burggraf, O., 1966, Analytical and numerical studies of the structure of steady separated flows, J. Fluid Mech., 24, 113-151.

Burk, C., 1965, Geology of the Alaska Peninsula - Island arc and continental margin, Geol. Soc. Amer. Mem., 99, 3 parts, 250 p.

Carpenter, E., Marshall, P., and Douglas, A., 1967, The amplitude-distance curve for short period teleseismic P-waves, Geophys. J. R. Astr. Soc., 13, 61-70.

Cathles, L., 1971, The viscosity of the earth's mantle, unpublished Ph.D. thesis, Princeton University, 330 pp.

Cleary, J., 1967, Analysis of the amplitudes of short-period P waves recorded by Long-Range Seismic Measurements stations in the distance range 30° to 102°, J. Geophys. Res., 72, 4705-4712.

Coats, R., 1962, Magma type and crustal structure of the Aleutian arc, Amer. Geophys. Union Mon., 6, 92-109.

Crittenden, M., 1967, Viscosity and finite strength of the mantle as determined from water and ice loads, Geophys. J. R. Astr. Soc., 14, 261-279.

Davies, D., and Julian, B., 1972, A study of short period P-wave signals from Longshot, Geophys. J. R. Astr. Soc., 29, 185-202.

Davies, D., and McKenzie, D., 1969, Seismic travel-time residuals and plates, Geophys. J. R. Astr. Soc., 18, 51-63.

Dewey, J., and Bird, J., 1970, Mountain belts and the new global tectonics, J. Geophys. Res., 75, 2625-2647.

Dickinson, W., 1968, Cicum-Pacific andesite types, J. Geophys. Res., 73, 2261-2269.

Dickinson, W., and Hatherton, T., 1967, Andesite volcanism and seismicity around the Pacific, Science, 157, 801-803.

Dickinson, W., and Luth, W., 1971, A model for plate tectonic evolution of mantle layers, Science, 174, 400-404.

Elsasser, W., 1967, Convection and stress propagation in the upper mantle, Princeton Univ. Tech. Rept. 5, June 15.

Engdahl, R., 1971, Explosion effects and earthquakes in the Amchitka Island region, Science, 173, 1232-1235.

Ernst, W., Seki, Y., Onuki, H., and Gilbert, M., 1970, Comparative study of low-grade metamorphism in the California Coast ranges and the outer metamorphic belt of Japan, Geol. Soc. Amer. Mem., 124, 276 pp.

Ewart, A., and Stipp, J., 1968, Petrogenesis of volcanic rocks of the Central North Island, New Zealand, as indicated by a study of Sr_{87}/Sr_{86} ratios and Sr, Rb, K, U and Th abundances, Geochim. et Cosmochim. Acta, 32, 699-736.

Faizullaev, D., 1969, Laminar Motion of Multiphase Media in Conduits, Consultants Bureau, Eng. Trans., New York, 144 p.

Fitch, T., 1970, Earthquake mechanisms in the Himalayan, Burmese and Andaman regions and the continental tectonics in central Asia, J. Geophys. Res., 75, 2699-2710.

Fitton, J., 1971, The generation of magmas in island arcs, Earth Planet. Sci. Lett., 11, 63-67.

Forbes, R. and Kuno, H., 1965, Peridotite inclusions and basaltic host rocks, in: Upper Mantle Symposium, New Delhi, 1964, edited by Smith and Sorgenfrei, pp. 161-179, Berlingske Bogtrykkeri, Copenhagen.

Forbes, R., Ray, D., Katsura, T., Matsumoto, H., Haramura, H., and Furst, M., 1969, in: Proceedings of the Andesite Conference, Ore. Dept. Geol. Mineral Industries Bull.,65, 111-120.

Fukao, Y., 1972, Source process of a large deep-focus earthquake and its tectonic implications, The western Brazil earthquake of 1963, Phys. Earth. Planet. Interiors, 5, 61-76.

Gill, J., 1970, Geochemistry of Viti Levu, Fiji and its

evolution as an island arc, Contr. Mineral. and Petrol., 27, 179-203.

Gorshkov, G., 1969a, Geophysics and petrochemistry of andesite volcanism of the circum-Pacific belt in: Proceedings of the Andesite Conference, Ore. Dept. Geol. Mineral Industries Bull., 65, 91-98.

Gorshkov, G., 1969b, Intraoceanic islands, East Pacific ridge, island arcs; volcanism and upper mantle, Tectonophys., 8, 213-221.

Gorshkov, G., 1970, Volcanism and the Upper Mantle; Investigations in the Kurile Island Area, Plenum Press, New York, 385 pp. (English trans.).

Green, D., and Ringwood, A., 1967a, The genesis of basaltic magmas, Contr.Mineral. Petrol., 15, 103-190.

Green, D., and Ringwood, A., 1967b, The stability fields of aluminous pyroxene peridotite and garnet peridotite and their relevance to upper mantle structure, Earth Planet. Sci. Letters, 3, 151-160.

Green, T., 1972, Crystallization of calc-alkaline andesite under controlled high-pressure hydrous conditions, Contr. Mineral. and Petrol., 34, 150-166.

Green, T., Green, D., and Ringwood, A., 1967, The origin

of high-alumina basalts and their relationships to

quartz tholeiites and alkali basalts, Earth Planet. Sci.

Lett., 2, 41-51.

Green, T., and Ringwood, A., 1966, Origin of the calc-

alkaline igneous rock suite, Earth Planet. Sci. Letters,

1, 307-316.

Green, T., and Ringwood, A., 1968a, Genesis of calc-alkaline

igneous rock suite, Contr. Miner. and Petrol., 18,

105-162.

Green, T., and Ringwood, A., 1968b, Origin of garnet

phenocrysts in calc-alkaline rocks, Contr. Miner. and

Petrol., 18, 163-174.

Green, T., and Ringwood, A., 1969, High pressure experimental

studies on the origin of andesites, in: Proceedings

of the Andesite Conference, Ore. Dept. Geol. Mineral

Industries Bull., 65, 21-32.

Griggs, D., 1972, The sinking lithosphere and the focal

mechanism of deep earthquakes, in: Nature of the Solid

Earth, Robertson, ed., McGraw-Hill, New York, pp. 361-

384.

Gutenberg, B., and Richter, C., 1956, Magnitude and energy

of earthquakes, Annali di Geofisica, 9, 1-15.

Hanks, T., 1971, The Kuril trench-Hokkaido rise system: large shallow earthquakes and simple models of deformation, Geophys. J. R. Astr. Soc., 23, 173-189.

Hanks, T., and Whitcomb, J., 1971, Comments on paper by J.W. Minear and M. Nafi Toksöz: "Thermal regime of a downgoing slab and new global tectonics," J. Geophys. Res., 76, 613-616.

Hart, S., 1971, K, Rb, Cs, Sr, and Ba contents and Sr isotope ratios of ocean floor basalts, Proc. Roy. Soc. Lond., A 268, 573-587.

Hasebe, K., Fujii, N., and Uyeda, S., 1970, Thermal processes under island arcs, Tectonophysics, 10, 335-355.

Hatherton, T., and Dickinson, W., 1969, The relationship between andesitic volcanism and seismicity in Indonesia, the Lesser Antilles, and other island arcs, J. Geophys. Res., 74, 5301-5310.

Hays, J. and Ninkovich, D., 1970, North Pacific deep sea ash chronology and age of present Aleutian under-thrusting, Geol. Soc. Amer. Mem., 126, 263-290.

Hedge, C., 1966, Variation in radiogenic strontium found in volcanic rocks, J. Geophys. Res., 71, 6119-6126.

Hedge, C., Hildreth, R., and Henderson, W., 1970, Strontium isotopes in some Cenozoic lavas from Oregon and Washington, Earth Planet. Sci. Letters, 8, 434-438.

Hedge, C., and Knight, R., 1969, Lead and strontium isotopes in volcanic rocks from northern Honshu, Japan, Geochem. J., 3, 15-24.

Hedge, C., and Peterman, Z., 1970, The strontium isotope composition of basalts from the Gordo and Juan de Fuca rises, northeastern Pacific ocean, Contr. Miner. and Petrol., 27, 144-120.

Heirtzer, J., Dickson, G., Herron, E., Pitman, W., and Le Pichon, X., 1968, Marine magnetic anomalies, geomagnetic field reversals, and the motions of the ocean floor and continents, J. Geophys. Res., 73, 2119-2136.

Herrin, E., 1968, 1968 seismological tables for P phases, Bull. Seismol. Soc. Amer., 58, 1193.

Hess, H., 1965, Mid-ocean ridges and tectonics of the sea floor, in Whittard, W., and Bradshaw, R., eds., Submarine Geology and Geophysics, Colston Research Society Symposium, London, England, Buttersworth, 317-332.

Holmes, A., 1965, Principles of Physical Geology, Nelson, London, 1288 p.

Hurley, P., 1968a, Absolute abundance and distribution of Rb, K, and Sr in the earth, Geochim. Cosmochim. Acta, 32, 273-283.

Hurley, P., 1968b, Correction to 'Absolute abundance and distribution of Rb, K, and Sr in the earth', Geochim. Cosmochim. Acta, 32, 1025-1030.

Ichikawa, M., 1966, Mechanism of earthquakes in and near Japan, 1950-1962, Papers Meteorol. Geophys. Tokyo, 16, 201-229.

Isacks, B., Oliver, J., and Sykes, L., 1968, Seismology and the new global tectonics, J. Geophys. Res., 73, 5855-5899.

Isacks, B., and Molnar, P., 1971, Distribution of stresses in the descending lithosphere from a global survey of focal mechanism solutions of mantle earthquakes, Rev. Geophys. Space Phys., 9, 103-174.

Isacks, B., Sykes, L., and Oliver, J., 1969, Focal mechanisms of deep and shallow earthquakes in the Tonga-Kermedec region and the tectonics of island arcs, Bull. Geol. Soc. Amer., 80, 1443-1470.

Jacob, K., 1970, Three-dimensional seismic ray tracing in
a laterally heterogeneous spherical earth, J. Geophys.
Res., 75, 6675-6689.

Jacob, K., 1972, Global tectonic implications of anomalous
seismic P travel times from the nuclear explosion
longshot, J. Geophys. Res., 77, 2556-2573.

Jakes, P., and Gill, J., 1970, Rare earth elements and the
island arc tholeiitic series, Earth Planet. Sci. Letters,
9, 17-28.

Jakes, P., and White, A., 1970, K/Rb ratios of rocks from
island arcs, Geochim. Cosmochim. Acta., 34, 849-856.

Jakes, P., and White, A., 1971, Composition of island arcs
and continental growth, Earth Planet. Sci. Letters,
12, 224-230.

Jeffreys, H., and Bullen, K., 1958, Seismological Tables,
British Assoc. for the Advancement of Science, Gray
Milne Trust, London.

Joplin, G., 1964, A Petrography of Australian Igneous Rocks,
American Elsevier Publishing Company, New York, p 214.

Julian, B., 1970, Ray tracing in arbitrarily heterogeneous
media, Technical Note, 1970-45, Lincoln Laboratory,
Massachusetts Institute of Technology, Lexington, Mass.,
17 pp.

Julian, B., and Anderson, D., 1968, Travel times, apparent velocities and amplitudes of body waves, Bull. Seismol. Soc. Am., 58, 339-366.

Kaila, K., 1970, Decay rate of P-wave amplitudes from nuclear explosions and the magnitude relations in the epicentral distance range 1° to 98°, Bull. Seismol. Soc. Am., 60, 447-460.

Kanamori, H., 1971a, Great earthquakes at island arcs and the lithosphere, Tectonophysics, 12, 187-198.

Kanamori, H., 1971b, Seismological evidence for a lithospheric normal faulting - the Sanriku earthquake of 1933, Phys. Earth Planet. Interiors, 4, 289-300.

Kanamori, H., 1972, Relation between tectonic stress, great earthquakes and earthquake swarms, Tectonophysics, 14, 1-12.

Karig, D., 1970, Ridges and basins of the Tonga-Kermedec island arc system, J. Geophys. Res., 75, 239-254.

Karig, D., 1971a, Origin and development of marginal basins in the western Pacific, J. Geophys. Res., 76, 2542-2651.

Karig, D., 1971b, Structural history of the Mariana island arc system, Bull. Geol. Soc. Amer., 82, 323-344.

Karig, D., 1972, Remnant arcs, Geol. Soc. Amer. Bull., 83, 1057-1068.

Karig, D., and Glassley, W., 1970, Dacite and related sediment from the West Mariana ridge, Philipine Sea, Bull. Geol. Soc. Amer., 81, 2143-2146.

Kay, R., Hubbard, N., and Gast, P., 1970, Chemical characteristics and the origin of oceanic ridge volcanic rocks, J. Geophys. Res., 75, 1585-1613.

Kraus, E., 1971, Die Entwicklungsgeschichte der Kontinent und Ozeane, Berlin, Akademie-Verlag, 429 p.

Kuno, H., 1950, Petrology of Hakone volcano and the adjacent area, Japan, Geol. Soc. Amer. Bull., 61, 957-1020.

Kuno, H., 1966, Lateral variation of basalt magma type across continental margins and island arcs, Bull. Volcanol., 29, 195-222.

Kuno, H., 1968, Origin of andesite and its bearing on island arc structure, Bull. Volcanol., 32, 141-176.

Kuno, H., 1969, Andesite in time and space, in: Proceedings of the Andesite Conference, Ore. Dept. Geol. Mineral Industries Bull.,65, 13-20.

Kurasawa, H., 1968, Isotopic composition of lead and concentrations of uranium, thorium, and lead in

volcanic rocks from Dogo of the Oki Islands, Japan,
Geochem. Jour., 2, 11-28.

Kushiro, I., 1970, Systems bearing on melting of the upper
mantle under hydrous conditions, Carnegie Inst. Wash.
Yearb., 68, 240-245.

Lambert, D., von Seggern, D., Alexander, S., and Galat, G.,
1970, The longshot experiment (2 vols.), Seismic Data
Laboratory Report no. 234, Alexandria, Virginia.

Lambert, I., and Wyllie, P., 1970, Melting in the deep crust
and upper mantle and the nature of the low velocity
layer, Phys. Earth Planet. Interiors, 3, 316-322.

Langseth, M., Le Pichon, X., and Ewing, M., 1966, Crustal
structure of mid-ocean ridges, 5, Heat flow through
the Atlantic Ocean floor and convection currents,
J. Geophys. Res., 71, 5321-5355.

Laughlin, A., Brookins, D., Kudo, A., and Causey, J., 1971,
Chemical and strontium isotopic investigations of
ultramafic inclusions and basalt, Bandera Crater, New
Mexico, Geochim. Cosmochim. Acta, 151, 107-113.

Leggo, P., and Hutchinson, R., 1968, A Rb-Sr isotope study
of ultrabasic xenoliths and their basaltic host rocks
from massif central, France, Earth Planet. Sci. Letters,
5, 71-75.

Le Pichon, X., 1968, Sea-floor spreading and continental drift, J. Geophys. Res., 73, 3661-3697.

Lewis, J., 1968, Trace elements, variation in alkalis, and the ratio Sr^{87}/Sr^{86} in selected rocks from the Taupo volcanic zone, N.Z. Jl. Geol. Geophys. 11, 608-629.

Luyendyk, B., 1970, Dips of the downgoing lithospheric plates beneath island arcs, Bull. Geol. Soc. Amer., 81, 3411-3416.

MacDonald, G., 1959, Calculations on the thermal history of the earth, J. Geophys. Res., 64, 1967-2000.

MacDonald, G., 1963, The deep structure of continents, Rev. Geophys., 1, 587-665.

Mammerickx, J., 1970, Morphology of the Aleutian abyssal plain, Bull. Geol. Soc. Amer., 81, 3457-3464.

Matsuda, T., and Uyeda, S., 1971, On the Pacific type orogeny and its model-extension of paired belts concept and possible origin of marginal seas, Tectonophysics, 11, 5-27.

McBirney, A., 1968, Petrochemistry of the Cascade andesite volcanoes, in: Andesite Conference Guildbook, Ore. Dept. Geol. Mineral Industries Bull., 62, 101-107.

McBirney, A., 1969 Compositional variations in Cenozoic calc-alkaline suites of Central America, in: Proceedings of the Andesite Conference, Ore. Dept. Geol. Mineral Industries Bull., 65, 185-189.

McBirney, A., and Weill, D., 1966, Rhyolite magmas of Central America, Bull. Volcanol., 29, 435-448.

McConnell, R., 1968, Viscosity of mantle from relaxation time spectra of isostatic adjustment, J. Geophys. Res., 22, 7089-7105.

McKenzie, D., 1966, The viscosity of the lower mantle, J. Geophys. Res., 71, 3995-4010.

McKenzie, D., 1969, Speculations on the consequences and causes of plate motions, Geophys. J. R. Astr. Soc., 18, 1-32.

McKenzie, D., 1971, Comments on Paper by John W. Minear and M. Nafi Toksöz, 'Thermal regime of a downgoing slab and new global tectonics,' J. Geophys. Res., 76, 607-609.

McKenzie, D., and Sclater, J., 1968, Heat flow inside the island arcs of the northwest Pacific, J. Geophys. Res. 73, 3137-3179.

Menard, H., 1967, Transitional types of crust under small ocean basins, J. Geophys. Res., 72, 3061-3073.

Menard, H., 1972, History of the Ocean basins, in: The Nature of the Solid Earth, Robertson, ed., McGraw-Hill, New York, pp. 440-460.

Minato, M., Gorai, M. and Hunahashi, M., 1965, The Development of the Japanese Islands, Tsukiji Shokan, Tokyo, 442 p.

Minear, J., and Toksöz, N., 1970a, Thermal regime of a downgoing slab and new global tectonics, J. Geophys. Res., 75, 1397-1419.

Minear, J., and Toksöz, M., 1970b, Thermal regime of a downgoing slab, Tectonophysics, 10, 367-390.

Minear, J., and Toksöz, M., 1971, Reply, J. Geophys. Res., 76, 610-612.

Mitronovas, W., and Isacks, B., 1971, Seismic velocity anomalies in the upper mantle beneath the Tonga-Kermadec island arc, J. Geophys. Res., 76, 7154-7180.

Moffatt, H., 1964, Viscous and resistive eddies near a sharp corner, J. Fluid Mech., 18, 1-18.

Molnar, P., and Oliver, J., 1969, Lateral variations of

attenuation in the upper mantle and discontinuities in the lithosphere, J. Geophys. Res., 74, 2648-2682.

Morgan, W., 1965, Gravity anomalies and convection currents, 1, A sphere and cylinder sinking beneath the surface of a viscous fluid, J. Geophys. Res., 70, 6175-6187.

Morgan, W., 1968, Rises, trenches, great faults, and crustal blocks, J. Geophys. Res., 73, 1959-1982.

Murauchi, S., Den, N., Asano, S., Hotta, H., Yoshii, T., Asanuma, K., Ichikawa, K., Sata, T., Ludwig, W., Ewing, J., Edgar, N., and Houtz, R., 1968, Crustal structure of the Philippine Sea, J. Geophys. Res., 73, 3143-3171.

Murdock, J., 1969a, Crust-mantle system in the central Aleutian region - a hypothesis, Bull. Seismol. Soc. Amer., 59, 1543-1558.

Murdock, J., 1969b, Short-term seismic activity in the central Aleutian region, Bull. Seismol. Soc. Amer., 59, 789-797.

Nuttli, O., 1972, The amplitudes of teleseismic P waves, Bull. Seismol. Soc. Amer., 62, 343-356.

O'Hara, M., 1963a, Melting of garnet peridotite at 30 kilobars, Carnegie Inst. Wash. Yr. Bk., 62, 71-76.

O'Hara, M., 1963b, Melting of bimineralic eclogite at 30 kilobars, Carnegie Inst. Wash. Yr. Bk., 62, 76-77.

O'Hara, M., 1965, Primary magmas and the origin of basalts, Scottish J. Geol., 1, 19-40.

O'Hara, M., Richardson, S., and Wilson, G., 1971, Garnet-peridotite stability and occurrence in crust and mantle, Contr. Mineral. and Petrol., 32, 48-68.

O'Neil, J., Hedge, C., and Jackson, E., 1970, Isotopic investigations of xenoliths and host basalts from the Honolulu volcanic series, Earth Planet. Sci. Lett., 8, 253-257.

Osborn, E., 1969a, Experimental aspects of calc-alkaline differentiation, in: Proceedings of the Andesite Conference, Ore. Dept. Geol. Mineral. Industries Bull., 65, 33-42.

Osborn, E., 1969b, The complementariness of orogenic andesite and alpine peridotite, Geochim. Cosmochim. Acta, 33, 307-324.

Osborn, E., 1969c, Genetic significance of V and Ni content of andesites: Comments on a paper by Taylor, Kaye, White, Duncan, and Ewart, Geochim. Cosmochim. Acta, 33, 1553-1554.

Oversby, V., 1971, Lead in oceanic islands, Faial, Azores and Trinidade, Earth Planet. Sci. Letters, 11, 401-406.

Oversby, V., and Gast, P., 1968, Lead isotope compositions and uranium decay series disequilibrium in recent volcanic rocks, Earth Planet. Sci. Letters, 5, 199-206.

Oversby, V., and Gast, P., 1970, Isotopic composition of lead from oceanic islands, J. Geophys. Res., 75, 2097-2114.

Oversby, V., Lancelot, J., and Gast, P., 1971, Isotopic composition of lead in volcanic rocks from Tenerife, Canary Islands, J. Geophys. Res., 76, 3402-3413.

Oxburgh, E., and Turcotte, D., 1970, Thermal structure of island arcs, Bull. Geol. Soc. Amer., 81, 1665-1688.

Oxburgh, E., and Turcotte, D., 1971, Origin of paired metamorphic belts and crustal dilation in island arc regions, J. Geophys. Res., 76, 1315-1327.

Ozima, M., Zashu, S., and Ueno, N., 1971, K/Rb and $(^{87}Sr/^{86}Sr)_o$ ratios of dredged submarine basalts, Earth Planet. Sci. Letters, 10, 239-244.

Pan, F., and Acrivos, A., 1967, Steady flows in rectangular cavities, J. Fluid Mech., 28, 643-655.

Peaceman, D., and Rachford, H., 1955, The numerical
solution of parabolic and elliptic differential
equations, J. Soc. Ind. Appl. Math., 3, 28-41.

Peacock, M., 1931, Classification of igneous rocks, J. Geol.,
39, 54-67.

Peterman, Z., Carmichael, I., and Smith, A., 1970a, Strontium
isotopes in quaternary basalts of southeastern
California, Earth Planet. Sci. Lett., 7, 381-385.

Peterman, Z., Carmichael, I., and Smith, A., 1970b,
Sr^{87}/Sr^{86} ratios of quaternary lavas of the Cascade
range, northern California, Bull. Geol. Soc. Amer., 81,
311-318.

Peterman, Z., Lowder, G., and Carmichael, I., 1970c,
Sr^{87}/Sr^{86} ratios of the Talasea series, New Britain,
Territory of New Guinea, Bull. Geol. Soc. Amer., 81,
39-40.

Powell, J., and DeLong, S., 1966, Isotopic composition of
strontium in volcanic rocks from Oahu, Science, 153,
1239-1242.

Press, F., 1970, Earth models consistent with geophysical
data, Phys. Earth Planet. Interiors, 3, 3-22.

Pushkar, P., 1968, Strontium isotopic ratios in volcanic rocks of three island arc areas, J. Geophys. Res., 73, 2701-2714.

Pushkar, P., McBirney, A., and Kudo, A., 1972, The isotopic composition of strontium in central American ignimbrites, Bull. Volcanol., 35, 265-294.

Raleigh, C., and Lee, W., 1969, Sea-floor spreading and island-arc tectonics, in: Proceeding of the Andesite Conference, Ore. Dept. Geol. Mineral Industries Bull., 65, 99-110.

Rikitake, T., 1969, The undulation of an electrically conductive layer beneath the islands of Japan, Tectonophys., 7, 257-264.

Ringwood, A., 1969, Composition and evolution of the upper mantle, Geophys. Mon., 13, 1-17.

Ringwood, A., 1970, Phase transformations and composition of the mantle, Phys. Earth Planet. Interiors, 3, 109-155.

Ringwood, A., 1972, Phase transformations and mantle dynamics, Earth Planet. Sci. Lett., 14, 233-241.

Rodolfo, K., 1969, Bathymetry and marine geology of the

Andaman basin and tectonic implications for southeast Asia, Bull. Geol. Soc. Amer., 80, 1203-1230.

Schatz, F., 1971, Thermal conductivity of earth materials at high temperature, Ph.D. Thesis at M.I.T., Cambridge, Mass.

Scheidegger, A., 1960, The Physics of Flow Through Porous Media, Macmillan, New York, 313 p.

Scheinmann, Yu., 1968, Tectonics of the upper parts of the mantle under geosynclines and island arcs, in: The Crust and Upper Mantle of the Pacific Area, Amer. Geophys. Union. Geophys. Monogr., 12, 466-472.

Scheinmann, Yu., 1971, Tectonics and the Formation of Magma, New York, Consultants Bureau (Eng. Trans.), 173 p.

Schubert, G., and Turcotte, D., 1971, Phase changes and mantle convection, J. Geophys. Res., 76, 1424-1432.

Sclater, J., Anderson, R., and Bell, M., 1971, Elevation of ridges and evolution of the central eastern Pacific, J. Geophys. Res., 76, 7888-7915.

Sclater, J., and Francheteau, J., 1970, The implications of terrestrial heat flow observations on current tectonic and geochemical models of the crust and upper mantle of the earth, Geophys. J. R. Astr. Soc., 20, 493-509.

Sclater, J., Hawkins, J., Mammerickx, J., and Chase, C., 1972, Crustal extension between the Tonga and Lau ridges: Petrologic and geophysical evidence, <u>Bull. Geol. Soc. Amer.</u>, <u>83</u>, 505-518.

Sclar, C., 1970, High pressure studies in the system $MgO-SiO_2-H_2O$, <u>Phys. Earth Planet. Interiors</u>, <u>3</u>, 333.

Sen Gupta, M., and Julian, B., in preparation, Teleseismic P-wave travel time anomalies.

Sleep, N., 1969, Sensitivity of heat flow and gravity to the mechanism of sea-floor spreading, <u>J. Geophys. Res.</u>, <u>74</u>, 542-549.

Sleep, N., and Toksöz, N., 1971, Evolution of marginal basins, <u>Nature</u>, <u>233</u>, 548-550.

Smith, A., and Toksöz, M., 1972, Stress distribution beneath island arcs, <u>Geophys. J. R. Astr. Soc.</u>, in press.

Solomon, S., 1972, Seismic-wave attenuation and partial melting in the upper mantle of North America, <u>J. Geophys. Res.</u>, <u>77</u>, 1483-1502.

Sorrells, G., Crowley, J., and Veith, K., 1971, Methods for computing ray paths in complex geologic structures, <u>Bull. Seism. Soc. Amer.</u>, <u>61</u>, 27-53.

Stauder, W., 1968, Mechanism of the Rat Island earthquake sequence of February 4, 1965, with relation to island arcs and sea-floor spreading, J. Geophys. Res., 73, 3847-3858.

Sugimura, A., 1967, Chemistry of volcanic rocks and the seismicity of the earth's mantle in island arcs, Bull. Volcanol., 30, 319-334.

Sugimura, A., 1968, Spatial relations of basaltic magmas in island arcs, in Baslts, The Poldervaart Treatise on Rocks of Basaltic Composition, edited by H.H. Hess, vol. 2, pp. 537-572, Interscience, New York.

Sykes, L., 1966, The seismicity and deep structure of island arcs, J. Geophys. Res., 71, 2981-3006.

Tatsumoto, M., 1966a, Genetic relations of oceanic basalts as indicated by lead isotopes, Science, 153, 1094-1101.

Tatsumoto, M., 1966b, Isotopic composition of lead in volcanic rocks from Hawaii, Iwo-Jima and Japan, J. Geophys. Res., 71, 1721-1733.

Tatsumoto, M., 1969, Lead isotopes in volcanic rocks and possible ocean-floor thrusting beneath island arcs, Earth Planet. Sci. Letters, 6, 369-376.

Tatsumoto, M., and Knight, R., 1969, Isotopic composition of lead in volcanic rocks from central Honshu with regard to basalt genesis, Geochem. J., 3, 53-86.

Taylor, S., 1969, Trace element chemistry of andesites and associated calc-alkaline rocks, in: Proceedings of the Andesite Conference, Ore. Dept. Geol. Mineral Industries Bull., 65, 21-32.

Taylor, S., Kaye, M., White, A., Duncan, A., and Ewart, A., 1969, Genetic significance of Co, Cr, Ni, Sc, and V content of andesites, Geochim et Cosmochim Acta, 33, 275-286.

Taylor, S., Kaye, M., White, A., Duncan, A., and Ewart, A., 1969b, Genetic significance of V and Ni content of andesites; Reply to Prof. E.F. Osborn, Geochim. Cosmochim. Acta, 33, 1555-1557.

Taylor, S., and White, A., 1966, Trace element abundances in andesites, Bull. Volcanol., 29, 177-194.

Tokarev, P., 1971, On the focal layer, seismicity and volcanicity of the Kurile-Kamchatka zone, Bull. Volcanol., 35, 230-242.

Toksöz, M., Minear, J., and Julian, B., 1971, Temperature field and geophysical effect- of a downgoing slab, J. Geophys. Res., 76, 1113-1138.

Turcotte, D., and Oxburgh, E., 1968, A fluid theory for the deep structure of dip-slip fault zones, Phys. Earth Planetary Interiors, 1, 381-386.

Turcotte, D., and Oxburgh, E., 1969, Convection in a mantle with variable physical properties, J. Geophys. Res., 74, 1458-1474.

Utsu, T., 1971, Seismological evidence for anomalous structure of island arcs with special reference to the Japanese region, Rev. Geophys. Space Phys., 9, 839-890.

Uyeda, S., and Horai, K., 1964, Terrestrial heat flow in Japan, J. Geophys. Res.,69, 2121-2141.

Vening Meinesz, F., 1951, A third arc in many island arc areas, Proc. Koninkl. Ned. Akad. Wetensch., ser. B., 54, 432-442.

Verhoogen, J., 1965, Phase changes and convection in the earth's mantle, Trans. Roy. Soc. London, A258, 276-283.

Ward, R., 1971, Synthesis of teleseismic P-waves from sources near transition zones, unpublished Ph.D. thesis, M.I.T., Cambridge, Mass., 206 p.

Weertman, J., 1970, The creep stength of the earth's mantle, Rev. Geophys., 8, 145-168.

Weertman, J., 1971, Theory of water-filled crevasses in glaciers applied to vertical magma transport beneath oceanic ridges, J. Geophys. Res., 76, 1171-1183.

Welke, H., Moorbath, S., and Cumming, G., 1968, Lead isotope studies on igneous rocks from Iceland, Earth Planet. Sci. Lett., 4, 221-231.

Wiggins, R., 1971, Consequences of a gravitational driving mechanism for plate tectonics, abstract T74, Trans. Am. Geophys. Un., 52, 355.

Wyss, M., 1970, A comparison of apparent stresses of earthquakes on ridges with earthquakes in trenches, Geophys. J. R. Astr. Soc., 19, 479-484.

Yasui, M., Epp, D., Nagasaka, K., and Kishii, T., 1970, Terrestrial heat flow in the seas around the Nansei Shoto (Ryukyu Islands), Tectonophys., 10, 225-234.

Yasui, M., Hashimoto, Y., and Uyeda, S., 1967, Geomagnetic studies of the Japan Sea, 1. Anomaly pattern of the Japan Sea, Oceanogr. Mag., 19, 221-231.

Yoder, H., 1965, Diopside-anorthite-water at five and ten kilobars and its bearing on explosive volcanism: Carnegie Inst. Washington Year Book 64, 82-89.

Yoder, H. Jr., 1969, Calcalkalic andesites: experimental

data bearing on the origin of their assumed

characteristics, in: Proceedings of the Andesite

Conference, Ore. Dept. Geol. Mineral. Industries Bull.,

65, 77-89.

APPENDIX A

Numerical Methods

This paper is concerned with solving equations of heat and mass transfer applicable to flow in this interior of the earth. A full solution of the problem is not attempted but rather the temperature field is determined in regions where the velocity field can be directly estimated from observations. The fluid flow equation is also solved for limited regions for which control on the boundary conditions can be obtained directly from knowledge of plate motions.

The relevant equations are the Navier-Stokes equation

$$\rho \frac{\partial v}{\partial t} + \rho (v \cdot \text{grad}) v = -\text{grad } p + \eta \nabla^2 v - \rho \alpha g T \qquad (A.1)$$

and the heat flow equation

$$\frac{\partial T}{\partial t} + v \cdot \text{grad} T = \frac{1}{\rho C} \text{div}(k \text{ grad} T) + \frac{H}{\rho C} \qquad (A.2)$$

The notation is

    v   velocity

    ρ density

    t   time

    p   pressure

    η viscosity

    α coefficient of thermal expansion

    g   acceleration of gravity

T   temperature

C   .specific heat (at constant pressure)

H   internal heat production

k   thermal conductivity

For the earth, the inertial terms on the left hand side of equation (A.1) can be ignored.

A.1 Calculation of slab models

The computation scheme used herein is similar to that used by Toksöz et al. (1971). The basic model consists of a slab of material moving downward into the mantle at an angle to the surface. The surrounding mantle is assumed to be fixed (Figure A.1). The computational scheme consists of explicitly translating temperatures between grid points in the slab and allowing the slab to warm up over a time interval Δt, which corresponds to the amount of movement at the assumed velocity. The heat flow equation was solved after each translation step using the alternating-direction implicit finite difference scheme (Peaceman and Rachford, 1955). This technique used by Toksöz et al. (1971) was modified so that the slab could dip at an arbitrary angle and a self-adjoint form was used for the derivatives. The finite difference equation implicit in the x direction is

$$\frac{T_{n,m}^{\rho+1} - T_{n,m}^{\rho}}{\Delta t} = \frac{\beta}{\Delta x^2} \left\{ (k_{n+1,m} + k_{n,m})(T_{n+1,m}^{\rho+1} \right.$$

$$- T_{n,m}^{\rho+1}) - (k_{n-1,m} + k_{n,m})(T_{n,m}^{\rho+1}$$

$$\left. - T_{n-1,m}^{\rho+1}) \right\} + \frac{\beta}{\Delta z^2} \left\{ (k_{n,m+1} + k_{n,m})(T_{n,m+1}^{\rho} \right.$$

$$\left. - T_{n,m}^{\rho}) - (k_{n,m-1} + k_{n,m})(T_{n,m}^{\rho} - T_{n,m-1}^{\rho}) \right\}$$

$$+ \beta H \qquad\qquad (A.3)$$

where

$$x = n\Delta x$$

$$z = m\Delta z$$

$$t = \rho\Delta t$$

$$\beta = (\rho C)^{-1}$$

This set of equations can be written as

$$A_n T_{n-1,m}^{\rho+1} + B_n T_{n,m}^{\rho+1} + C_n T_{n+1,m}^{\rho+1} = D_n \qquad (A.4a)$$

where

$$A_n = -(k_{n-1,m} + k_{n,m})(0.5\beta/\Delta x^2) \qquad (A.4b)$$

$$B_n = \Delta t^{-1} + (0.5\beta/\Delta x^2)(k_{n-1,m} + k_{n+1,m} + 2k_{n,m}) \qquad (A.4c)$$

$$C_n = -(k_{n+1,m} + k_{n,m})(0.5\beta/\Delta x^2) \qquad (A.4d)$$

$$D_n = (0.5\beta/\Delta z^2) - (k_{n,m-1} + k_{n,m+1} + 2k_{n,m})T_{n,m}{}^{\rho}$$

$$+ (k_{n,m-1} + k_{n,m})t_{n,m-1}{}^{\rho} + (k_{n,m+1} + k_{n,m})T_{n,m+1}{}^{\rho}$$

$$+ T_{n,m}{}^{\rho}/\Delta t + \beta H \tag{A.4e}$$

For each grid line the set of implicit equations can be solved as a tridiagonal matrix. The iteration is completed by solving for $T_{n,m}{}^{\rho+2}$ using equations that are implicit in z. The relevant formulae can be obtained by adding 1 to the index ρ and interchanging x with z and m with n.

Boundary conditions were zero heat-flux on the sides n = 1 and n = N, zero temperature at the surface, and heat flux of F at the bottom, m = 1.

A.1.1 Thermal conductivity

Two formulations were used for calculating thermal conductivity. One set of models used a formulation by MacDonald (1959)

$$k = k_1 + (16n^3 sT^3)/(n\varepsilon_0 + 120\pi\sigma_0 \exp(-E/KT)) \tag{A.5}$$

where

k_1 lattice conductivity, 0.25×10^6 erg/cm-sec-°C

T   absolute temperature

K   Boltzmann's constant

E   width of energy gap for electronic conduction, 3 e.v.

s   Stefan-Boltzmann constant

n   index of refraction, 1.7

ε_0 low temperature opacity, 10 cm^{-1}

σ_0 electrical conductivity, $10 \text{ ohm}^{-1}\text{cm}^{-1}$

The other set of models used the experimental results of Schatz (1971) on olivine. In this case the lattice con-ductivity is the larger of

$$k_1 = (30.6 + 0.21T)^{-1} \qquad\qquad (A.6a)$$

$$k_1 = 0.003 + (3 \times 10^{-6})z \qquad\qquad (A.6b)$$

where z is in kilometers, T in °K and the unit of conduc-tivity is cal/cm-sec-°C. The radiative conductivity is given by

$$k_r = 0 \qquad T \leq 500°K \qquad\qquad (A.7a)$$

$$k_r = 5.5 \times 10^{-6}(T - 500) \qquad T > 500°K \qquad (A.7b)$$

A.1.2 Phase changes

An improved method was used for calculating heating due to phase changes. The amount of each phase present was evaluated at points where a phase change might occur assuming that the fraction of the high pressure phase increases linearly with depth over a finite depth interval and the depth of the interval is dependent on temperature. The function A is evaluated

$$A = (\frac{\partial T}{\partial z_i} z + T_0 - T)/B \tag{A.8}$$

and then limited by 0 and 1 to give the mass fraction of phase i

$$f_i^{\rho+1} = 0 \qquad A \leq 0 \tag{A.9a}$$

$$f_i^{\rho+1} = A \qquad 0 \leq A \leq 1 \tag{A.9b}$$

$$f_i^{\rho+1} = 1 \qquad A \geq 1 \tag{A.9c}$$

The amount of phase change heating in one translation step is given by

$$\Delta t H_i = \rho \Delta f_i (T_{abs} \Delta S_i - p \Delta V_i) \tag{A.10}$$

Δt = length of time step

H_i = power production from phase i

ΔS_i = entropy of phase change

ΔV = volume of phase change

The following phase changes were included in various models

		T_0,°C	$\frac{\partial T}{\partial z}$,$\frac{°C}{km}$	B,°C	ΔS,10^6erg/g°C	ΔVgcm^3/g
1.	basalt-eclogite	-80	17	50	-1.17	-0.065
2a.	olivine-spinel	-1120	9	50	-0.713	-0.0265
2b.	olivine-spinel	-1380	9	300	-0.713	-0.0265
3.	post-spinel	-87000	150	50	-0.594	-0.0262

A.1.3 Convective geotherm

The migration of ridges with respect to trenches
precludes a permanent region of trapped flow at the core
of a convection cell in the upper mantle. The minimum
amount of average upward velocity in the upper mantle, not
including slabs, is that amount needed to produce the
spreading oceanic lithosphere. This average velocity can
be used to approximate a geotherm if the surface heat
flux is "known". Starting with the z-component of the
heat flow equation in steady state

$$\rho c V_z \frac{\partial T}{\partial z} - \frac{\partial}{\partial z} k \frac{\partial T}{\partial z} = H \tag{A.11}$$

the vertical derivative of vertical heat flux can be
found by differentiating by parts

$$\frac{\partial F}{\partial z} = \frac{\partial}{\partial z}(-k\frac{\partial T}{\partial z} + \rho c V_z T) = T\frac{\partial}{\partial z}(\rho c V_z) + H \tag{A.12}$$

F = vertical heat flux.

This equation can be solved by a self-consistent iteration
procedure

$$F_{j+1}^{\rho+1} = F_j^{\rho+1} + H_j^{\rho}\Delta z + [(\rho c V_z)_{j+1} - (\rho c V_z)_j] * T_j^{\rho} \tag{A.13}$$

ρ (superscript)   iteration number

j (subscript)   vertical increment number (+ = up)

Δz vertical grid spacing

The bottom heat flux, $F_0^{\rho+1}$, is adjusted such that the

surface heat flux has the assumed value. An improved temperature was obtained by numerically integrating downward from the known surface temperature using the expression for vertical heat flux solved for temperature

$$T_j^{\rho+1} = (F_{j+1}^{\rho+1} + T_{j+1}^{\rho+1} \cdot k_j^\rho / \Delta z) / [(\rho c V_z)_j + k_j^\rho / \Delta z] \qquad (A.14)$$

Conductivity, k_j^ρ, was evaluated at a temperature of $(T_{j+1}^\rho + T_j^\rho)/2$. The adiabatic and phase change heating parts of H_j^ρ were evaluated at T_j^ρ. The relevant formulae of calculating these parameters are given in Section A.1.1 and A.1.2.

The velocity v_z was adjusted so that mass was conserved in the main part of the flow. The mass flux was assumed to be

$$v_z = z/S \qquad 0 \le z \le L \qquad (A.15a)$$

$$\rho v_z = (L + A)\rho_0/2S + (z - A)^2 \rho_0 / 2S(L - A)$$
$$L \le z \le A \qquad (A.15b)$$

$$\rho v_z = (L + A)\rho_0/2S \qquad (A.15c)$$

For purposes of calculation the parameters were assumed to be

surface heat flux	F_n	= 71 ergs/cm^2-sec
grid spacing	Δz	= 1 km
replacement time of lithosphere	S	= 120 my
depth of base of lithosphere	L	= 80 km
depth of base of asthenosphere	A	= 150 km

weighted density of A and L $\rho_0 = 3.38 \text{ g/cm}^3$

The iteration converged in less than ten iterations starting from T = 0 everywhere. The calculation can be valid only away from those parts of the flow which thermally equilibrate with slabs and away from the bottom boundary layer of the convection cell. The estimate of temperature obtained by this method is at worst a smoothly varying solution which is adiabatic in the interior but conductive near the surface. At best it is a zero order solution to a much more complicated problem. Considering that the parameters in the calculation are poorly known, little improvement in the average geotherm of the mantle could be obtained from a more sophisticated calculation.

A.1.4 Accuracy and stability

A complete analysis of the stability and accuracy of the method used to calculate the geotherm in descending slabs would be intractable because the method is an exceedingly complicated mixture of explicit and implicit calculation. The scheme used herein is identical to the scheme used by Toksöz et al. (1971) except for the use of self-adjoint operators, which conserve energy, and for modification of the method used to calculate heat sources. The analyses for stability and accuracy of the earlier scheme (McKenzie, 1971; Minear and Toksöz, 1971; Toksöz et al.,

1971) also apply to the newer scheme. Rather than re-
peating the results of those papers, the importance of
different kinds of numerical errors to the final results
will be discussed.

The formulation of truncation error for the scheme
with constant conductivity is sufficient to illustrate the
numerical effects on the attenuation of thermal anomalies.
Wavenumbers perpendicular to the slab are the most strongly
excited during the calculation and also the most dangerous
with regard to numerical inaccuracies. After two time
steps (one implicit in $\underline{x}$, one implicit in $\underline{z}$), such a wave-
number is attenuated by a factor of (Peaceman and Rachford,
1955)

$$\theta = \left(\frac{1 - 2\beta \sin^2(\pi y/4)}{1 + 2\beta \sin^2(\pi y/4)} \right)^2$$

where

$$\beta \equiv 2\kappa\Delta t/\Delta x^2$$

$$y \equiv \lambda_{min}/\lambda$$

$$\lambda_{min} = 2^{\frac{3}{2}}\Delta x = \text{minimum wavelength on grid}$$

This compares with the exact attenuation factor

$$\Omega = \exp(\beta\pi^2 y^2/2) \tag{A.17}$$

For small β the scheme is thus accurate to the second order
in β.

In the problems considered here, the shortest

wavelength components of temperature are re-excited by

the heat sources and by the slab motion in each time step.

In this case more accuracy is needed than in problems

where short wavelengths decay, and one might expect that

a value of β much less than 0.5 might be needed. However,

even in this case, $\beta = 0.5$ is sufficient for accuracy.

This can be seen by considering a continuous heat source

that contributes an amplitude of 1 to the shortest wave-

length component in one time step. Then its contribution

from the previous time step is θ, and the total amplitude

expected is

$$T \sim \sum_{0}^{N} \theta^N = \frac{1}{1-\theta} \tag{A.18}$$

Unless θ is near unity, as would occur if β was larger than

1, the higher order terms of the series would have little

effect. It is sufficient for the purpose of this numerical

calculation to have wavelengths which have attenuated in

the exact solution attenuate in the model. Unless $\beta > 1$,

numerical errors build up on about the same time scale

as the wavelength attenuates. The criteria used by

McKenzie (1971) that the ratio of $|1 - \Omega/\theta| < 0.02$ for

20% accuracy is misleading, since this small numerical

error acts similarly to a 2% change in conductivity and

can cause a large relative error in the results only after

the thermal anomaly is mostly attenuated. It should be

remembered that long wavelengths are more accurate than

short wavelengths, and that the truncation error does not
effect total heat energy.

Another source of error is from the method used to
model the motion of the slab. The discrete translation
steps tend to excite the wavenumbers parallel to the
slab, perpendicular to the most strongly excited wave-
number. When an excessive translation distance was used
the effect was evident, and could thus be removed in
subsequent calculations.

A.2 Flow in stratified viscous fluid

In this section a numerical method for determining the
two-dimensional flow pattern in a stratified viscous fluid
is derived from the variational principle of minimum work.
It is convenient to define a stream function, ψ , such
that

$$v_x \doteq \partial\psi/\partial y \tag{A.19a}$$

$$v_y = -\partial\psi/\partial x \tag{A.19b}$$

since the fluid flow equation A.2 can be reduced to

$$\nabla^4\psi = 0 \tag{A.20}$$

The stream function has the property that particles in the
fluid remain on surfaces of constant ψ called streamlines.
The variational principle requires that the integral of
viscous dissipation over all years be a minimum

$$\delta \sum_{i,j} \int \eta \left[\frac{\partial v_i}{\partial x_k} \left(\frac{\partial v_i}{\partial x_k} + \frac{\partial v_k}{\partial x_i} \right) \right] \, dV = 0 \qquad (A.21)$$

when zero stress or constant velocity boundary conditions are assumed. In two dimensions the integrand can be written in terms of ψ

$$\eta \left\{ 4 \cdot \left(\frac{\partial^2 \psi}{\partial x \partial y} \right)^2 + \left(\frac{\partial^2 \psi}{\partial^2 y^2} - \frac{\partial^2 \psi}{\partial x^2} \right)^2 \right\} \qquad (A.22)$$

The boundary conditions at the boundary of two viscous fluids are that material is conserved at the boundary

$$\psi_1 = \psi_2 \qquad (A.23)$$

that velocity parallel to the boundary in the x direction is constant

$$\frac{\partial \psi_1}{\partial y} = \frac{\partial \psi_2}{\partial y} \qquad (A.24)$$

and that stress is continuous at the boundary

$$\eta_1 \left(\frac{\partial v_x}{\partial y} + \frac{\partial v_y}{\partial x} \right)_1 = \eta_2 \left(\frac{\partial v_x}{\partial y} + \frac{\partial x_y}{\partial x} \right)_2 \qquad (A.25)$$

where 1,2 denote evaluation layer 1 or 2. Thus

$$\frac{\partial^2 \psi_1}{\partial y^2} = \frac{\eta_2}{\eta_1} \frac{\partial^2 \psi_2}{\partial y^2} + \left(1 - \frac{\eta_2}{\eta_1} \right) \frac{\partial^2 \psi}{\partial x^2} \qquad (A.26)$$

The numerical relaxation scheme is derived by using the

variation principle to obtain an improved estimate of
the value of the stream function at some point 0 (Figure
A.2) while leaving the stream function at all other
points constant. The formula obtained is applied re-
peatably at all the points in the region until a con-
vergent solution is obtained. We assume that point 0 is
on the boundary and that no other boundary is within two
points of point 0. Only terms involving ψ_0 need be
included in the variational integral, since other terms
drop out when differentiation with respect to ψ_0 is
performed. The expression

$$\left(\frac{\partial^2 \psi}{\partial y \partial x} \right)^2$$

is most easily evaluated at points a, b, c, and d. The
boundary condition A.26 can be used to show that for
evaluation around point 1

$$\int_{x,y} dV \left[\frac{\eta_1}{2} \left(\frac{\partial^2 \psi_1}{\partial y^2} - \frac{\partial^2 \psi}{\partial x^2} \right)^2 + \frac{\eta_2}{2} \left(\frac{\partial^2 \psi_2}{\partial y^2} - \frac{\partial^2 \psi}{\partial x^2} \right)^2 \right]$$

(A.27)

$$= \frac{1}{h^2} \frac{\eta_1 \eta_2}{(\eta_1 + \eta_2)} (\psi_5 + \psi_8 - \psi_{12} - \psi_0)^2$$

h is the grid spacing.

Those terms in the variational integral containing ψ_0 are

$$2h^2 E_0 = 4\eta_1 (\psi_5 - \psi_1 - \psi_2 + \psi_0)^2 + 4\eta_1 (\psi_6 - \psi_3 - \psi_2 - \psi_0)^2$$

$$4\eta_2 (\psi_8 - \psi_1 - \psi_4 + \psi_0)^2 + 4\eta_2 (\psi_7 - \psi_3 - \psi_4 - \psi_0)^2$$

$$+ \eta_1 (\psi_9 - \psi_0 - \psi_5 - \psi_6)^2 + \eta_2 (\psi_{11} + \psi_0 - \psi_8 - \psi_7)^2$$

$$+ 2 \frac{\eta_1 \eta_2}{\eta_1 + \eta_2} \left((\psi_0 + \psi_{12} - \psi_8 - \psi_5)^2 \right.$$

$$\left. + (\psi_0 + \psi_{10} - \psi_6 - \psi_7)^2 \right) \tag{A.28}$$

By setting $\dfrac{\partial E_0}{\partial \psi_0} = 0$

we obtain the relaxation formula

$$\psi_0 = \left(9\eta_1 + 9\eta_2 + 4 \frac{\eta_1 \eta_2}{\eta_1 + \eta_2} \right)^{-1} \left[8\eta_1 \psi_2 + 4(\eta_1 + \eta_2)(\psi_1 + \psi_3) \right.$$

$$+ 8\eta_2 \psi_4 + (\psi_5 + \psi_6)\left(-3\eta_1 + 2 \frac{\eta_1 \eta_2}{\eta_1 + \eta_2} \right)$$

$$+ (\psi_7 + \psi_8)\left(-3\eta_2 + 2 \frac{\eta_1 \eta_2}{\eta_1 + \eta_2} \right) - \left((\psi_{12} + \psi_{10}) \right.$$

$$\left. 2 \frac{\eta_1 \eta_2}{\eta_1 + \eta_2} \right) - \eta_1 \psi_9 - \eta_2 \psi_{11} \right] \tag{A.29}$$

For $\eta_1 = \eta_2$ the formula reduces to the standard numerical expression for the biharmonic equation

$$\psi_0 = \frac{1}{20} \left(8(\psi_1 + \psi_2 + \psi_3 + \psi_4) - 2(\psi_5 + \psi_6 + \psi_7 + \psi_8) \right.$$

$$\left. - (\psi_9 + \psi_{10} + \psi_{11} + \psi_{12}) \right) \tag{A.30}$$

It is more convenient at interior points away from boundaries to use a two step relaxation formula due to Burgraff (1966)

$$\psi_0 = \frac{1}{4} \left(\psi_1 + \psi_2 + \psi_3 + \psi_4 + h^2 \Omega_0 \right) \qquad \text{(A.30a)}$$

$$\Omega_0 = \frac{1}{4} \left(\Omega_1 + \Omega_2 + \Omega_3 + \Omega_4 \right) \qquad \text{(A.30b)}$$

The boundary condition to a rigid wall normal to y

$$\psi_0 = \text{constant} \qquad \text{(A.31a)}$$

$$\Omega_0 = -(2/h^2)(\psi_4 - hV) \qquad \text{(A.31b)}$$

V the velocity of the wall

The two step relaxation procedure used in the interior is unconditionally stable (Burgraff, 1966). The program for computing was checked by comparison of the results with special cases (Burgraff, 1966; Pan and Acrivos, 1967) and by comparison with results obtained numerically for a fluid with a variable viscosity (D.J. Andrews, personal communication). Even when the viscosities of different layers differed by a factor of 1000, the program converged after a few hundred iterations.

FIGURE CAPTIONS

Figure A.1   Schematic representation of the computational

scheme, input parameters, and boundary con-

ditions used to calculate thermal models of

slabs.   (Modified after Toksöz et al., 1971).

Figure A.2   Finite difference grid is used to obtain an

improved value of the stream function at

point 0 by numerical relaxation.   The line

through points 12, 1, 0, 3 and 10 is the

boundary between the two fluids of different

viscosity.   The stream function is defined

at numbered points.   For convenience certain

derivatives were evaluated at letter points

during the derivation of the finite difference

formula.
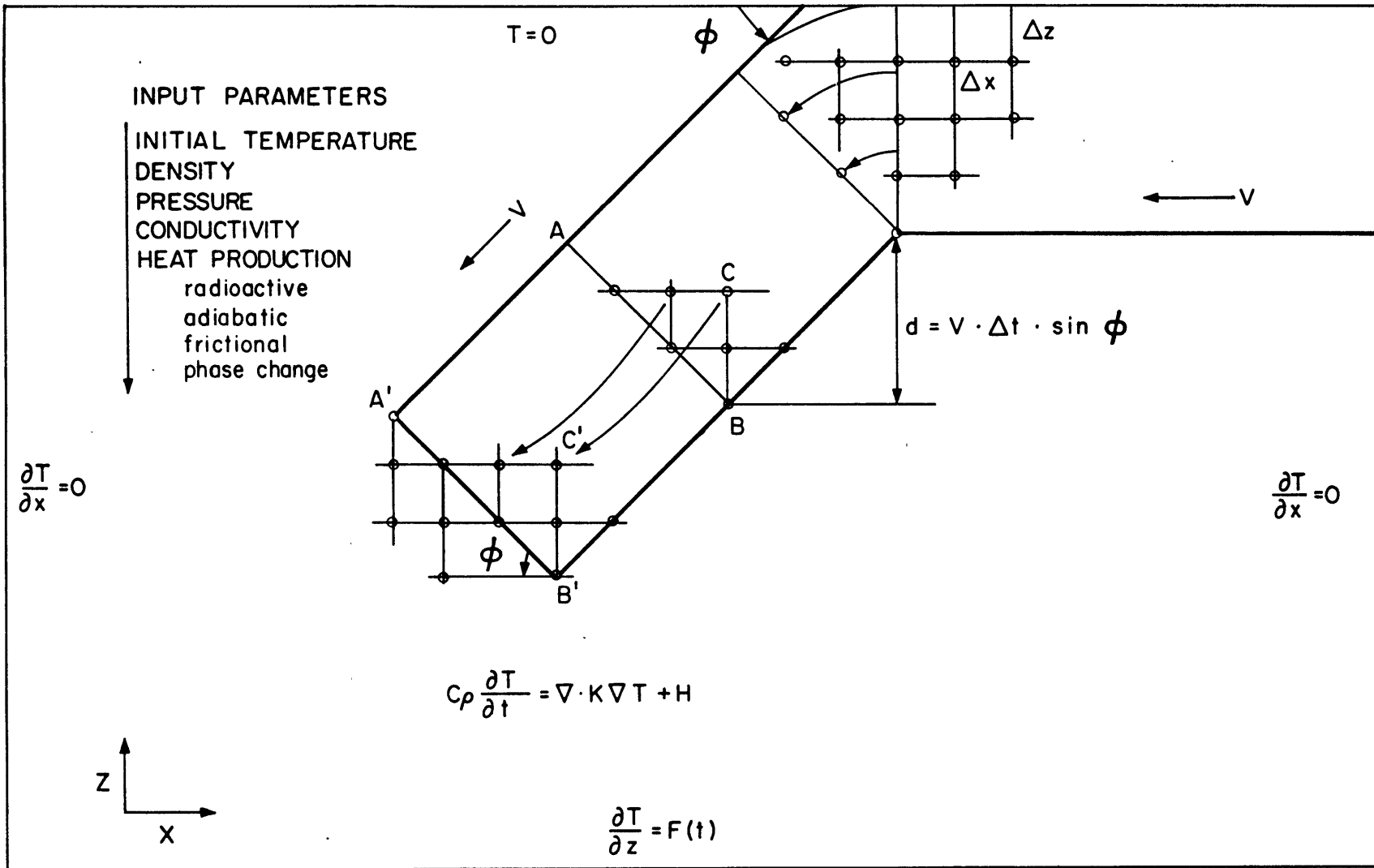
FIGURE A.1
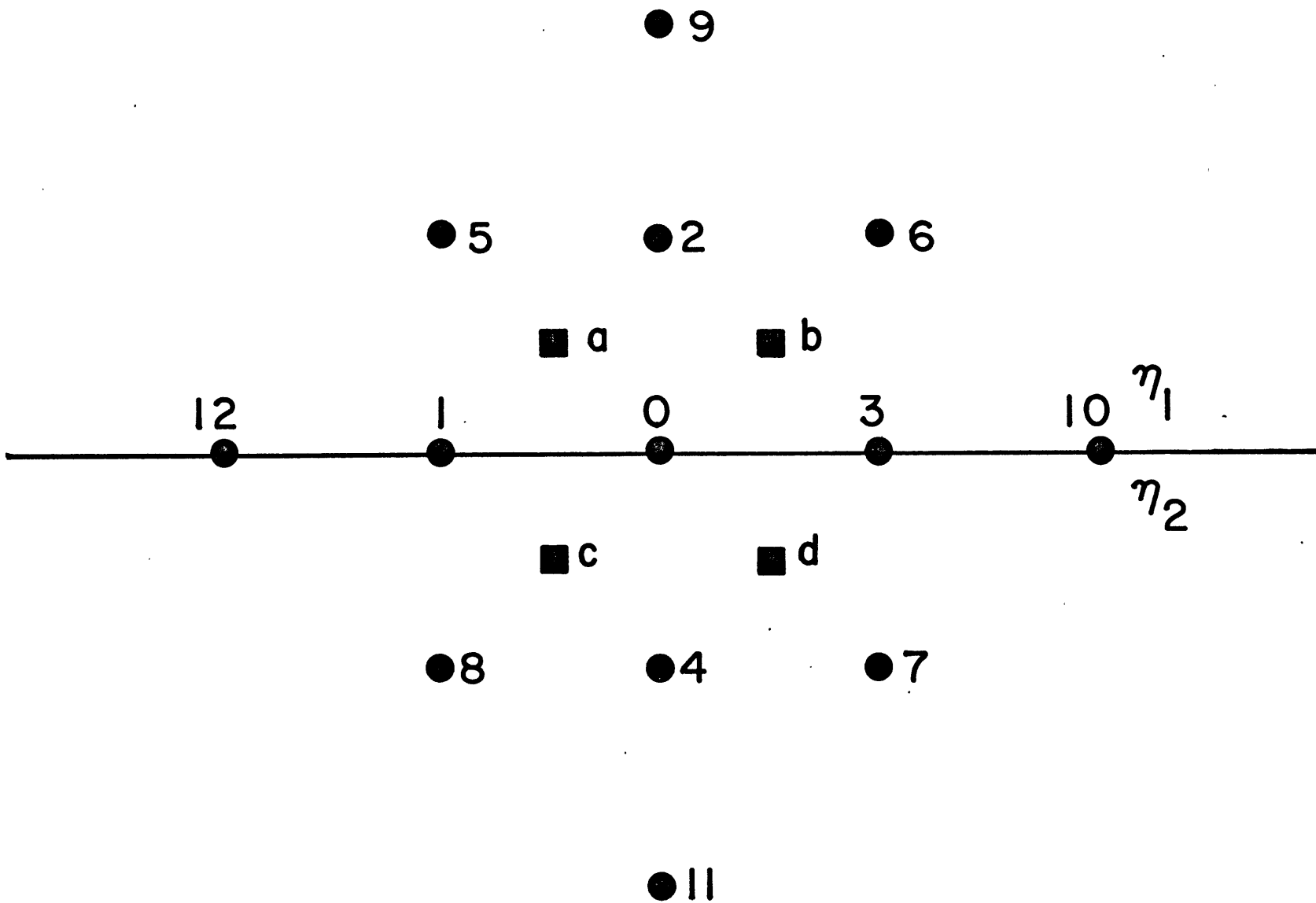
FIGURE A.2

APPENDIX B

Measured Earthquake Amplitudes

The measured amplitudes for the earthquakes and
nuclear explosions used in this study are plotted in
Figures B.1, B.2, B.4, B.6, B.8, B.9, B.11, B.12, B.13,
B.14, B.15, B.16, B.17, and B.18. The amplitudes could
not be computed on an absolute scale because the period
of the first motion could not be accurately measured.
Relative amplitudes for each event are sufficient for
the purpose of this paper. The amplitudes indicated by
a given amplitude on the scale of a figure or by a given
interval number should not be compared between earthquakes
or between the short and long periods of an earthquake,
since the scales have been adjusted to avoid large ordinate
or interval class values. The distribution of interval
class numbers with respect to terrestrial co-ordinates are
plotted for earthquakes which were not explicitly used in
the main text in Figures B.3, B.5, B.7, and B.10. The
earthquakes are grouped by location with the Aleutian
earthquakes plotted in Figures B.2 through B.11, the Tonga-
Kermedec earthquakes in Figures B.12 through B.17, and the
Kurile earthquake in Figure B.18. Within each group the
ordering is chronological.

FIGURE CAPTIONS

Figure B.1.   The amplitude of the first peak to peak motion

measured on the short period, vertical

component of WWSS records is plotted as a

function of distance for the LONGSHOT (above)

and MILROW (below) events. Stations in the

predicted shadow zone are indicated by circles.

The cross bars terminating lines extended from

the symbols are station corrected values.

Stations used for LONGSHOT in order of increasing

distance included: CMC, LON*, SEO* (This station

may have been dead for MILROW), BKS*, BOZ, GUA*,

NOR*, DUG, GSC, RCD, ANP, GOL, GDH*, TUC, ALQ*,

KEV*, HKC*, KTG*, BAG*, LUB, MDS, RAB, AAM*,

JCT, DAL, DAV*, AKU*, HNR*, OXF, AFI*, SCP,

NUR*, KON, NHA, OGD, ATL*, WES*, SHL, ESK*,

LAHI RARI NDI*, VAL*, CTA, MSH, QUE, STU*, BEC*,

TAB*, TRI, IST*, POO, SHI, PTO, RIV*, PDA, PTO,

RIV*, PDA, TOL*, KOD, BHP, SJG*, JER, MAL*, and

ADE. Stations used for both events are indicated

by '*'. Stations used only for MILROW included:

MAT, GEO, COP, and LOR. Numbered interval

classes differing by factors of two are

formed by the assumed amplitude-distance curve.

Figure B.2. Observed short (above) and long (below)

period amplitudes from the earthquake of

5 Feb 1965, at 9h (earthquake #4, Stauder,

1968a) are plotted as a function of epicentral

distance. The cross bars on top of lines

extending from symbols indicate the amplitude

as corrected for source mechanism. No

correction is plotted when the correction is

smaller than the symbols. Triangles indicate

stations between -50 and 50 degrees azimuth.

Other stations are indicated by circles. Open

symbols are less accurate measurements due to

small signal, high noise, or poor records.

The assumed long and short period amplitude

curves divided the data into interval classes

differing by factors of two. Stations in

order of increasing epicentral distance include:

CMC, LON, NOR, BOZ, RCD, GDH, GOL, HKC, BAG,

KEV, TUC, MAN-S, KTG, RAB, DAV, LUB, UME-S,

HNR-S, FLO, AAM, NUR, NHA, PMG, KON-L, SCP,

BLA, WES, GEO, COP, LAH-L, NDI-L, ESK, VAL,

CTA, QUE, STU, TRI, LEM, POO, LPS-S, SHI-L,

AQU, KOD-L, TOL, RIV-L, and SJG. Stations for

which only short or long period readings were

made are indicated by 'S' or 'L' respectively.

Figure B.3. The amplitudes for the earthquake of 5 Feb 1965, at 9h are plotted as in Figure 3.17.

Figure B.4. The amplitudes measured for the earthquake of 5 Feb 1965, at 20h (earthquake #5, Stauder, 1968a) are plotted as in Figure B.2. Stations included: CMC, NOR, BOZ, DUG-S, RCD, GDH, GOL, BAG, MAN, TUC, KEV, KTG, RAB, DAV, LUB, UME-S, AAM, PMG, NUR, KON, SCP, COP, NDI, ESK, VAL, QUE, STU, LEM, BEC, TRI, POO, LST, SHI, AQU, KOD-L, PTO, TOL, and SJG.

Figure B.5. The amplitudes for the earthquake of 5 Feb 1965, at 20h are plotted as in Figure 3.17.

Figure B.6. The amplitudes measured for the earthquake of 6 Feb 1965, (earthquake #6, Stauder, 1968a) are plotted as in Figure B.2. Stations included: CMC-S, NOR, DUG-S, RCD-S, GOL, GDH, TUC, BAG, KEV, MAN, KTG, RAB, LUB, DAV, HNR, FLO, UME-S, AAM-S, NUR-S, PMG-S, NHA-L, SHL-L, SCP, KON, BLA, COP, NDI, ESK, CTA-S, VAL, QUE, STU, BEC-L, TRI-S, LEM, POO, IST, SHI, AQU-S, PTO, JER, SJG, and ADE-L.

Figure B.7. The amplitudes for the earthquake of 6 Feb 1965, are plotted as in Figure 3.17.

Figure B.8. The amplitudes measured for the earthquake of 7 Feb 1965, at 2h are plotted as in Figure B.2. Stations included: CMC, LON, COR-L, BKS, ANP-L, NOR, BOZ, DUG, RCD, BAG, GDH, GOL, MAN, KEV, TUC, KTG, RAB, LUB, FLO, PMG, AAM, SHL, NUR, KON, SCP, BLA, LAH-L, NDI, COP, ESK, CTA, QUE, VAL, STU, POO, TRI, BEC, IST, SHI, AQU, KOD, RIV, PTO, ADE, and SJG-S.

Figure B.9. The amplitudes measured for the earthquake of 7 Feb 1965, at 9h (earthquake #8, Stauder, 1968a) are plotted as in Figure B.2. Stations included: CMC, LON, BKS, BOZ, NOR, DUG, RCD, GOL, TUC, KTG, BAG, LUB, FLO, AAM, DAV, UME-S, SCP-S, PMG, NUR-S, BLA, SHL-L, KON, COP-S, ESK, LAH, NDI, VAL, CTA, QUE-L, STU, IST-L, POO, SHI, RIV-L, KOD-L, and SJG.

Figure B.10 The amplitudes for the earthquake of 7 Feb 1965 at 9h are plotted as in Figure 3.17.

Figure B.11   The amplitudes measured for the earthquake of

2 Jun 1966 are plotted as in Figure B.2.

Stations included: KIP, CMC, SEO-S, LON, COR,

BKS, BOZ, NOR, DUG, GDH, HKC, TUC, ALQ, KEV,

KTG, RAB, LUB, HNR-L, FLO-L, AKU, UME-L, AAM-S,

PMG, NOR, SHL, CHG, SCP, KON, BLA, COP, LAH,

NDI, ESK, SNG, CTA, MSH, VAL, STU, BEC, LPS,

TRI, POO, IST, SHI, PTO, JER, ADE-S, and SJG.

This earthquake was used to obtain source

corrections for LONGSHOT.

Figure B.12   The amplitudes measured for the earthquake of

21 Jul 1964, are plotted as in Figure B.2

except that triangles denote stations between

210 and 330 degrees azimuth.   Hexagons indicate

low amplitude precursors.   Stations included:

TAU-S, CTA, PMG, ADE, KIP, SBA, GUA, MUN-S,

SPA-S, MAN, BAG, ANP, HKC, BKS, TUC, DUG, ALQ,

CHG, LUB, BOZ, NHA, and LPS-S.

Figure B.13   The amplitudes measured for the earthquake

of 5 Aug 1964, are plotted as in Figure B.12.

Stations included: CTA, ADE, PMG, SBA, MUN, GUA,

KIP, MAN, BAG, ANP, HKC, BKS, GSC-L, TUC, ANT,

CHG, NNA-S, and ALQ.

Figure B.14   The amplitudes measured for the earthquake of

18 Mar 1965, are plotted as in Figure B.12.

Stations included: RIV, RAB, CTA, PMG, TAU,

ADE-S, KIP-S, GUA, HKC, TUC, LON, DUG, ALQ,

COL, BOZ, GOL, RCB-S, and LUB-S.

Figure B.15   The amplitudes measured for the earthquake of

20 Aug 1965 are plotted as in Figure B.12.

Stations included: CTA, RAB, TAU-S, PMG, ADE,

KIP, GUA, SBA, MUN, SPA-S, MAN, MAT-S, BAG, LEM,

ANP-L, BKS, SEO, SOM, COR, TUC, DUG, ALQ, BOZ,

LUB, COL, and LPS.

Figure B.16   The amplitudes measured for the earthquake of

10 Aug 1966, are plotted as in Figure B.12.

Stations included: RIV, RAB, CTA, PMG-S, TAU, ADE,

KIP-S, GUA, SBA, MUN, DAV, SPA-S, MAN-L, MAT, BAG,

ANP, BKS, SEO, TUC, LON, DUG, ALQ, BOZ, COL,

LUB, GOL, JCT, PEL-S, and LPS.

Figure B.17   The amplitudes measured for the earthquake of

12 Aug 1967 are plotted as in Figure B.12.

Stations included: CTA, TAU-S, RAB, PMG, ADE-S,

KIP-S, GUA, SBA, MUN, DAV, SPA, MAN, BAG, MAT,

ANP-L, BKS, SEO, HKC, LON, ALQ, BOZ, LUB, COL,

and GOL.

Figure B.18 The amplitudes for the earthquake of 4 Aug 1964
are plotted as in Figure B.2 except that
triangles denote stations between -100 and 10
degrees azimuth. Stations included: COL, HKC,
BAG, MAN, KIP, CMC, NHA, RAB, NOR, PMG-L, HNR,
LON, KEV, NDI-L, LAH, BKS, BOZ, KTG, NUR, QUE,
DUG, CTA, GSC, AKU-S, RCD-S, KON, GOL, TUC,
COP-L, ALQ, SHI-S, IST, STU, RIV-S, VAL-L,
SCP-L, JER, MUN-S, and BLA.
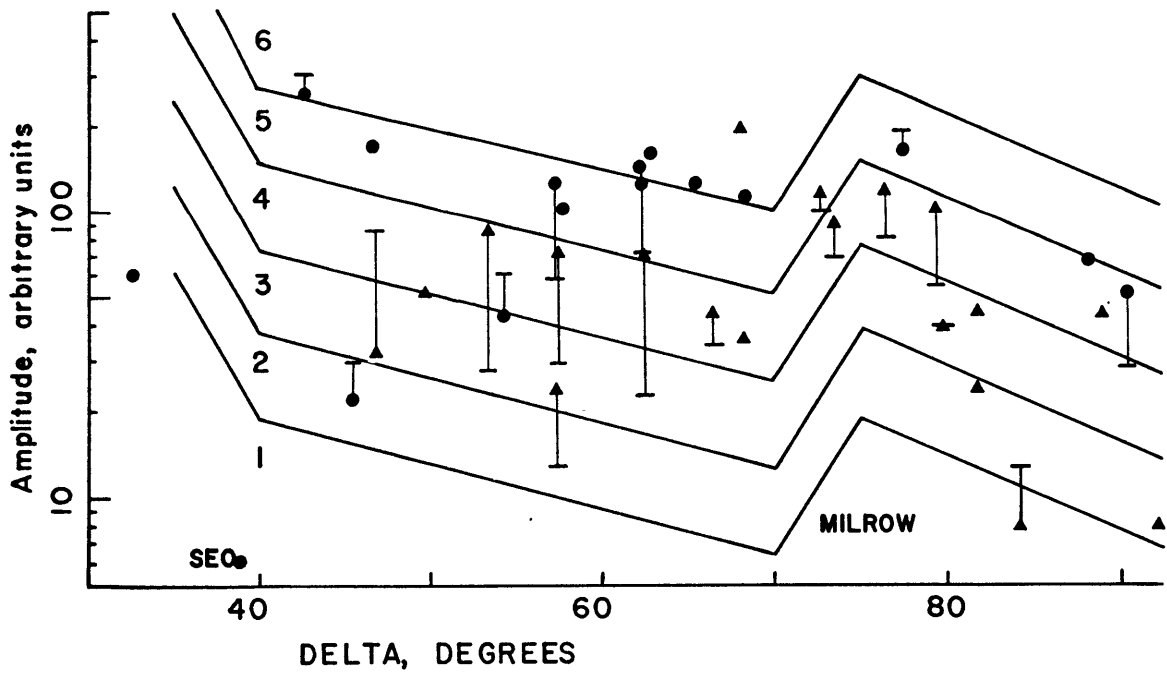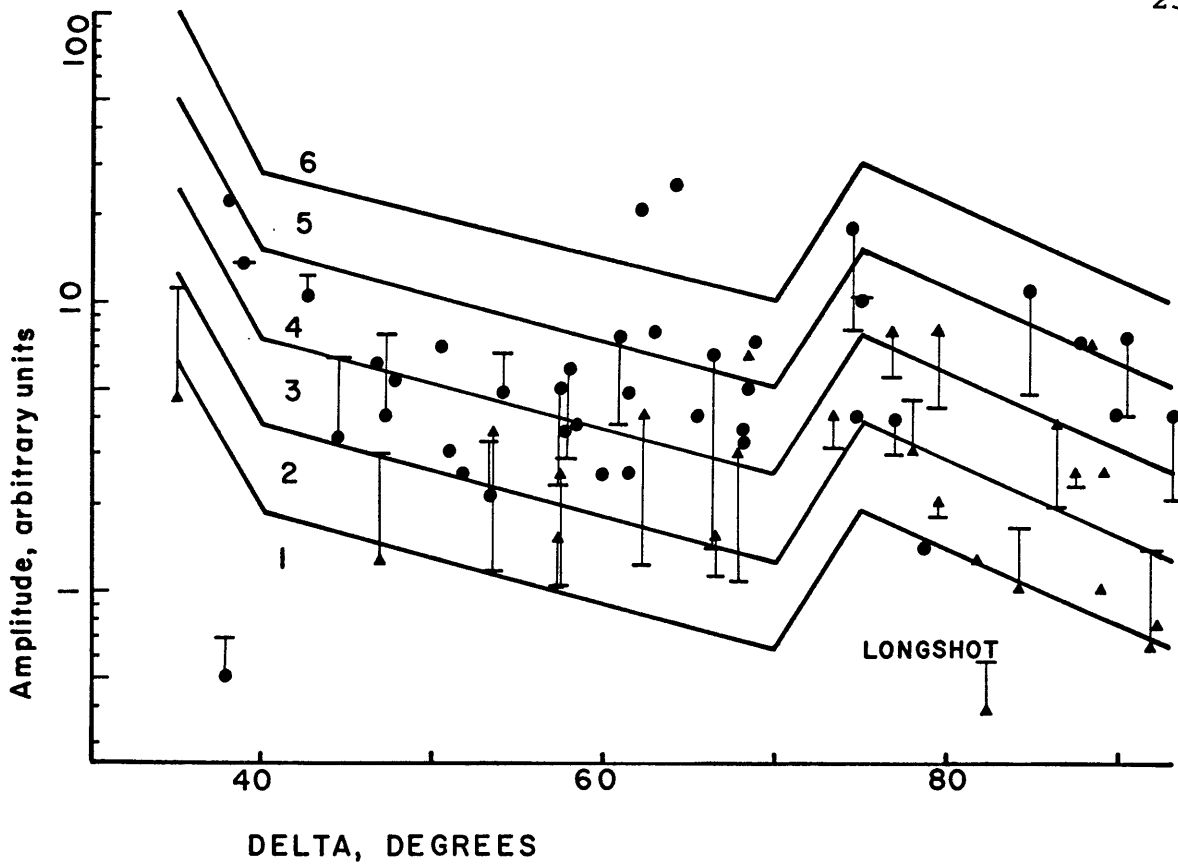
FIGURE B.1
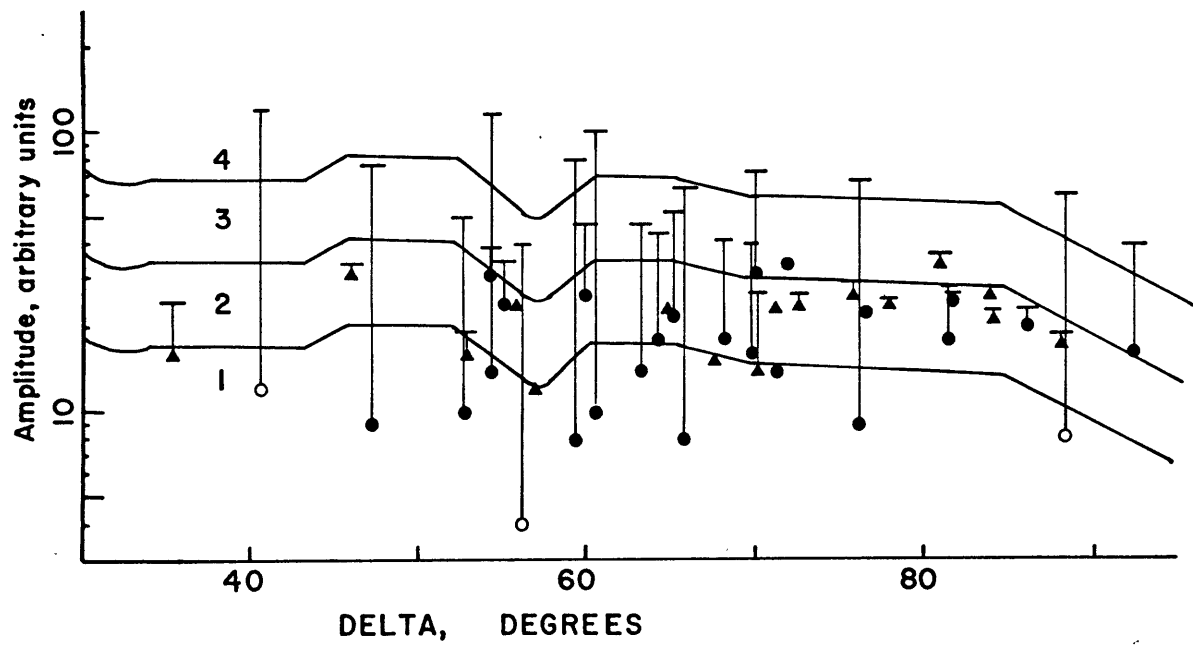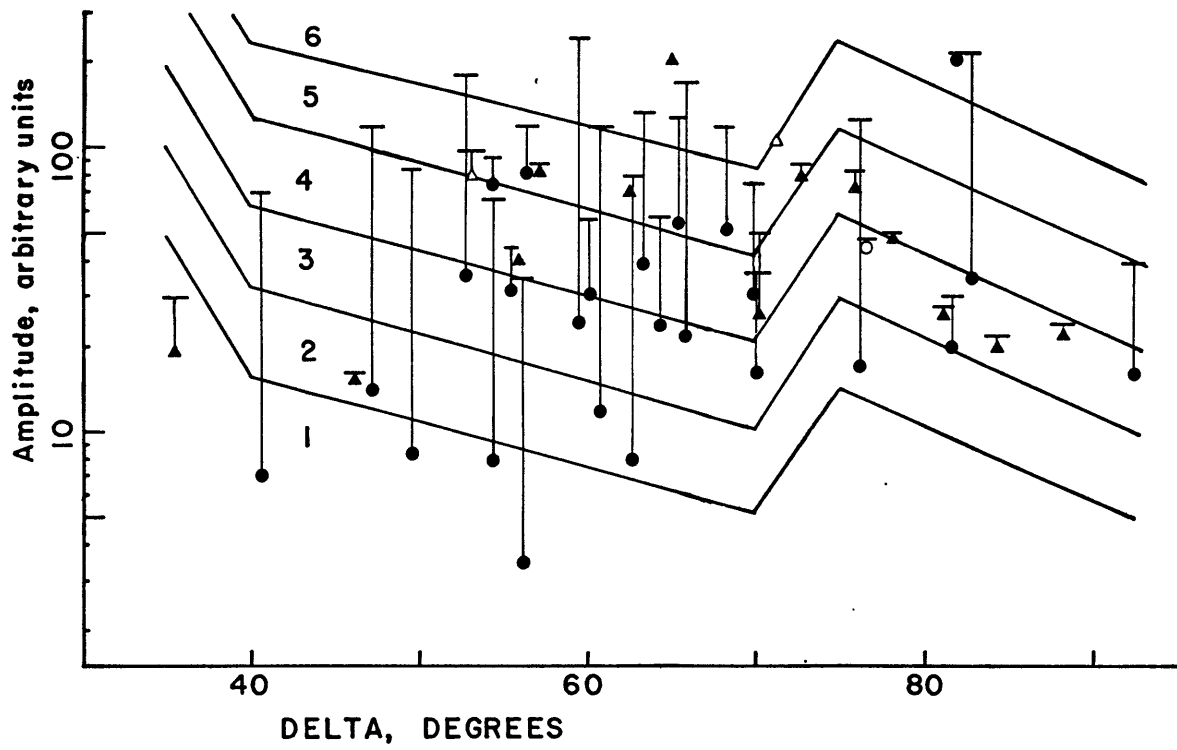
FIGURE B.2

FIGURE B.3

FIGURE B.4

SPZ

LPZ

20h
5 FEB 1965

SOURCE CORRECTED   UNCORRECTED

FIGURE B.5

FIGURE B.6

6 FEB 1965

SPZ

LPZ

SOURCE CORRECTED

UNCORRECTED
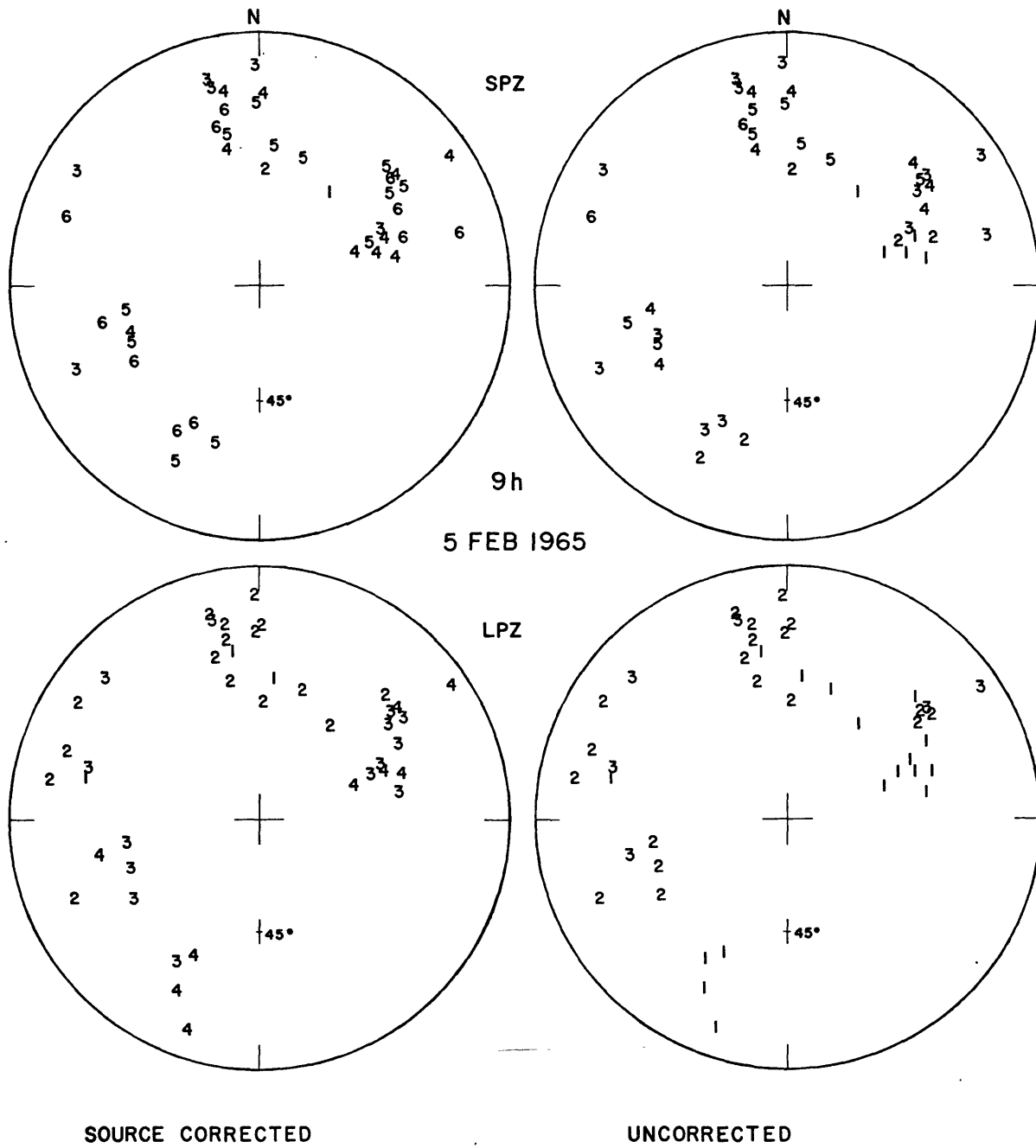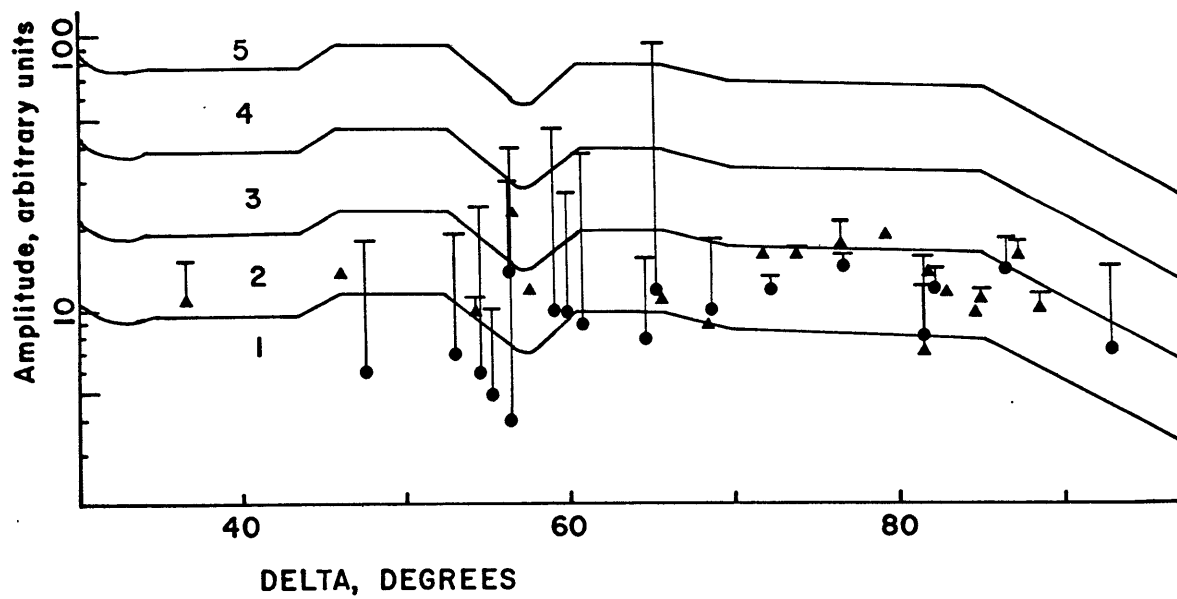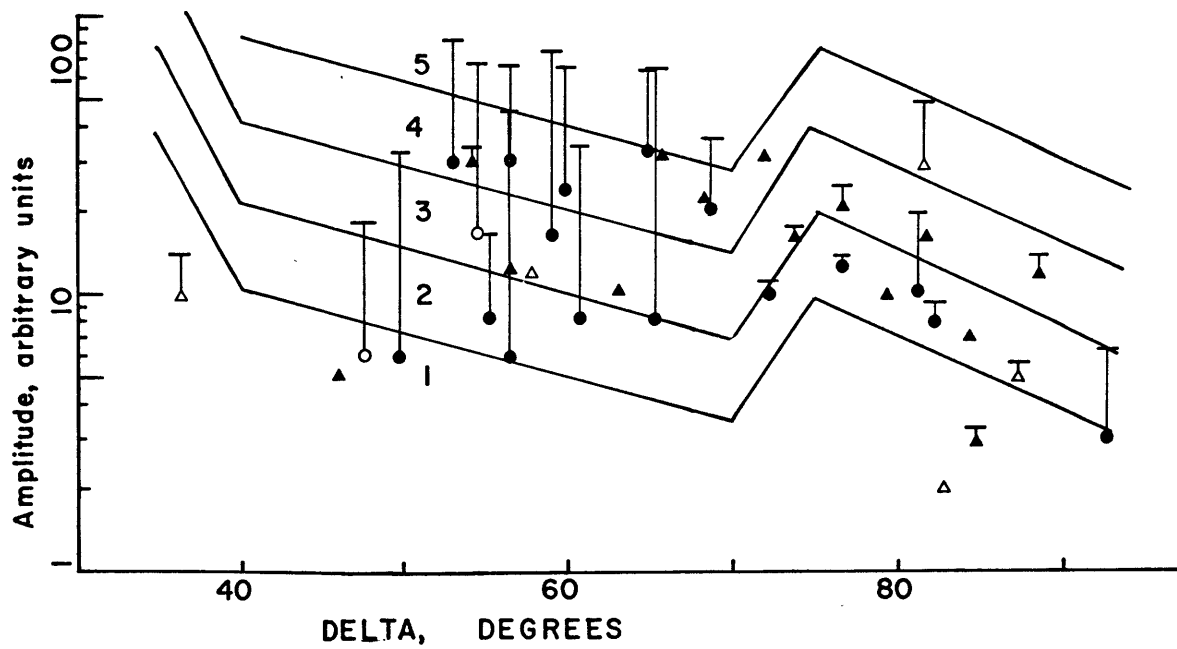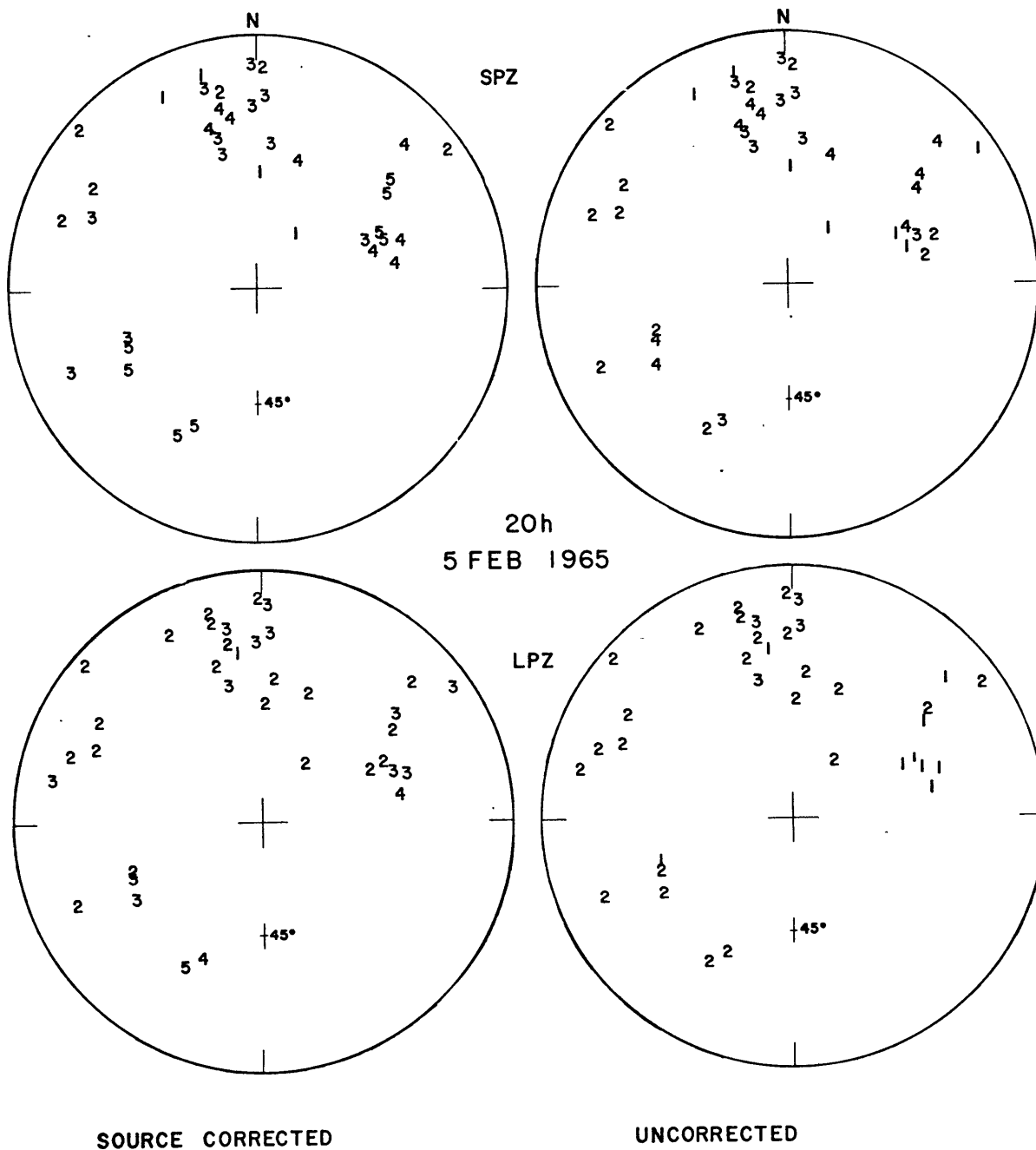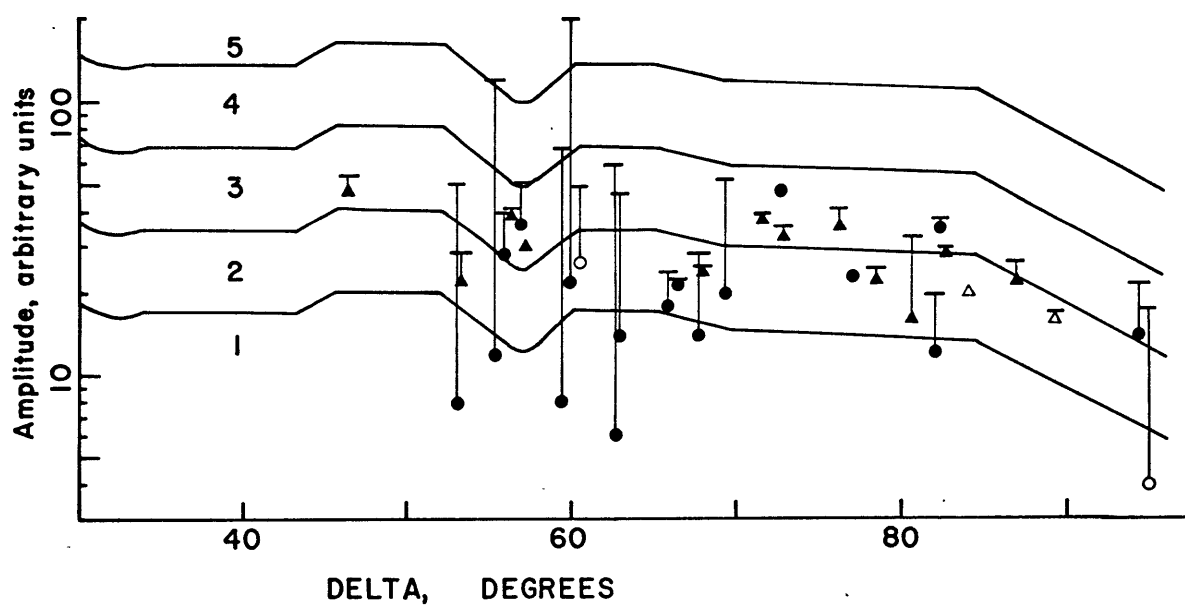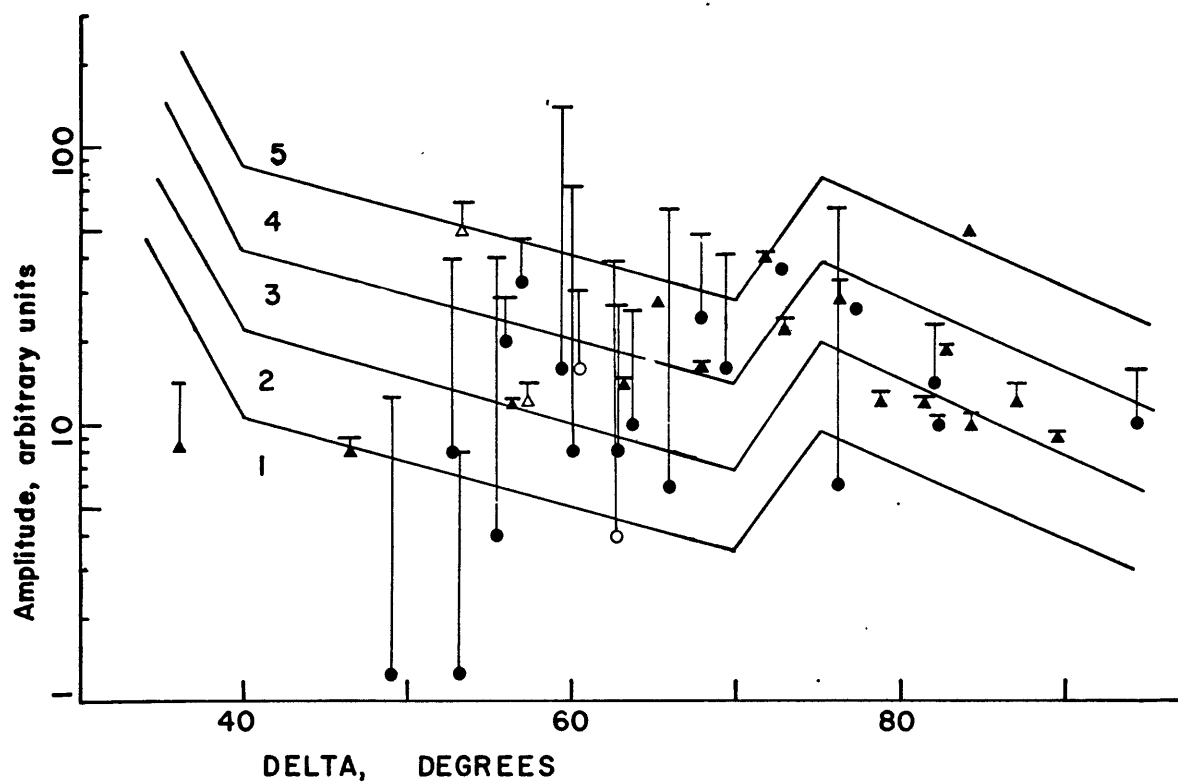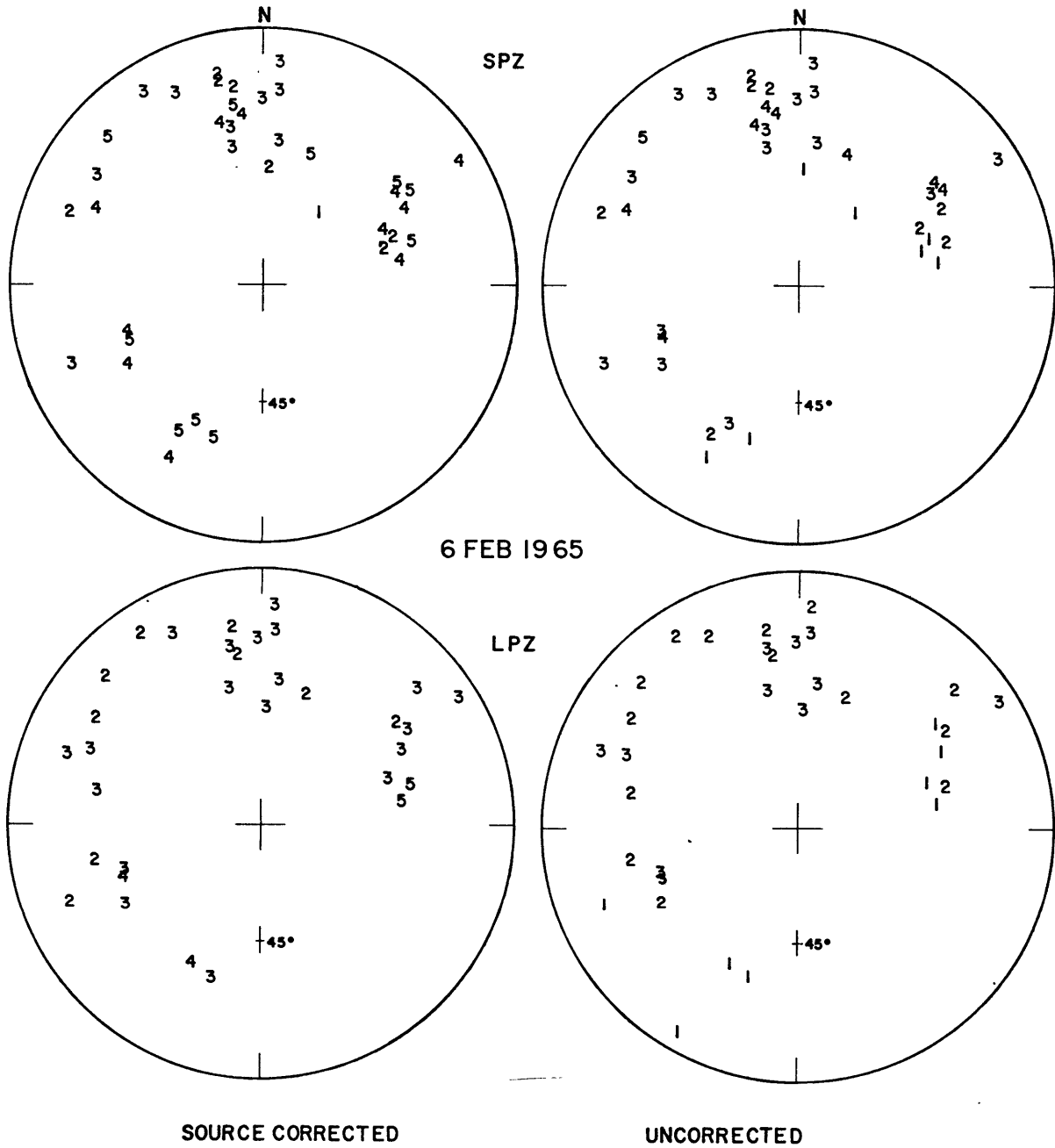
FIGURE B.7

FIGURE B.8

FIGURE B.9

SPZ

LPZ

9h
7 FEB 1965

SOURCE CORRECTED   UNCORRECTED
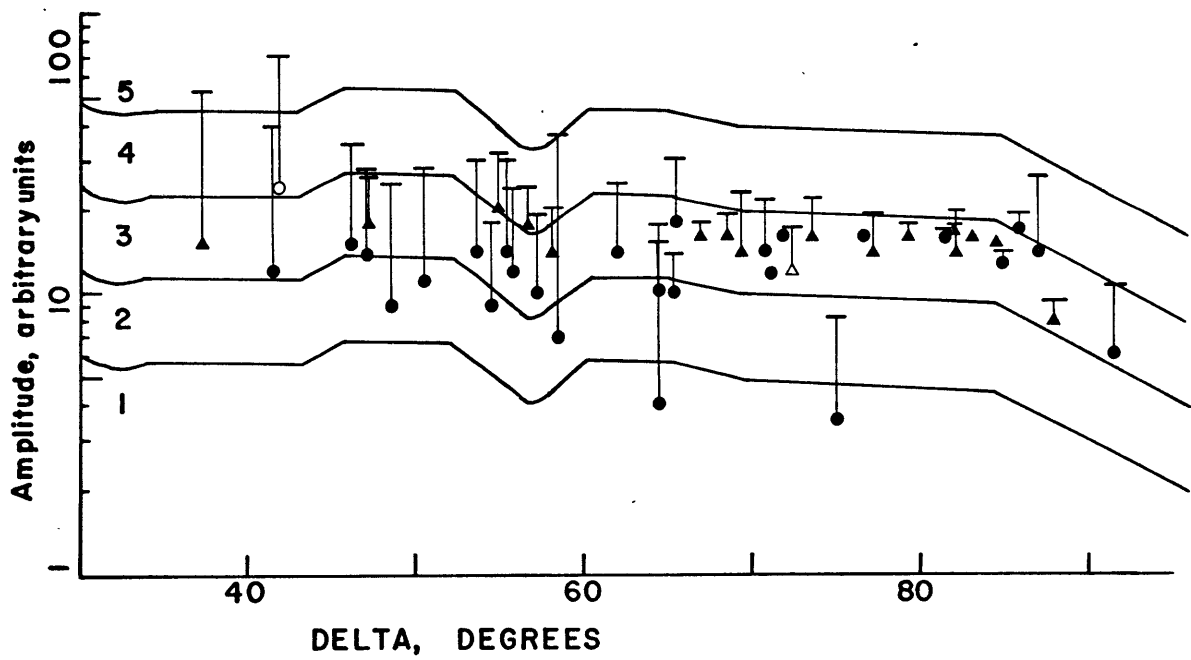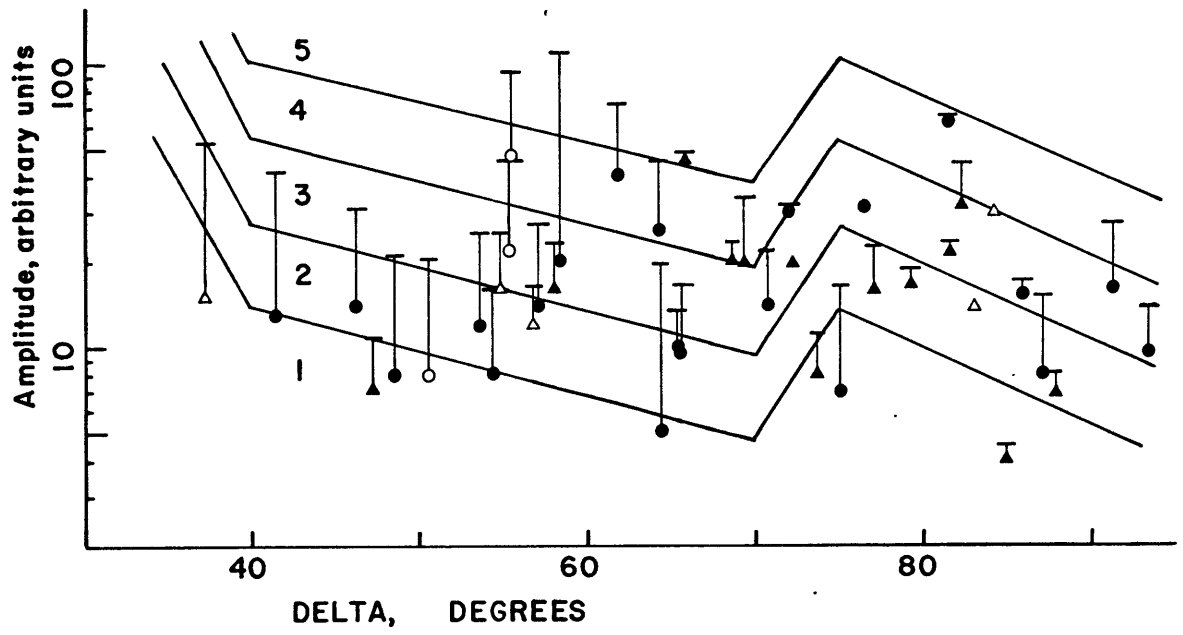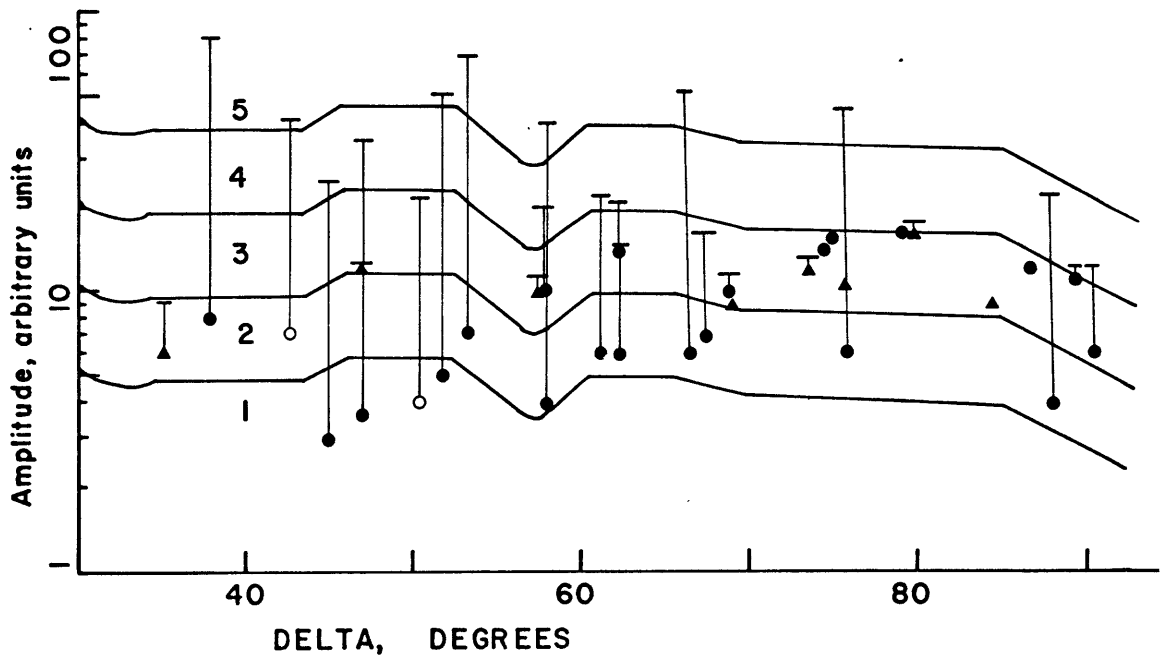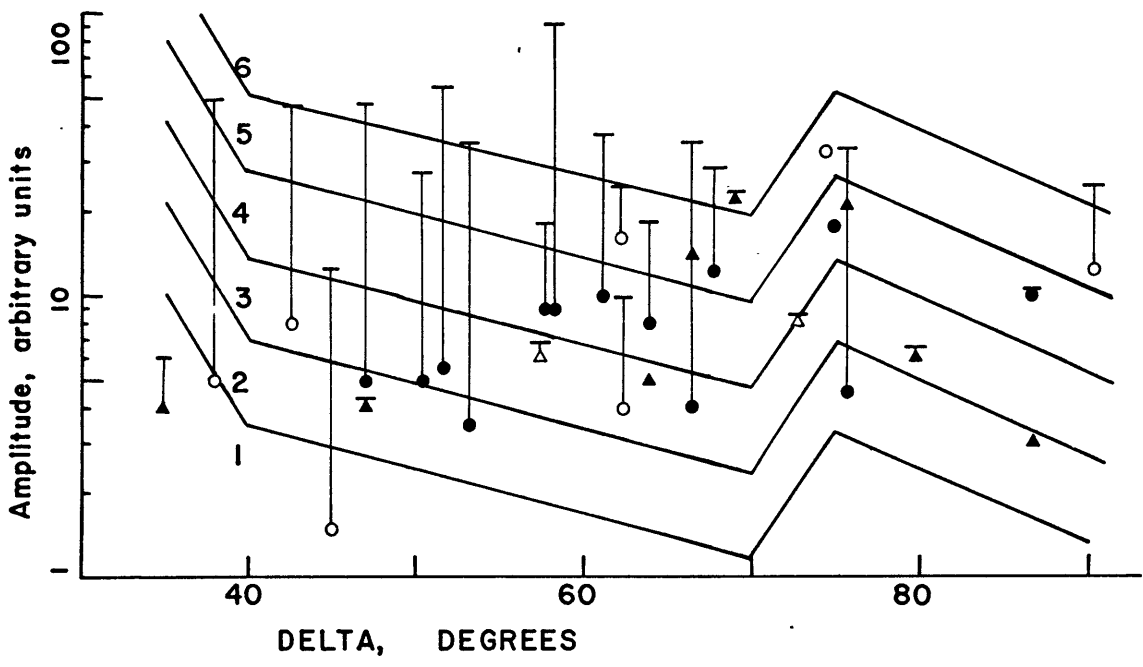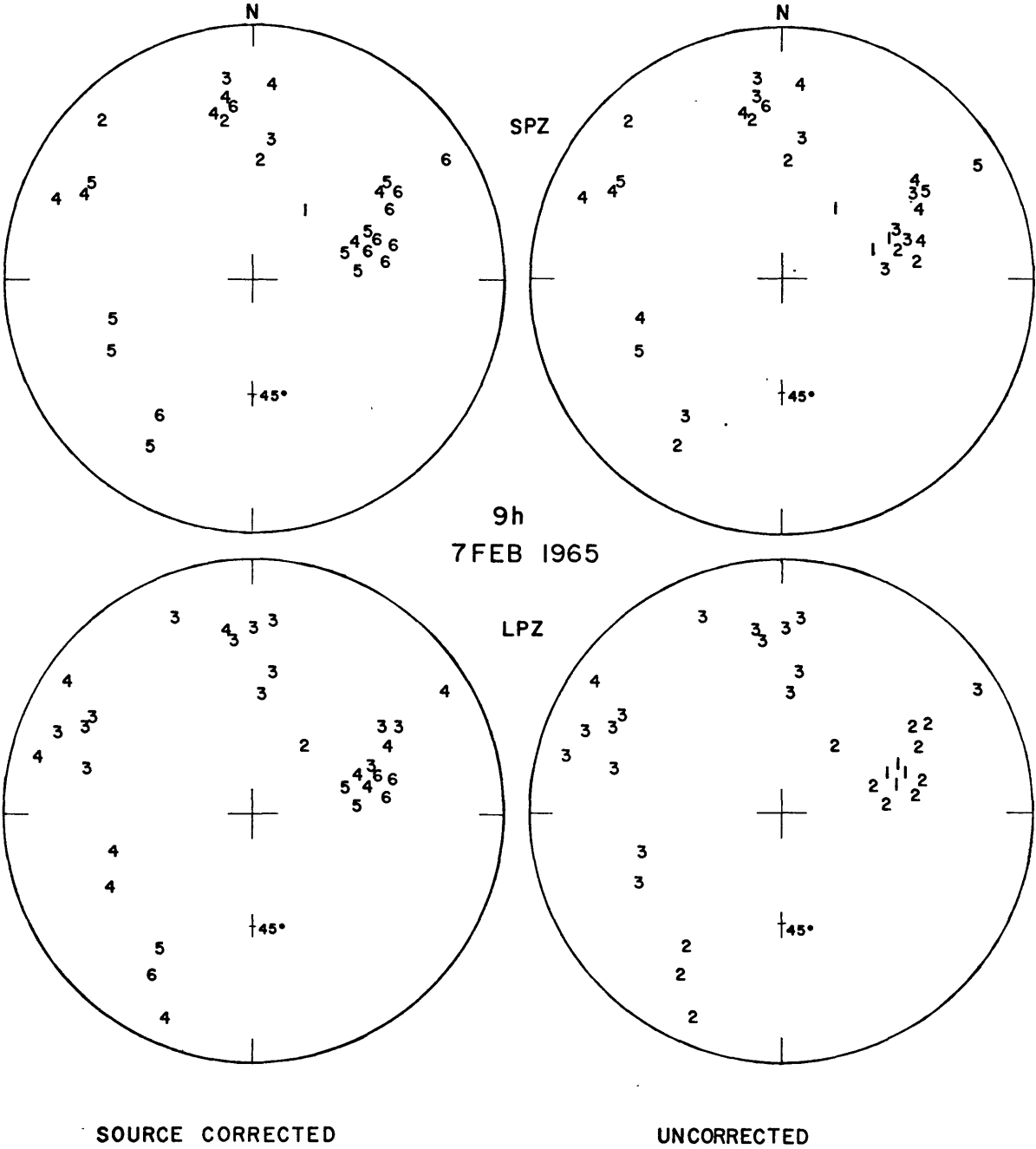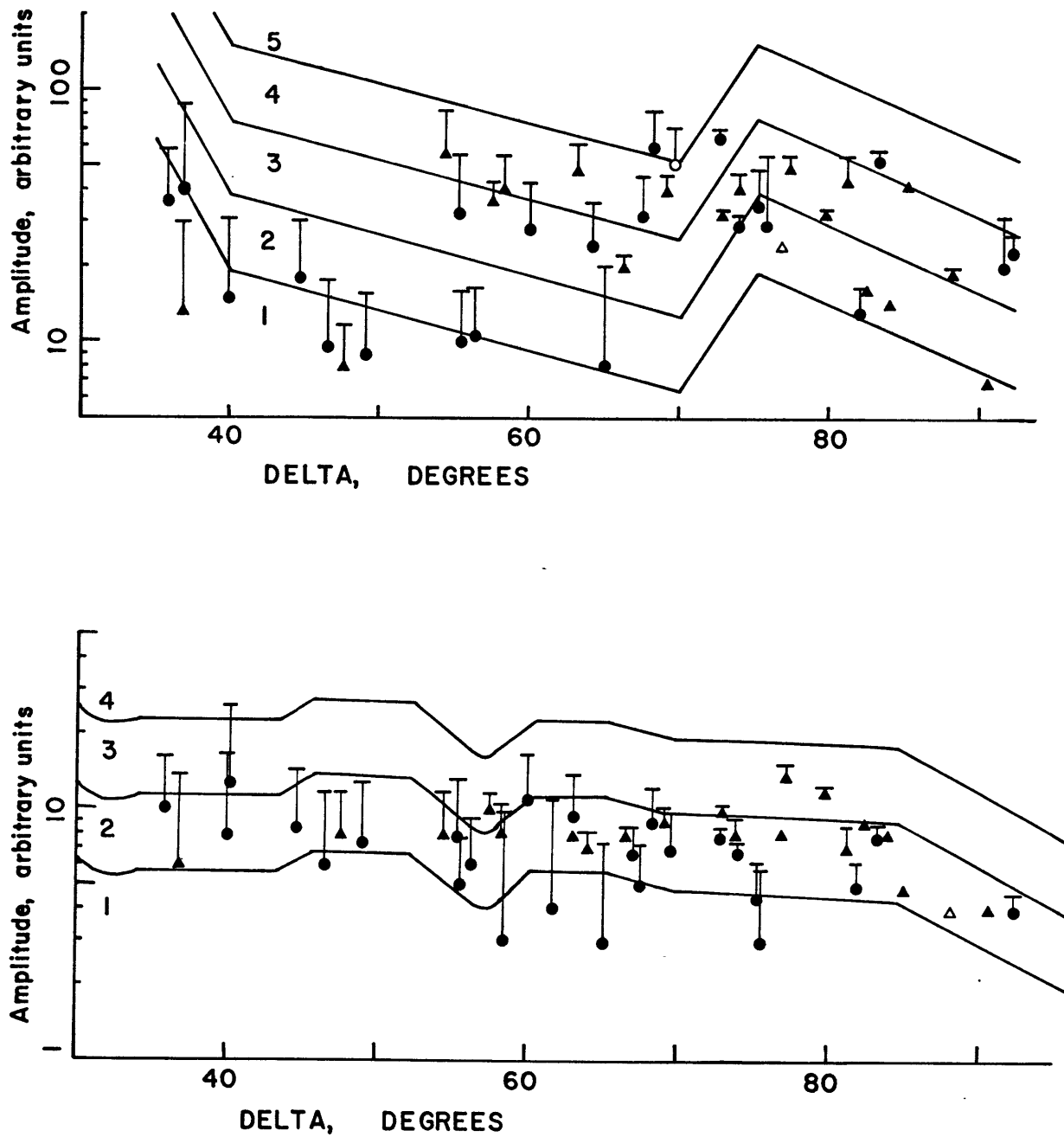
FIGURE B.10
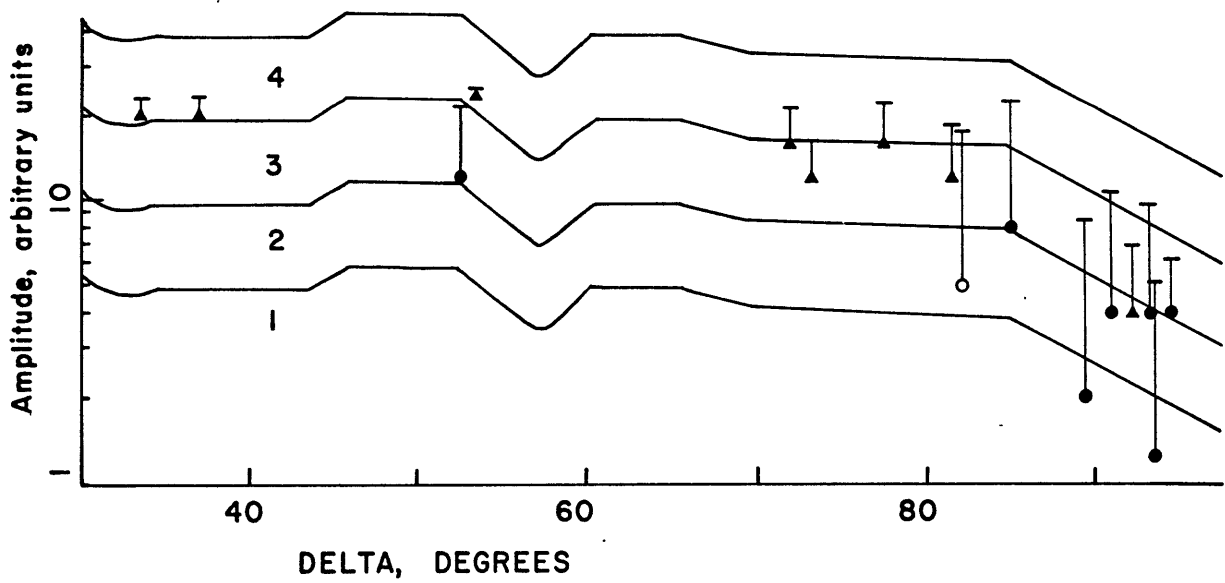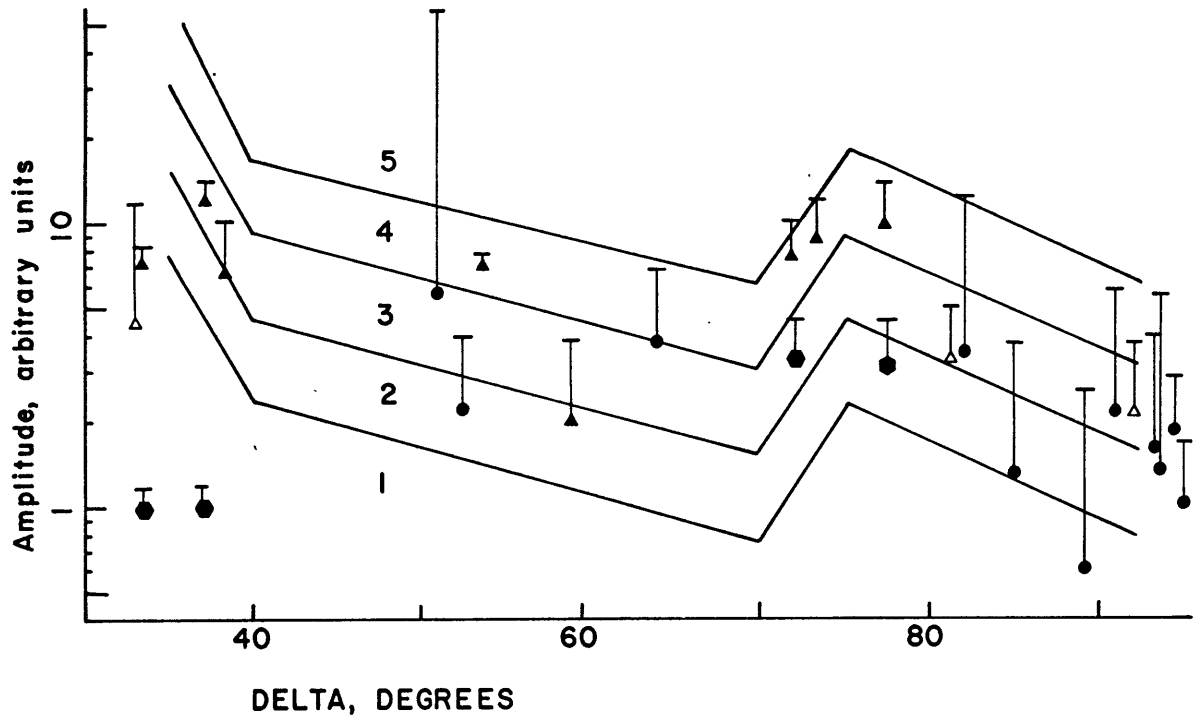
FIGURE B.11

FIGURE B.12
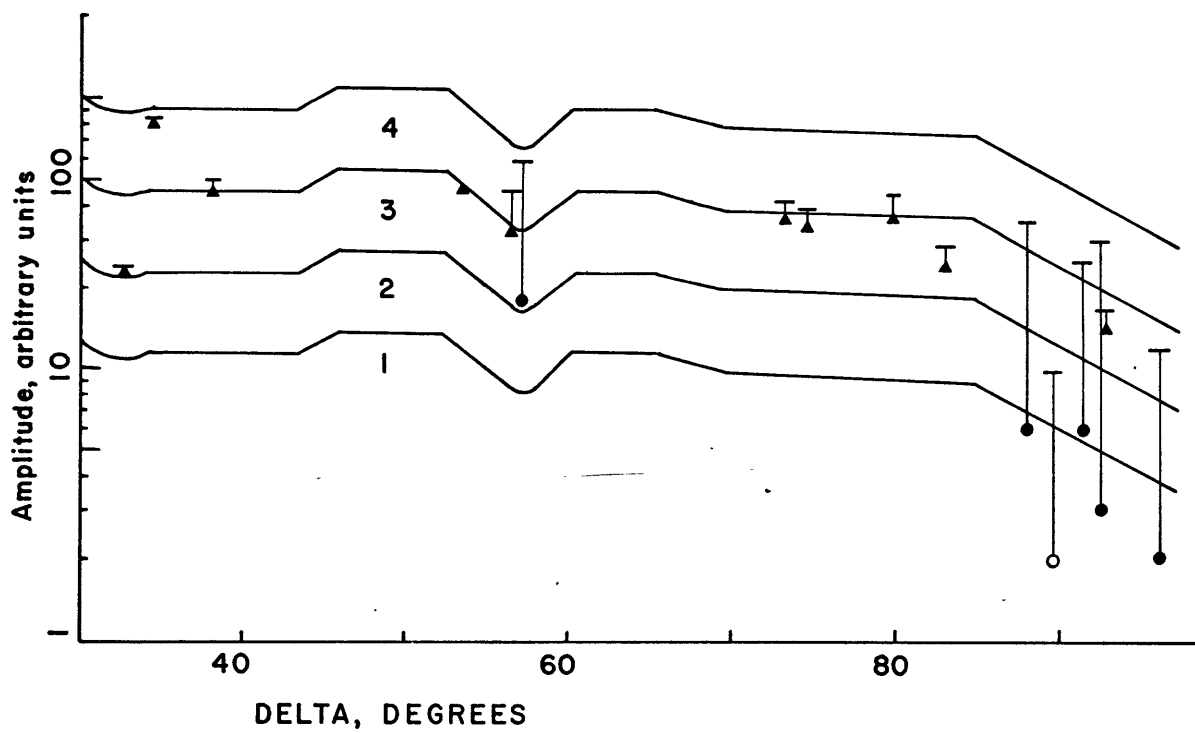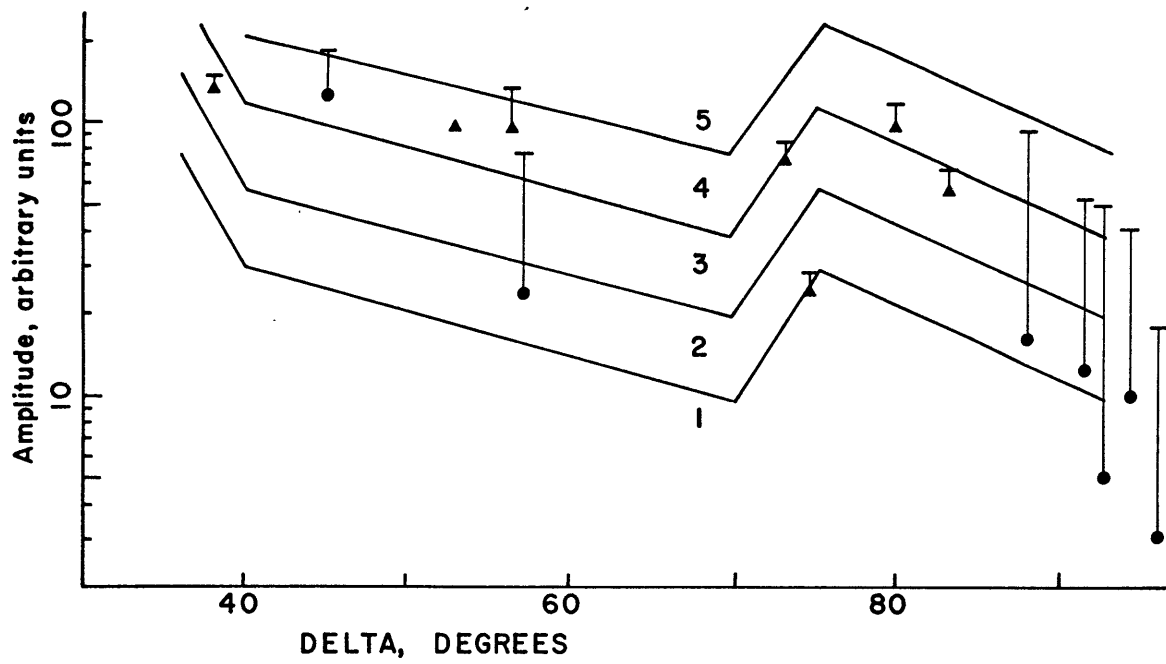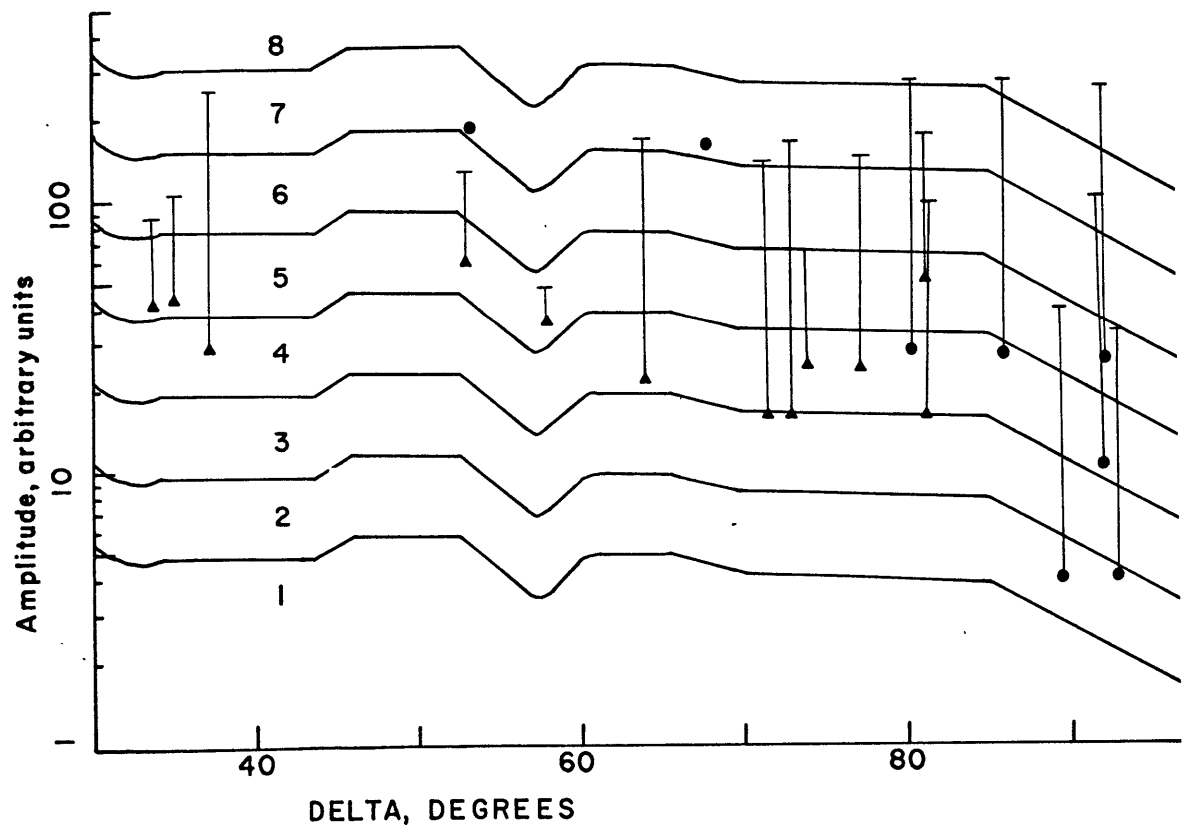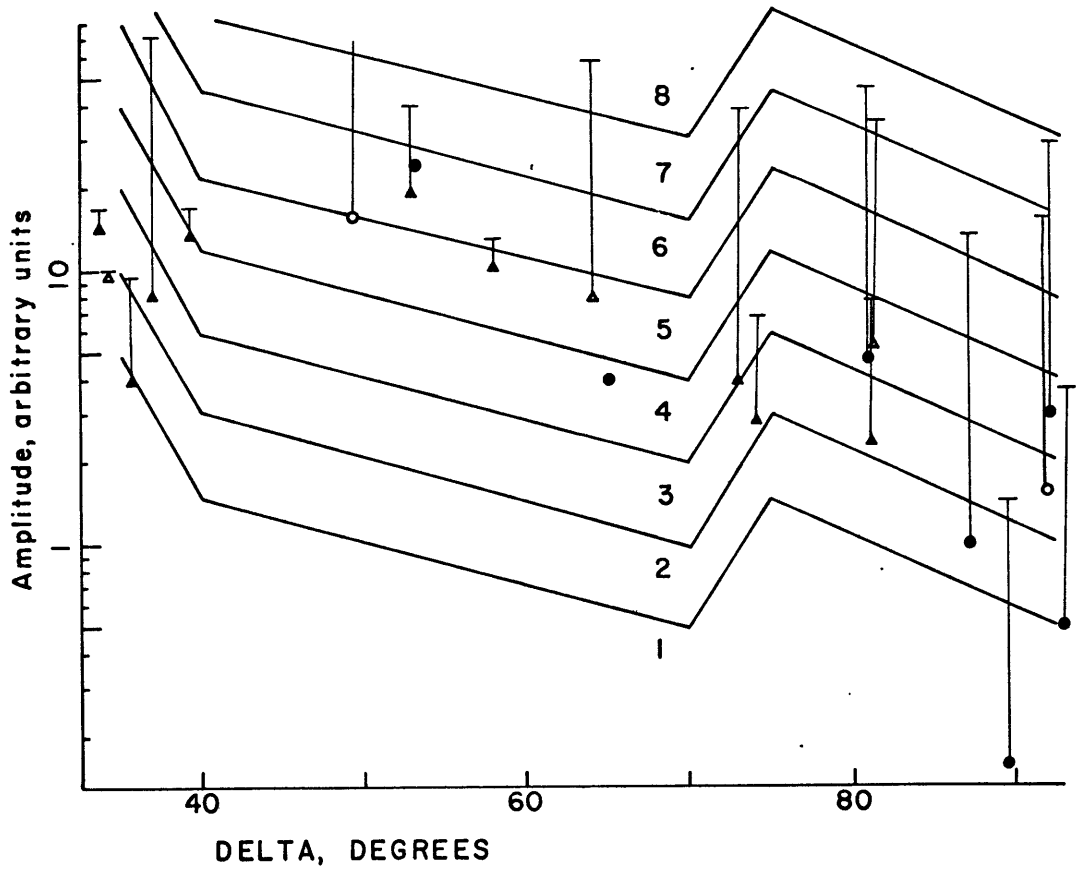
FIGURE B.13
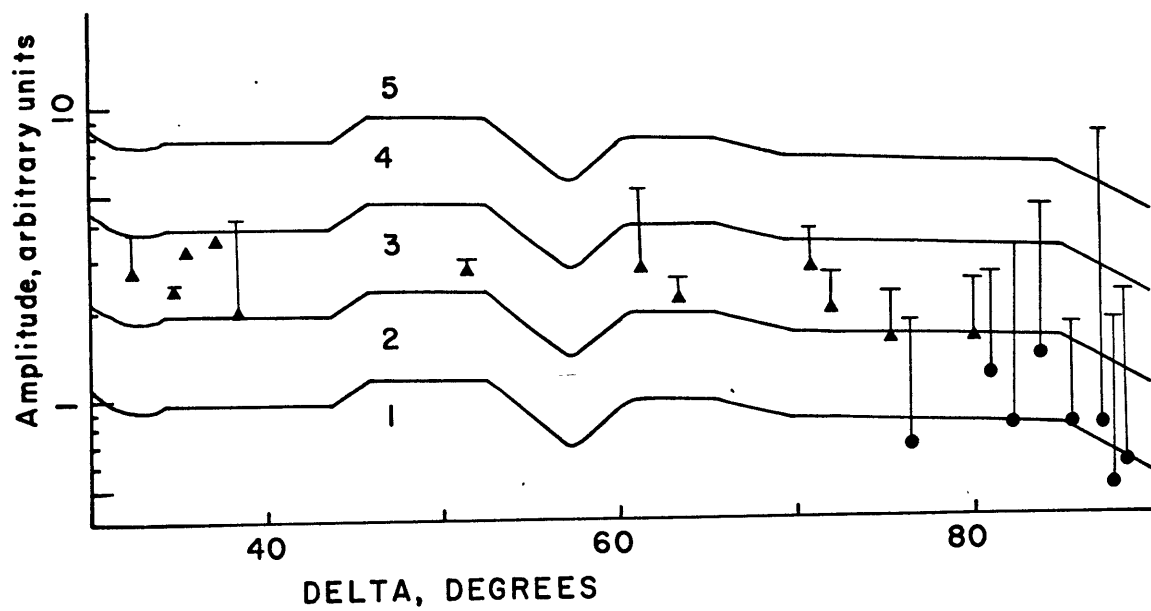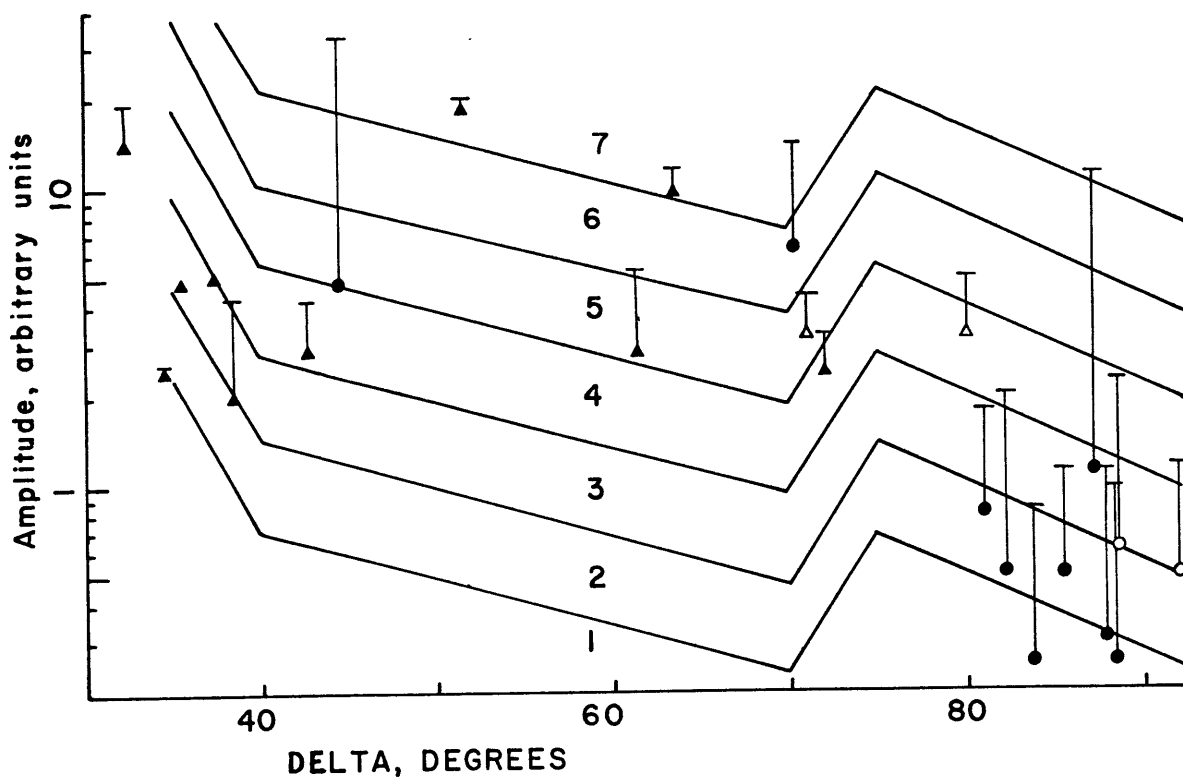
FIGURE B.14
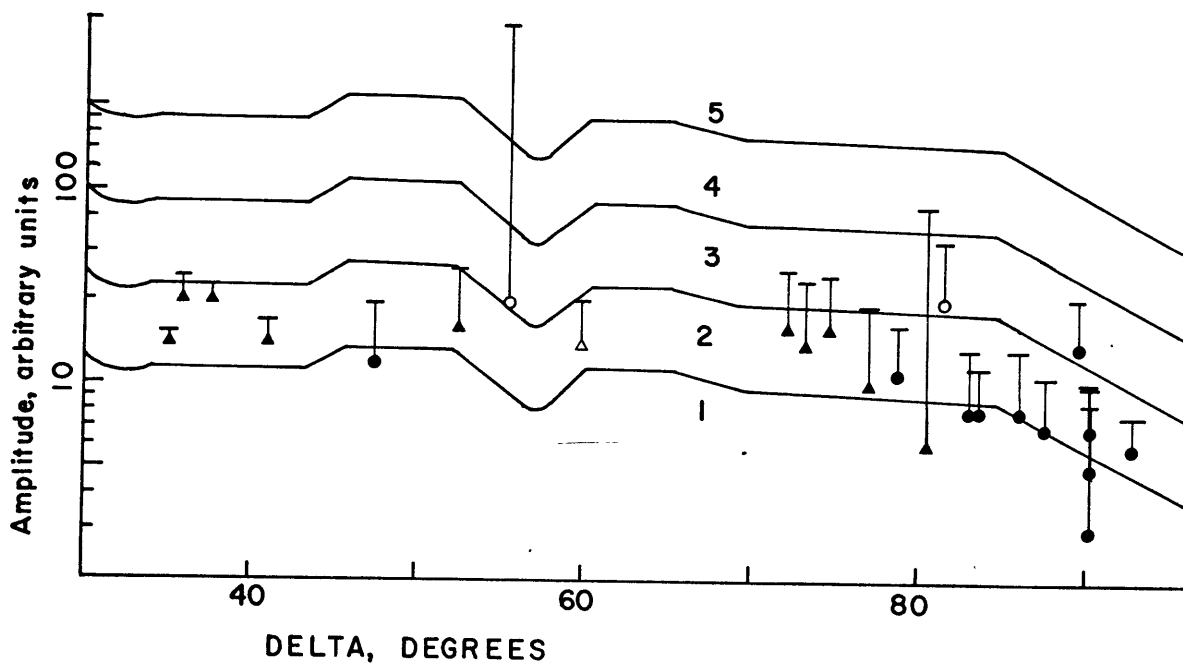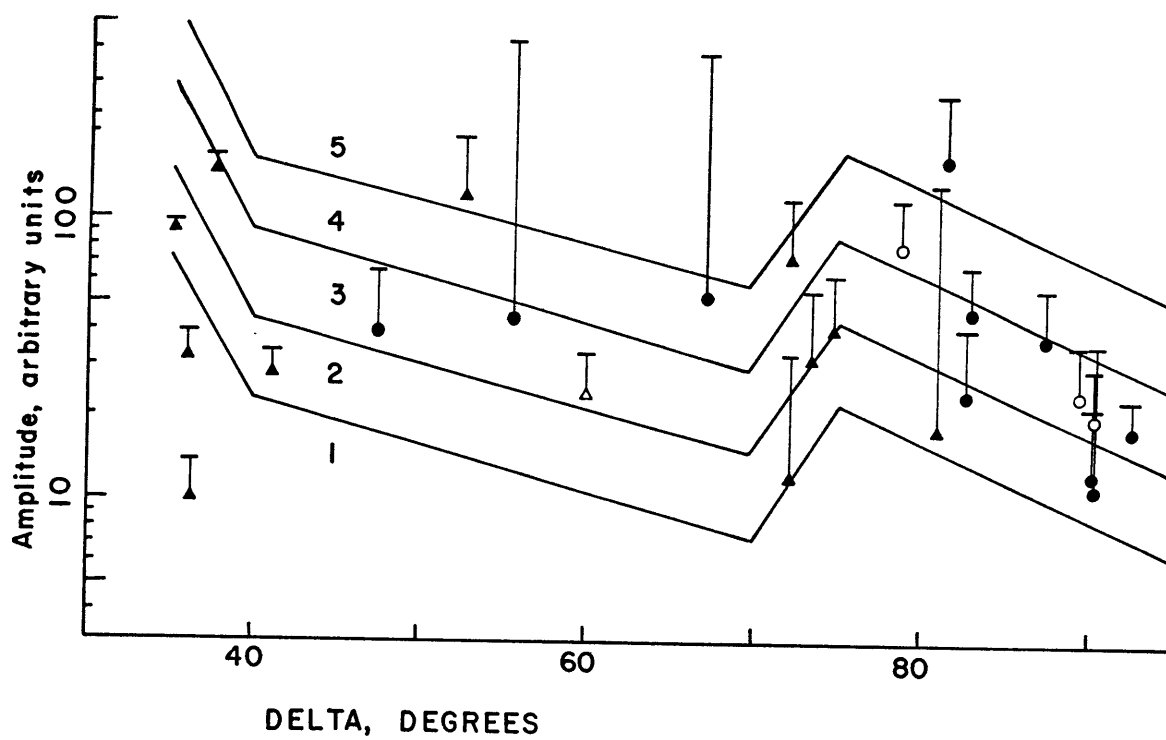
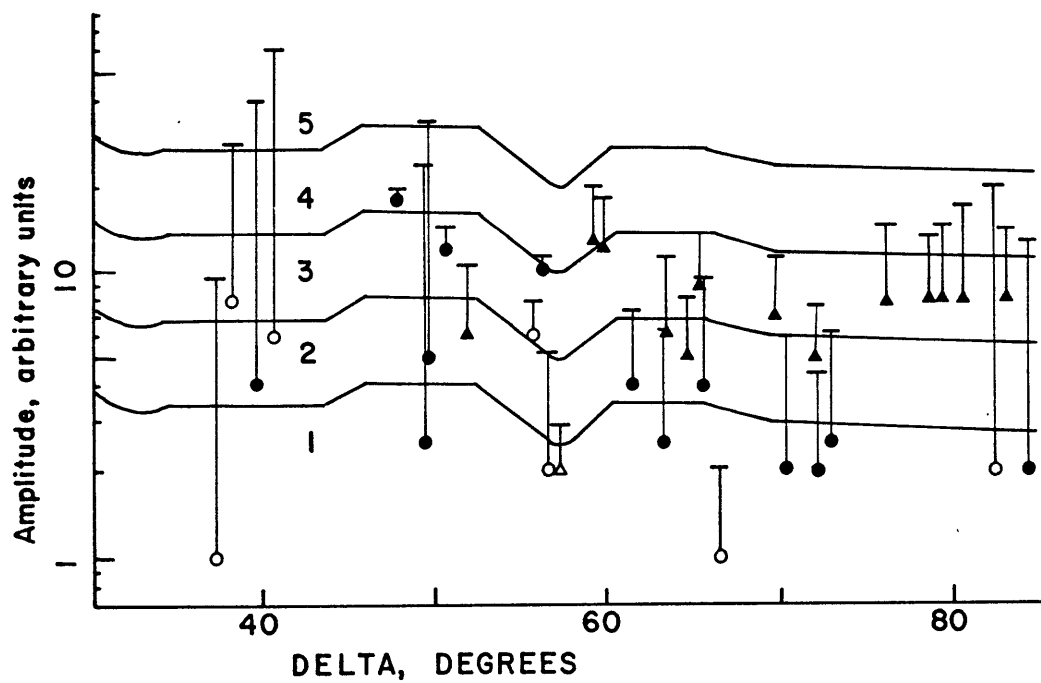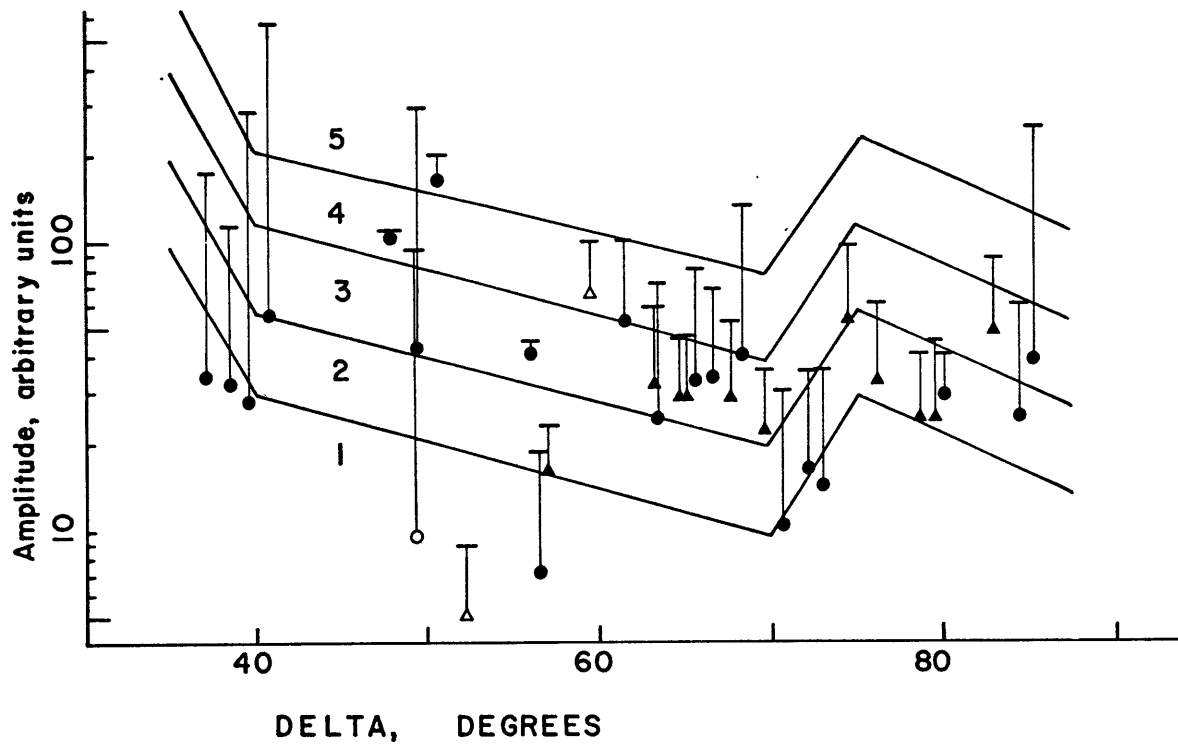FIGURE B.15
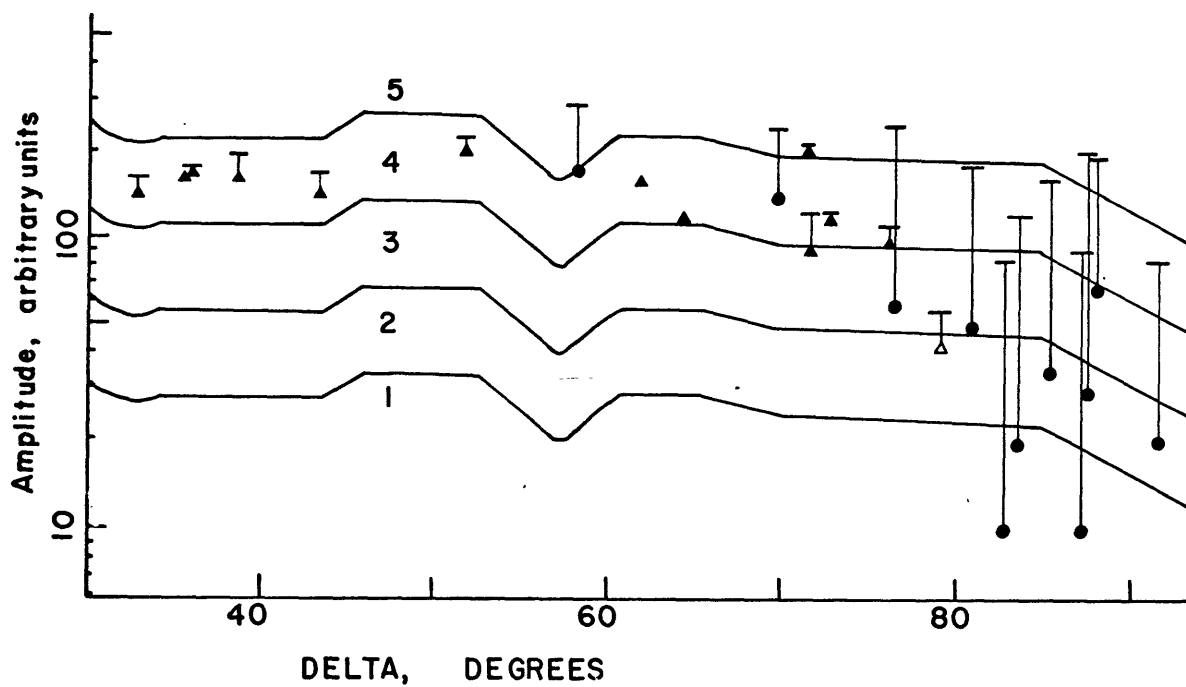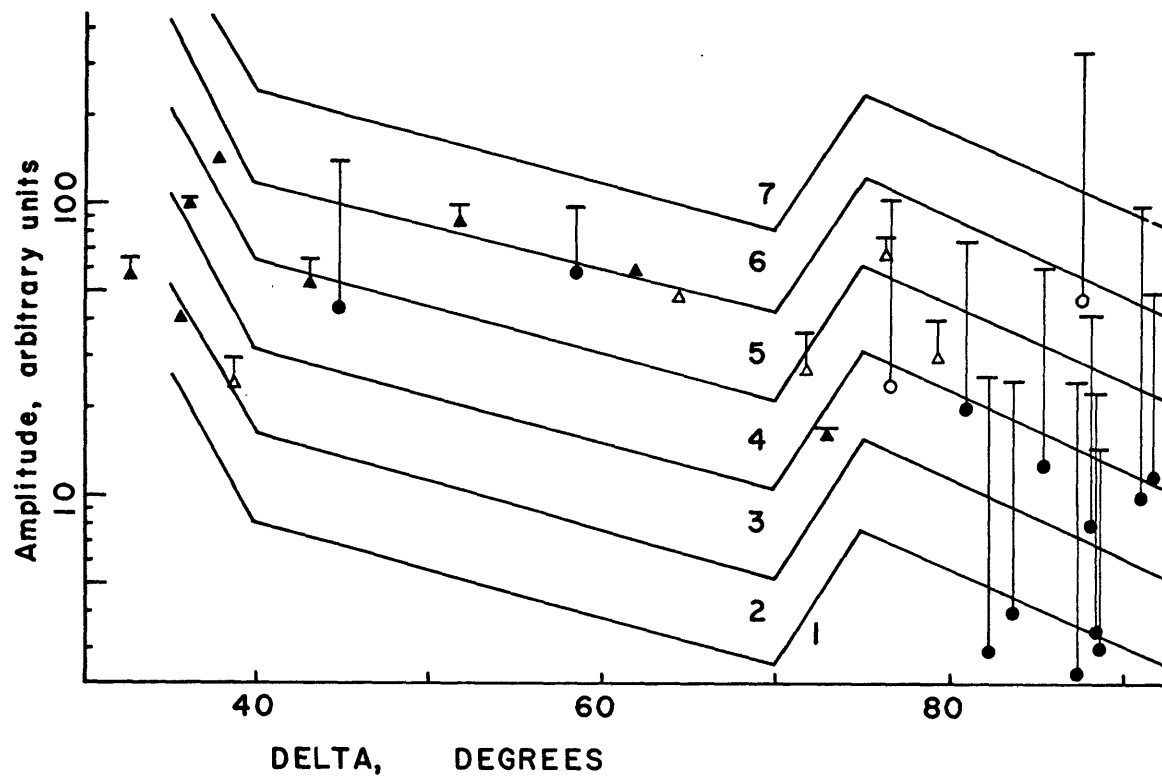
FIGURE B.16

FIGURE B.17

FIGURE B.18

BIOGRAPHICAL NOTE

The author was born in Kalamazoo, Michigan on February 14, 1945, the son of Norman C. Sleep and Caroline Sleep (neé Harvey). At age 5 his family moved to Parchment, Michigan, where he attended the Parchment Public Schools. After graduating from high school in 1963, he enrolled at Michigan State University, graduating with a B.S. in mathematics in 1967. During part of this time he was also employed in the paper industry in Parchment and Kalamazoo, Michigan. In September, 1967, he entered Graduate School at the Massachusetts Institute of Technology. He is the author of the following papers:

Sleep, N.H., Sensitivity of Heat Flow and Gravity to the Mechanism of Sea-Floor Spreading, J. Geophys. Res., 72, 542, 1969.

Sleep, N.H. and S. Biehler, Topography and Tectonics at the Intersections of Fracture Zones with Central Rifts, J. Geophys. Res., 75, 2748, 1970.

Sleep, N.H. and M.N. Toksöz, Evolution of Marginal Basins, Nature, 233, 548, 1971.

Sleep, N.H., Thermal Effects of the Formation of Atlantic Continental Margins by Continental Break Up, Geophys. J. Roy. Astron. Soc., 24, 325, 1971.

Sleep, N.H., Crustal Thinning on Atlantic Continental

    Margins: evidence from older margins, Proc. NATO

    Advanced Study Institute, Newcastle, England, in

    press, 1972.